NASA CR-134597

FRACTURE CONTROL METHODS FOR SPACE VEHICLES

Volume II

Assessment of Fracture Mechanics Technology for Space Shuttle Applications

By

R.M. Ehret

Prepared for

NATIONAL AERONAUTICS AND SPACE ADMINISTRATION

NASA Lewis Research Center

Contract NAS 3-16765

FRACTURE CONTROL METHODS FOR SPACE VEHICLES

Volume II

Assessment of Fracture Mechanics Technology for Space Shuttle Applications

by

R. M. Ehret

Contract NAS3-16765
NASA Lewis Research Center
Cleveland, Ohio

August 1974

1. Report No.	2. Government Accession No.	3. Recipient's Catalog No.
NASA CR-134597		

4. Title and Subtitle	5. Report Date
Fracture Control Methods for Space Vehicles, Volume II: Assessment of Fracture Mechanics Technology for Space Shuttle Applications	August 1974
	6. Performing Organization Code
7. Author(s)	8. Performing Organization Report No.
R.M. Ehret	SD 73-SH-0171-2
9. Performing Organization Name and Address	10. Work Unit No.
Space Division Rockwell International Corporation Downey, CA 90241	11. Contract or Grant No.
	NAS3-16765
12. Sponsoring Agency Name and Address	13. Type of Report and Period Covered
National Aeronautics and Space Administration 21000 Brookpark Rd. Lewis Research Center, Cleveland, OH 44135	Contractor Report June 1972 through March 1974
	14. Sponsoring Agency Code

15. Supplementary Notes

Project Manager, Gordon T. Smith
NASA Lewis Research Center
Cleveland, OH 44135

16. Abstract

A state-of-the-art review of the discipline of fracture mechanics was performed. Emphasis was placed on those engineering fracture mechanics concepts presently considered most applicable to the Space Shuttle vehicle. The concepts explored include fracture toughness, precritical flaw growth, failure mechanisms, inspection methods (including proof test logic), and crack growth predictive analysis techniques.

17. Key words (Suggested by Author(s))	18. Distribution Statement
Fracture Mechanics Space Vehicle Structure Fracture Control Procedures	Unclassified, Unlimited

19. Security Classif. (of this report)	20. Security Classif. (of this page)	21. No. of Pages	22. Price*
Unclassified	Unclassified		

FOREWORD

The work described in this report was performed by the Space Division of Rockwell International Corporation under Contract NAS3-16765, Fracture Control Methods for Space Shuttle Vehicles, for the Lewis Research Center of the National Aeronautics and Space Administration. The investigation was conducted under the technical direction of Mr. Gordon T. Smith of NASA/LeRC. The project study manager at the Space Division of Rockwell International Corporation was Mr. A. F. Liu, with Dr. Paul C. Paris of Del Research Corporation and Dr. Matthew Creager of Del West Associates, Inc., acting as primary technical consultants.

This report consists of three volumes:

Volume I. Fracture Control Design Methods (prepared by A. F. Liu)

Volume II. Assessment of Fracture Mechanics Technology for Space Shuttle Applications (prepared by R. M. Ehret)

Volume III. Space Shuttle Configurations (prepared by A. F. Liu and E. J. Mulcahy)

Mr. James E. Collipriest, Jr., provided overall techanical guidance in the preparation of Volume II. Mr. Edward J. Mulcahy and Mr. A. S. Musicman contributed significantly to the preparation of Section 1.1 (Space Shuttle Vehicle Structural Description) of Volume I. Mr. John Mamon and Mr. F. Stuckenburg aided substantially in the preparation of the nondestructive evaluation sections in Volumes I and II. Mr. R. E. O'Brien and Mr. R. M. Ehret contributed, respectively, Section 2.2 (Prevention of Cracks and Crack-Like Defects in Shuttle Vehicle Structure) and Section 2.3.8 (Required Material Properties Data for Space Shuttle Fracture Mechanics Analysis) of Volume I. Dr. Matthew Creager contributed Section 2.3.6 (Failure Under Complex Loading Conditions) and Section 2.3.7.4 (Damage Tolerance Analysis for Pressure Vessels) of Volume I and Section 2.2 (Thin Sheet Behavior) and a discussion of fracture behavior under combined in-plane loading in Section 1.2 (Linear Elastic Concepts of Fracture Behavior) of Volume II.

Mr. R. W. Westrup prepared the original proposal response to the RFP and established the basic frame work for the study program. The managerial guidance provided by Mr. R. P. Olsen, Engineering Manager, Materials and Processes, Space Division, is acknowledged by the authors.

NOMENCLATURE

a	Half-crack length or crack depth for part-through crack
A	Crack surface area
a_c	Critical crack size
a_e	Crack size plus plastic zone size
a_f	Flaw size at fracture
a_i	Initial crack size
a_o	Initial flaw size
a_p	Crack size plus plastic zone caused by an overload stress large enough to extend past a residual plastic zone
a_s	Maximum flaw size that can survive a proof load
a_u	Empirical material parameter
b	Half the major axis for an ellipsoidal cavity
B	Thickness
c	Surface flaw half length
C	Coefficient in crack growth rate expressions; or elastic compliance
c_B	Backside flaw half-length of a part-through crack following penetration
CCT	Center-cracked tension test specimen
c_F	Frontside flaw half-length of a part-through crack following penetration
C_m, C_m'	Empirical constant
COD	Crack opening displacement
C_p	Retardation parameter

CT	Compact test specimen
CVN	Charpy V-notch impact energy
C_1	Empirical constant
D	Empirical material parameter
da/dN	Crack growth per cycle of load
da/dt	Crack growth per unit of time
E	Elastic modulus
$\epsilon_x, \epsilon_y, \epsilon_z$	Rectangular components of displacement
G	Shear modulus of elasticity
G	Crack extension force (energy rate)
G_c	Crack extension force at instability
G_{Ic}	Plane-strain fracture toughness
G_r	Resistance level of available strain energy release rate
A	Empirical acoustic emission coefficient
J	Potential energy difference associated with the difference between two identically loaded bodies having neighboring crack sizes
J_{Ic}	Plane-strain fracture toughness
K	Stress intensity factor
K_c	Critical stress intensity factor
K_c, K_{IIc}, K_{IIIc}	Critical stress intensity factors associated with each mode of cracking
K_f	Effective toughness for a part-through crack
K_i, K_{Ii}	Initial stress intensity
K_{max}	Maximum applied stress intensity

K_Q	Apparent fracture toughness
K_r	Stress intensity factor associated with resistance to crack extension
K_s	Survival stress intensity for a part-through crack calculated using failure load and final flaw size
K_{Tc}	Through crack fracture toughness
K_{th}	Environmental cracking threshold
K_w, K_t, K_u, K'_u	Stress concentration factors
K_I, K_{II}, K_{III}	Stress intensity factors associated with each mode of cracking
K_{Ic}	Plane strain fracture toughness or critical value of K_c for Mode I in Mixed Mode Failure discussion
K_{IE}	Surface flaw fracture toughness calculated using failure load and initial flaw size
K_{Iscc}	Stress corrosion cracking threshold
m	Empirical material parameter
m	Exponent for accommodation of load ratio effects in effective stress intensity calculation
m	Crack growth retardation recovery parameter
m	Free surface stress intensity magnification factor for a part-through crack
M	Moment of inertia
M_B	Stress intensity magnification factor of a part-through crack subjected to bending
M_1	Front face stress intensity magnification factor for a part-through crack
M_2	Back face stress intensity magnification factor for a part-through crack
n	Exponent in crack growth rate expressions

N	Load cycle or number of load cycles
N	Total number of acoustic emission signals
NDE	Nondestructive evaluation
p	$\partial U_p / \partial a$
P	Applied load
P_L	Plastic limit load
PTC	Part-through crack
Q	Plasticity and shape normalizing factor for surface flaw
r	Radial coordinate from a crack tip
R	Materials resistance to crack extension
R	Load ratio (minimum load/maximum load)
R_{eff}	Effective load ratio
r_p	Full width of the plastic zone
r_y	Distance from apparent crack tip to the elastic-plastic boundary ahead of the crack tip
R_y	Yield zone size at current stress (retardation model)
s	Empirical material parameter
SEN	Single-edge notch test specimen
SF	Surface flaw test specimen
t	Time
t	Thickness
U	Total potential energy per unit thickness
U_E	Elastic potential energy per unit thickness
U_o	Potential energy per unit thickness prior to introduction of a crack

U_p	Energy per unit thickness consumed in plastic straining
U_S	Energy absorbed per unit thickness in creating a new crack surface
W	Width
W	Strain energy density
WOL	Wedge opening load test specimen
V	Stored energy
α	Proof factor; ratio of proof stress to operating stress
α	Flaw size dependent constant
β	Angular coordinate
β	Constant
γ	Surface tension
Δ	Displacement
δ	Load displacement
ΔK	Stress intensity excursion ($K_{max} - K_{min}$)
$\overline{\Delta K}$	Effective stress intensity range from $\overline{\Delta K} = (1 - R)^m K_{max}$
ΔK_ϕ	Cyclic crack growth threshold stress intensity range
θ	Angular coordinate measured from the crack plane
ν	Poisson's Ratio
ρ	Mass density
ρ	Crack tip radius
σ	Gross stress
σ_{ap}	Stress required to produce a crack length plus plastic zone equal to a_p

σ_B	Outer fiber stress of a plate subjected to bending
σ_c	Critical stress
σ_f	Net stress at failure
σ_{max}	Maximum applied gross stress
σ_n	Net stress
σ_{ol}	Overload stress
σ_{op}	Operating stress
σ_{opn}	Crack opening stress
σ_p, σ_{proof}	Proof stress
σ_{red}	Reduction in applied stress due to retardation
σ_u	Ultimate strength
σ_u	Empirical constant
σ_w	Working stress
σ_x, σ_y, σ_z	Rectangular components of tensile stress
σ_{ys}	Yield strength
τ	Shear stress
τ_{xy}, τ_{yz}, τ_{xz}	Rectangular components of shear stress
γ	Crack opening displacement
ϕ	An elliptic integral
ω	Empirical material parameter

CONTENTS

ILLUSTRATIONS

TABLES

INTRODUCTION

As performance requirements for space vehicles and military aircraft continue to increase, demands that maximum performance be exacted from the available materials will also increase. The resulting trend toward higher strength materials and higher applied stresses will often have a tendency to increase a structure's sensitivity to the presence of flaws. Applied fracture mechanics attempts to provide techniques for characterization of this sensitivity in a quantitative manner.

The contract for design and fabrication of the Space Shuttle vehicle specifically requires that fracture control methods be employed to prevent catastrophic structural failures resulting from cracks or crack-like defects. The Space Shuttle structure is a unique combination of aircraft and spacecraft. The multitude and extremes of anticipated configurations, environments and loads present a significant challenge regarding the application of fracture mechanics technology. To avoid an inefficient (overly conservative) design or potentially dangerous simplifying assumptions, immediate steps must be taken to reconcile existing discrepancies between those material data and analysis methods currently available and those necessary for evaluation of Space Shuttle structural components. The following review of the state of the art of the discipline of fracture mechanics is intended to emphasize those engineering fracture mechanics concepts presently considered most applicable to the Space Shuttle vehicle.

If there has been one overriding goal in the past 20 years of fracture mechanics activity, it has been to characterize fracture phenomena in terms of measurable material properties relating applied stress to flaw size at fracture—i.e., fracture toughness. An equally, if not more important, product of fracture mechanics methodology is the developing ability to characterize the behavior of flaws prior to fracture. Such information provides tools for estimating the useful service life of structures while considering the presence of crack-like defects, including situations where defect sizes are below the limits of conventional detectability. These two topics, fracture and precritical growth, occupy a major portion of the following review. Section 2 examines the nature of plane strain fracture toughness, K_{I_c}, and evaluates the applicability of that material property to the Space Shuttle. The contrasting behavior and analysis methods associated with fracture of thin sheet material are also reviewed. Additionally, analysis of the fracture behavior of the surface flaw as a unique defect geometry requiring special consideration is included.

Section 3 examines the phenomenon of pre-critical (or sub-critical) flaw growth behavior with consideration of such topics as flaw growth under monotonic load application, cyclic load-induced flaw growth behavior including environmental effects and crack growth retardation, and sustained load crack growth behavior.

Section 4 briefly reviews the microscopic and macroscopic aspects of the fracture process, in addition to providing an evaluation of several available techniques for characterizing the phenomenon of penetration or transition of a surface flaw to a stable through-the-thickness crack (leak-before-burst).

Because the application of fracture mechanics principles assumes some prior knowledge or finite measure of flaw size, Section 5 gives a brief review of conventional flaw detection methods and the current applicability of acoustic emission technology as a fracture mechanics tool. The value of the proof test as a viable means of establishing flaw sizes is examined, and an attempt is made to identify the salient ingredients of a comprehensive proof test logic.

Incorporation of fracture mechanics principles into service life predictive analysis programs is a natural product of a comprehensive fracture control effort. Therefore, Section 6 briefly outlines the necessary considerations for proper implementation of predictive analysis techniques associated with pre-critical flaw growth behavior.

1.0 THEORETICAL ASPECTS OF FRACTURE ANALYSIS

1.0 THEORETICAL ASPECTS OF FRACTURE ANALYSIS

The fundamentals of linear elastic fracture mechanics theory are available through several comprehensive reviews of the subject (References 1, 2, and 3). A brief review of these fundamentals is presented in this section to provide technical continuity with subsequent sections. Additionally, the topics of combined in-plane loading, multiple parameter failure criteria, and the J-integral approach to fracture analysis are briefly discussed as subjects of current endeavor with regard to the theoretical aspects of fracture analysis.

1.1 APPROACHES TO FRACTURE ANALYSIS

Several approaches to the evaluation of fracture behavior are available. These can generally be classified to include residual strength analysis, transition temperature approach, and stress analysis methods. The residual strength of a structure containing a defect is simply a measure of the load carrying ability of a specific configuration containing a specific defect. Such an approach does not rely on stress intensity solutions or toughness values. This "damage tolerance" approach is often expedient for complex structural configurations associated with airframes where extensive design verification testing is usually performed.

In less complex structures, the fracture stress may be represented by some empirical or graphic relationship with defect size, allowing assessment of damage tolerance at various stress levels.

The obvious shortcoming of such an approach is the necessity of extensive test data generation. All test results must then remain closely tied to the test specimen configuration and extrapolation to other configurations must be approached with considerable caution.

Empirical residual strength analysis generally depends on comparison of equivalent test values to determine the best material or structural configuration. Similarly, structural adequacy is verified by demonstration that crack sizes grossly exceeding inspection detectability do not reduce the residual strength below design limit values, or that with a readily-detectable sized crack, residual strength significantly exceeds design values. Only limited application of an empirical residual strength approach is anticipated for the Space Shuttle program.

The transition temperature approach for evaluating brittle fracture has been used for many years. A comprehensive review of the transition temperature approach relative to fracture mechanics principles can be found in Reference 3. The basic philosophy is relatively simple—some ferritic materials have a characteristic temperature below which they are susceptible to low stress brittle fracture in the presence of sharp defects, and above which brittle fracture rarely occurs. Weight considerations and the temperature extremes anticipated for Space Shuttle materials will limit selection of any alloys which exhibit an abrupt ductile-to-brittle transition behavior. Additionally, the qualitative nature of the transition temperature approach, when compared to linear elastic fracture mechanics, does not allow for convenient solution of specific problems, especially when attempting to characterize pre-critical flaw growth. Therefore, further consideration of such analysis methods is not within the scope of this review.

In the stress analysis approach to fracture prediction, some property of the stress-strain distribution is used as the prediction criterion. The most notable in recent literature are those developed by Neuber (Reference 4 and 5) and Kuhn (Reference 6 and 7) in addition to the elastic crack tip stress field approach. Each of these methods uses an elastic stress analysis to determine the general character of redistribution of force transmission around cracks. Also, each of these analyses draws attention to a phenomenon at the crack tip which is regarded as that which precipitates failure, More specifically, these phenomena are respectively: (1) developing a plastic particle of critical size, (2) developing an ultimate stress at a specific radius from the crack tip (discussed further in Section 2), and (3) developing an elastic stress field approaching a critical magnitude ahead of the crack.

The stress field approach requires no assumptions regarding physical phenomena, and the strength and generality of linear elastic fracture mechanics are, in part, due to the absence of such assumptions. In essence, linear elastic fracture mechanics represents the most sophisticated, yet, the most direct and quantitative method currently available for addressing the problems associated with fracture.

A review of various stress analysis approaches to fracture analysis is contained in Reference 2. For Space Shuttle application, it is anticipated that linear elastic theory, specifically the stress intensity concept of fracture behavior, will dominate fracture control analysis methods. Therefore the remainder of this discussion will focus directly on that subject.

1.2 LINEAR ELASTIC CONCEPTS OF FRACTURE BEHAVIOR

In recent years linear elastic fracture mechanics has evolved to a position of widespread acceptance as a viable tool for use in fracture analysis of structural materials. This "fracture toughness" technology provides a unique structural design concept which yields quantative relationships between applied stress, flaw size, and material behavior. The theory can be developed in terms of either an energy approach or a stress field approach. Both approaches are closely related and lead to equivalent results.

Energy Approach as a Failure Criterion

Griffith (Reference 8) provided the first analysis of equilibrium and stability of cracks in 1920. He based his analysis on viewing the change in potential energy of a body into which a crack is introduced. His analysis is applicable to "perfectly brittle" materials, for which experiments with glass provided reasonable verification of his theory.

Griffith proposed that brittle material contains many small cracks which produce stress concentrations of sufficient magnitude so that the theoretical cohesive strength is reached in localized regions at a nominal stress which is well below the theoretical value. When one of the cracks spreads, it produces an increase in the surface area of the sides of the crack. This requires energy to overcome the cohesive force of the atoms, i.e., an increase in surface energy. A significant source of the increased surface energy is the reduction in elastic potential energy which is made available as the crack spreads.

Consider an infinite sheet of elastic material subject to uniform tensile stress, σ, into which a through-crack of length, 2a, is introduced (Figure 1-1). The potential energy balance of such a system can be written as

$$U = U_o + U_E + U_s \tag{1}$$

where U is the total potential energy of the system and U_o is the potential energy prior to introducing the crack. U_E is the energy per unit thickness

available to create the new crack surfaces resulting from the central through-crack. In accordance with the stress analysis of Inglis (Reference 9), this elastic potential energy decrease is expressed as

$$U_E = - \pi a^2 \sigma^2 / E \tag{2}$$

The term U_s is the energy absorbed for unit thickness in creating the new crack surfaces and is expressed by

$$U_s = 4a\gamma \tag{3}$$

with γ being the surface tension of the material.

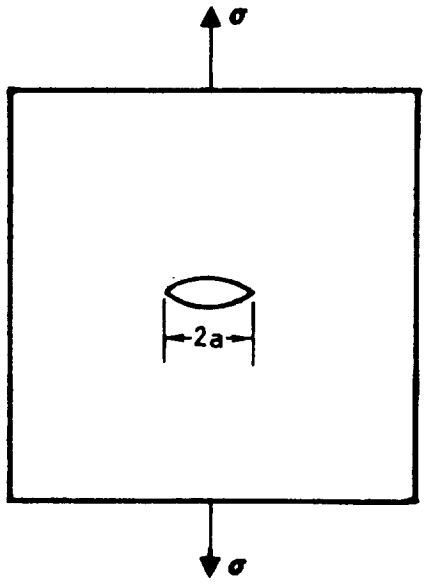

Figure 1-1. An Infinite Cracked Sheet With Uniform Normal Stress at Infinity

The change in the potential energy with respect to crack size, a, is expressed by the derivative of Equation (1) where

$$dU = \frac{\partial}{\partial a} [U_o + U_E + U_s] \, da \tag{4}$$

Setting this result equal to zero (equilibrium position) and for non-zero variation ($da \neq o$), conditions for unstable crack propagation can then be expressed by

$$\frac{\partial}{\partial a}\left[U_E + U_s\right] \leq 0 \tag{5}$$

or

$$\frac{\sigma^2 \pi a}{E} \geq 2\gamma \tag{6}$$

This relationship states that a crack will propagate when the decrease in elastic potential energy is at least equal to the energy required to create the new crack surface.

In subsequent fracture mechanics discussions, Equation (6) is interpreted in the following manner: designating the left side of Equation (6) as the elastic energy release rate, or alternately, the crack-extension force, G, and interpreting this value as the elastic energy available for infinitesimal crack extension, yields,

$$G = \sigma^2 \pi a/E \tag{7}$$

The right hand side of Equation (6) is then the material's resistance to crack extension, R, in terms of energy required to extend the crack per unit area of new surface created or, $R = 2\gamma$, for an ideally brittle material.

This energy rate viewpoint of crack stability can be put in graphic terms as shown in Figure 1-2, where both G and R are plotted as a function of crack size, a, for an initial crack size of a_o. The ideally brittle material's resistance, R, is a constant except that because of the irreversibility of crack growth, the R-curve begins with a vertical line from the initial crack size. The available energy rate, G, according to Equation (6), is a straight line through the origin whose slope increases with increasing applied stress. Therefore, upon loading, the state at any time is the first intersection of the G and R curves, and loading may proceed until the instability point is reached.

Independently, Orowan (Reference 10) and Irwin (Reference 15) suggested that the Griffith relationship could be made more compatible with brittle fracture in metals by inclusion of the energy consumed in plastic straining in the region at the crack tip. The instability criterion of Equation (5) can then be expressed by adding a plastic work term, U_p, so that

$$\frac{\partial}{\partial a}\left[U_E + U_s + U_p\right] \leq 0 \tag{8}$$

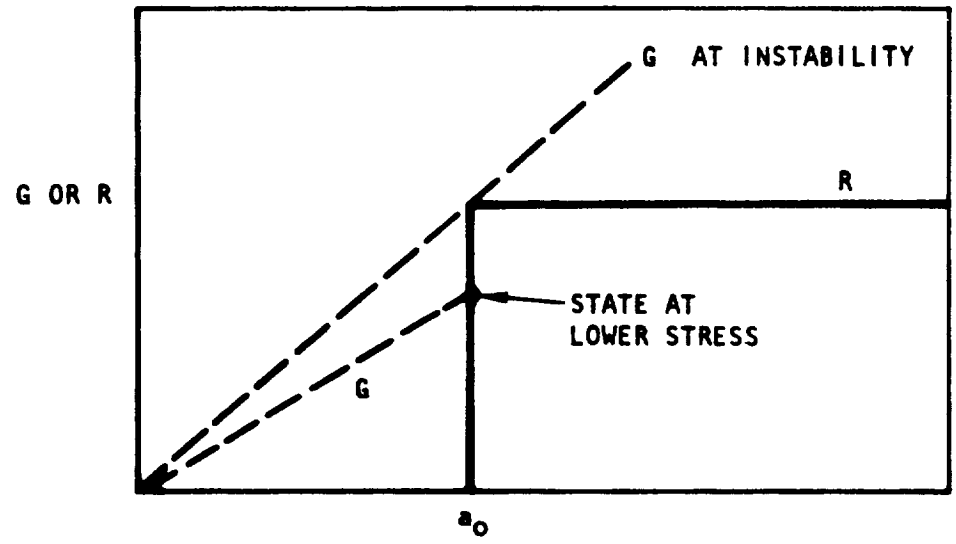

Figure 1-2. Available Crack Extension Energy and Resistance Versus Crack Size for an Ideally Brittle Material

The surface energy term is frequently neglected, because estimates of the plastic work term are generally much larger; and Equation (8) then reduces to

$$\frac{\partial}{\partial a}\left[U_E + U_p\right] \leq 0 \tag{9}$$

Letting

$$\frac{\partial U_p}{\partial a} = p \tag{10}$$

Equation (9) then, for one-half the total crack length, reduces to

$$\frac{\pi \sigma^2 a}{E} = p \tag{11}$$

The crack extension force, G, is then relatable to Orowan's plastic work factor, p. The value of G at the point of instability can be calculated from measurements of the load and the instantaneous crack length at that point. It is designated G_c and is taken as the fracture toughness of the material.

Applying the crack growth resistance interpretation to the fracture of metals, then Equation (10) would represent the resistance to crack extension; however, its variation with crack size is not specifically defined. The actual flaw size dependence, as determined by experiment, is illustrated in Figure 1-3. The contour of the R-curve results from stable crack extension accompanying a rising load. Materials which exhibit less stable growth prior to instability will be characterized by the more abrupt contour of the R-curve approaching the "perfectly brittle" behavior previously illustrated in Figure 1-2.

The failure criteria resulting from this approach is that the critical strain-energy release rate be achieved and that further crack extension causes the increase in G to occur at a rate greater than or equal to the rate of increase of crack growth resistance; or,

$$G = G_c \text{ and } \frac{\partial G}{\partial a} \geq \frac{\partial R}{\partial a} \tag{12}$$

and instability is initiated at the point when

$$G = G_c \text{ and } \frac{\partial G}{\partial a} = \frac{\partial R}{\partial a} \tag{13}$$

or, as illustrated in Figure 1-3, when the R-curve and G-curve become tangent.

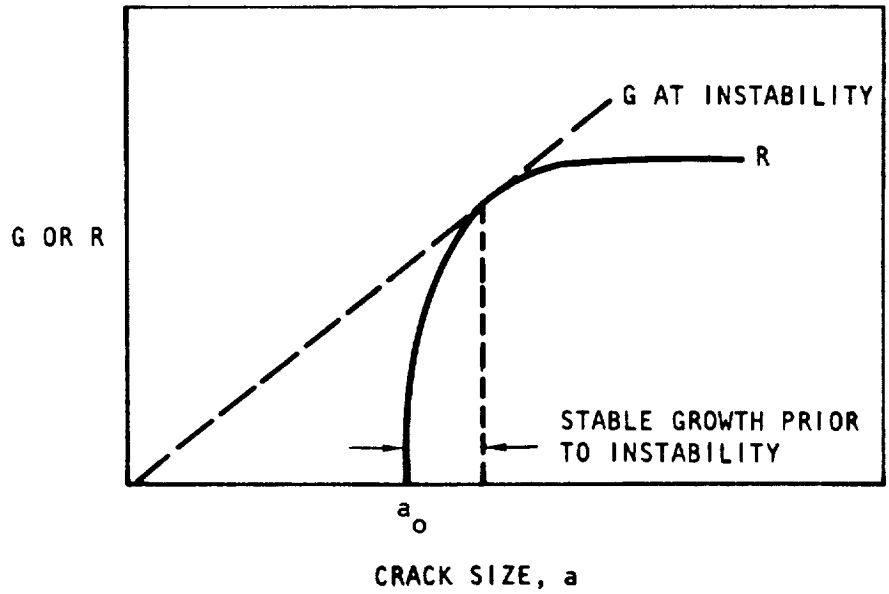

Figure 1-3. Crack Extension Energy and Resistance Vs Crack Size for a "Ductile" Material

From an engineering viewpoint, the energy concepts of fracture analysis are difficult to relate directly to hardware. However, the behavioral insight into the nature of the fracture process that is provided, especially when related to R-curve analysis, is extremely desirable. This characteristic ability to depict crack growth during load application, a reality with ductile materials, has led to an increase in popularity of R-curve techniques as discussed further in Sections 2 and 5.

Stress Intensity Approach as a Failure Criterion

In a structure containing a flaw, the surfaces of the crack being free from normal stress provide the dominating influence on the distribution of stresses near the crack tip. Other finite boundaries and remotely applied loads will affect only the intensity of the local stress field. To accommodate further discussion of these local stress fields, the coordinates measured from the leading edge of a crack and the stress components in the crack tip stress field are specified in Figure 1-4.

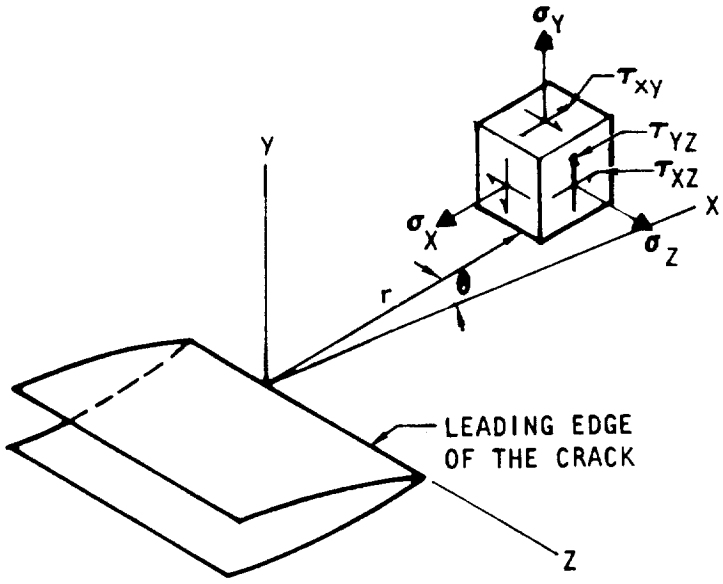

Figure 1-4. Coordinates and Stress Components of a Crack Tip Field

The state of stress throughout most bodies falls between the limits defined by the states of plane stress and plane strain. In the mathematical theory of elasticity and plasticity, a state of plane stress exists when (referring to Figure 1-4 for notation) $\sigma_z = \tau_{xz} = \tau_{yz} = 0$. This two dimensional state of stress is frequently assumed in practice when one of the dimensions of the body is small relative to the others. In a thin plate loaded in the plane of the plate, there will be virtually no stress acting perpendicular to the plate. The remaining stress system will consist of the two normal stresses σ_x and σ_y and a shear stress τ_{xy}.

Similarly, a state of plane strain exists when $\epsilon_z = \tau_{xz} = \tau_{yz} = 0$ which ensures that $\sigma_z = \nu(\sigma_x + \sigma_y)$. In such a system, all displacements can be considered to be limited to the xy-plane, so that strains in the z-direction can be neglected in the analysis. Since a plastic material tends to deform in all directions, to develop a plane strain condition it is necessary to constrain the flaw in one direction.

Near the leading edge of a crack, the magnitude of stresses and strains is very high compared to values at some relatively greater distances away. Because of this high degree of tensile deformation, the material near the

crack front tends to shrink (a Poisson's ratio effect) in a direction parallel to the leading edge. However, this shrinkage is constrained by any surrounding material which is less deformed. If the leading edge length is long compared to other dimensions of the plastically deformed zone, then it is highly constrained against shrinkage parallel to the leading edge and is considered to be in a state of localized plane strain. Conversely, if the plastic zone dimensions are large compared to the leading edge length of the crack, by viewing the plastic zone as a short cylinder with free ends, it is bound to be relatively unconstrained or in a state of localized plane stress. Naturally, plane stress conditions would still exist at free surfaces of a thick plate containing a flaw while localized plane strain conditions would prevail in the interior of the plate. The above considerations are equally relevant for three-dimensional cracks with curved crack fronts.

Neither total plane strain nor total plane stress conditions are found in real structural configurations. However, in stress field analysis, employment of either of these constraints allows for two-dimensional solutions of three-dimensional problems, which provides the foundation for linear elastic fracture mechanics theory as it is applied today.

Stress fields near the crack tips are three basic types, each characterized by a local mode of deformation. "Opening," Mode I, is characterized by local displacement in which the crack surfaces move directly apart. "Edge sliding," Mode II, is characterized by displacements in which the crack surfaces slide over one another perpendicular to the leading edge of the crack. "Tearing," Mode III, is characterized by crack surfaces sliding with respect to one another and parallel to the leading edge of the crack. The superposition of these three modes is sufficient to describe the most general case of crack tip deformation and stress fields. A direct approach for determining the elastic stress and displacement fields associated with each of these modes was developed by Irwin (References 11 and 12) based on the method of Westergaard (Reference 13). The resulting stress and displacement fields corresponding to the appropriate displacement mode are given in Figure 1-5. The equations for Modes I and II were written for the case of plane strain (that is, $\epsilon_z = 0$) but can be changed to plane stress by taking $\sigma_z = 0$ and replacing Poisson's ratio, ν, in the displacements with an appropriate value.

The parameters K_I, K_{II}, and K_{III} in the equations are termed stress intensity factors for the corresponding three types of stress displacement fields. These stress intensity factors may be physically interpreted as parameters which reflect the redistribution of stress in a body due to the introduction of a crack; and in particular, they indicate the type (mode) and magnitude of force transmission through the crack tip region.

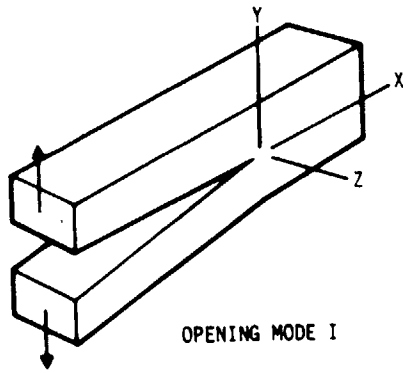

OPENING MODE I

$$\sigma_X = \frac{K_I}{(2\pi r)^{1/2}} \cos\frac{\theta}{2}\left[1 - \sin\frac{\theta}{2}\sin\frac{3\theta}{2}\right]$$

$$\sigma_Y = \frac{K_I}{(2\pi r)^{1/2}} \cos\frac{\theta}{2}\left[1 + \sin\frac{\theta}{2}\sin\frac{3\theta}{2}\right]$$

$$\tau_{XY} = \frac{K_I}{(2\pi r)^{1/2}} \sin\frac{\theta}{2}\cos\frac{\theta}{2}\cos\frac{3\theta}{2}$$

$$\sigma_Z = \nu(\sigma_X + \sigma_Y),\ \tau_{XZ} = \tau_{YZ} = 0$$

$$\epsilon_X = \frac{K_I}{G}\left[(r/(2\pi)\right]^{1/2} \cos\frac{\theta}{2}\left[1 - 2\nu + \sin^2\frac{\theta}{2}\right]$$

$$\epsilon_Y = \frac{K_I}{G}\left[(r/2\pi)\right]^{1/2} \sin\frac{\theta}{2}\left[2 - 2\nu - \cos^2\frac{\theta}{2}\right]$$

$$\epsilon_Z = 0$$

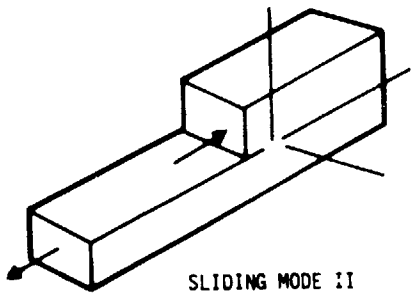

SLIDING MODE II

$$\sigma_X = \frac{-K_{II}}{(2\pi r)^{1/2}} \sin\frac{\theta}{2}\left[2 + \cos\frac{\theta}{2}\cos\frac{3\theta}{2}\right]$$

$$\sigma_Y = \frac{K_{II}}{(2\pi r)^{1/2}} \sin\frac{\theta}{2}\cos\frac{\theta}{2}\cos\frac{3\theta}{2}$$

$$\tau_{XY} = \frac{K_{II}}{(2\pi r)^{1/2}} \cos\frac{\theta}{2}\left[1 - \sin\frac{\theta}{2}\sin\frac{3\theta}{2}\right]$$

$$\sigma_Z = \nu(\sigma_X + \sigma_Y),\ \tau_{XZ} = \tau_{YZ} = 0$$

$$\epsilon_X = \frac{K_{II}}{G}\left[r/(2\pi)\right]^{1/2} \sin\frac{\theta}{2}\left[2 - 2\nu + \cos^2\frac{\theta}{2}\right]$$

$$\epsilon_Y = \frac{K_{II}}{G}\left[r/(2\pi)\right]^{1/2} \cos\frac{\theta}{2}\left[-1 + 2\nu + \sin^2\frac{\theta}{2}\right]$$

$$\epsilon_Z = 0$$

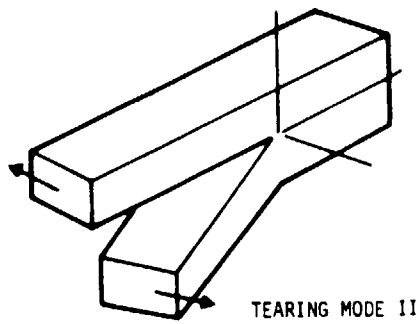

TEARING MODE III

$$\tau_{XZ} = \frac{-K_{III}}{(2\pi r)^{1/2}} \sin\frac{\theta}{2}$$

$$\tau_{YZ} = \frac{K_{III}}{(2\pi r)^{1/2}} \cos\frac{\theta}{2}$$

$$\sigma_X = \sigma_Y = \sigma_Z = \tau_{XY} = 0$$

$$\epsilon_Z = \frac{K_{III}}{G}\left[(2r)/\pi\right]^{1/2} \sin\frac{\theta}{2}$$

$$\epsilon_X = \epsilon_Y = 0$$

G = SHEAR MODULUS OF ELASTICITY

ν = POISSON'S RATIO

Figure 1-5. Crack Displacement Modes and Associated Stress Field Relationships

An infinite plate subjected to a uniform tensile stress, σ, into which a transverse crack length, 2a, has been introduced is shown in Figure 1-6a. As a two-dimensional problem of theory of elasticity, only two characteristic dimensions are present, σ and a. Since this configuration is symmetrical to the crack plane, only the Mode I fields are present. From dimensional consideration with the Mode I stress field relationships, Paris (Reference 14) developed the following crack tip stress intensity relationships:

$$K_I = C_1 \sigma \sqrt{a}; \; K_{II} = K_{III} = 0 \tag{14}$$

where C_1 has been determined to be equivalent to $\sqrt{\pi}$.

Consideration of this plate under a uniform shear stress τ (Figure 1-6b) results in stress intensity factors of:

$$K_{II} = \tau \sqrt{\pi a}; \; K_I = K_{III} = 0 \tag{15}$$

Shear stress applied parallel to the tunnel crack (Figure 1-6c) results in stress intensity factors of

$$K_{III} = \tau \sqrt{\pi a}; \; K_I = K_{II} = 0 \tag{16}$$

The similarity between the above relationships and the previously discussed Griffith energy criteria for crack stability indicates that instability occurs at a constant value of K. Additionally, the stress field equations (Figure 1-5) indicate that the stress conditions near the crack tip are of similar distributions and vary only in stress intensity from one case to another. Therefore, it follows that unstable crack extension will take place when the stress intensity factor, K, reaches a critical value; that is, when any combination of load, crack geometry, and configuration becomes critical. This occurs, then, when K approaches K_c (where the subscript (c) denotes criticality) whose absolute value is assumed to be a property of the material.

By restriction of the concept of K_c to particular displacement modes, criticality would then be represented by the terms K_{Ic}, K_{IIc} and K_{IIIc}. Historically, as dependence of critical stress intensities upon the state of stress at the crack tip became evident, the term K_{Ic} was corrupted to specifically denote the Mode I critical stress intensity under conditions of plane strain. The term K_{Ic}, used in such a context, is synonymous with plane strain fracture toughness. For conditions other than plane strain, criticality is then simply denoted by the term K_c (without regard for

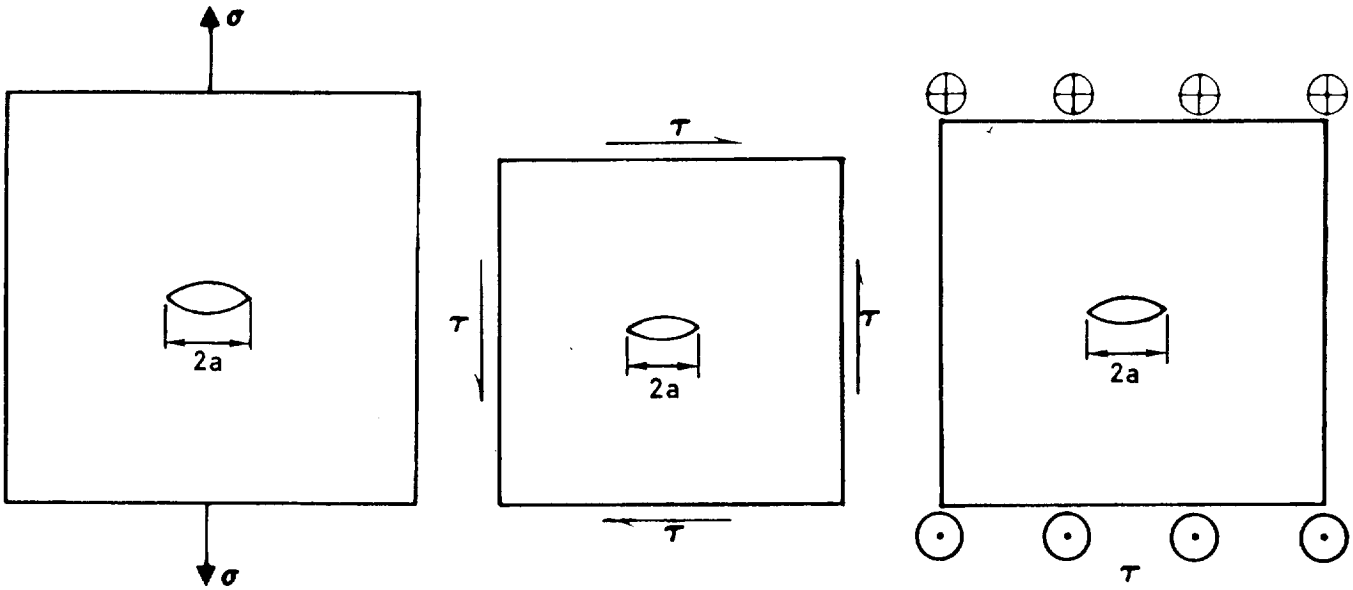

a) Normal Stress b) In-Plane Shear c) Out of Plane Shear

Figure 1-6. Modes of Force Transmission Through a Cracked Plate (Reference 1)

identification of the displacement mode). Further confusion with nomenclature results when either conditions of mixed stress states (partially plane strain and partially plane stress) or conditions of combined loading producing more than one displacement mode at the crack tip are both referred to as "mixed mode" behavior.

The arguments leading to the concept of criticality are not limited to perfectly elastic activity. If a small zone of non-linearity (e.g., plasticity) is present at the crack tip, it is embedded within the elastic field. In a material of given properties, the non-linearity will disturb the elastic field, and consequent failure will occur at a measured critical stress intensity. The implication is that the criticality relationships can then be applied for real engineering materials showing small amounts of ductile behavior.

Compliance Considerations

The Griffith crack extension process was defined in terms of the elastic potential energy (strain energy and loading force potential) made available to the process of crack extension. The energy rate can be examined in more detail using the elastic compliance of a body (References 15 and 16).

During an increment of crack extension, creating a new crack surface area, dA, the work done by the loading force, P, is $P\,d\Delta$ where Δ is the displacement of the force in its own direction. The stored energy, V, is always positive and contributes to its own release during crack extension. Therefore, collecting the contributions to the energy rate, G,

$$G = P \frac{d\Delta}{dA} - \frac{dV}{dA} \tag{17}$$

The elastic compliance, C (inverse spring constant), relates load to displacement by

$$\Delta = C\,P \tag{18}$$

The compliance depends only on the elastic modulus of the material and the geometry of the body, including the crack size.

Since the strain energy can be written as the work done during loading at a constant crack length, or

$$V = \frac{P\Delta}{2} = \frac{C\,P^2}{2} \tag{19}$$

and by appropriate substitutions

$$G = \frac{P^2}{2} \frac{dC}{dA} \tag{20}$$

and when $dA = Bda$, where B is the plate thickness

$$G = \frac{P^2}{2B} \frac{dC}{da} \tag{21}$$

This result implies that the method of load application does not affect the available energy rate for infinitesimal crack extension, G.

The fracture criteria associated with the energy rate and stress field approaches to fracture are respectively:

$$G = G_c$$

and (22)

$$K = K_c$$

In both cases, the left sides of these equations are elastically analyzed causes of the local crack tip conditions promoting fracture and, in fact, are equivalent concepts. Their interrelationship is derived in detail in Reference 1 and is expressed by

$$G = \frac{K^2}{E} \text{ (plane stress)} \tag{23}$$

and

$$G = \frac{(1 - \nu^2)K^2}{E} \text{ (plane strain)} \tag{24}$$

where E is the modulus of elasticity and ν is Poisson's ratio. Thus, using the compliance relationship of Equation 21 and Equation 23 relating K to G, we have

$$K^2 = E\,G = \frac{E\,P^2}{2B}\,\frac{dC}{da} \tag{25}$$

Elastic compliance in the case of generalized plane stress can be normalized by thickness and elastic modulus, and the functional dependence upon relative crack depth (a/W) can be experimentally evaluated, to provide:

$$C\,E\,B = f\,(a/W) \tag{26}$$

Combination of Equations 25 and 26 results in

$$K^2 = E\,G = \frac{1}{2}\left(\frac{P}{B}\right)^2 \frac{1}{W}\,\frac{d\,(C\,E\,B)}{d\,(a/W)} \tag{27}$$

This provides a method for relating the stress intensity factor directly to the applied load when the compliance behavior of the particular geometry has been experimentally determined.

It should be noted that the above relationship was developed using the plane stress equivalency relationship between K and G (Equation 23), and that the correction factor, $(1 - \nu^2)$, should be employed for plane strain calculations of stress intensity. However, it is also necessary to note that this correction factor has not been incorporated into the published standard for measuring plane strain fracture toughness (Reference 17).

Crack Tip Plasticity Adjustments

The preceding analyses of K and G used linear theory of elasticity to obtain the results. The use of elasticity in characterizing crack extension does not preclude the possibility of the presence of some plasticity in the material's resistance to crack extension. That is, a small amount of plasticity at a crack tip does not disturb the usefulness of elasticity in determining the general redistribution of forces in a body due to the presence of a crack. To ensure that the plastic zone accompanying a crack tip is small, it is relevant to develop a means of estimating its size.

As a first estimate, the elastic stress field equations for a crack tip may be regarded as a reasonable approximation of the stresses outside the boundary of the zone of plasticity. In such a case, the stress in the elastic region will approach the conditions for yielding as the elastic-plastic boundary is approached. Using distortion energy yield criteria, the distribution of the plane stress and plane strain plastic zone have been described by

$$\frac{r}{r_y} = \cos^2\frac{\theta}{2}\left(1 + 3\sin^2\frac{\theta}{2}\right) \text{(plane stress)} \tag{28}$$

and

$$\frac{r}{r_y} = \cos^2\frac{\theta}{2}\left((1 - 2\nu)^2 + 3\sin^2\frac{\theta}{2}\right) \text{(plane strain)} \tag{29}$$

where

$$r_y = \frac{1}{2\pi}\left(\frac{K}{\sigma_{ys}}\right)^2 \text{ from } \sigma_y = \sigma_{ys} = \frac{K}{\sqrt{2\pi r_y}} \tag{30}$$

from the plane stress solution it can be noted that r_y is the distance, r, from the origin (the apparent crack tip location) to the elastic-plastic boundary, directly ahead of the crack ($\theta = 0$). Therefore, it is termed the plane stress plastic zone radius. The extent of plasticity predicted for plane strain is considerably less than for plane stress since the constraint will promote triaxiality of stresses and will inhibit yielding.

The origin of the coordinates r and θ is not truly the crack tip itself. The plasticity of the crack tip causes the elastic portion of the specimen to respond as if the crack were slightly longer than it really is. Thus, the effective crack tip is somewhere within the plastic zone; and from results of Mode III plastic zone analysis, it is located about one plastic zone radius ahead of the actual crack tip, or

$$a_{effective} = a_{actual} + r_y \tag{31}$$

where

$$r_y = \frac{1}{2\pi}\left(\frac{K}{\sigma_{ys}}\right)^2 \quad \text{(plane stress)} \tag{32}$$

and

$$r_y = \frac{(1-2\nu)^2}{2}\left(\frac{K}{\sigma_{ys}}\right)^2 \quad \text{(plane strain)} \tag{33}$$

Several other estimates are available which are closely related to the above equations (Reference 18). One popular estimate for plane strain plastic zone radius is

$$r_y = \frac{1}{6\pi}\left(\frac{K}{\sigma_{ys}}\right)^2 \tag{34}$$

Irwin (Reference 19) estimates the plastic zone radius associated with a surface crack by

$$r_y = \frac{1}{4\sqrt{2}\pi}\left(\frac{K}{\sigma_{ys}}\right)^2 \tag{35}$$

Plasticity at the crack tip causes some redistribution of stresses to maintain equilibrium and therefore the full width of the plastic zone, r_p, is estimated at just twice the above results (i.e., $r_p = 2r_y$). It is emphasized that the zone size results are merely estimates since work-hardening, large strains, and other obvious influences are ignored.

For valid measurement of plane strain fracture toughness, one criterion within the specification (Reference 17) is that the thickness, B, (and certain other planar dimensions) of the test specimen be sufficient such that

$$B \geq 2.5\left(\frac{K_{Ic}}{\sigma_{ys}}\right)^2 \tag{36}$$

which is approximately 50 times the plane strain plastic zone radius. This relationship was developed empirically and is subject to change.

The above estimates of plastic zone size are by no means inclusive. Many similar relationships can be found in the literature which are formulated either by analytical methods (References 20, 21, 22) or physical measurements of plastic zone dimensions (Reference 23).

Three-Dimensional Considerations

Since the majority of naturally occurring defects in aircraft structures are present in the form of cracks from holes and surface flaws (Reference 24), the need for accurate stress intensity solutions for such crack geometrics is readily apparent. These solutions require three-dimensional analysis of the stress fields under consideration and the resulting increase in computational difficulty when compared to the two-dimensional cases is often a limiting factor in the development of functional solutions.

Using a method employing Fourier transforms, Sneddon (Reference 25) treated the case of a circular disk crack of radius, a, in an infinite solid subjected to uniform tension, σ, normal to the cracked plane. His results for crack tip stress field expansions lead to

$$K_I = 2\sigma\left(\frac{a}{\pi}\right)^{1/2}; \quad K_{II} = K_{III} = 0 \tag{37}$$

The analysis of stresses near ellipsoidal cavities in infinite bodies subjected to tension has been discussed by Sadowsky (Reference 26) and Green (Reference 27). However, difficulties arise in their results when the stresses are computed near the crack edge and when the ellipsoid is degenerated into a crack. Subsequently Irwin (Reference 28) calculated the stress intensity factor at any location on the crack border, described by the angle, β, by comparing Green's results for displacements with the stress field equations from Figure 1-5. Referring to Figure 1-7, the formulas obtained are

$$K_I = \frac{\sigma(\pi a)^{1/2}}{\phi}\left(\sin^2\beta + \frac{a^2}{b^2}\cos^2\beta\right)^{1/4} \tag{38}$$

when

$$\phi = \int_0^{\pi/2} \left[1 - \left(\frac{b^2 - a^2}{b^2} \right) \cos^2 \beta \right]^{1/2} d\beta \qquad (39)$$

This analysis has formed the foundation for stress intensity solutions for partially through-the-thickness cracks (surface flaws). Modifications of the Irwin analysis for plasticity and free surface magnification factors have been quite extensive and the resulting applicability to the surface flaw problem is discussed further in Section 2.3.

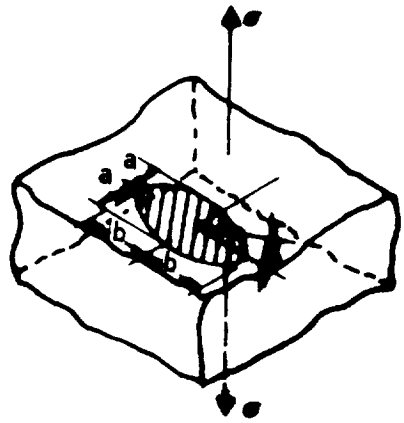

Figure 1-7. An Elliptical Crack in an Infinite Body Subjected to Uniform Tension

Stress-Intensity Solutions

Utilization of linear elastic stress field concepts requires the availability of stress-intensity solutions for particular structural and flaw configurations. It is not within the scope of this contract to catalogue these solutions. Several well-prepared catalogues are currently available (References 1, 29, and 30) which provide approximate or exact solutions to many practical configurations. In many instances, however, it is necessary to estimate solutions, a process which is recommended only for those well versed in the field of applied mechanics.

Combined In-Plane Loading

The effect of combined in-plane loading (Mode I and Mode II) has not received as much attention as many other aspects of fracture mechanics. This is primarily because it is recognized that under cyclic loading cracks tend to grow perpendicular to the direction of maximum tensile loading and

in a manner such that the local crack tip stress field, after sufficient growth, corresponds to a Mode I (tensile) stress distribution. Thus, it can be anticipated that fatigue cracks will always be aligned perpendicular to the principal direction of loading and that cracks from sources other than fatigue will align themselves in a similar manner after a few cycles of loading. This line of thinking is supported by the fact that analysis of structural failures, where existing cracks have been identified as the source, has usually indicated that the load which caused the failure was perpendicular to the existing crack. However, in those cases where there is more than one primary loading direction, a capability of predicting the failure of cracks under combined Mode I and Mode II is still desirable.

An additional reason for the minimum of work performed is the lack of stress intensity solutions for branched crack problems. Although solutions have been reported in the literature (Reference 31), they have subsequently been shown to be incorrect. The branched crack problem is important since cracks under combined Mode I and Mode II loadings do not propagate along the original crack line. This was clearly demonstrated by Erdogan and Sih in their paper of 1963 (Reference 32). See Figure 1-8.

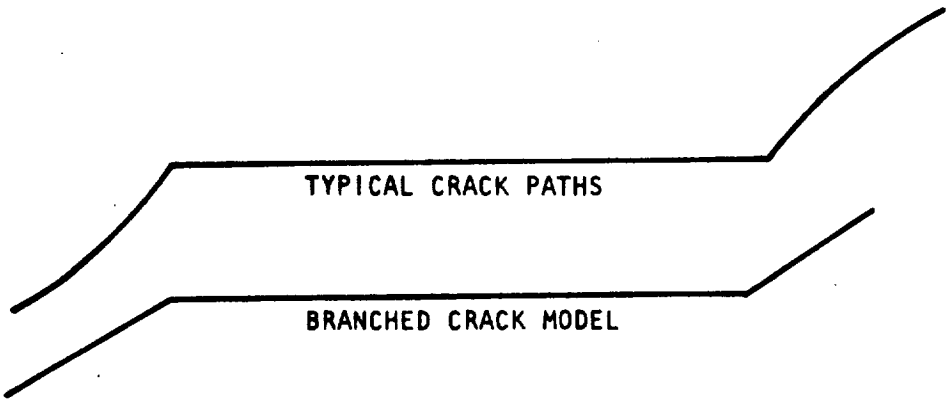

Figure 1-8. Branched Cracks

There they postulated that crack growth proceeded along a line going through the crack tip and perpendicular to the line of maximum local circumferential stress. Since the circumferential stress near the crack tip is a function of K_I and K_{II}, it is a simple matter to find the value θ, which makes the circumferential stress a maximum for various values of K_I and K_{II}. This value of θ is the direction of crack growth. The governing equation is

$$K_I \sin \theta + K_{II} (3 \cos \theta - 1) = 0 \qquad (40)$$

Note that θ varies from 0 degrees for pure Mode I to 70.5 degrees for pure Mode II. These predictions were confirmed by tests on plexiglass sheet. It should be noted here that because stress intensity factors are not available for the branched crack problem, strain energy release rates for combined loading are not available either. Although the literature contains expressions for the Mode II strain energy release rate (K^2_{II}/E for plane stress), these expressions assume crack growth along the line of the crack and hence do not conform to physical reality. Although the initial crack growth under combined loading is predictable, the capability of predicting the loads at which crack growth occurs is not as well established.

A fact that has not been brought out in the literature is that once a straight crack under combined loading grows, the stress field that the branched crack immediately sees is pure Mode I. This can be shown analytically by noting that the line of local maximum tangential stress along which the crack grows is a principal stress direction and hence has zero shear; thus, the stresses that are relieved as the crack grows are purely tensile stresses perpendicular to the current crack line and produce a tensile singularity only. Additionally, the fact, that after initial branching, crack paths are continuous, is evidence that only Mode I stress distributions are present. If Mode II stress distributions were present at any subsequent position, branching and corners could be observed. Thus, it can be seen that for materials where slow stable growth occurs, stress intensity factors for the branched crack problem in conjunction with resistance curve concepts may, in the future, enable more rational predictions to be made.

As stated above, capability is not currently available for predicting from basic Mode I failure data, the loads at which failure occurs when Mode II stress intensity factors are present. Present alternatives require testing under combined loading conditions. A common method of indicating the interaction of Mode I and Mode II loading is a plot of $\frac{K_I}{K_{Ic}}$ versus $\frac{K_{II}}{K_{IIc}}$ at failure. K_{Ic} and K_{IIc} are the critical stress intensities based on maximum load and initial crack length for pure Mode I and pure Mode II, respectively. All of the available data on aluminum alloys have been plotted in this manner by Liu (Reference 33) and are shown in Figure 1-9. There is a reasonably wide range of material behavior presented. Part of this disparity may be attributed to the fact that Liu used a shear panel test whereas all the other tests were conducted on center-cracked tensile panels. The test configurations and stress intensities are given in Figure 1-10. Note that non-zero pure Mode II cannot be achieved in the tensile test. The values of K_{IIc} used in constructing Figure 1-9 are extrapolated in those cases. Although there were differences in K_{Ic} and K_{IIc} in all these tests, the variation was always less than 20% and no real trends are apparent. Thus on the basis of these

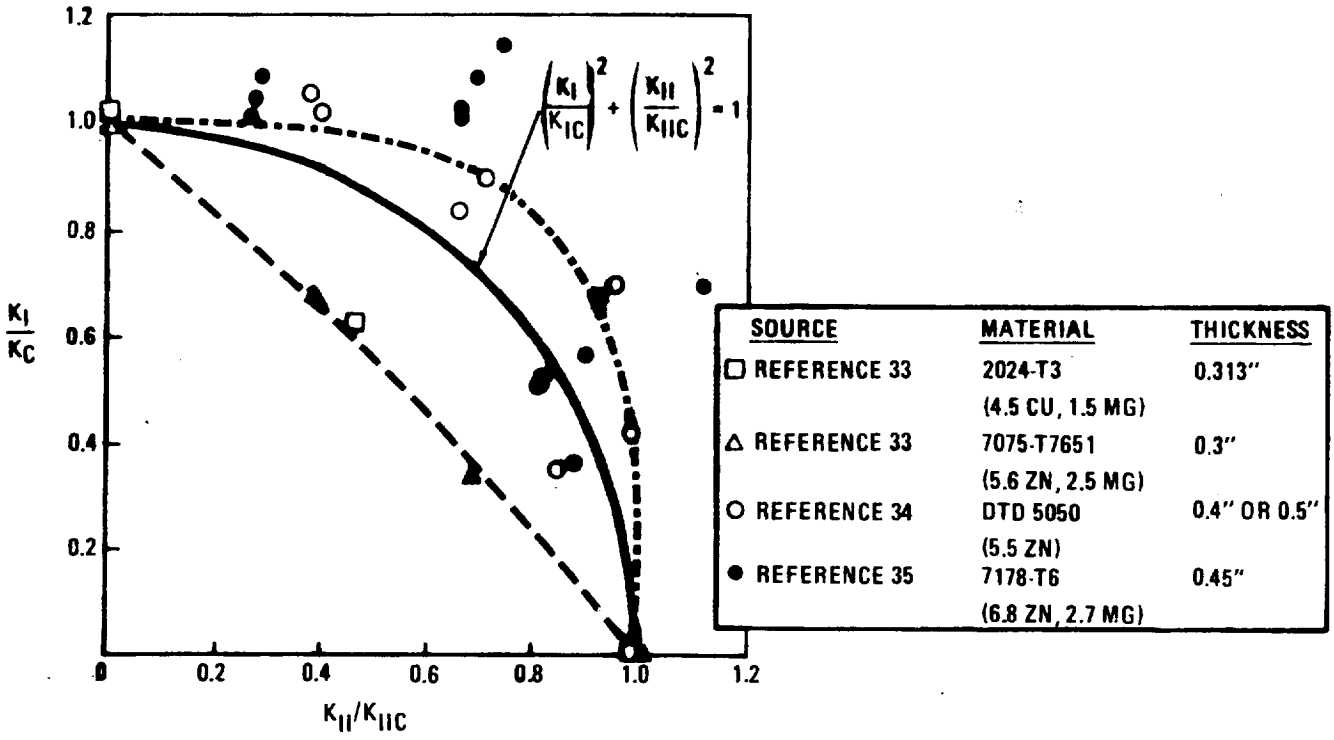

Figure 1-9. Mode I - Mode II Interactions

limited tests, the assumption that $K_{IIc} = K_{Ic}$ is probably reasonable in light of our current prediction capability. It seems that a straight line extending from K_{Ic} to K_{IIc} represented by the equation:

$$\left(\frac{K_I}{K_{Ic}}\right) + \left(\frac{K_{II}}{K_{IIc}}\right) = 1 \tag{41}$$

would be a conservative estimate of an interaction curve to be used in design. Liu indicates that a quadratic form of the interaction curve goes through the

$$\left(\frac{K_I}{K_{Ic}}\right)^2 + \left(\frac{K_{II}}{K_{IIc}}\right)^2 = 1 \tag{42}$$

midrange of the data he considered.

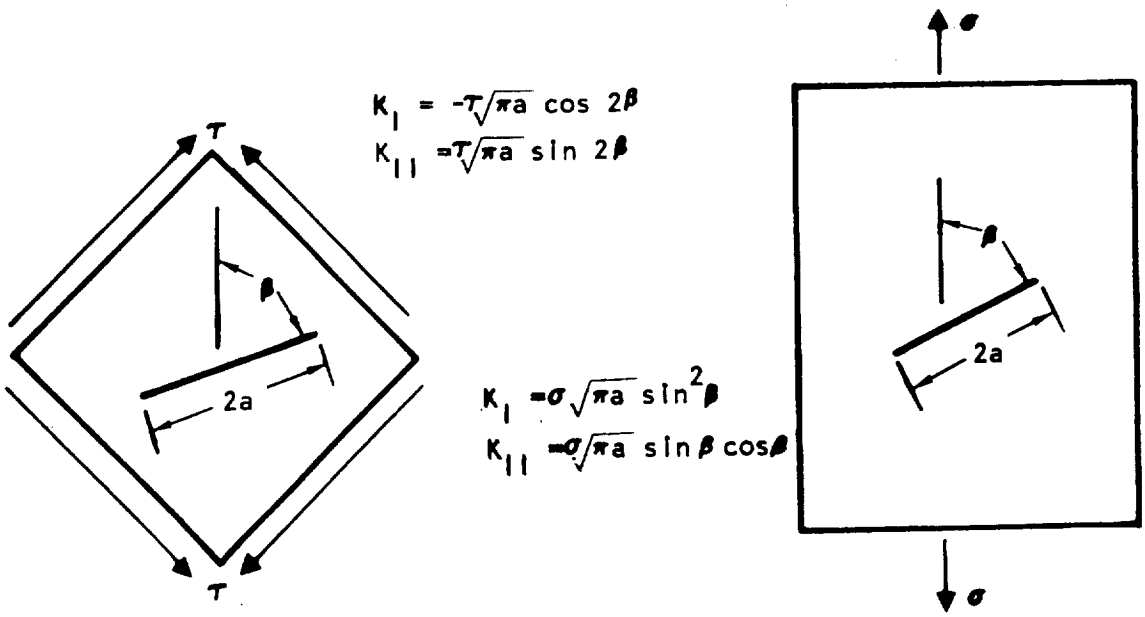

Figure 1-10. Combined Loading Test Configurations

Recently Sih (Reference 36) has introduced an analysis technique based on the energy density in the immediate path of the crack tip. He refers to this as the S_c method. Crack growth supposedly occurs when a quantity S reaches a critical value S_c. S is a function of the applied stress intensity factors, the angle of growth and basic material properties. The angle of growth according to this theory is not only a function of the relative amounts of Modes I and II, but is also a function of Poisson's ratio and the degree of constraint (plane stress versus plane strain) as well. Thus the Mode I and Mode II interaction curve varies with material and constraint condition. For normal values of Poisson's ratio, however, the variations in the interaction are much smaller than present accuracy in the testing of metals under combined loads. In fact the difference between this interaction curve and Equation 42 is less than experimental accuracy at this time. There appears to be no reason to utilize an unproved, unnecessary complication of this type.

1.3 MULTIPLE-PARAMETER APPROACHES

When a particular stress intensity solution, dependent only upon flaw size and applied stress, fails to consolidate test data into a single value of

fracture toughness, alternate solutions are often pursued. For example, Newman (Reference 37) uses Neuber's notch factor relationship (Reference 4), to derive a relation between the linear elastic stress intensity factor, the applied stress and three "material" parameters. For the case of the surface flaw, the Neuber equation was generalized for an elliptical crack in a three-dimensional solid. The two-parameter fracture criterion for cracked plates was given by

$$K_f = \frac{K_{IE}}{1 - m\left(\frac{\sigma_n}{\sigma_u}\right)} \tag{45}$$

where K_{IE} is the linear elastic stress intensity factor for cracked plates subjected to uniform remote loading. σ_n and σ_u are the applied net stress and the material's ultimate strength, respectively. The parameters K_f and m are then "material constants" evaluated by least squares methods from test data. These parameters are constant in the same limited sense as the ultimate tensile strength; that is, the parameters vary with material thickness, state of stress, temperature, and rate of loading.

For values of m near zero, K_f is equivalent to K_{IE}, and the equation would be applicable to brittle materials. If m equals unity, the equation is similar to that obtained by Kuhn (Reference 38) and is applicable to ductile materials. Unfortunately, the apparent lack of applicability of such an approach to characterization of precritical flaw growth behavior will severely limit its desirability as an engineering tool.

Bockrath et al. (Reference 39) have offered an expression for evaluating ductile fracture which contains parameters that are determinable from the uniaxial stress strain curve. For a thin section containing a through-the-thickness crack of half-length, a, the expression is

$$\sigma(a)^{\frac{1}{2+\omega}} = \sigma_u (a_u)^{\frac{1}{2+\omega}} = K_{T_c} = \text{constant} \tag{46}$$

where K_{T_c} is the toughness associated with the through-crack, σ is the applied stress, and σ_u is again the material's ultimate strength. The quantities a_u and ω are the two parameters that are required to compute toughness and may be determined either by fracture tests or from a uniaxial stress-strain curve.

For the surface flaw, the expression is

$$\sigma(\lambda a)^{\frac{1}{2+\omega}} = \sigma_u (\lambda a_u)^{\frac{1}{2+\omega}} = K_{PTc} \tag{47}$$

for which the quantity λa is equivalent to the more familiar value a/ϕ^2 for significant values of flaw aspect ratio (a/2c). This theory is said to be applicable in stress regions above and below a material's yield strength. Additionally, cyclic flaw growth rates (da/dN) are also proposed to be evaluated by an expression of the form

$$\frac{da}{dN} = D\sigma^m (a^s) \text{ for a through-crack} \tag{48}$$

and

$$\frac{d(\lambda a)}{dN} = D\sigma^m (\lambda a)^s \text{ for a surface flaw} \tag{49}$$

where D, m and s are experimentally determined from test data.

Although increasing the number of "material parameters" will usually provide for improved representation of fracture data, the added complexity is sometimes self-defeating in the pursuit of a viable, economical test method and predictive analysis procedure.

1.4 J-INTEGRAL APPROACH

The stress intensity factor approach to fracture analysis encounters its major difficulty when attempting to evaluate non-linear (elastic-plastic) behavior in the vicinity of a crack tip. An alternate failure criterion has been formulated by Begley and Landes (Reference 40) whereby a single parameter, in the form of the path independent J-integral, is employed to characterize fracture behavior.

Referring to Figure 1-11, the J-integral is defined for two-dimensional problems and is given by

$$J = \int_r W\,dy - \vec{T} \cdot \frac{\partial \vec{u}}{\partial x}\,ds \tag{50}$$

where W is the strain energy density as defined by

$$W = \omega(x, y) = \omega(\epsilon_{mn}) = \int_{o}^{\epsilon_{mn}} \sigma_{ij} \cdot d\epsilon_{ij} \tag{51}$$

and r is any contour surrounding the crack tip. $\vec{T}$ is the traction vector defined according to the outward normal along r, or

$$\vec{T}_i = \sigma_{ij}\, n_j \tag{52}$$

$\vec{u}$ is the displacement vector and ds is an element of the arc along r.

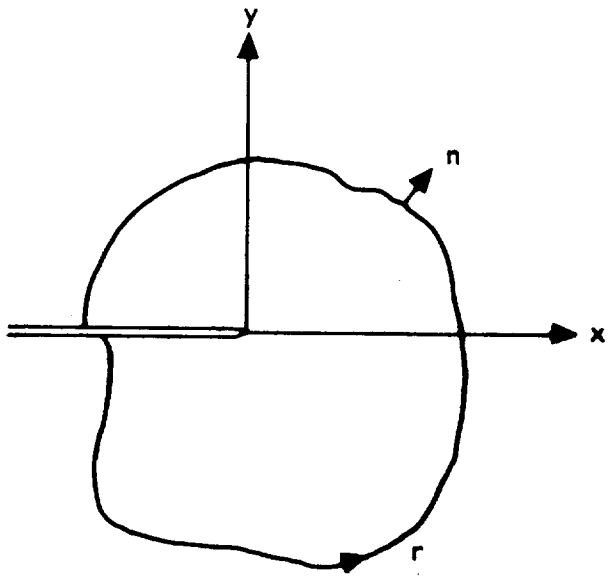

Figure 1-11. Crack Tip Coordinate Orientation and Arbitrary Line Integral Contour (Reference 41)

For any elastic or elastic-plastic material treated by deformation theory of plasticity, Rice (Reference 42) has proven path independence of the J-integral.

Additionally, Rice has shown that the J-integral may be interpreted as the potential energy difference between two identically loaded bodies having neighboring crack sizes a and a + da. This is stated mathematically as

$$J = \frac{-d\,(U/B)}{da} \tag{53}$$

where U/B is the potential energy normalized per unit thickness B and defined by

$$U/B = \iint_A W\,dx\,dy - \int_{r_t} \vec{T} \cdot \vec{U}\,ds \tag{54}$$

where the first term is the integrated strain energy density or simply the work done on the body in loading to a given condition. In the second term, r_t refers to that portion of the boundary over which stresses are prescribed as boundary conditions.

In analogy with the linear elastic fracture mechanics interpretation of the energy release rate, the area between two monotonic load-deflection curves for the neighboring crack sizes is $JB \cdot \Delta a$. The interpretation is illustrated in Figure 1-12 and suggests procedures for calculating J.

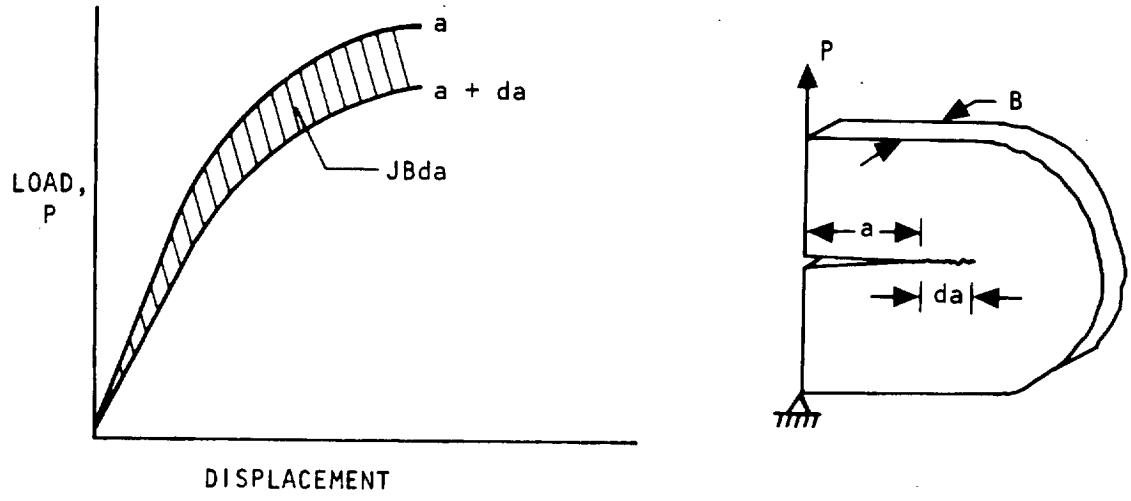

Figure 1-12. Interpretation of J-Integral (Reference 41)

Because J is a function of crack length and displacement, a critical value of J for crack initiation, J_{Ic}, can be determined through measurement of a critical value of displacement. However, defining crack initiation and determining its onset are perhaps the most difficult part of measuring J_{Ic}. Procedures for estimating the value of the J-integral are presented by Bucci et al. in Reference 41.

For the case of small-scale yielding or linear-elastic behavior, the J-integral is identical to G, the energy release rate per unit crack extension.

Therefore, a J failure criterion for the linear elastic case is identical to the K_{Ic} failure criterion in that

$$J_{Ic} = G_{Ic} = \frac{1 - \nu^2}{E} K_{Ic}^2 \tag{55}$$

It remains, however, an open question as to the suitability of such a one-parameter characterization in conditions of large-scale yielding.

The actual role of the J-integral approach as a failure criteria applicable to the Space Shuttle is naturally dependent upon the amount of development effort applied toward eliminating difficulties associated with displacement measurements and to extending applicability of the concept to stable crack extension and general yielding conditions.

REFERENCES

1. Paris, P.C. and Sih, G.C., "Stress Analysis of Cracks," Fracture Toughness Testing and its Applications, Special Technical Publication No. 381, ASTM, p. 51 (1965).

2. Wilhem, D.P. Fracture Mechanics Guidelines for Aircraft Structural Applications. Air Force Flight Dynamics Laboratory, Wright-Patterson AFB, Ohio, Technical Report AFFDL-TR-69-111 (February 1970).

3. Wessel, E.T., Clark, W.G. Jr., and Wilson, W.K., Engineering Methods for the Design and Selection of Materials Against Fracture. Westinghouse Research Laboratories, Final Technical Report TR-A0-801005 (June 1966).

4. Neuber, H., "Theory of Stress Concentration for Shear-Strained Prismatical Bodies with Arbitrary Nonlinear Stress-Strain Law." Transactions of ASME, Series E, Journal of Applied Mechanics, Volume 28, No. 4 pp. 544-550 (December 1961).

5. Neuber, H., "Fracture Mechanics," Structural Mechanics, New York, Pergamon Press (1960).

6. Kuhn, P., The Prediction of Notch and Crack Strength Under Static and Fatigue Loading, presented to the SAE-ASME meeting, New York, N.Y. (April 1964).

7. Kuhn, P., and Figge, I.E., Unified Notch Strength Analysis for Wrought Aluminum Alloys, NASA TN D-1259 (1962).

8. Griffith, A.A., "The Phenomena of Rupture and Flow in Solids," Transactions, Royal Society of London, Vol. 221 (1920).

9. Inglis, C.E., "Stresses in a Plate Due to the Presence of Cracks and Sharp Corners," Proceedings, Institute of Naval Architects, Volume 60 (1913).

10. Orowan, E., "Fundamentals of Brittle Behavior of Metals," Fatigue and Fracture of Metals, New York: John Wiley and Sons, Inc. (1952).

11. Irwin, G.R., "Analysis of Stresses and Strains Near the End of a Crack Transversing a Plate," Transactions of ASME Journal of Applied Mechanics (1957).

12. Irwin, G.R., "Fracture Mechanics," Structural Mechanics, New York: Pergamon Press (1960).

13. Westergaard, H. M., "Bearing Pressures and Cracks," Transactions of ASME Journal of Applied Mechanics (1939).

14. Paris, P. C., Stress-Intensity-Factors by Dimensional Analysis, Lehigh University Institute of Research Report (1961).

15. Irwin, G.R., and Kies, J.A., "Critical Energy Rate Analysis of Fracture Strength," Welding Journal (Research Supplement) (1954).

16. Irwin, G.R. and Kies, J.A., "Fracturing and Fracture Dynamics," Welding Journal (Research Supplement) pp. 95 S-100S (1952).

17. Tentative Method of Test for Plane Strain Fracture Toughness of Metallic Materials. ASTM E 399-70T, Annual Book of ASTM Standards, Part 31, pp. 919-935 (1971).

18. McClintock, F.A., and Irwin, G.R., "Plasticity Aspects of Fracture Mechanics," Fracture Toughness Testing and its Applications, ASTM STP 381, p. 84 (1965).

19. Irwin, G.R., "Plastic Zone Near a Crack and Fracture Toughness," Seventh Sagamore Ordnance Materials Research Conference (August 1960).

20. Bilby, B.A., and Swinden, K.H., "Representation of Plasticity at Notches by Linear Dislocation Arrays," Proceedings of the Royal Society (London), Series A, Vol. 285, pp. 22-23 (1965).

21. Rice, J.R., "Mathematical Analysis in the Mechanics of Fracture," Fracture, Vol. 2; Mathematical Fundamentals, New York: Academic Press Inc., pp. 191-311 (1969).

22. Keer, L.M., and Mura, T. "Stationary Crack and Continuous Distributions of Dislocations," Proceedings of the First International Conference on Fracture, Sendai, Japanese Society for Strength and Fracture of Materials, Vol. 1, pp. 99-116 (1965).

23. Francis, P.H., and Davidson D. L., "Experimental Characterization of Yield Induced by Surface Flaws," The Surface Crack: Physical Problems and Computational Solutions, ASME, pp. 63-78 (1972).

24. Little, C.D., and Bunting, P.M., "The Surface Flaw in Aircraft Structures and Related Fracture Mechanics Analysis Problems," The Surface Crack: Physical Problems and Computational Solutions, ASME, pp. 11-42 (1972).

25. Sneddon, I.N., "The Distribution of Stress in the Neighborhood of a Crack in an Elastic Solid," Proceedings, Royal Society, London, Vol. A-187 (1946).

26. Sadowsky, M.A., and Sternberg, E.G., "Stress Concentration Around A Triaxial Ellipsoidal Cavity," Transactions, ASME, Journal of Applied Mechanics (1949).

27. Green, A.E., and Sneddon, I.N., "The Stress Distribution in the Neighborhood of a Flat Elliptical Crack in an Elastic Solid," Proceedings, Cambridge Philosophical Soc., Vol. 46 (1950).

28. Irwin, G.R., "The Crack Extension Force for a Part-Through Crack in a Plate," Transactions, ASME, Journal of Applied Mechanics (1962).

29. Tada, H., Paris, D.C., and Irwin, G.R. Stress Analysis of Cracks Handbook. Hellerstown, Pa.: Del Research Corp. (1973).

30. Sih, G.C., Handbook of Stress Intensity Factors for Researchers and Engineers, Institute of Fracture and Solid Mechanics, Lehigh University, Bethlehem, Pennsylvania (1973).

31. Anderson, A., "Stress-Intensity Factors at the Tips of a Star Shaped Contour in an Infinite Tensile Sheet," Journal of the Mechanics and Physics of Solids, Vol. 17 pp. 405 to 417 (1969).

32. Erdogan, F., and Sih, G.C., "On the Crack Extension in Plates Under Plane Loading and Transverse Shear," Journal of Basic Engineering (December 1963).

33. Liu, A.F., Crack Growth and Failure of Aluminum Plate Under In-Plane Shear, Presented at the AIAA 11th Aerospace Sciences Meeting, Washington, D.C. (January 1973).

34. Pook, L.P., "The Effect of Crack Angle on Fracture Toughness," Engineering Fracture Mechanics, Vol. III, No. 3 (October 1971).

35. Wilson, W.K., Clark, W.G. Jr., and Wessel, E.T., Fracture Mechanics For Combined Loadings and Low to Intermediate Strength Metals, Technical Report No. 10276, TACOM (Vehicular Components and Materials Lab. U.S. Army, Tank Automotive Command, Warren, Michigan) (November 1968).

36. Sih, G. C., Some Basic Problems in Fracture Mechanics and New Concepts, Presented at the Symposium on Fracture and Fatigue, Washington, D.C. (May 1972).

37. Newman, J.C. Jr., Fracture Analysis of Surface and Through-Cracked Sheets and Plates, NASA Langley Research Center, Hampton, Virginia, Presented at the Symposium on Fracture and Fatigue, Washington, D. C. (May 1972).

38. Kuhn, P., Residual Tensile Strength in the Presence of Through Cracks or Surface Cracks," NASA TN D-5432 (1970).

39. Bockrath, G.E., Glassco, J.B., and Wysocki, E.V., Fracture Control of Ductile Fracture, MDAC Paper WD 2075, Presented to WESTEC Conference, ASM, Los Angeles, California (March 1973).

40. Begley, J.A., and Landes, J.D., "The J-Integral as a Fracture Criterion," Fracture Toughness, Proceedings of the 1971 National Symposium on Fracture Mechanics, Part II, ASTM STP 514, pp. 1-20 (1972).

41. Bucci, R.J., Paris, P.C., Landes, J.D., and Rice, J.R., "J-Integral Estimation Procedures," Fracture Toughness, Proceedings of the 1971 National Symposium on Fracture Mechanics, Part II, ASTM STP 514, pp. 40-69 (1972).

42. Rice, J.R., "A Path Independent Integral and the Approximate Analysis of Strain Concentration by Cracks and Notches," Transactions, ASME Journal of Applied Mechanics, Vol. 35, pp. 379-386 (1968).

2.0 FRACTURE TOUGHNESS

2.0 FRACTURE TOUGHNESS

In recent years, much emphasis has been placed upon characterization of the material property called "fracture toughness." Generically, fracture toughness is represented by the minimum crack tip stress intensity that will initiate unstable crack growth. Ideally, when armed with an accurate measure of both flaw size and fracture toughness, the investigator can calculate the residual strength of a structure with the aid of an appropriate stress intensity solution. However, owing to the fact that real engineering materials do not behave in a purely elastic manner on fracturing, the analysis must be modified to take into account the finite sizes of structural members and the presence of crack tip plasticity. As a result, the application of fracture toughness as an oversimplified panacea for prevention of fracture problems must be avoided, and its actual role in the design of fracture critical hardware must be specifically defined.

In the rush to quantify fracture toughness for real engineering materials, the presence of a strong thickness dependency soon became evident. The effect is illustrated by the data shown in Figure 2-1. The fact that the measured critical stress intensity factor, K_c, decreases markedly with increasing thickness challenges the concept that fracture toughness is an intrinsic

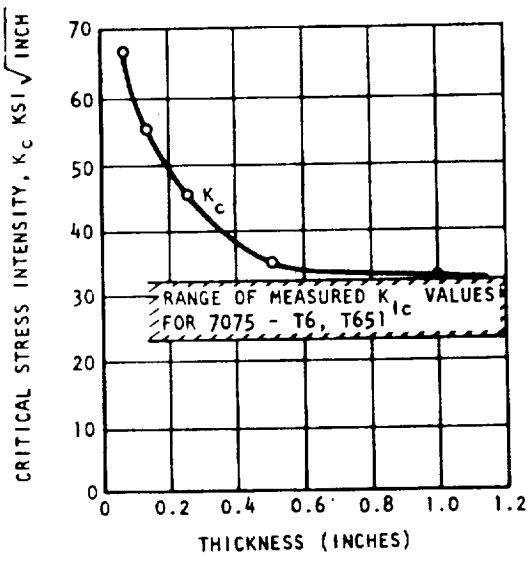

Figure 2-1. Thickness Effect Upon the Measured Critical Stress Intensity an of Aluminum Alloy

material property. Further investigation had led to the conclusion that stress state (plane strain or plane stress) is a primary contributing factor. When the material thickness is sufficient to produce nearly total plane strain conditions in the vicinity of the crack, the resulting (lower bound) critical stress intensity is referred to as plane strain fracture toughness, K_{Ic}. When the local stress state becomes significantly mixed (plane strain and plane stress), the value of the resulting critical stress intensity appears to be a function of the degree of stress-state mixing. The magnitude of the increase in apparent toughness with decreasing thickness may also be enhanced by phenomenological differences associated with measurements of plane-strain versus plane-stress critical stress intensities. Under plane-strain conditions, K_{Ic} is based on the lowest load at which significant measurable extension of the crack occurs. On the other hand, K_c testing will often acknowledge that some crack extension will occur before instability, and consequently relates fracture to the maximum achieved load and to the crack length at instability. The compounding influence of both stress state and flow measurement discrepancies requires considerable attention when the attempt is made to use "toughness" numbers in an analysis.

In the following paragraphs, those fundamental fracture mechanics concepts which are intended to evaluate the load carrying ability of a flawed structure are evaluated. The significance and applicability of plane strain fracture toughness as a material property are examined. Approaches for characterizing thin sheet fracture behavior are presented, and analysis methods and behavioral characteristics associated with the surface flaw are reviewed.

2.1 PLANE STRAIN FRACTURE TOUGHNESS, K_{Ic}

It is anticipated that much of the fracture analysis on Space Shuttle hardware will consider non-plane-strain stress states. However, because of the general popularity of K_{Ic} as a material property, in addition to a few plane strain application requirements, significant K_{Ic} testing and analysis will undoubtedly be performed. Therefore, the following paragraphs are presented to define K_{Ic} and its relationship with other material properties, and to identify the limits of applicability in Space Shuttle analysis.

K_{Ic} Testing

As a result of the activity of the ASTM committee on fracture toughness (ASTM Committee E-24), plane strain fracture toughness, K_{Ic}, has been explicitly defined. Specification ASTM E399-72 identifies a standard method for measuring fracture toughness as a basic material property. Test procedures, specimen size, and material behavior must meet several specific requirements to ensure that plane-strain conditions, free from excessive

plasticity will prevail. As a welcome result of the ASTM effort, plane-strain fracture toughness is redefined as that material property which, when measured in accordance with the requirements of Specification ASTM E-399-72, meets all the criteria specified therein. If any test result fails to meet all the specification criteria, this apparent fracture toughness (termed K_Q) should not be cataloged, disseminated, or evaluated as K_{Ic}.

Historically, a variety of specimens have been considered for determining K_{Ic}, the first perhaps being the notched round specimen (Figure 2-2a); however, the large amount of material and large testing machines required for this type of test and difficulties associated with instrumentation initially discouraged its wide use. Center-cracked-tension (CCT) specimens (Figure 2-2b) were also used, but again, material and testing system problems governed, and attention was soon focused on what commonly is called the single-edge-notch (SEN) tension specimen (Figure 2-2c). Greater testing experience soon led to the observation that even the use of SEN tension specimens for relatively tough materials resulted in problems in loading capacity and gripping. The immediate solution to the problem was simply to rotate the plane of the specimen 90 degrees and conduct a bend test. Events at the crack tip were identified, and the differing stress gradient were accounted for in the equations for calculating stress intensity. As a result, the notch bend specimen (Figure 2-3a) was incorporated into the ASTM test standard for fracture toughness measurements.

Results from independent research on the fracture toughness of nuclear vessel materials (Reference 2) led to the conclusion that a compact (CT) specimen (Figure 2-3b) provided a more efficient use of material than the notched bend specimen. Attention was then focused on the development of the details of the test procedure with this particular specimen, and Specification ASTM E-399-72 was expanded to incorporate the compact tension as well as the notch bend specimen.

In this test method, measurement of K_{Ic} is based on the lowest load at which significant measurable extension of the crack occurs. Significant measurable extension is measured in terms of a specified deviation from linearity of a load versus crack-opening-displacement test record. In some instances, this may coincide with the maximum load, but frequently the specimen will sustain a higher load than that at which significant crack extension occurs. The procedure involves bend or tension testing of notched specimens which have been precracked in fatigue. Load versus crack-opening-displacement is recorded autographically. Testing may be done in various machines having suitable load sensing devices for instrumenting to an autographic recorder. A summary of test criteria associated with the compact tension test specimen is presented in Reference 9 and illustrates the exacting detail which the ASTM specification requires to ensure that plane strain fracture toughness, representing a consistent material property, are being measured.

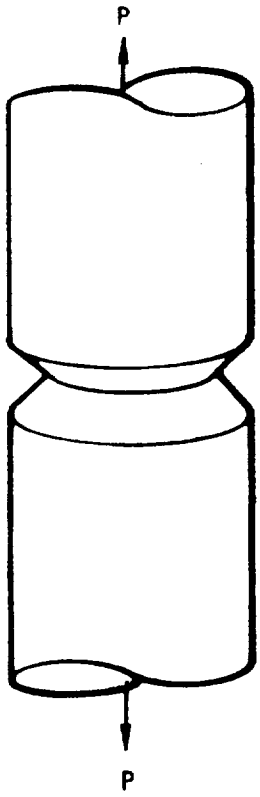

(A) NOTCHED ROUND TENSION SPECIMEN

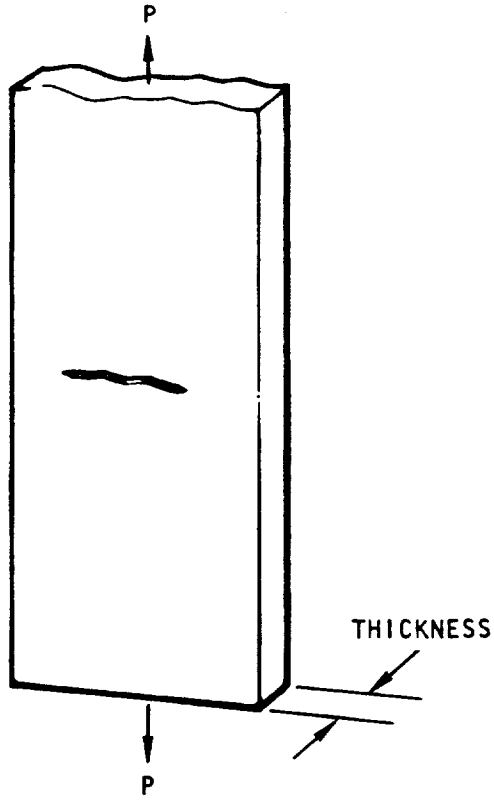

(B) CENTER CRACKED TENSION SPECIMEN

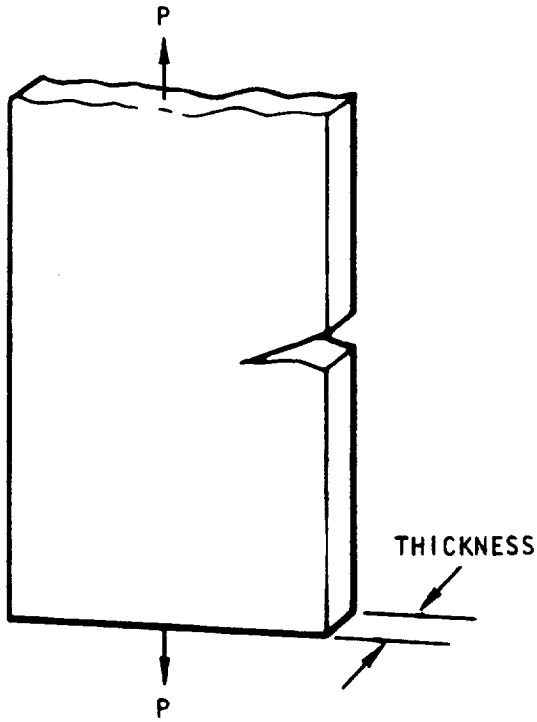

(C) SINGLE-EDGE NOTCH

Figure 2-2. Original Test Specimens for Measuring Fracture Toughness

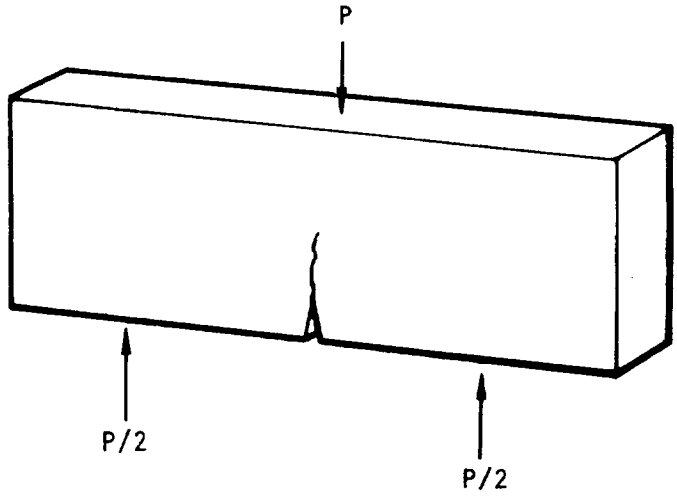

(A) NOTCH BEND SPECIMEN

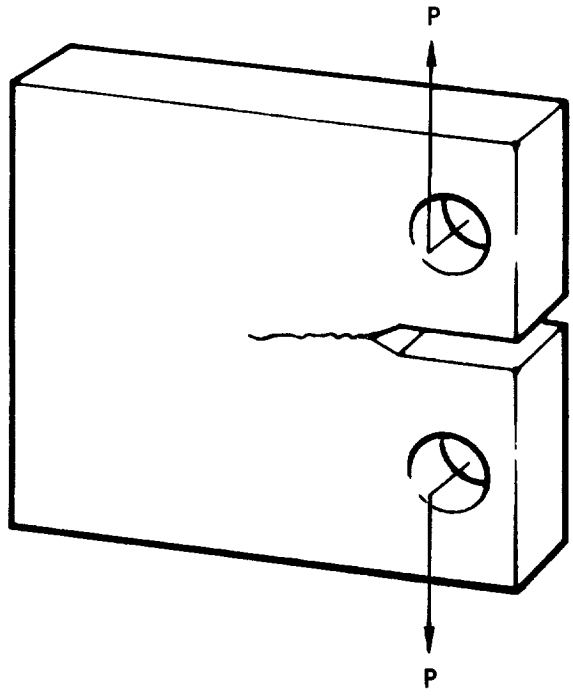

(B) COMPACT SPECIMEN

Figure 2-3. Current Test Specimens Used for Measuring K_{Ic}

Correlation of K_{Ic} With Other Material Properties

Since the numerous "validity" considerations associated with testing for K_{Ic} make it an expensive property to measure, there have been numerous attempts to correlate K_{Ic} values with other, less costly, or more commonly measured, material properties. The best documented of the proposed correlations involve conventional tensile characteristics or the Charpy V-notch impact energy.

Hahn and Rosenfield (Reference 3) have proposed to calculate K_{Ic} from a strain hardening index and other quantities that could be derived from a conventional tension test. A relation proposed by Krafft (References 4 and 5) also involves a strain hardening index as well as a fracture process zone size that would have to be determined by some independent means. However, as discussed by Jones and Brown (Reference 6), a fundamental difficulty with relations involving a strain hardening index is the variety of definitions used for this quantity. No single parameter can characterize strain hardening over a wide range of plastic strains; and as yet, there is no way of knowing what portion of the stress strain curve is of most importance in the fracture process of cracked specimens.

It has been observed for many years that the strength of sharply notched bars of high-strength steels generally increases as the tensile strength decreases. An inverse relation between K_{Ic} and yield strength has been evaluated by several investigators (References 6, 7, and 9) whereby $K_{Ic} \propto 1/(YS)^m$ where the parameter m varies over a significant range. However, while K_{Ic} values generally increase with decreasing yield strength, a simple power relationship between these two quantities is likely to apply only over a limited range of their values. Also, it would be safe to assume that any processing which normally alters the yield strength of a material would also affect K_{Ic}, and additional testing would be required to quantify the difference. As illustrated by Brown and Srawley (Reference 9), correlation of K_{Ic} with other tensile properties such as tensile elongation and reduction in area is virtually nonexistent.

The convenience and economy of the Charpy V-notch test to alloy producers have led to investigations of correlations between Charpy V-notch impact results and K_{Ic} values. While no generally acceptable method has been developed whereby K_{Ic} can be determined from CVN test results, the use of this less expensive test for material control can still be acceptable. When sufficient data are available comparing Charpy V-notch with K_{Ic} for a particular alloy system (and distinct relationship identified), the use of the test for process control testing would be economically prudent. Similarly, recent work at Alcoa Research Laboratories (Reference 10) has demonstrated a correlation between the conventional notch-yield ratio and K_{Ic} for some aluminum alloys, as shown in Figure 2-4. Again, if such test results are

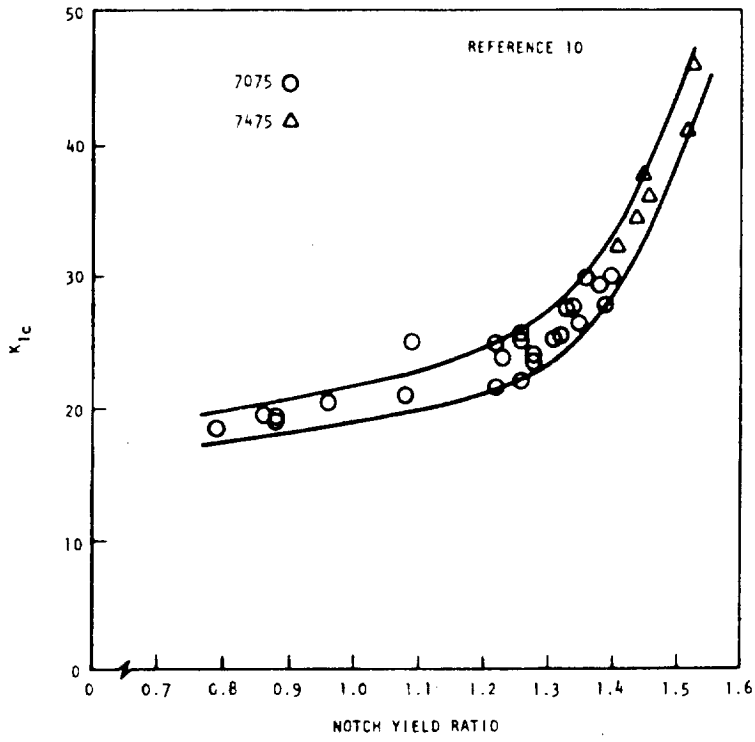

Figure 2-4. Correlation of Notch Yield Ratio With Fracture Toughness of Aluminum

shown to adequately correlate with K_{Ic} for a particular alloy system, the advantages of the testing method for material qualification or product verification cannot be ignored.

Application of Plane Strain Fracture Toughness

It must not be expected that publication of a standard test method will allow immediate incorporation of a minimum level K_{Ic} into material specifications. Actually, after the procedure has been developed, it is necessary to obtain significant quantities of data showing the amount of scatter in the results and the influence of production variation (test direction, product dimension, product heat treatment) on the values, as has been done with tension test specifications. Additionally, it must be noted that the specimen size requirements of the ASTM test method will preclude determination of K_{Ic} for many product forms and service thicknesses, and specification of K_{Ic} for these materials would be meaningless.

Original requirements for fracture toughness measurements resulted from attempts to characterize relatively brittle materials. As a result, the standard test method concentrates on determination of the stress intensity

at which initial extension of a flaw will occur, presuming that fracture is imminent. A natural extension of K_{Ic} measurements to materials with high toughness, in addition to substantially increasing "valid" specimen size requirements, introduces the problem of significant stable crack extension prior to fracture, which increases the difficulty in meeting other specification requirements. Additionally, since actual fracture behavior is no longer being measured, applicability of such data is subject to dispute, and alternate test methods (Reference 11) and analysis techniques are being suggested for these materials.

Material Screening

Contrary to the opinions of many, an invalid value of K_{Ic} (that is, a value determined by a test which does not meet all of the criteria for validity) is not a reliable and useful relative measure of toughness. Therefore, while the temptation to use the invalid values "just for screening" is strong, it may give false information and must be avoided. The reason for this is that there is no way to gauge how far away from the true value for K_{Ic} the invalid number really is, and whether the K_Q is larger or smaller than K_{Ic}. For some materials, an invalid value may be equal to K_{Ic}; for another material, an equally invalid number (that is, invalid for identical reasons) may be far removed from the real value.

Product form often prohibits K_{Ic} measurements by the currently specified test method because of specimen size requirements. In such instances, attempts are often made to obtain an "engineering estimate" of K_{Ic} using subsize specimens (i. e., specimens uniformly decreased in all dimensions from valid specimen size requirements). However, subsize specimens have been demonstrated to be totally without reliability for estimates of K_{Ic} (Reference 6). The applicability of subthickness specimens, however, may often provide a useful approximation to K_{Ic} (References 12 and 13); that is, by following the ASTM test method in all aspects, except the limitation on thickness, an engineering approximation to K_{Ic} can be obtained. However, the proximity of the value to actual K_{Ic} cannot be accurately evaluated, and its applicability in plain stress (K_c) analysis is not known. It must also be emphasized that attempts to estimate K_{Ic} by some empirical method are of dubious value when plane strain failure is not a design consideration.

The Conservative Nature of K_{Ic}

Since the ASTM test method has been structured to ensure that plane strain conditions prevail at the crack tip, the resulting K_{Ic} measurement represents a lower bound critical stress intensity. This lower bound value, therefore, automatically carries with it an aura of conservatism. In most

cases, K_{Ic} will be a truly conservative value; however, the effects of this characteristic must be fully understood to avoid extensive overdesign.

It would not be an uncommon occurrence for the K_{Ic} value of a Space Shuttle material to differ from some design configuration critical stress intensity, K_c, by a factor of two. In such an instance, since critical or initial detectable flaw size varies as the square of the toughness (i. e., a_c, $a_i \alpha (K_c/\sigma_{ys})^2$), the initial flaw size that must be found by some inspection technique may be reduced by 75 percent. Use of K_{Ic} values in such a case, although truly conservative, can impart significant restrictions on cost, weight, material selection, and overall design flexibility. As a result, improper fracture mechanics analysis can easily become self-defeating.

Application of K_{Ic} values can also produce results that are not conservative. In proof test logic, for example, the use of lower bound K_{Ic}, which neglects slow stable flaw growth, can result in a significant underestimate of the maximum size flaw that can survive proof application. Additionally, the subsequent calculation of remaining life may be overestimated, resulting in an analysis that is not conservative (see Section 5).

The use of conservative K_{Ic} data for screening materials not intended for application or analysis under conditions of plane strain may also lead to results that are not conservative. It would not be an unlikely occurrence if the thickness dependency of the critical stress intensity, for two materials, were to behave in a manner illustrated by Figure 2-5. In such an instance, material A might prematurely be considered inferior to material B (with all other variables compensating) because of its lower K_{Ic}. However, if the structural application under consideration dictates thin gauge or a plane stress-influenced stress state (as will often be the case for Space Shuttle material applications), a material choice based on K_{Ic} or K_Q may be entirely inaccurate. Even in the event that the data of Figure 2-5 were available, two questions of considerable importance must be evaluated before a selection could responsibly be made.

1. What test method was used to generate the non-K_{Ic} data (since CT specimen data may not necessarily correspond with notch bend or CCT test results under these mixed stress-state conditions)?

2. Are the numbers readily transferable for analysis of structural situations such as center-cracked panels or surface flaws?

Most investigators would agree that the most reliable method for minimizing the uncertainty in the applicability of such data would be to use only those results where transferability to the "design configuration" has been experimentally verified. Even in such instances, caution must be exercised

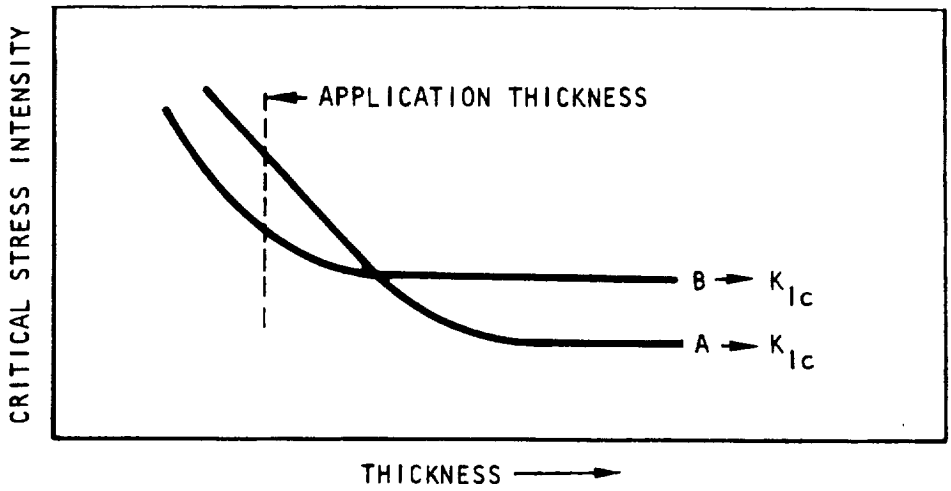

Figure 2-5. Use of K_{Ic} for Screening Materials

when applying the data, and the temptation to extrapolate the transferability must be resisted. Of course, as mixed stress-state behavior becomes more explicitly defined and the transferability of K_c data from specimen to specimen and to hardware is demonstrated, the test complexities will decrease and material screening will thereby be simplified.

Available K_{Ic} Data

Despite the magnitude of interest in fracture toughness testing, there are relatively few summary documents containing "valid" K_{Ic} data for several alloy systems. This is primarily a result of the recency of the standard method of test for K_{Ic}. Moreover, early data sources usually do not contain sufficient information to determine whether the rigorous requirements of the ASTM test method have been met.

The Damage Tolerant Design Handbook, prepared by Battelle's Columbus Laboratories (Reference 14), and Fracture Mechanics Data (Reference 15), prepared at Rockwell's Rocketdyne Division, are two documents containing valid K_{Ic} data for some of the alloy systems under consideration for Space Shuttle applications. However, due primarily to the fact that so little is known regarding those processing variables affecting K_{Ic}, it is necessary to acquire data in each product form, grain orientation, and heat treatment under consideration. In view of this fact, it is anticipated that much K_{Ic} data will be generated at Rockwell and subcontractors as part of the Space Shuttle material characterization programs.

2.2 THIN SHEET BEHAVIOR

The following paragraphs deal with the prediction of failure in thin metal sheets cracked through the thickness. There are two significant reasons for considering this specific phenomenon. First, major sections of the Space Shuttle will be composed of thin sheet structures, and thus a description of this phenomenon is directly applicable. Secondly, many failures of part-through cracks in tough materials exhibit much of the same phenomenological behavior as through cracks in thin sheet, and thus conclusions drawn from this somewhat simpler problem may be more generally applicable to the more complex problem of the failure of part through cracks.

Crack tip behavior is controlled by the plastic processes occurring at the crack tip. Since the plastic deformation processes at the crack tip are highly dependent upon the constraints in the direction parallel to the crack front, the thickness of thin sheet specimens has a significant effect on the fracture processes. Therefore, all "material" properties which describe thin sheet fracture behavior must be considered to be functions of thickness as well as chemical and processing variables. This fact will be implicit in the ensuing discussion.

The general problem of predicting failure of damaged (cracked) thin sheet structure under arbitrary loading conditions (including pressure, shear, tension, bending, etc.) has not yet been considered in a single comprehensive approach. The general analysis (stresses, strains) would be very difficult and would have to include complex interaction effects of structure as well as buckling and large deformation theory. In addition, the material behavior, which includes effects such as slow stable tear, is very complex and not completely understood. Due to the compounding complexities of material behavior and structural analysis as well as the high cost of testing complex structures, most investigators have concentrated on the relatively simple structural configuration of a center-cracked panel loaded in uniaxial tension.

The following discussion of various failure prediction techniques for the most part will depend heavily upon the center-cracked tension panel also. However, the discussion will also consider which of these techniques may be used for more complex structures and loading, although the manner in which this is done often depends upon the type of structure and loading considered and is at present dependent upon a great deal of engineering judgment as well.

A typical test used to simulate a structural application and which the various failure prediction techniques attempt to depict may be described as follows: a thin sheet structure which contains a "natural" crack is loaded monotonically at a moderate rate. As the load is increased, the crack is often observed to grow slowly and stably (if the load is not increased, the crack does not grow). In most structures, a maximum load is reached at which unstable growth occurs, and the structure is said to have failed.

It is usually accepted that for purposes of design, significant correlations would involve the initial crack length and maximum load. For material characterizations, however, other correlations may be acceptable (e.g., load and crack length at instability).

Other methods than those discussed are available but were not considered due to constraints of time and space. Most of these additional methods are similar to, and combine aspects of, the discussed techniques. An example of this is the work of Newman (Reference 16) which combines notch strength analysis and critical stress intensity concepts. A brief description of four prediction techniques follows. This is followed by a discussion of the use and applicability of each of the techniques.

Description of Concepts

Notch Strength or Crack Strength Analysis

Notch strength analysis is a technique developed primarily by Kuhn (References 17 and 18) from notch strength analysis concepts proposed in Europe. It utilizes the results of an approximate elastic analysis of elliptical holes in finite width sheets in which the stress concentration factor K_t is given by

$$K_t = 1 + 2 K_w \sqrt{a/\rho} \tag{1}$$

where a is the semimajor axis for the elliptical hole, ρ is the radius of the tip

$$K_w = \left[\frac{1 - \frac{2a}{w}}{1 + \frac{2a}{w}}\right]^{1/2}, \text{ center hole} \tag{2}$$

$$K_w = \left[1 - 2\frac{a}{w}\right]^{1/2}, \text{ edge hole}$$

and w is the panel width.

Kuhn has modified his basic theory for application to crack problems and refers to this modified theory as "crack strength analysis." Here the governing equations are

$$\left.\begin{aligned} \sigma_f &= \frac{\sigma_u}{K_u} \\ K_u &= 1 + C_m K_w \sqrt{a} \end{aligned}\right\} C_m \text{ method} \tag{3}$$

$$\left.\begin{aligned} \sigma'_f &= \frac{\sigma'_u}{K_u} \\ K'_u &= 1 + C'_m K_w \sqrt{a} \end{aligned}\right\} C'_m \text{ method}$$

where

σ_f is the net section stress at failure

σ_u is the ultimate tensile strength

σ'_u, C_m, C'_m are additional constants

The C_m and C'_m methods are obviously similar. The C'_m method is used when notch strengthening is important and when, according to Kuhn, the actual ultimate strength does not control fracture. Both methods are essentially two-parameter curve fits of failure stress versus crack length. Note that the above crack lengths are initial crack length and that slow stable growth is not directly accounted for in this method. Where slow stable growth occurs, (C_m) or (C'_m) is probably configuration dependent.

Stress Intensity Concepts

The concept of a critical stress intensity factor has been one of the basic fracture mechanics concepts. The stress intensity factor is defined as $K = \sigma\alpha$ where α is the geometric factor. It is a relatively simple (one-parameter) method of correlating fracture data, and is perhaps the most widely used concept in fracture mechanics. However, no standard procedure is available for determining the critical value of K, that is, K_c. Variations in K_c values with geometry are the principal reason for the inability of a standard test procedure to be established. Figure 2-6 indicates these planar geometric variations for center cracked panels.

The term K_c, plotted in this form, is usually (but not always) based on center-cracked panel tests where the width is sufficiently wide for the value of K_c to have stabilized. The stress and crack length used in the stress intensity calculation are usually (but not always) maximum stress and initial crack length. There is not direct consideration of slow, stable growth.

An additional consideration within the stress intensity concept is the plasticity term which is usually added to the crack length term. The plastic zone is taken to be

$$r_y = \frac{1}{2\pi} \left(\frac{K}{\sigma_{ys}}\right)^2$$

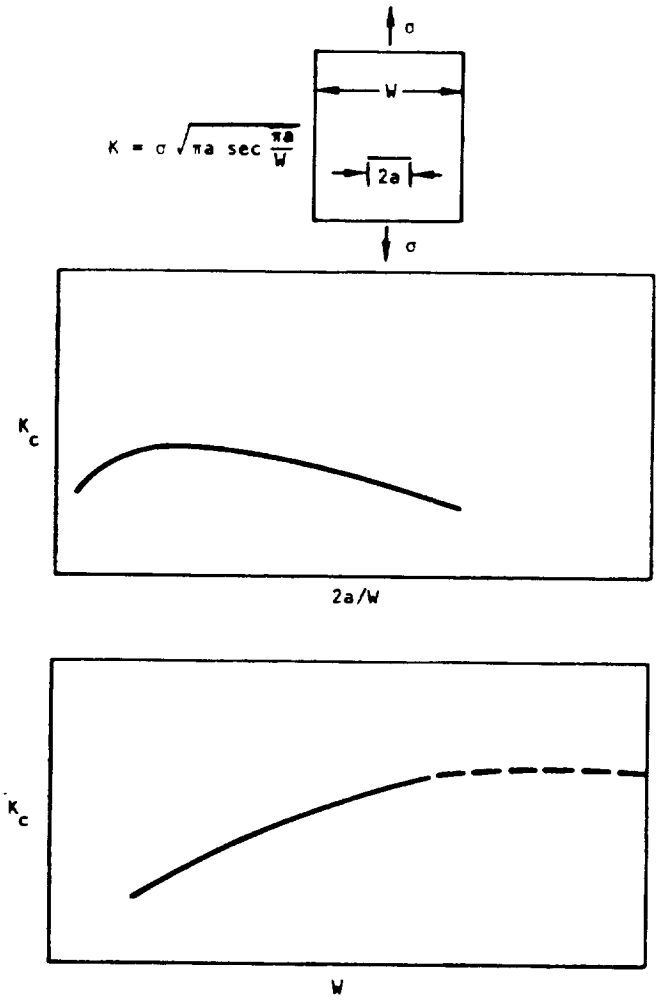

Figure 2-6. Effects of Geometry on K_c

For wide (compared to the crack length) center-cracked panels

$$K_c = \sigma_c \sqrt{\pi (a + r_y)}$$

$$K_c = \frac{\sigma_c \sqrt{\pi a}}{\sqrt{1 - 1/2 \left(\frac{\sigma_c}{\sigma_{ys}}\right)^2}} \qquad (4)$$

Note that if σ_{ys} is replaced by an unknown "flow stress," the above equation becomes a two-parameter equation, similar in form to the crack strength analysis method of Kuhn.

DMIC (Fedderson) Data Display Technique

Fedderson's observations of data generated at Battelle has led him to suggest a simplification of the data analysis of center-cracked tension panel fracture behavior (Reference 19). The method makes use of a curve relating gross stress to crack size for a particular panel width, as shown in Figure 2-7. The central portion of the curve is described by

$$\sigma_c = \frac{K_c}{\sqrt{\pi a}} \tag{5}$$

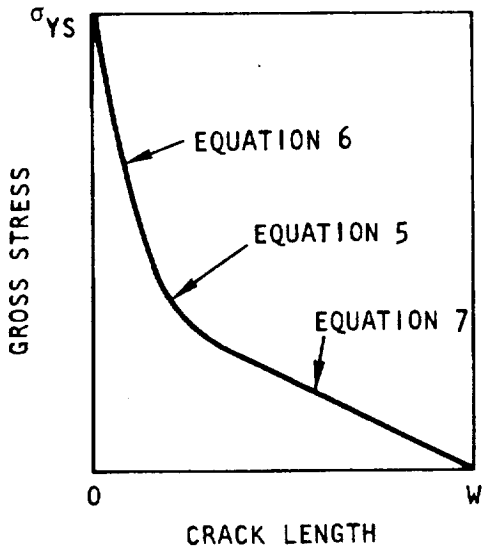

Figure 2-7. DMIC (Fedderson) Data Display Technique

A separate curve is developed for each panel width. This includes the determination of a distinct value of K_c for each width. The left portion is a straight line, tangent to the K curve and going through the yield stresses at a = 0. It is described by

$$\sigma = \sigma_{ys}\left[1 - \frac{4\pi^3}{(1+2\pi)^3}\left(\frac{\sigma_{ys}}{K_c}\right)^2 a\right] \tag{6}$$

The right portion is a straight line tangent to the K curve and going through zero stress when 2a = w. It is described by

$$\sigma = \frac{(1 - 2a/w)K_c}{2\left(\frac{\pi}{1+2\pi}\right)^{3/2}\sqrt{\frac{w}{2}}} \tag{7}$$

Fedderson uses this type of curve to describe various degrees of damage such as initiation and critical instability. The entire theoretical relationship between σ and a for a particular damage level can be described if a "valid K_c" exists and the yield strength is known. A "valid" K_c is one for which

$$\sigma \leq \frac{2}{3}\sigma_{ys},\ 2a < \frac{w}{3}$$

at the condition under consideration (e.g., crack initiation or instability).

Points which violate this condition lie on one of the tangents, rather than the K curve. Note that in some cases the two tangents can degenerate into the line which represents net section yielding. In these degenerate cases, an artificial

$$K_c = 2\sigma_{ys}\left(\frac{\pi}{1 + 2\pi}\right)^{3/2}\sqrt{\frac{w}{2}}$$

reduces the above equations into the appropriate straight line.

Resistance Curve Concepts

The resistance curve is a material property curve which relates the applied stress intensity factor (or strain energy release rate) to the amount that a crack has grown. There is, of course, a thickness dependency due to the effect of lateral constraint as there is in other fracture indices. Resistance curve concepts are the only techniques presently available that can adequately explain the effect of width and initial crack length on the failure of center-cracked panels. In addition, resistance curve concepts are the only techniques which attempt to take into account the exact slow, stable growth behavior which occurs when a thin metal sheet is loaded.

This concept was initially presented by Kraft, Sullivan, and Boyle (Reference 20). They postulated that for a given material and thickness there is a unique relationship between the amount that a crack grows and the applied stress intensity factor, as shown schematically in Figure 2-8. They called this a crack growth resistance curve (R-curve). Resistance was defined as the level of available strain energy release rate, G_r, required to grow a crack a given amount. This level changes as the crack grows. For plane stress $G = K^2/E$, therefore, strain energy release rates and stress intensity factors are directly analogous, and the term "resistance" has been applied to both in the recent literature.

Kraft et al. also presented a failure criterion based on the crack growth resistance concept. A crack will grow stably as long as the increase in

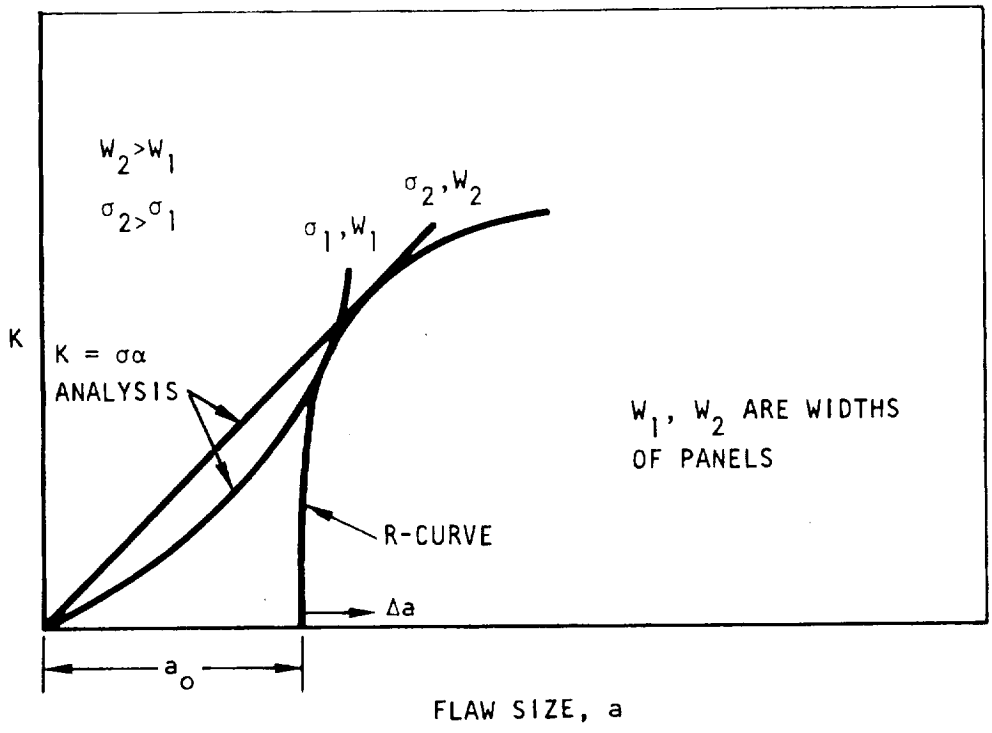

Figure 2-8. Center-Crack Panel Resistance Curve Failure Prediction

resistance, as the crack grows, is greater than the increase in applied stress intensity. Otherwise, unstable fast fracture will occur; that is, failure will occur when

$$\frac{\partial K}{\partial a} \geq \frac{\partial K_r}{\partial a} \tag{8}$$

$$K \geq K_r \tag{9}$$

Graphically, the failure point is determined when the applied K-curve for a given load is tangent to the R-curve as in Figure 2-8. The way in which the structure can affect the amount of slow, stable growth is seen by the example in Figure 2-8 for a finite width sheet. For different initial crack lengths, the resistance curve is simply shifted to the left or right, and the critical crack length and failure load will change accordingly.

The correctness of the above phenomenological description has been fairly well determined, most notably by Heyer and McCabe (References 21 and 22). They have used a displacement-controlled test specimen to generate crack resistance curves for a number of materials. In this test, K decreases with increasing crack length over a range of crack lengths, which enables them to develop a major portion of the resistance curve. Note that a test on

a more stable configuration (lower gradient in K), such as a wide center-cracked panel, is needed to predict the failure on a less stable configuration such as a narrow center-cracked panel. As may be seen from Figure 2-8, it is impossible to predict the results of the wide panel test from the narrow panel test, because an insufficient portion of the resistance curve will be available.

Since the resistance curve describes more of the detailed motion of the crack tip, it would be expected that predictions made by using this concept are more accurate than those using other techniques. There is, of course, an accompanying difficulty in developing material properties as they relate to resistance concepts, because a material curve, K_r, rather than a single parameter, is necessary to make the failure prediction. Not only is the necessary input information more extensive, but the actual failure prediction is more complex due to the presence of an unknown in addition to the failure load. The crack length (or alternatively, the stress intensity factor) at instability is not known a priori. For this reason, general design curves using the resistance curve concept are difficult to generate. However, a simple technique employing a transparency has been developed which makes the task of failure prediction easier (Reference 23). This graphical technique is summarized in Figure 2-9. It uses a log plot of α (stress intensity divided

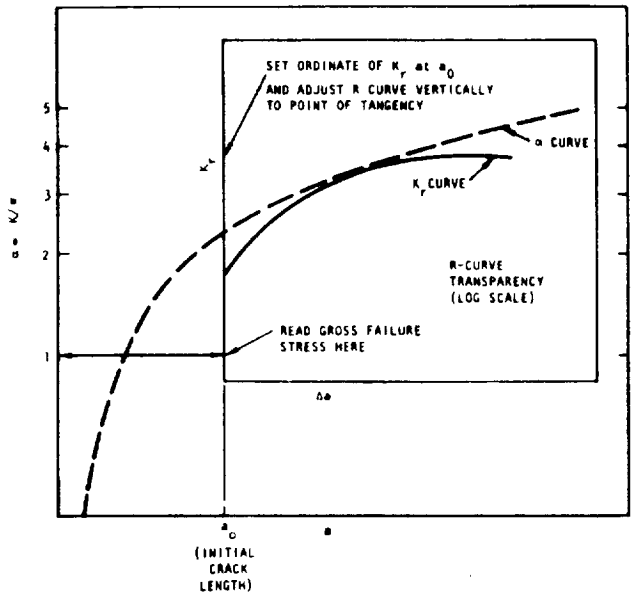

Figure 2-9. Schematic of Resistance Curve Prediction Procedure

Table 2-1. Plane-Stress and Transitional Fracture Toughness of 0.250-Inch-Thick Aluminum 7075-T7351 Alloy Plate

Crack Orientation is L-T, Buckling of Crack Edges Restrained

SPECIMEN IDENT	TEST TEMP	TENSILE PROPERTIES YIELD STR	TENSILE PROPERTIES ULT STR	SPECIMEN DIMENSIONS THICKNESS (T)	SPECIMEN DIMENSIONS WIDTH (W)	SPECIMEN DIMENSIONS CRACK LENGTH INITIAL 2C(I)	SPECIMEN DIMENSIONS CRACK LENGTH FINAL 2C(F)	STRESS MAXIMUM S(C)	STRESS ONSET S(O)	MATERIAL TOUGHNESS APPRNT K(APP)	MATERIAL TOUGHNESS CRITCL K(C)	MATERIAL TOUGHNESS ONSET K(O)	NET STRESS RATIO APPRNT	NET STRESS RATIO CRITCL	NET STRESS RATIO ONSET
	F	KSI	KSI	INCH	INCH	INCH	KSI			KSI-SQRT(INCH)					
28	70	60.5	72.0	0.254	8.043	0.773	0.000	46.80	27.70	51.76*	0.00	30.64	0.855	0.000	0.506
29	70	60.5	72.0	0.254	8.040	1.220	-0.000	43.40	27.70	60.95*	0.00	38.90	0.846	0.000	0.540
30	70	60.5	72.0	0.257	8.040	1.660	2.900	39.30	31.30	65.18*	91.32*	51.91	0.819	1.016	0.652
31	70	60.5	72.0	0.258	8.040	2.050	3.060	36.30	27.20	66.91	86.33*	53.14	0.799	0.957	0.598
32	70	60.5	72.0	0.258	8.043	2.473	3.400	33.70	20.00	70.53*	87.77*	41.86	0.804	0.965	0.477
33	70	60.5	72.0	0.253	8.000	2.860	3.800	30.60	19.30	70.50	87.24*	44.46	0.787	0.963	0.497
34	70	60.5	72.0	0.259	8.030	3.233	4.450	28.20	14.50	70.71	92.47*	46.39	0.780	1.046	0.512
35	70	60.5	72.0	0.257	8.030	3.650	4.900	25.20	16.70	69.41	92.22*	46.00	0.764	1.069	0.506
36	70	60.5	72.0	0.259	8.046	4.010	5.050	23.30	17.50	68.58	87.23*	52.18	0.758	1.022	0.577
37	70	60.5	72.0	0.256	8.043	4.353	5.100	20.80	12.70	66.92	79.87*	41.50	0.749	0.940	0.466
38	70	60.5	72.0	0.256	8.030	4.773	5.610	17.80	11.40	64.67	78.04*	41.42	0.748	0.972	0.479
39	70	60.5	72.0	0.255	8.050	5.233	5.850	15.50	10.20	61.44	72.83*	40.43	0.731	0.937	0.481
41	70	60.5	72.0	0.255	8.030	5.650	6.000	13.60	9.20	60.47	67.14*	40.91	0.758	0.889	0.513
43	70	60.5	72.0	0.260	8.020	6.000	-0.000	11.50	8.20	56.87	0.00	40.55	0.755	0.000	0.538
44	70	60.5	72.0	0.253	8.020	6.420	6.600	8.50	6.80	48.62	52.23	38.89	0.704	0.794	0.563
45	70	60.5	72.0	0.257	8.020	6.693	7.000	7.40	7.00	47.12	54.85*	44.58	0.733	0.854	0.693
46	70	60.5	72.0	0.260	8.030	7.270	7.300	4.70	4.00	41.27*	42.19*	35.12	0.621	0.655	0.599
47	70	60.5	72.0	0.255	8.040	7.663	-0.000	1.90	1.40	24.20	0.00	22.93	0.664	0.000	0.629
								AVERAGE VALUE		59.72	0.00	41.60			
								STANDARD DEV.		13.21	0.00	7.19			
48	70	60.5	72.0	0.252	15.900	1.580	0.000	46.30	23.50	71.80*	0.00	37.25	0.831	0.000	0.431
49	70	60.5	72.0	0.252	15.950	3.169	-0.000	35.80	19.90	81.75	0.00	45.44	0.738	0.000	0.410
50	70	60.5	72.0	0.252	15.910	4.840	7.000	31.30	19.30	91.59	118.24*	56.47	0.744	0.524	0.458
51	70	60.5	72.0	0.252	16.020	6.473	8.600	24.90	23.00	88.09	111.77*	81.70	0.688	0.885	0.638
52	70	60.5	72.0	0.251	15.960	8.150	10.200	19.70	14.60	84.67	107.93*	62.75	0.668	0.908	0.495
53	70	60.5	72.0	0.253	15.910	9.550	10.850	16.30	12.00	82.47	97.22*	60.71	0.675	0.847	0.497
54	70	60.5	72.0	0.248	15.920	11.453	13.500	11.40	8.90	74.00	107.95*	57.77	0.671	1.240	0.524
55	70	60.5	72.0	0.252	15.910	12.930	-0.000	8.30	6.20	66.95	0.00	51.89	0.706	0.000	0.547
56	70	60.5	72.0	0.252	15.860	14.503	14.700	3.70	3.30	47.87	52.10*	38.81	0.734	0.823	0.571
								AVERAGE VALUE		77.17	0.00	54.76			
								STANDARD DEV.		14.17	0.00	13.66			
89	70	60.5	72.0	0.259	36.120	7.353	9.250	29.98	17.40	98.32	102.92	60.68	0.537	0.575	0.306
90	70	60.5	72.0	0.259	36.120	18.888	24.888	15.88	10.28	94.73	136.84	64.42	0.494	0.797	0.336
91	70	60.5	72.0	0.253	36.123	28.838	33.188	7.88	4.58	94.81	155.42*	54.24	0.639	1.342	0.369
								AVERAGE VALUE		93.82	115.88	59.78			
								STANDARD DEV.		2.36	23.99	5.15			

*NOTE- NET SECTION STRESS EXCEEDS 80 PERCENT OF YIELD STRENGTH. VALUE NOT INCLUDED IN AVG. VALUE OR STD. DEV.

by load) versus a and a transparency of a log plot of resistance versus Δa. The use of logarithms enables these two curves to be sufficient for relating initial crack size to failure stress for all stress levels. Of course, other techniques (such as those employing a computer) may be used to simultaneously solve the nonlinear Equations 8 and 9.

Prediction Techniques

Instead of discussing prediction techniques in a relatively abstract sense, speculating upon the advantages and disadvantages of each, it will be far simpler and clearer to discuss them with a particular data set as an example. The data set to be used is the result of a program run at Battelle Memorial Institute by C. Fedderson on 0.25-inch-thick 7075-T73 aluminum, and is one of the most comprehensive sets of data on a single sheet of material. In addition, it is probable that the materials used on the Shuttle will exhibit basic failure properties like those of this material.

Table 2-1 is a reproduction of data taken from Reference 14. Three panel widths and a number of crack lengths at each panel width were tested. Data recorded during the test were maximum load, load at which crack growth began, and crack length at instability. Maximum load is a quantity that can be determined with reasonable accuracy, but the load at which crack growth initiates cannot be as accurately known, since a judgment of exactly when crack growth has started must be made. The last quantity, the crack length at instability, is wholly a matter of judgment and is a relatively inaccurate quantity. However, the fact that this last crack length was recorded is a significant aid in understanding the advantages and disadvantages of each of the failure prediction techniques.

The data recorded in Table 2-1 include test temperature, yield strength, ultimate strength, panel thickness, and panel width; these require no explanation. Also listed are total crack lengths at initiation and instability. Since many structures contain a single crack tip (as opposed to two in a center-cracked panel), the use of the half-crack length, a, in a center-cracked panel is of more general use. The quantities termed "maximum stress" and "onset (of growth) stress" are gross stresses equal to load/WB. The "material toughness" listed in the table is a stress intensity factor where K (APP) is calculated using the initial crack length and maximum load, K (C) is calculated using the crack length at instability and maximum load, and K (O) is calculated using the initial crack length and the load at the onset of slow, stable growth.

Each of the techniques listed above will be considered in its capacity to predict one portion of the test data from another portion. Although attention is being focused upon a single set of center-cracked panel data, the

general objective of describing prediction techniques for complex structure will be kept in mind. The discussion will not be concerned simply with the collapsing of data onto a single line.

Crack Strength Analysis

Crack strength analysis as described above uses the initial crack size, a, and does not anywhere in its development take into account the fact that slow, stable growth occurs. Due to the extensive stable tear evident in this data set (and usually present in the tougher engineering alloys), it is pertinent to ask what effect this should have upon the usefullness of this approach. Kuhn, in his presentation of crack strength analysis, made a number of statements regarding slow, stable growth, He noted that, for design purposes, the initial crack length had to be used as a base datum. This is certainly true. He felt that a procedure for relating final crack size to initial crack size did not exist. This may not be true any longer (see the section below on resistance curves). He stated,

> A number of investigators have concluded that the relation (critical crack length) = (initial crack length) X constant holds either with good accuracy, or at least with acceptable accuracy. Under these circumstances, the difference between using either the critical or the initial length is essentially a constant numerical factor attached to the "notch toughness" number, and such a difference is immaterial. The question remains open, of course, when the relation between initial and critical length is more complex.

Figure 2-10 contains plots of the ratio of critical crack length to initial crack length versus initial crack length for the three panel widths. In spite of the difficulties and inaccuracies associated with such a measurement, the data trends are clear and may be relied upon. Thus, it is obvious that the relationship between initial crack length and critical length cannot be expressed as a simple constant ratio. The relationship is apparently a more complex function of crack length and panel width. However, the impact on failure predictions is not clear; and to actually evaluate the method, the technique must be applied to the actual failure data.

Kuhn points out that the use of his "modified method" often improves the correlation of test results obtained from specimens of different widths. It was initially felt that this might take into account in some way the effects of differences in slow growth behavior. However, when this was attempted using data from one 36-inch panel and one 8-inch panel to get C_m and σ'_u, the value of σ'_u obtained was less than the actual ultimate strength of 72 ksi and the approach had to be abandoned. Since the crack strength method automatically fits data to zero crack length ($\sigma'_c = \sigma_u$), it seems that the larger

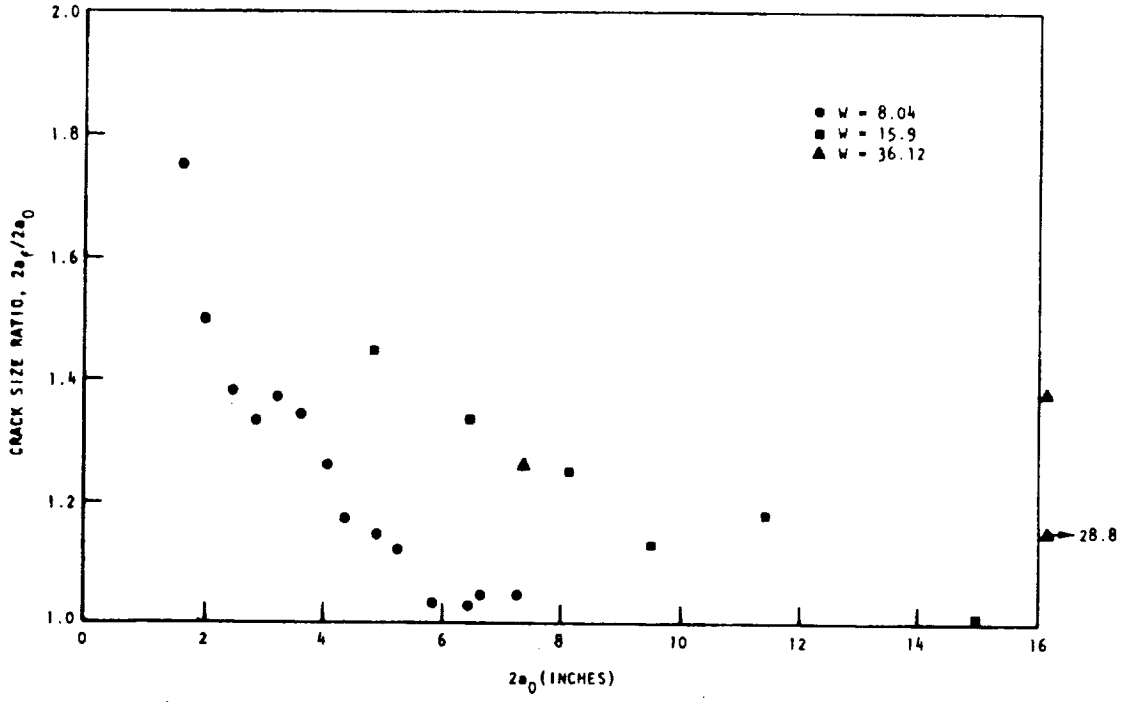

Figure 2-10. Slow, Stable Growth

test specimens would be the most appropriate for determining C_m. On the other hand, Specimen 91 had an unusually large initial crack length and a reported net stress ratio to yield a stress ratio of 1.5 at failure. Since this test result might be unreliable, Specimen 90 was used to determine C_m. Substitution of the appropriate values into the equation

$$C_m = \left[\left[\frac{\sigma_u}{\sigma_c}\right] - 1\right]\left[\frac{1 + \frac{2a}{w}}{1 - \frac{2a}{w}}\right]^{1/2} \frac{1}{\sqrt{a}} \qquad (10)$$

yields a value of C_m equal to 0.81. Using this value, failure predictions can be made for each of the initial crack lengths reported in the data set. As can be seen in Figure 2-11, the correlation is quite good. In light of the fact that slow, stable growth was totally ignored and yet was significant during the test, the remarkable correlation becomes a contradiction. It seems that the failure criterion assumed (basically a critical stress) and the analysis performed have "errors" that, at least in this case, compensate for the effects of slow, stable growth.

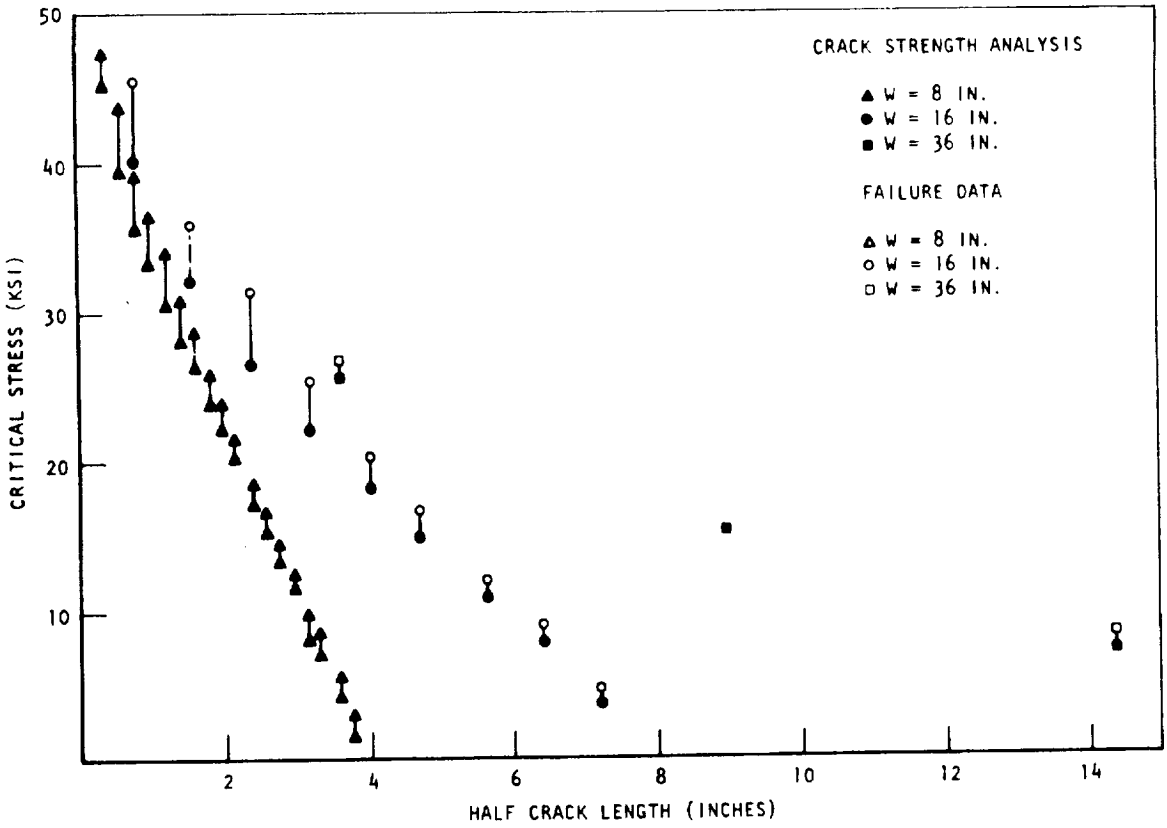

Figure 2-11. Crack Strength Analysis Failure Prediction

For high values of C_m, the "1" in Equation (3) is insignificant, and the crack strength method essentially becomes the critical stress intensity method discussed below. It appears that for materials that have low values of C_m (tough materials) and that also exhibit little slow, stable growth, the resulting relationship between σ_f and a will not be appropriate. It is probably true, however, that for most materials used in thin section structure, slow growth is significant, and crack strength analysis will correlate the data reasonably accurately.

In this stress analysis, Kuhn utilizes the quantity

$$K_t = 1 + 2 K_w \sqrt{a/\rho}$$

to determine the stresses near the crack tip which cause failure. In general, the quantity K_w can be related to the fracture mechanics analysis parameter α. However, the first part of the K_t expressions generally is a constant other than 1. Thus, to analyze a structure other than a center-cracked panel using crack strength analysis, a stress analysis of a structure with a notch must be analyzed for a number of notch sizes (ρ) to establish the proper expression for K_t. In general, analyses such as this are not available and would be

difficult and expensive to obtain. In addition, complex structural interactions may affect slow, stable growth behavior in a significantly different manner than occurs in center-cracked panels; thus, the effects of slow, stable tear may not be properly compensated for. The extreme example of this is a structure in which the local crack tip stresses decrease as the crack grows; this would produce results significantly different from those in tests in which the local stresses increase with increasing crack length.

Critical Stress Intensity

The critical stress intensity analysis approach, like that of crack strength analysis, also does not account for the slow, stable growth behavior directly. To be completely rational in this approach, then, requires either that the assumption that little slow, stable growth occurs or that the amount of slow, stable growth is proportional to the initial crack length. It has been shown previously that these assumptions are not generally true, and therefore, the pertinent question is how much this deviation from reality affects the failure predictions. In addition to these inherent assumptions with regard to slow, stable growth behavior, the critical stress intensity approach contains assumptions about the overall gross stress at failure. The development of K as a significant parameter is dependent on the ratio of the applied stress to yield stress being low. This is violated in most practical situations and in the data set under consideration as well.

However, the J-integral concept (References 24 and 25) is one that is valid even at the yield stress, and Irwin (Reference 26) has recently noted that (at least for center-cracked panels) the value of J calculated by a numerical technique (which included nonlinear material behavior) and of G (which is directly related to K and which included a plastic zone correction) were in close agreement up to a net-stress/yield-stress ratio of 0.8. Thus we may expect K (with a plastic zone correction) to be a significant parameter for a wide range of test and application situations.

The data set was analyzed by determining a value of K_c from a single test. Specimen 90 was chosen for reasons mentioned previously. The equations used were

$$K_c = \sigma_c \sqrt{\pi a_e \sec\left(\frac{\pi a_e}{w}\right)} \qquad (11)$$

where

$$a_e = \frac{1}{2\pi}\left(\frac{K_c}{\sigma_{ys}}\right)^2 + a \qquad (12)$$

Using a yield strength of 60.5 ksi, a value of $K_c = 95$ ksi $\sqrt{\text{in.}}$ was found to satisfy the above equation for Specimen 90. Failure stress predictions were then made for the remaining panels using the above relations.

The results are plotted in Figure 2-12. The predictions are not as bad as the inconsistency with the slow growth behavior might imply. However, Kuhn's notch strength analysis predictions are better. It appears that the fracture mechanics approach does not have the compensating errors present in notch strength analysis and thus the lack of consideration of slow, stable growth has a greater impact.

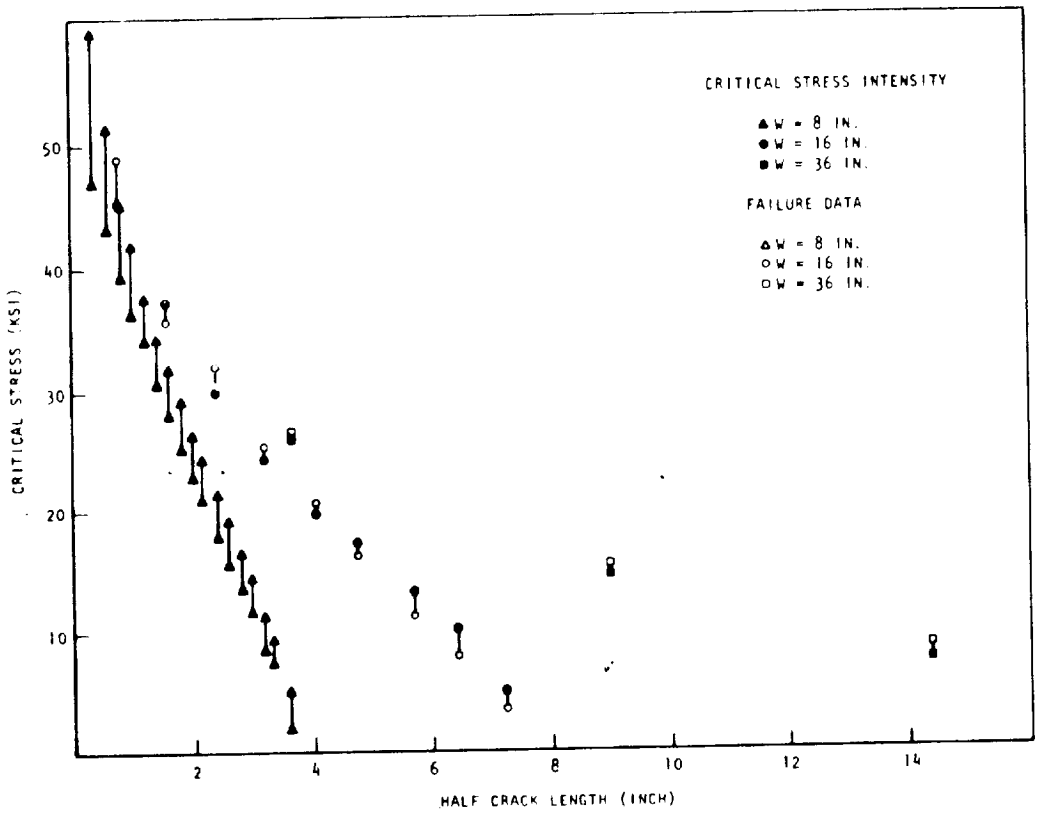

Figure 2-12. Critical Stress Intensity Failure Prediction

DMIC Data Display Technique

This technique is more of a data correlation technique than a prediction technique, and therefore, the failure data were not used in the evaluation. A review of the literature indicates that this method seems to correlate center-cracked panel data reasonably well. However, it should be noted that no procedure is given for going from the threshold of growth stresses to the critical instability stresses (slow, stable growth is not described). Therefore, the method may only be used for failure prediction where stable growth is not significant, or is always consistent. A great deal of testing, and expense, is involved in developing enough data for the empirical analysis, particularly since a test series must be run for each panel width under consideration. In

addition, the dependence on the center-cracked panel is total, and generalization to other structural configurations would be very difficult. Most of these comments are appropriate to the vast majority of data correlation approaches.

Resistance Curve Techniques

The stress intensity factor is basic to the present use of resistance curves. However, the stress intensity factor is defined on the basis of linear elasticity, and therefore the use of it at net section stresses at or near the yield stress requires modification to the basic concept. This can be accomplished by using the Kyield approach described in page 66, Volume I.

Since a resistance curve for the data set under consideration was not available, one was constructed utilizing the available information. Test Specimens 89 and 90 were used. The test information was employed in the following manner. The largest value of K recorded prior to catastrophic failure was 137. Therefore, the resistance curve was constructed to be asymptotic to a K of about 140. The value of K at Δa = 3 inches was set at about 135. Since Test 90 had a Δa of 0.95 at a K of 103, the resistance was drawn through that point also. Finally, it was assumed that discernible crack growth first began at a K of 60. Using this rather scanty information, the resistance curve in Figure 2-13 was constructed. Note that if a resistance curve had been the object of the test program which generated the failure data, sufficient information to generate the entire curve precisely could be obtained from a single test.

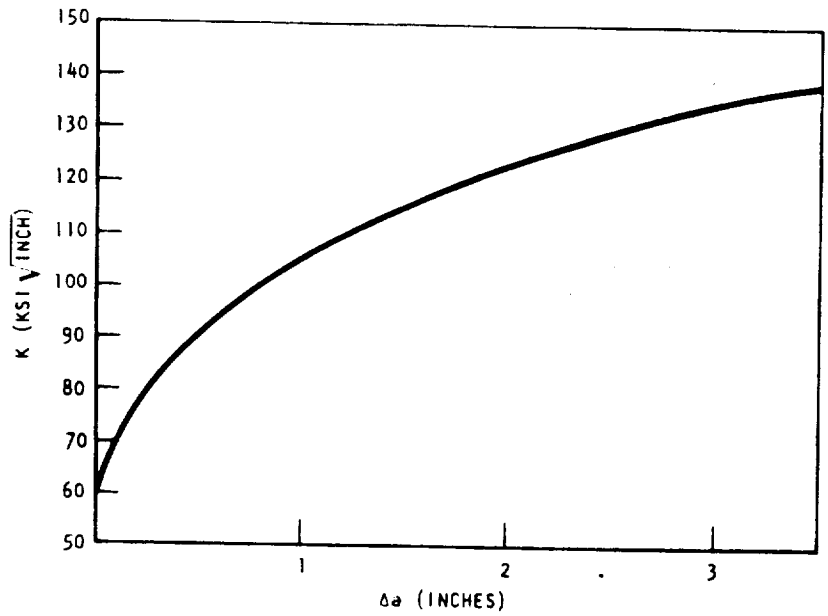

Figure 2-13. Constructed Resistance Curve

Since this resistance curve was generated so crudely, it was felt that the added complication of a plastic zone correction was not called for. The transparency technique described in preceding paragraphs was used in conjunction with the K_{yield} approach. The prediction results are presented in Figure 2-14. Note that except for the extremely short crack lengths, the resistance curve techniques make significantly better predictions than any of the other techniques.

The lack of good fit to the short crack length data may be attributed to the fact that a plastic zone correction was not used. Since more of the known behavior was used (the slow, stable growth description), it is not surprising that this method produced the most accurate predictions. More important, however, is the fact that because of the greater rationality of this approach, it would be expected to be accurate for other structural configurations as well. This can be seen in Reference 27 where the resistance curve approach was applied successfully to complex reinforced structural configurations.

In summary, it may be concluded that the resistance curve may be expected to fit the data generated on center-cracked panels better than any other approach. Moreover, the resistance curve appears to be the most general approach and would allow an analyst to be more confident in extrapolating predictions to geometries other than those from which the basic failure data were generated. On the other hand, crack strength analysis fits the data investigated remarkably well and is a very simple technique. Because of the simplicity of its use, crack strength analysis may be the superior analysis methodology for structures which closely resemble the configuration used to generate the basic failure data (i. e., the center-cracked panel).

2.3 THE SURFACE FLAW

Much analytical and experimental research has been conducted on fatigue growth and fracture behavior of structural materials containing surface flaws. This effort was undertaken because the surface flaw has been considered a prevalent type in many classes of structures, particularly welded, both pressurized and nonpressurized, and pressure vessels containing corrosive fluids and gases. Weld defects are common origins of surface flaws in welded joints. Other origins of surface flaws are inclusions, stringers, or corrosion pits in the stressed surfaces exposed to corrosive environments.

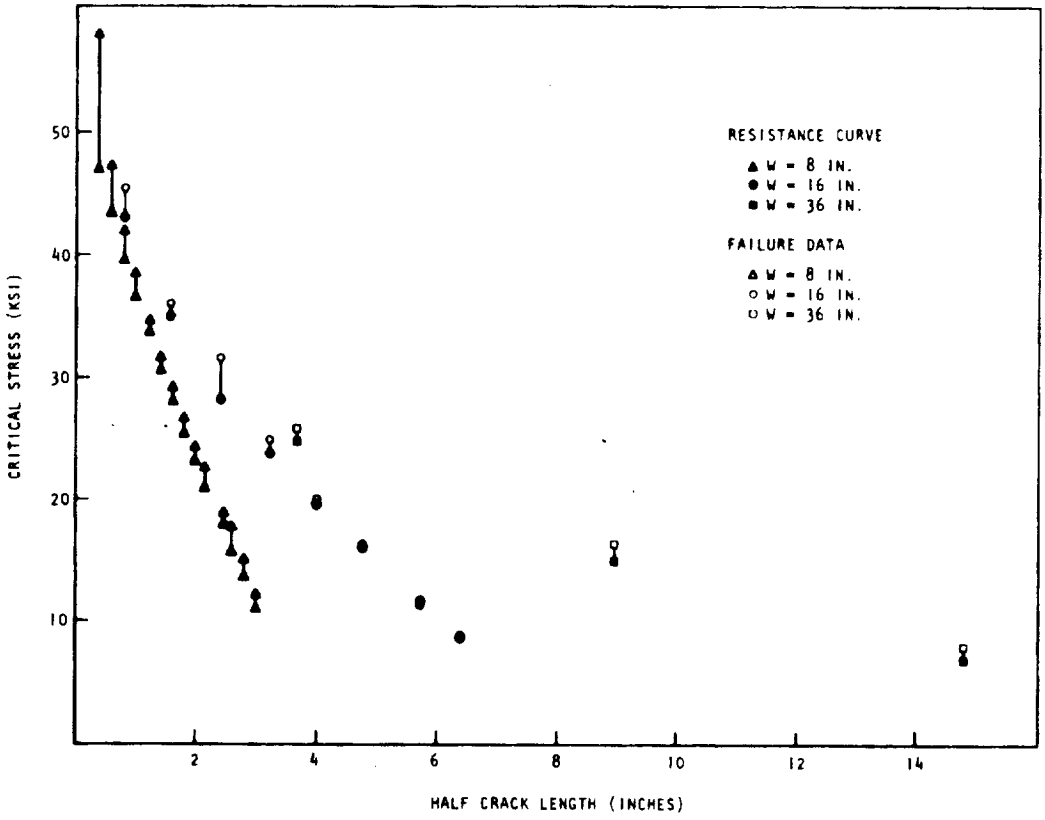

Figure 2-14. Resistance Curve Failure Predictions

The statistical frequency with which surface flaws are known to have caused failure in aircraft structures was investigated by Little and Bunting (Reference 28). The results of that study indicated that the surface flaw, although not the most prevalent type of defect in aircraft structures (cracks originating in bolt and rivet holes are the most prevalent), is a significant origin of failure.

Because there are a variety of nomenclatures applied to the surface flaw or part-through-crack (PTC), Figure 2-15 is presented in the interest of clarity for this discussion. The flaw is presented as a planar discontinuity extending into a material in the thickness direction and is oriented normal to the primary stress axis. The surface through which the crack extends is referred to as the front surface and the surface toward which it extends is called the back surface. The material has a finite thickness, t, and width, w. The crack size is described by its surface length, 2c, and depth, a. The two-dimensional flaw system is usually represented as a regular semi-ellipse with the a and 2c dimensions corresponding to the minor and major axes respectively.

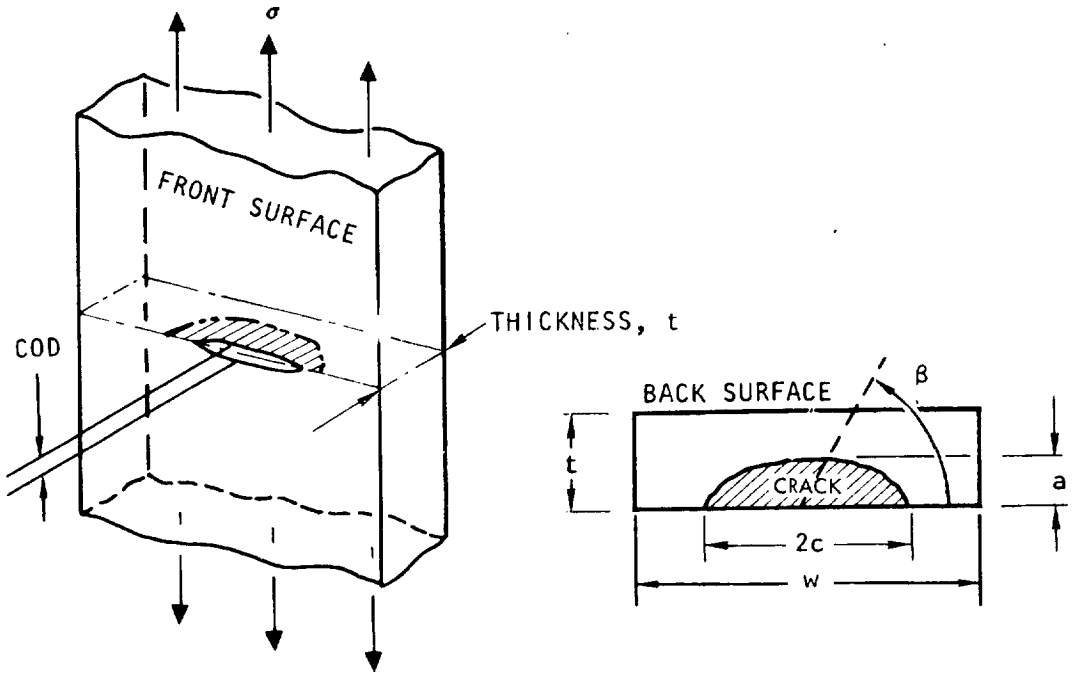

Figure 2-15. Orientation and Crack-Dimensioning System

Stress Intensity Solutions

As discussed in Section 1, the stress intensity factor, K, around the perimeter of a buried elliptical sharp crack in an infinite elastic solid under uniform normal tensile stress, σ, is described by:

$$K = \sigma \sqrt{\pi a/\phi^2} \left| \sin^2 \beta + (a/c)^2 \cos^2 \beta \right|^{\frac{1}{4}} \tag{19}$$

where β designates the location along the crack front, and a and c are defined by Figure 2-15. A shape normalizing factor, ϕ, is expressed by

$$\phi = \int_0^{\pi/2} \sqrt{1 - k^2 \cos^2 \beta}\, d\beta; \quad k = \sqrt{1 - a^2/c^2} \text{ for } c > a \tag{20}$$

Values of ϕ are published in handbooks as the complete elliptic integral of the second kind. A very useful expression developed by Rawe (Reference 29) for approximating ϕ^2 is

$$\phi^2 = 1 + 4.593\,(a/2c)^{1.65} \tag{21}$$

and is known to be very accurate for flaw aspect ratios (a/2c) between 0.05 and 0.5.

Irwin (Reference 30) adapted the expression given by Equation 19 to the case of the part-through surface crack under uniform tensile stress by applying a multiplying factor of about 1.1. This factor was originally meant to represent the combined effects of both the front and back free surfaces being made free from normal shear stresses.

For the surface flaw, Equation 19 could then be rewritten as

$$K = 1.1\sigma \sqrt{\pi a/\phi^2} \left| \sin^2 \beta + \left(\frac{a}{c}\right)^2 \cos^2 \beta \right|^{\frac{1}{4}} \tag{22}$$

In the depth direction (β = 90 deg),

$$K = 1.1\sigma \sqrt{\pi a/\phi^2} \tag{23}$$

and in the length direction (β = 0 deg),

$$K = 1.1\sigma \sqrt{\pi a/\phi^2} \cdot \sqrt{a/c} \tag{24}$$

Irwin also proposed adding an estimate of the size of the plastic zone ahead of the crack tip to the crack size. Adding the estimated plastic zone radius, r_y to the crack depth, a, gives for the surface flaw in the depth direction

$$K = \frac{1.1\sigma}{\phi} \sqrt{\pi(a + r_y)} \tag{25}$$

For plane strain conditions, r_y was estimated from

$$r_y = \frac{1}{4\sqrt{2}\pi}(K/\sigma_{ys})^2 \tag{26}$$

Substituting Equation 26 into Equation 25 and solving for K then gives

$$K = 1.1\sigma \sqrt{\pi a} / \sqrt{\phi^2 - 0.212\,(\sigma/\sigma_{ys})^2} \tag{27}$$

The expression under the radical in the denominator is identified as Q (the Irwin flaw shape and plasticity factor) and Equation 27 can be written

$$K = 1.1\sigma \sqrt{\pi a/Q} \tag{28}$$

It should be noted that the quantity 0.212 results from $(1.1)^2/4\sqrt{2}$ and that with consideration of more exact free surface factors, the value of that expression will change.

In addition, agreement regarding the applicability of the plastic zone solution used by Irwin, Equation 26, is not universal. Employing an electrolytic etching technique to measure plastic zones associated with deep surface flaws in tension loading, Francis and Davidson (Reference 31) concluded that none of the available models for plastic zone size estimates is adequate to determine the deformation state at the tip of the crack. The plane strain estimates of Liu (Reference 32) and Irwin were found to underestimate the measured zone size while the plane stress estimates of Rice (Reference 33) overestimated the actual zone size.

The limits of applicability of Equation 28 to predict surface flaw fracture are illustrated by Figure 2-16. For very small flaws, fracture is controlled by the strength of the material — not the fracture toughness. Zone 1 represents stress intensity values that would be calculated if the failure stress were between the yield and ultimate strength of the material. These values would underestimate the nominal toughness for the material. Zone 2 represents typical material toughness which theoretically should remain constant as the flaw size increases. As the flaw depth approaches the back surface, however, the fracture stress (and the calculated stress intensity) drops off rapidly (Zone 3). Such behavior (precluding an influence of net section stress effects) requires formulation and use of more accurate back surface stress intensity magnification factors. High toughness, lower strength, and material "thinness" all contribute to diminishing the size of Zone 2 and increase the required dependence upon free surface correction factors for accurate prediction of surface flaw fracture behavior.

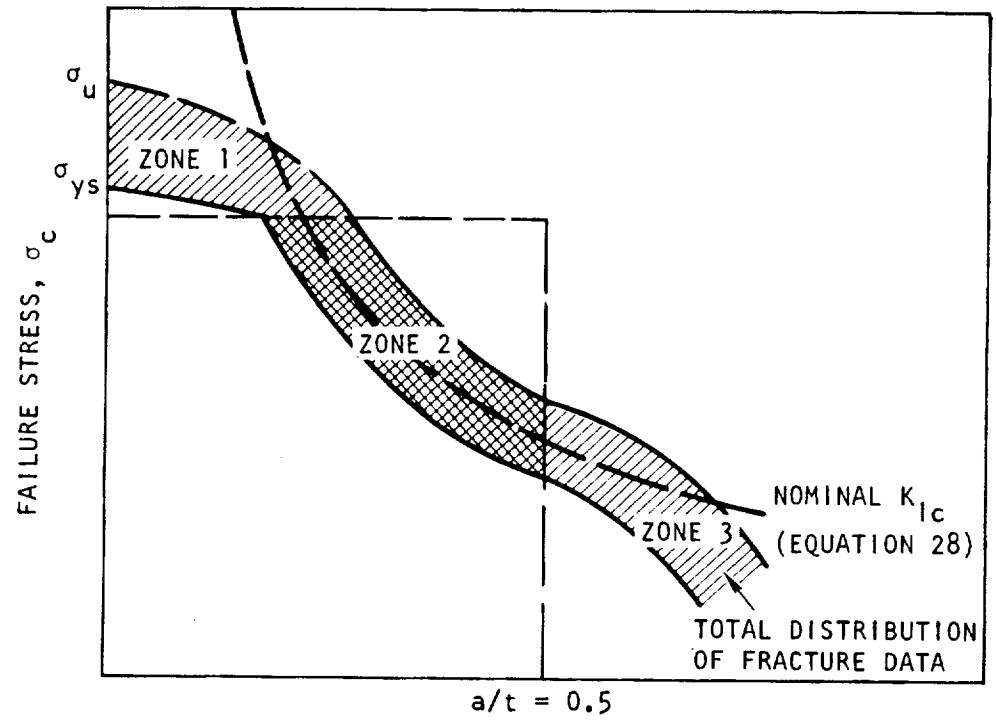

(A) STRESS VS. SIZE

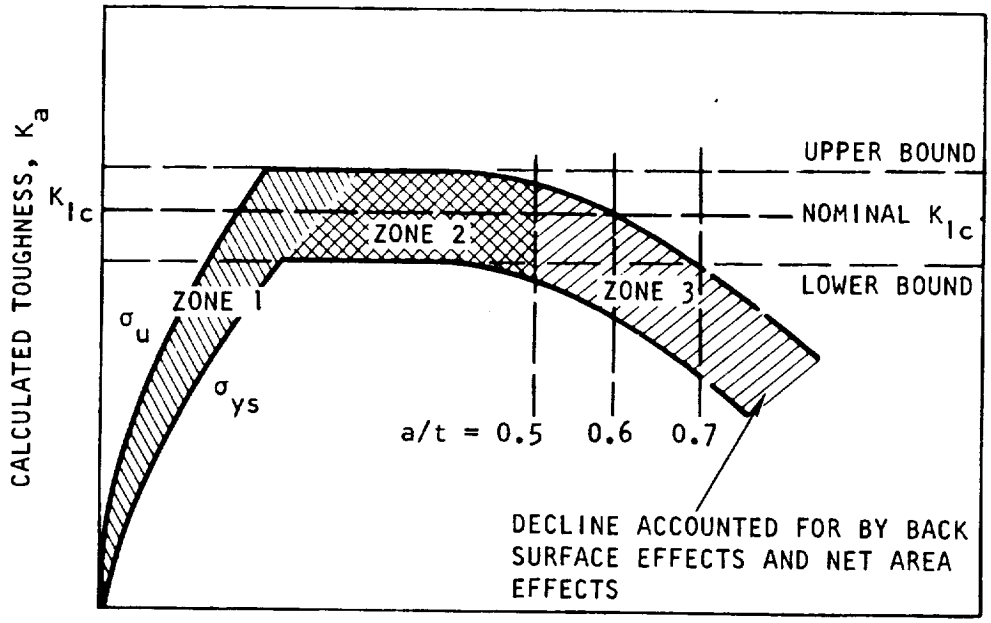

(B) K VS. SIZE

Figure 2-16. Schematic Representation of Surface Flaw Fracture Data

Free Surface Correction Factors

Following Irwin's analysis, attempts were made by many investigators to develop improved estimates of the effect on K of making the front and back faces free of normal and shear stresses. Equation 23 has been rewritten to accommodate free surface correction factors in the following generalized form:

$$K = \frac{M_1 M_2}{\phi} \sigma \sqrt{\pi a} \qquad (29)$$

where M_1 and M_2 are the front and back face magnification factors, respectively. Estimates are usually made for only the stress intensity factor in the depth direction, presuming that to be the location of maximum stress intensity and thereby avoiding the problem of estimating the variation of M_1 and M_2 with β. This omission, while not originally considered to be of significance for the monotonic load-to-failure type of analysis, can induce considerable deficiencies when the attempt is made to estimate or predict precritical flaw growth behavior (specifically fatigue) and associated flaw shape changes.

Figure 2-17 is a plot of a combined front and back surface magnification factor formulated by Kobayashi and Shah (Reference 35). This factor results from combining the front face factor suggested by Kobayashi and Moss (Reference 36) of

$$M_1 = 1 + 0.12 (1 - a/2c)^2 \qquad (30)$$

with a back face factor, M_2, obtained from an existing solution to the problem of a pair of coplanar elliptical cracks under uniform tension and a plane of symmetry located midway between the two cracks. Included in Figure 2-17 is a three-dimensional representation of this combined magnification factor.

This type of elastic magnification factor has been demonstrated to depict accurately surface flaw fatigue crack propagation (Reference 37) which can be considered as primarily an elastic process. In addition, efforts to determine the relative ability of the various stress intensity solutions to consolidate a variety of surface flaw fracture data indicate that Equation 29, using M as illustrated in Figure 2-17, correlates adequately with the test results (Reference 35). It is anticipated, therefore, that this solution will be used in Shuttle analysis.

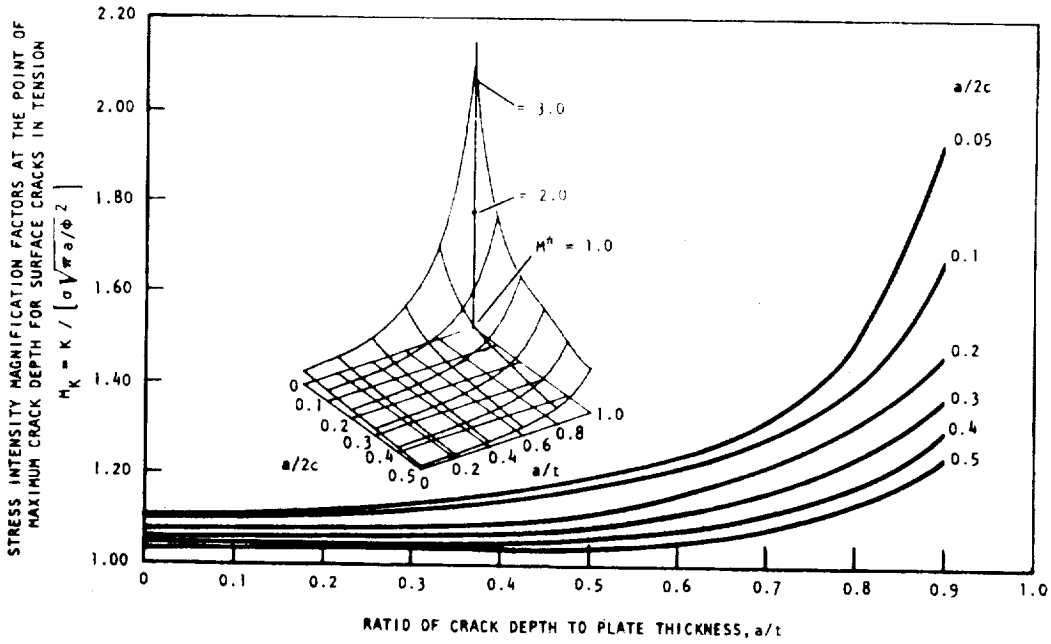

Figure 2-17. Magnification Factor, $M_1 \cdot M_2$, Versus a/t

Many other available PTC stress intensity solutions are well reviewed and summarized by Merkle in Reference 38. One result of his review was the observation that none of the current PTC stress intensity solutions attempts to accommodate bending due to eccentricity of the net section, which could significantly contribute to stress intensity in thin sheet material.

Formulation or application of empirical representations of free surface correction factors in the manner of Masters (Reference 39) is not recommended because of the error induced by necessary assumptions of the flaw size at the onset of crack instability; that is, since surface flaw growth prior to fracture is not usually measured, its contribution to the calculated magnification factor cannot be assessed, and therefore, transferability to other configurations cannot be assumed.

To aid in understanding or visualizing the damage potential of various surface flaw configurations, it is often useful to display graphically the stress intensity as a function of plate thickness, crack size, aspect ratio, or combination of variables. In addition, within certain limitations, convenient normalizations can be made. Figure 2-18 is a plot of stress intensity normalized by applied stress as a function of crack depth for several aspect

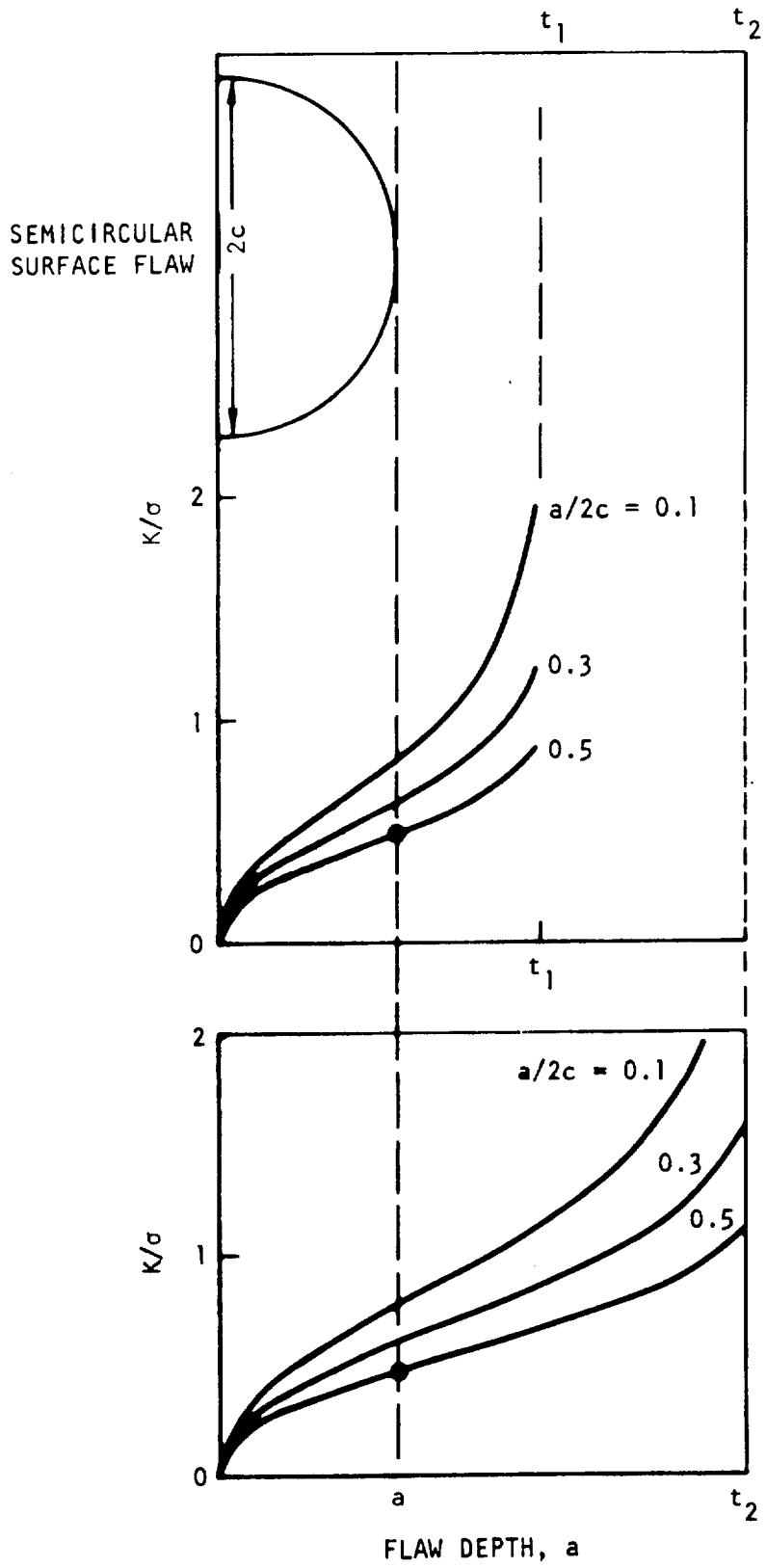

Figure 2-18. Surface Flaw Stress Intensity Gradients

ratios, using Equation 29 and the magnification factor from Figure 2-17. Naturally, longer flaws of equivalent depth produce the higher stress intensity. The slope of the curve is referred to as the stress intensity gradient for this particular flaw-specimen geometry.

Bending

Surface flaws subjected to bending loads are of particular interest in many structural analyses. Although the majority of PTC work has been confined to models depicting tension load application, some efforts to describe stress intensity factors in bending have been completed. Kobayashi and Shah analyzed the embedded elliptical crack in an infinite solid and combined the results with the estimated stress intensity factors for a semi-elliptical surface crack subjected to uniform tension to estimate the stress intensity factors for a semi-elliptical surface crack in a plate subjected to bending (Reference 35). The results of that analysis are given in Figure 2-19.

This stress intensity solution has been employed in a crack growth predictive analysis program used as an aid in precracking laboratory test specimens in bending (Reference 40). For that program the stress intensity solution properly accounted for observed crack growth rates and flaw shape changes.

Application and Analysis

In the last several years it has become common practice to measure and report plane strain fracture toughness values (K_{Ic}) obtained from surface flaw tests. Confidence in these values resulted from their apparent direct transferability to structural applications. It is argued that the type of constraint around the surface flaw contributes to essentially plane strain conditions at the crack tip and that ensuing fracture is controlled by the material plane strain fracture toughness. Application of this type of toughness measurement has primarily involved the proof test logic. Unfortunately, there is a fundamental difference between the plane strain fracture toughness value obtained from ASTM E-399-72 test method and the numbers obtained from the surface flaw test. That is, the standard test method is constructed to measure the minimum stress intensity at which measurable extension of a crack will occur, while the surface flaw test measures that stress intensity corresponding to the initial flaw size and failure stress. Since it has been well established that significant extension of a surface flaw can occur during monotonic load application (see Section 3), the equivalency of the two test methods cannot be assumed or, in the majority of cases, even expected.

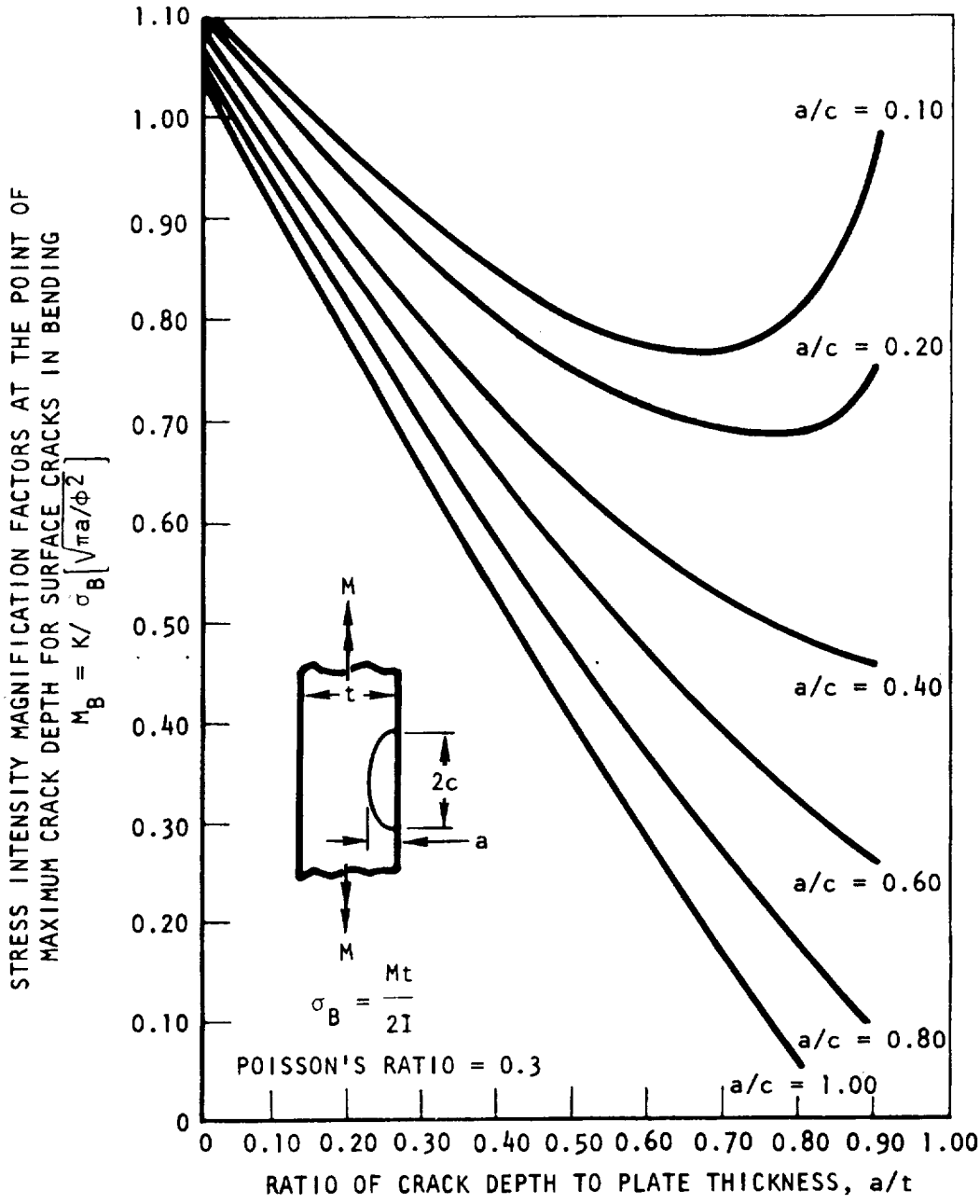

Figure 2-19. Estimated Elastic Stress Intensity Magnification Factors at Maximum Crack Depth for Surface Cracks in Bending

Increased recognition of this discrepancy has resulted in redesignation of K_{IE} as the stress intensity value obtained by using the initial flaw size and the fracture stress for the surface flaw test. The primary applications of this value, therefore, must be restricted to evaluating the residual strength of a structure containing a known defect and to screening candidate materials of application thickness to determine relative tolerance to the presence of flaws.

Problems unique to the surface flaw are usually associated with difficulties in obtaining accurate measurement of flaw size during testing. The recent availability of an elastic compliance calibration for the part-through-crack in thin sheet material has improved the situation significantly (Reference 41). However, sufficient data characterizing flaw growth during monotonic load application has not been generated and standard test techniques for supplying such information are not available.

Currently, the potential of the crack growth resistance curve as as analysis tool for surface flaw fracture behavior is not well-defined. R-curves generated from center-cracked tension panels may not be appropriate for characterizing surface flaw behavior because of an apparent influence of stress state on the magnitude of the resistance curves. Since the stress state experienced by the surface flaw is not well defined, it is necessary to generate R-curves specifically from surface flaw specimens, a difficult and costly task.

Assuming the availability of R-curves applicable to the surface flaw, an analysis chart (Figure 2-20) can be constructed. At a specified stress level, stress intensity curves are plotted for various flaw aspect ratios using Equation 29. In this example, criticality is determined by moving the R-curve left or right until it becomes tangent with the particular aspect ratio/stress intensity curve of interest. The initial flaw depth that will result in failure at this aspect ratio and the specified stress level is found at a_0. The potential flaw extension which may precede fracture is depicted by the difference of $a_f - a_0$. The actual point of tangency represents the flaw depth and stress intensity at failure. The more commonly measured value of K_{IE} also can be found at the intersection of a_o and the stress intensity curve. Conversely, if the initial flaw depth is specified, the failure stress at various aspect ratios can be determined in a manner similar with that described for analysis of thin sheet behavior.

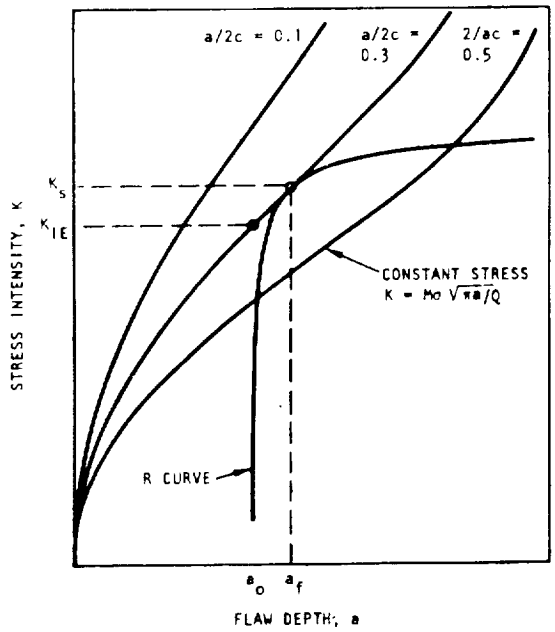

Figure 2-20. Illustration of Resistance Curve Application to Surface Flaw Analysis

Also it should be pointed out that the example illustrated in Figure 2-20 indicates that while the flaw of aspect ratio of 0.3 (at the given a_o) would "just fail" at the applied stress, σ. The flaw of aspect ratio 0.1 and same initial depth would have failed prior to reaching σ, while the 0.5 aspect ratio flaw would have grown a discrete amount during loading without failure.

An implicit assumption in the preceding simplified analysis is that as the flaw depth extends from a_o to a_f, the shape of the flaw remains constant. Since the applied stress intensity varies around the crack front, and since the value of the R-curve may differ around the crack front, a change in aspect ratio is often expected during monotonic load application. In many instances, the flaw may lose its elliptical shape by tunneling, as shown in Figure 2-21, thereby further complicating the analysis. Before employing R-curve techniques for surface flaws, the sensitivity of the analysis to assumptions regarding flaw shape or the potential of two-dimensional stable flaw growth analysis must be assessed carefully.

For Space Shuttle applications, it is anticipated that the surface flaw will be analyzed by the more conventional, K_{IE}-type values for residual strength calculations, and K_S-type estimates (maximum flaw size and failure stress) for determination of the maximum size flaw that might survive a proof test.

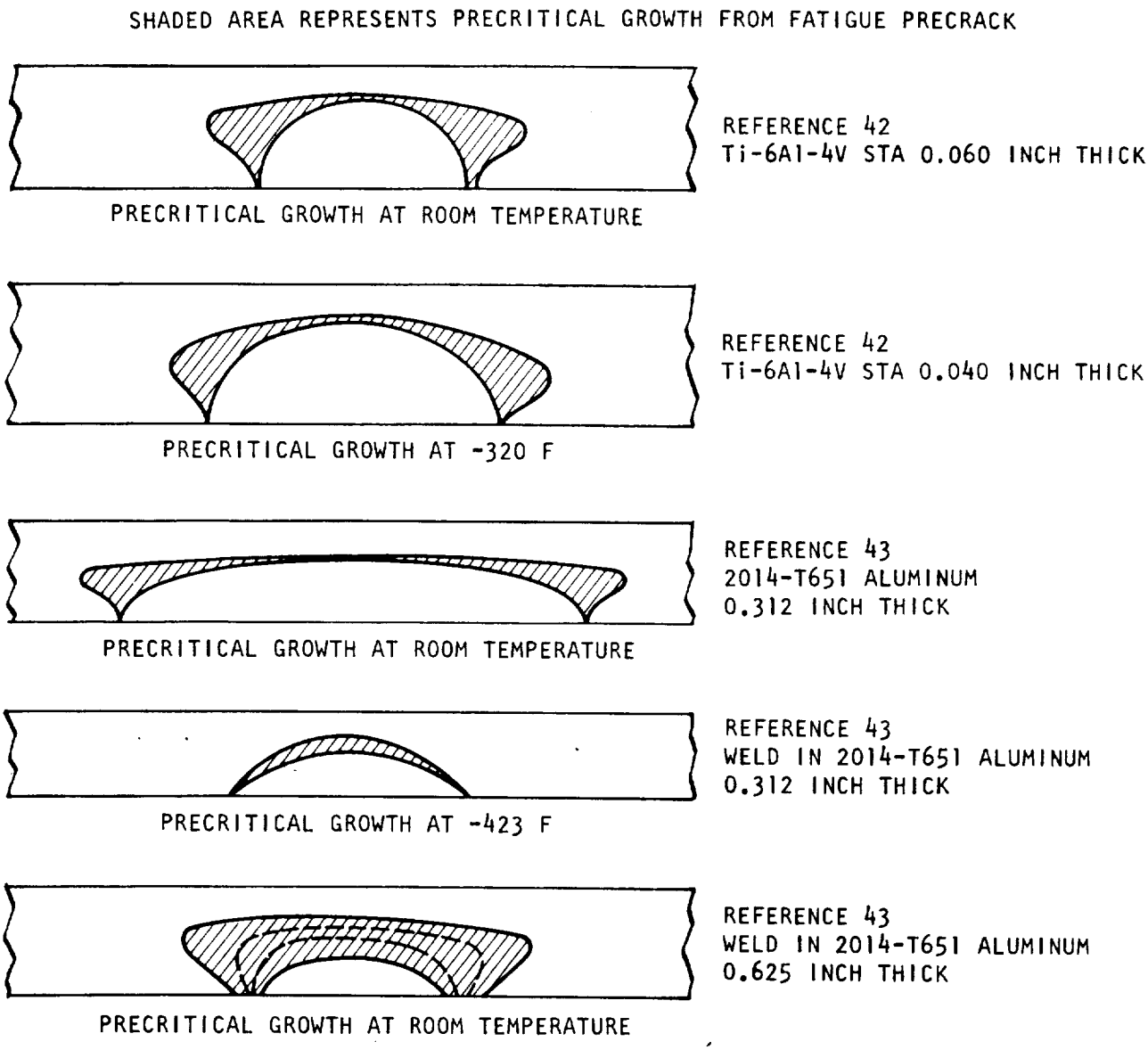

Figure 2-21. Fracture Surface Reproductions of Precritical Crack Growth

REFERENCES

1. Kaufman, J. G. "Progress in Fracture Testing of Metallic Materials," Review of Developments in Plane Strain Fracture Toughness Testing. American Society for Testing and Materials, ASTM STP 463 (1970), pp. 3-21.

2. Manjoine, M. J. Biaxial Brittle Fracture Tests. American Society of Mechanical Engineers Paper 64-MET-3 (May 1964).

3. Hahn, G., and A. Rosenfield. "Source of Fracture Toughness: The Relation Between K_{Ic} and Ordinary Tensile Properties of Materials," Applications Related Phenomena in Titanium Alloys. American Society for Testing and Materials, ASTM STP 432 (1968).

4. Krafft, J. "Fracture Toughness of Metals," Report of Progress. U.S. Naval Research Laboratory, Washington, D.C. (November 1963).

5. Krafft, J. "Correlation of Plane Strain Crack Toughness With Strain Hardening Characteristics of a Low, Medium, and a High Strength Steel," Applied Materials Research, Vol. 3 (1964), p. 88.

6. Jones, M.H., and W.F. Brown, Jr. "The Influence of Crack Length and Thickness in Plane Strain Fracture Toughness Tests," Review of Development in Plane Strain Fracture Toughness Testing. American Society for Testing and Materials, ASTM STP 463 (1970), pp. 63-101.

7. Krafft, J.M., and A.M. Sullivan. "Effects of Speed and Temperature on Crack Toughness and Yield Strength in Mild Steel," Transactions Quarterly, American Society for Metals, Vol. 56 (1963), p. 160.

8. Steigerwald, E.A. Plane Strain Fracture Toughness for Handbook Presentation. TRW AFML-TR67-187 (July 1967).

9. Brown, W.F., Jr. and J.E. Srawley. "Commentary on Present Practice," Review of Developments in Plane Strain Fracture Toughness Testing. American Society for Testing and Materials, ASTM STP 463 (1970), pp. 216-248.

10. Kaufman, J.G. Notch-Yield Ratio as a Quality Control Index for Plane Strain Fracture Toughness. Alcoa Research Laboratories, New Kensington, Pa., Al Report No. 9-73-20 (May 7, 1973).

11. Vroman, G.A. Reconsideration of the Cracked Round Bar Specimen. Rocketdyne Division, Rockwell International Corporation, Pub 572-K-11 (April 1973).

12. Rolfe, S.T., and S.R. Novak. Written discussion to The Influence of Crack Length and Thickness in Plane Strain Fracture Toughness Tests. American Society for Testing and Materials, ASTM STP463 (1970) p. 92.

13. Kaufman, J.G. Thickness Effects on Aluminum Alloys. Presented at ASTM Committee E-24 Meeting, September 23, 1969.

14. Campbell, J.E., W.G. Berry, and C.E. Fedderson, Damage Tolerant Design Handbook. Prepared by Battelle Memorial Institute, Columbus Laboratories, under the U.S. Air Force sponsorship, MCIC-HB-01 (December 1972).

15. Vroman, G.A., and R.F. Fields. Fracture Mechanics Data. Rocketdyne Division, Rockwell International Corporation, SR2112-5036 (October 1972).

16. Newman, J.C. Fracture Analysis of Surface- and Through-cracked Sheets and Plates. Presented at the Symposium on Fracture and Fatigue, Washington, D.C., May 1972.

17. Kuhn, Paul. Residual Strength in the Presence of Fatigue Cracks. Presented to the AGARD Structures and Materials Panel, 1967.

18. Kuhn, Paul, and I.E. Figgee. Unified Notch-Strength Analysis for Wrought Aluminum Alloys. NASA TN D-1259 (1962).

19. Fedderson, C.E. "Evaluation of the Residual Strength of Center-Cracked Tension Panels," Damage Tolerance in Aircraft Structures. American Society for Testing and Materials, ASTM STP 486 (1971).

20. Kraft, J.M., A.M. Sullivan, and R.W. Boyle. "Effects of Dimensions on Fast Fracture Instability of Notched Sheets," Vol. I of Proceedings, Crack Propagation Symposium. College of Aeronautics, Cranfield, England, September 1961.

21. Heyer, R.H., and D.E. McCabe. Plane Stress Fracture Toughness Testing Using Crack-Line Loaded Specimen. Paper presented at the National Symposium on Fracture Mechanics at Lehigh University, August 1969.

22. Heyer, R.H., and D.E. McCabe. Crack Growth Resistance in Plane-Stress Fracture Testing. Paper presented at the National Symposium on Fracture Mechanics at Carnegie-Mellon University, August 24-26, 1970.

23. Creager, M. "A Note on the Use of a Simple Technique for Failure Prediction Using Resistance Curves," Fracture Toughness by R-Curve Methods. American Society for Testing and Materials, ASTM STP 527 (1971).

24. Begley, J.A., and J.D. Landes. "The J-Integral as a Failure Criterion," Fracture Toughness Proceedings of the 1971 National Symposium on Fracture Mechanics, Part II. American Society for Testing and Materials, ASTM STP 514 (1971).

25. Bucci, R.J., P.C. Paris, J.D. Landes, and J.R. Rice. "J-Integral Estimation Procedures," Fracture Toughness Proceedings of the 1971 National Symposium on Fracture Mechanics, Part II. American Society for Testing and Materials, ASTM STP 514 (1971).

26. Irwin, G.R. Presented to ASTM Committee E-24 (unpublished).

27. Creager, M., and A.F. Liu. The Effect of Reinforcements on the Slow Stable Tear and Catastrophic Failure of Thin Metal Sheet. AIAA 9th Aerospace Sciences Meeting, New York, New York, 1971.

28. Little, C.D., and P.M. Bunting. "The Surface Flaw in Aircraft Structures and Related Fracture Mechanics Analysis Problems," The Surface Crack: Physical Problems and Computational Solutions. American Society of Mechanical Engineers (November 1972), pp. 11-42.

29. Rawe, R.E. Fracture Mechanics and Safe Life Design. Douglas Aircraft Corporation, DAC 59591 (August 1970).

30. Irwin, G.R. "The Crack Extension Force for a Part-Through Crack in a Plate," Transaction of ASME, Series E: Journal of Applied Mechanics, Vol. 29, No. 4 (December 1962), pp. 651-654.

31. Francis, P.H., and D.L. Davidson. "Experimental Characterization of Yield Induced by Surface Flaws," The Surface Crack: Physical Problems and Computational Solutions. ASME (November 1972), pp. 63-78.

32. Liu, H. W. Discussion to "The Effect of Size and Stress History on Fatigue Crack Initiation and Propagation." Proceedings of the Cranfield Crack Propagation Symposium, Vol. 2 (1962), p. 514.

33. Rice, J.R. "Mathematical Analysis in the Mechanics of Fracture," Mathematical Fundamentals, in Fracture, Vol 2. New York: Academic Press Inc. (1969), pp. 191-311.

34. Collipriest, J.E., Jr. Part-Through-Crack Fracture Mechanics Testing, An IR&D Summary Report. Space Division, Rockwell International Corporation, SD 71-319 (June 1971).

35. Kobayashi, A.S., and R.C. Shah. "On the Surface Flaw Problem," The Surface Flaw: Physical Problems and Computational Solutions. ASME (November 1972), pp. 79-124.

36. Kobayashi, A.S., and W.L. Moss. "Stress Intensity Magnification Factors for Surface-Flawed Tension Plate and Notched Round Tension Bar." Proceedings of the Second International Conference on Fracture, Brighton, England (1969).

37. Collipriest, J.E., Jr., and R.M. Ehret. Computer Modeling of Part-Through Crack Growth. Space Division, Rockwell International Corporation, SD 72-CE-0015A (1972).

38. Merkle, J.G. A Review of Some of the Existing Stress Intensity Factor Solutions for Part-Through Surface Cracks. Oak Ridge National Laboratory, ORNL-TM-3983 (January 1973).

39. Masters, J.N., W.P. Harse, and R.W. Finger. Investigation of Deep Flaws in Thin-Walled Tanks. NASA CR-72606 (December 1969).

40. Ehret, R.M. Part-Through Crack Growth in Bending, Hewlett-Packard Computer Program 9810-3001. Space Division, Rockwell International Corporation, (1972).

41. Ehret, R.M. Part-Through-Crack Elastic Compliance Calibration. Space Division, Rockwell International Corporation, SD 71-329 (October 1971).

42. Hoeppner, D.W., D.E. Pettit, C.E. Fedderson, and W.S. Hyler. Determination of Flaw Growth Characteristics of Titanium 6AL-4V Sheet in the Solution-Treated and Aged Condition. Battelle Memorial Institute, Columbus Laboratories, NASA CR-65811 (January 1968).

43. Collipriest, J. E., Jr., and D. E. Kizer. Final Report - Saturn S-II Fracture Mechanics Research Program. Space Division, Rockwell International Corporation, SD 68-659 (December 1968).

3.0 PRECRITICAL FLAW GROWTH

3.0 PRECRITICAL FLAW GROWTH

Because engineering structures are required to function at alternating or sustained loads throughout a dedicated lifetime (or inspection interval), the growth characteristics of preexisting flaws at operating stresses become a necessary and useful analytical tool. By establishing the size and shape of flaws that can grow to critical dimensions during service, the flaw detection requirements, inspection intervals, and other operational criteria can be defined.

Precritical or subcritical flaw growth behavior (i.e., flaw growth occurring at stress intensities below K_{Ic} or K_c) is discussed in three general categories: growth-upon-loading, cyclic-load-induced crack growth, and sustained load flaw growth.

3.1 GROWTH-UPON-LOADING

Significant precritical flaw extension resulting from a single increasing load application has been observed and reported by many investigators. As demonstrated in preceding paragraphs, the concept of K_c testing explicitly acknowledges flaw growth upon loading. Unfortunately, many fracture mechanics application approaches conveniently ignore the phenomenon and thereby risk significant error in subsequent analysis.

For example, simplified proof test logic (Reference 1) purports to identify that flaw size which will survive a given proof load. If, however, the toughness level used for flaw size calculations was based on initial flaw size and failure loads, and significant flaw growth on loading does in fact occur, the maximum flaw size estimated to survive the proof test may be seriously underestimated. This discrepancy is illustrated in Figure 3-1. Striking examples of growth on loading of surface flaws simulating proof test survival are shown in Figure 3-2 for 6Al-4V titanium and Inconel 718 (both 0.25 inch thick). In both instances, the survival stress intensity (K_s) exceeds the "normal K_{Ic}" values by a significant degree.

A second analysis approach where growth upon loading may play a significant role is spectrum or random loading profiles. Accumulative damage effects, including retardation mechanisms, are accounted for in many flaw growth analysis programs; however, accommodation of growth-upon-loading

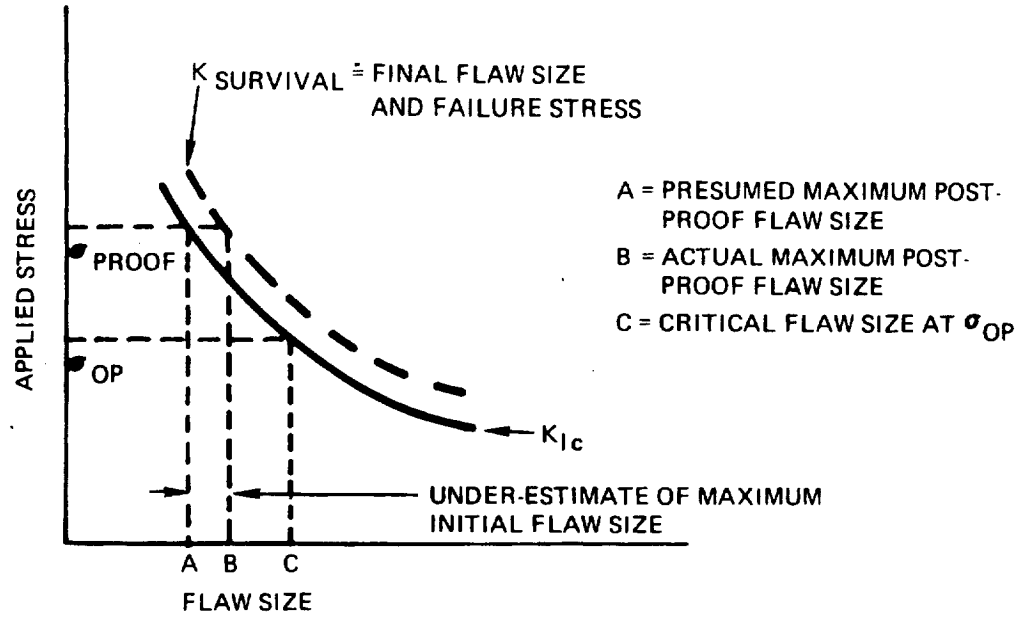

Figure 3-1. Influence of Flaw Growth-Upon-Loading on Proof Test Logic

between loading steps within a spectrum is seldom performed. This omission may result in overlooking a most significant portion of the flaw growth behavior, as illustrated in Figure 3-3.

Many measurements of growth on loading at stress intensities significantly below a critical stress intensity have been made. For example, investigators (Reference 2) in a study of crack growth retardation mechanisms reported "stretch zones" on microscopic surfaces corresponding with peak overload cycles. The sizes of these bands were reportedly more than twice the normal anticipated cyclic growth for the corresponding stress intensity range as shown in Figure 3-4. Other investigators have also reported that the measured growth upon loading is large with respect to a single-cycle fatigue rate. This may be attributed in part to crack growth attendant to the formation of a new plastic zone at the crack tip or possible stable crack geometry changes associated with differing stress levels.

Another area of analysis that demands consideration of growth upon loading is sustained load growth testing in various environments. Environmental effects are commonly evaluated by loading a preflawed specimen to

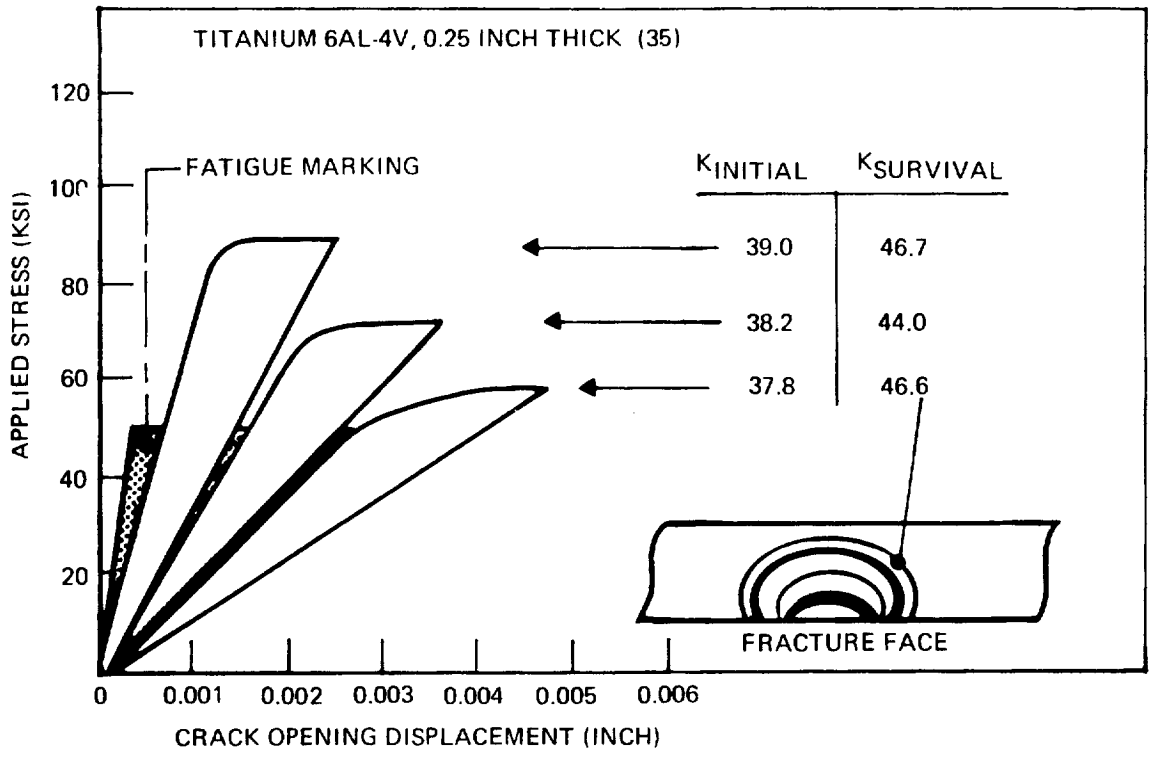

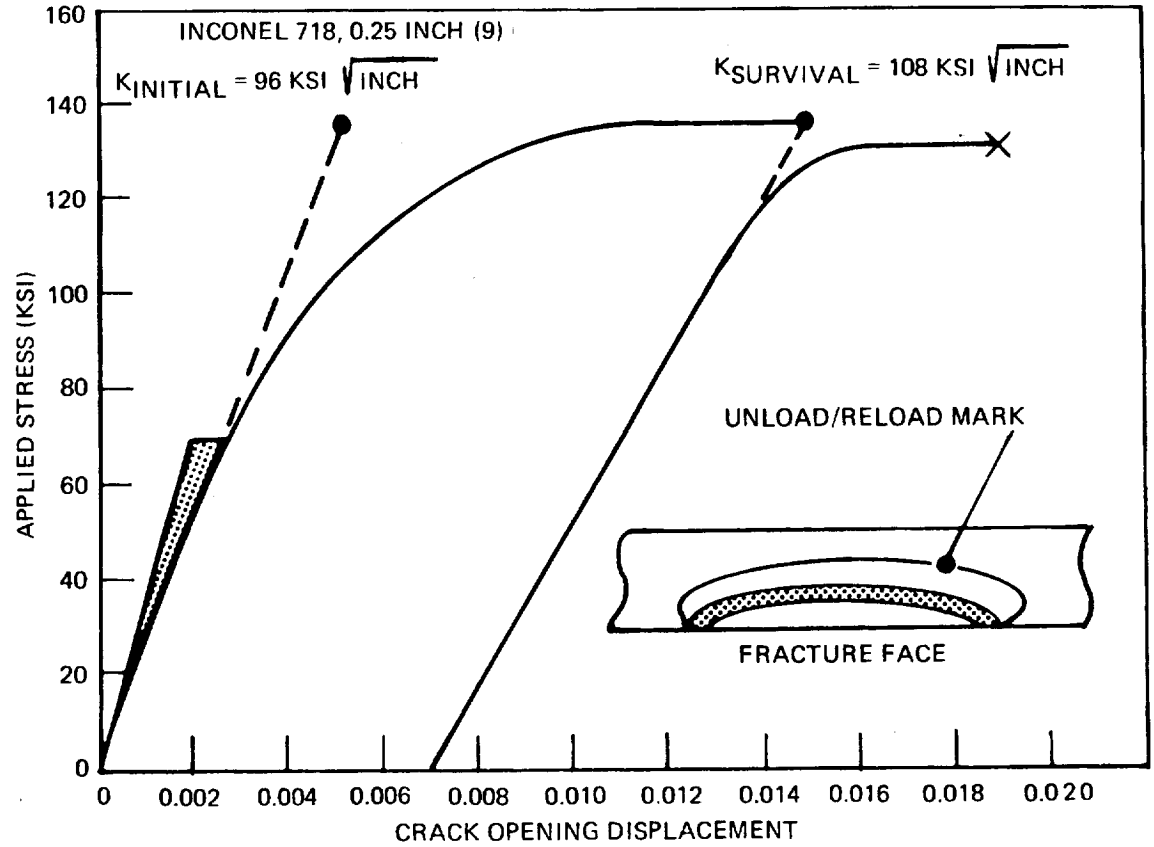

Figure 3-2. Examples of Growth-Upon-Loading During Proof Test Simulation

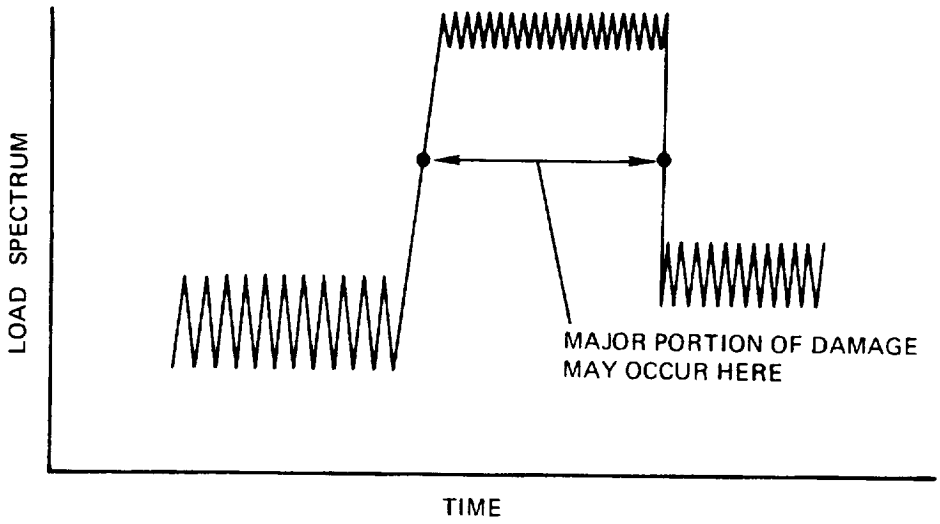

Figure 3-3. Variable Loading Profile Requiring Consideration of Crack Growth-Upon-Loading

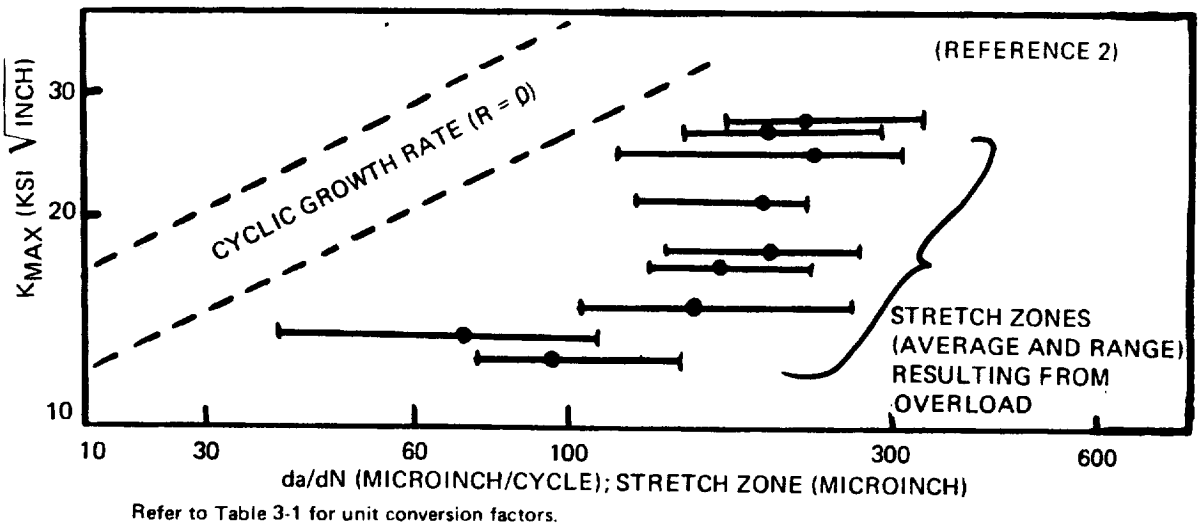

Refer to Table 3-1 for unit conversion factors.

Figure 3-4. Comparison of Cyclic Flaw Growth Rates With Microscopic "Stretch Zones" for 2024-T3 Aluminum

some predetermined stress or stress intensity level and maintaining the load for a prescribed amount of time. The fracture surface is often fatigue marked, and the measured increase in flaw size is recorded. Without proper consideration of the amount of growth on loading experienced during the initial load application, a true assessment of the effects of the environment cannot be made. An example of the type of data required to quantify growth upon loading behavior is shown in Figure 3-5 for 2219-T87 aluminum weldments.

For deep surface flaws in thin material growth upon loading will often precipitate flaw breakthrough and result in a stable through-crack (References 3, 4, 5) The subsequent failure stress and surface flaw length will often correspond to the materials' center-cracked-tension fracture toughness. Figure 3-6 shows results from a study (Reference 3) where surface flaw length, 2c, proved to be the critical flaw dimension in the PTC fracture test.

In view of the above discussion, the necessity for consideration of flaw growth on loading for fracture mechanics analysis need not be further emphasized. The real need, however, as with much of the science of fracture mechanics, is the standardization of test methods to properly quantify the phenomenon for all critical alloy systems. Crack growth resistance curve techniques, discussed in the previous section, appear to offer the greatest potential for quantitative analysis of this type of flaw behavior. Until such techniques become available for specific applications, critical Space Shuttle configurations that require consideration of growth-on-loading will require experimental verification of the analysis results.

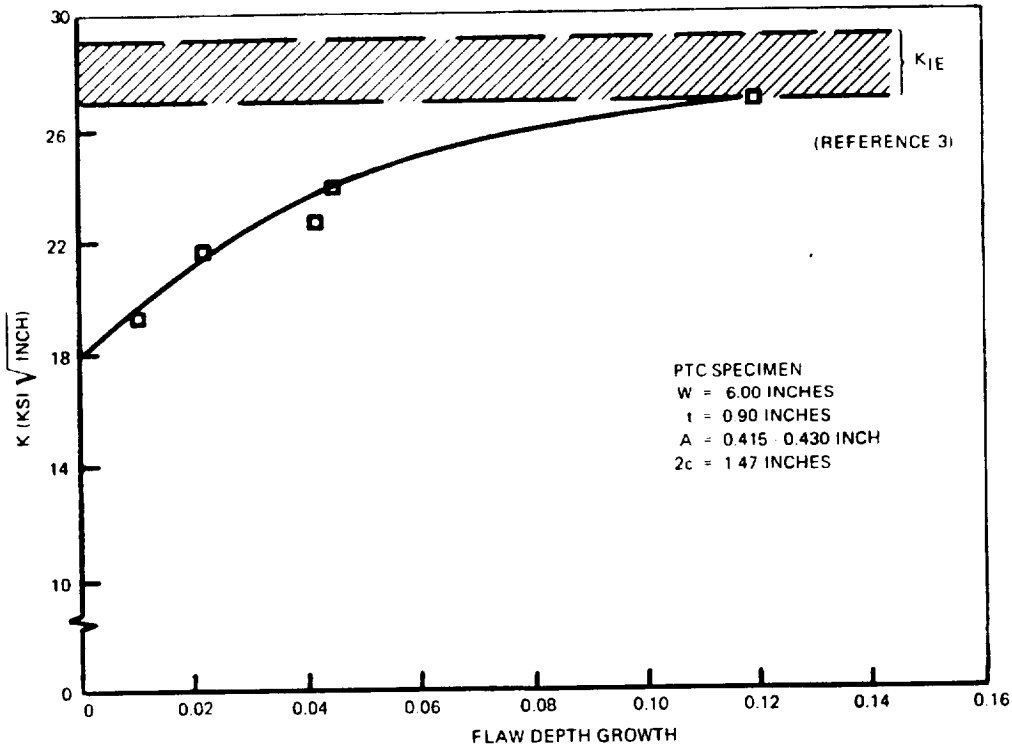

Figure 3-5. Surface Flaw Growth-Upon-Loading for 2219 Aluminum Welds

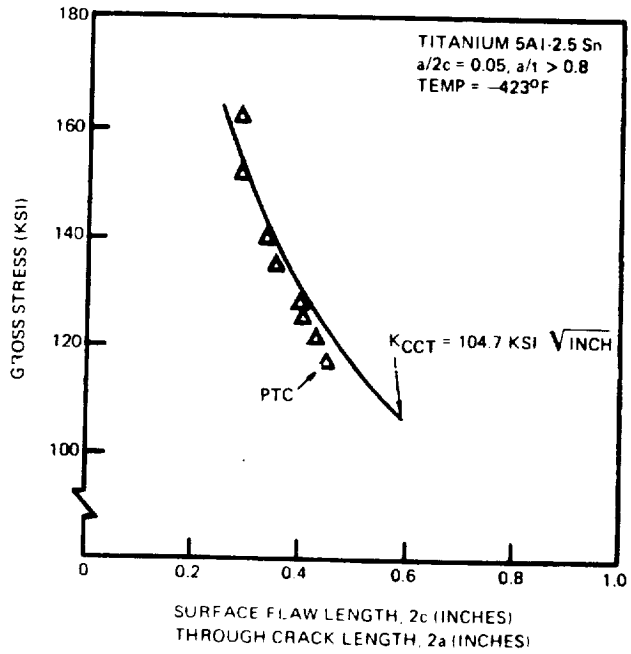

Figure 3-6. Comparison of Surface Flaw and Center-Cracked Data for Titanium Alloy

3.2 CYCLIC-LOAD CRACK PROPAGATION

Application of fracture mechanics theory to precritical flaw growth characterization has been most successful in the area of fatigue crack propagation. This may be attributed primarily to the conspicuous nature of the phenomenon which contributes to relatively convenient measurements of flaw growth. Additionally, cyclic flaw growth is generally attendant to conditions of elastic behavior which lends itself most favorably to the linear elastic fracture mechanics analysis formulations.

The following paragraphs attempt to evaluate the available fatigue crack propagation expressions, crack growth retardation theories, and environmental effects of fatigue crack growth rates.

Constant Amplitude Fatigue Crack Propagation

The first detailed work involving the stress intensity approach to fatigue crack propagation was performed by Paris and Erdogan (Reference 6). By subjecting preflawed specimens to tension-tension loading, incremental flaw extension, Δa, following a discrete number of load cycles, ΔN, was recorded and a crack growth rate, $\Delta a/\Delta N$, was calculated. The stress intensity corresponding to the maximum applied tensile stress was evaluated

using an appropriate stress intensity solution. By comparing the stress intensity excursion between minimum and maximum loads (K_{max} - K_{min} - ΔK) and the corresponding crack growth rates, a linear relationship between log ΔK and log $\Delta a/\Delta N$ was realized. Such a relationship is described by the simple power equation:

$$\Delta a/\Delta N = C(\Delta K)^n \quad (1)$$

with n corresponding to the reciprocal slope of the function on a log-log plot and C being a growth rate intercept corresponding to a unity value of ΔK, as illustrated in Figure 3-7. Test data indicate that the values of the constants C and n are dependent on material, product form, test environment, and the ratios of minimum load to maximum load, R.

As more data became available, it was observed that as the maximum cyclic stress intensity approached some critical value, K_c, the growth rate increased beyond the linear behavior illustrated in Figure 3-7. Additionally, at relatively small stress intensities, the growth rate was observed to diminish, approaching a threshold value of stress intensity below which measurable crack growth would not occur. These observations result in the sigmoidal growth rate characteristics illustrated in Figure 3-8.

To accommodate the K_c influenced crack growth rates and to provide for observed stress ratio affects, Forman (Reference 7) expanded the power relationship of Equation 1 to

$$da/dN = C\,\Delta K^n/[(1-R)\,K_c - \Delta K] \quad (2)$$

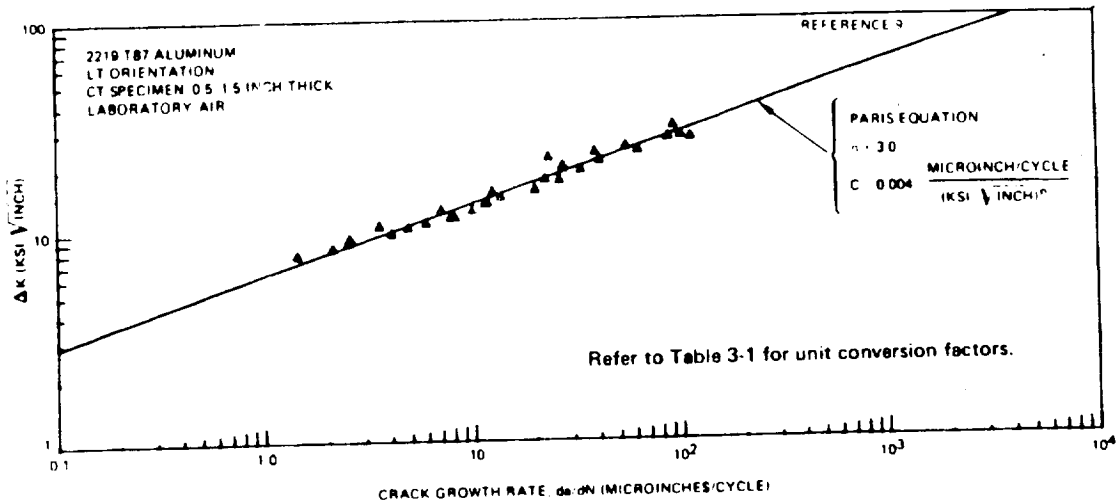

Figure 3-7. 2219 Aluminum Crack Growth Rate Data Plotted With Paris Equation

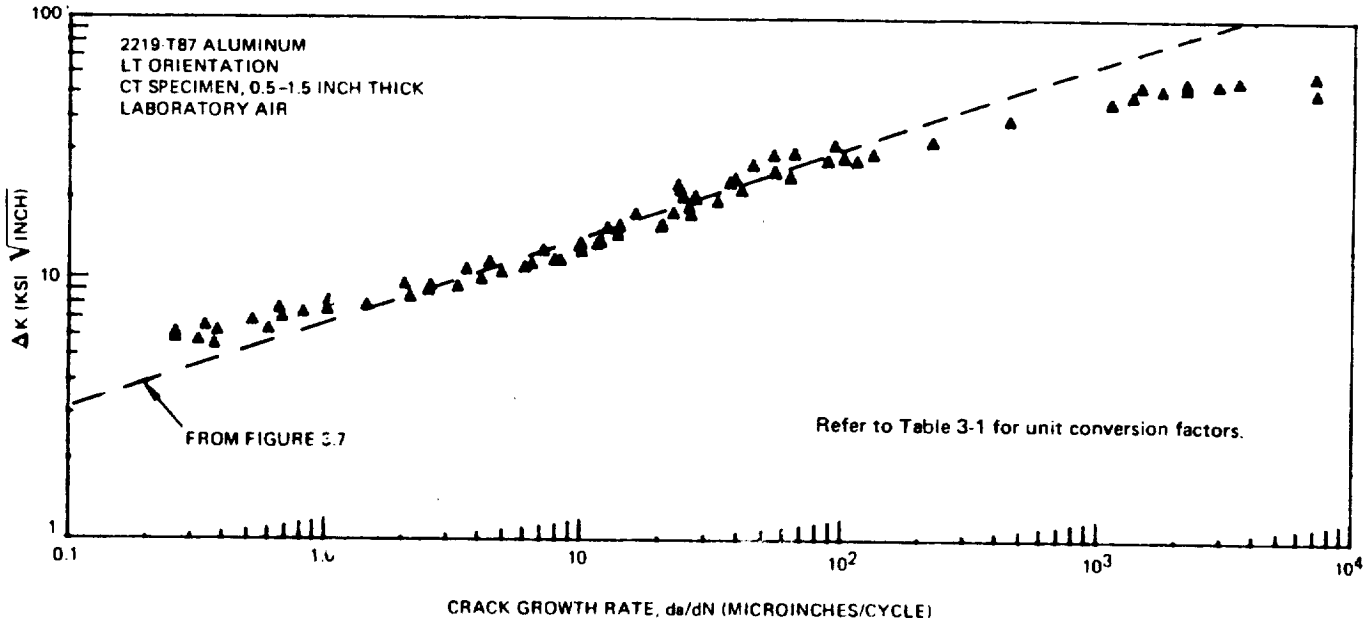

Figure 3-8. Sigmoidal Behavior of 2219 Aluminum Crack Growth Rate

The values of C and n in the Forman equation are similar to the Paris equation coefficients in origin; however, they are not numerically equivalent.

To include the growth threshold effect into a crack growth rate expression, Collipriest (Reference 8) formulated the following equation:

$$\frac{da}{dN} = \exp\left[n\left(\frac{\ln K_c - \ln \Delta K_o}{2}\right) \operatorname{arctanh}\left(\frac{\ln \Delta K - \frac{\ln\left|K_c(1-R)\right| + \ln \Delta K_o}{2}}{\frac{\ln\left|K_c(1-R)\right| - \ln \Delta K_o}{2}} \right) \ln\left(C\left[\exp\left(\frac{\ln K_c + \ln \Delta K_o}{2} n \right) \right] \right) \right]$$

Or, as arranged in a different but mathematically equivalent form (3)

$$da/dN = C\,(K_c \Delta K_o)^{n/2}\ \mathrm{EXP}\left[\ln(K_c/\Delta K_o)^{n/2} \operatorname{arctanh}\left\{ \frac{\ln\left|\Delta K^2 / \left|(1-R)K_c \Delta K_o\right|\right|}{\ln\left|(1-R)K_c/\Delta K_o\right|} \right\} \right]$$

This empirical relationship simply forces the natural sigmoidal characteristics of a hyperbolic tangent function through the test data. This equation, although much more formidable looking than the Paris or Forman equations, requires only four material-related constants,

- C = Empirical cofficient
- n = Empirical exponent
- K_c = Stress intensity for fracture
- ΔK_0 = Threshold stress intensity range for growth

and the normal input variables,

ΔK = Cyclic stress intensity range
R = Load ratio

Figure 3-9 illustrates how each of the above crack growth rate expressions approximates the growth behavior of 2024-T851 aluminum alloy. The limit of the range of applicability for each equation is clearly evident, and the accommodation of load ratio effects is also shown. It should be noted that, although the values of C and n are equivalent for Equations 1 and 3 by definition, many of the Paris equation coefficients reported in the literature attempt to accommodate data beyond the linear range. Subsequently, incorporation of Paris coefficients into Equation 3, without proper attention to the data they were extracted from, can produce erroneous results. Additionally, caution must be exercised when attempting to utilize published values of the growth rate coefficients C and n. In each instance, the units for C, ΔK, and the resulting da/dN must be known and must correspond with one another. Special care must be taken when transferring the value of coefficients between SI and English systems. Table 3-1 contains conversion factors for the basic values of the growth rate expressions.

The three empirical cyclic crack growth rate expressions identified in the preceding paragraphs require a relatively small amount of carefully measured test data to identify the coefficients and thereby characterize a material systems behavior. Each of the three equations can be easily linearized allowing statistical determination of the coefficients C and n by least-square regression analysis of crack growth data.

Presently, it does not appear correct to assume that any single treatment of load ratio (R) effects will properly describe fatigue crack growth rates for every alloy system subject to fracture mechanics analysis for Space Shuttle. The load ratio effect on many aluminum and titanium alloys does appear to be adequately described by Equations 2 or 3. Crack growth rates in 9Ni-4Co steel, however, appear to require some different treatment to accommodate load ratio effects. Recent works attempting to incorporate the observed load ratio effects into a single driving force parameter have met with moderate success. Several investigators (References 10, 11, 12) recommended a more general equation for expressing flaw growth rates using a coupling parameter, m. The analysis identifies an effective stress intensity range termed $\overline{\Delta K}$ corresponding to the following relationship:

$$\overline{\Delta K} = (1 - R)^m K_{max}$$

The value of the constant m was determined experimentally (Reference 13) for two aluminum alloys to be approximately 0.5. In the event that such a simplified relationship is shown to adequately accommodate load ratio effects for many materials, its application in other areas, especially in crack growth retardation studies will be truly appreciated.

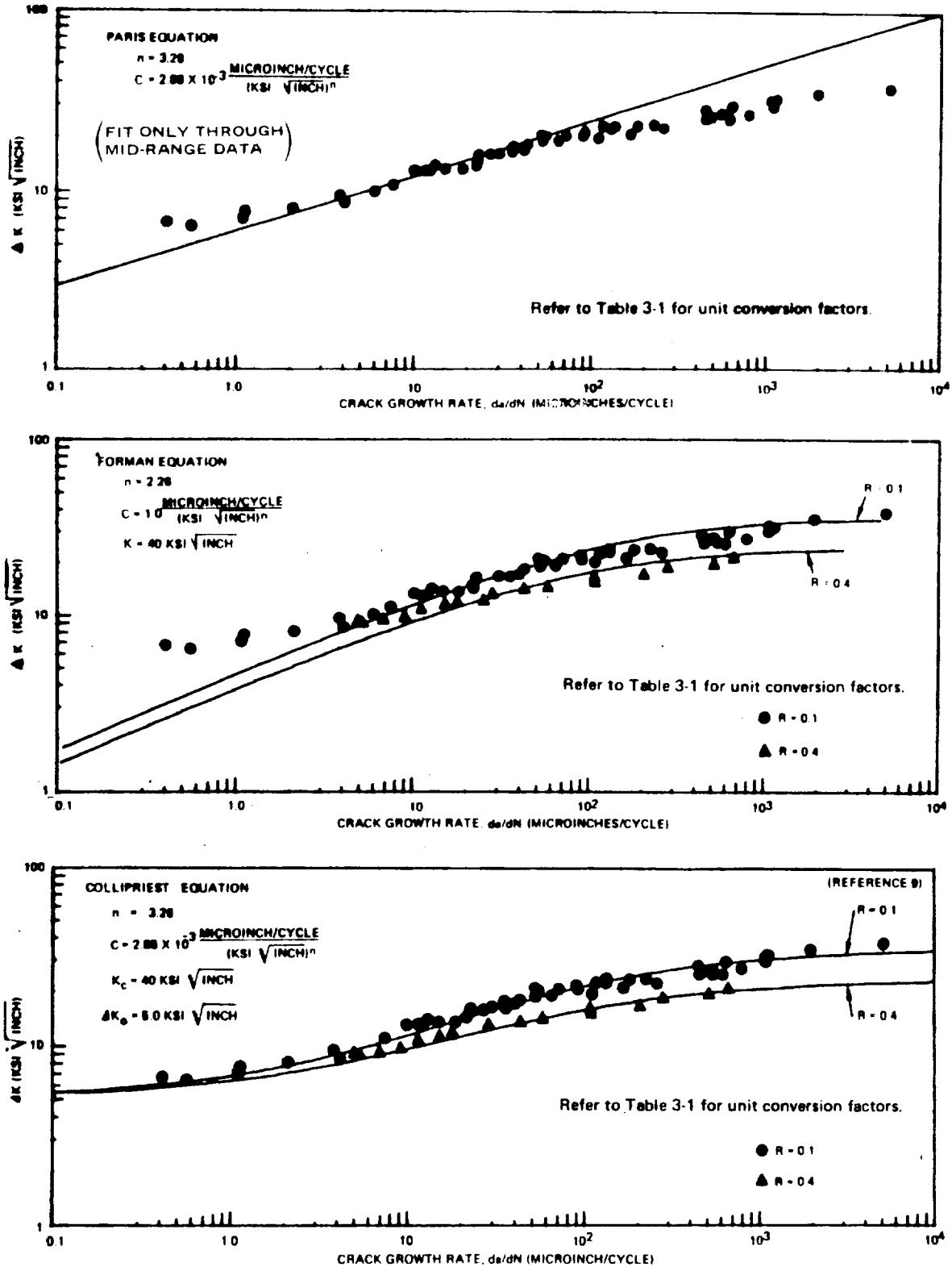

Figure 3-9. Accommodation of 2024-T851 Aluminum Crack Growth Rate Data by Three Growth Rate Expressions

Table 3-1. Conversion Factors for Crack Growth Rate Values

Multiply	By	To Obtain
ΔK, ksi $\sqrt{\text{inch}}$	1.0988	ΔK, $MN(m)^{3/2}$
da/dN, microinch/cycle	25.4	da/dN, nanometer/cycle
C, $\frac{\text{microinch/cycle}}{(\text{ksi}\sqrt{\text{inch}})^n}$	$\frac{25.4}{(1.0988)^n}$	C, $\frac{\text{nanometer/cycle}}{(MN(m)^{3/2})^n}$

Several other formulations involving secondary parameters have been offered (Reference 14). The value of such expressions is, however, self-limiting when large amounts of data are necessary to statistically characterize various "material constants." That is, with enough material data available, simple graphical display, best-fit polynomial expressions, or linear interpolation schemes will provide sufficient characterization of the materials' fatigue crack growth behavior. These statements are not intended to imply that better expressions relating crack growth rates would not be appreciated; however, emphasis towards more mechanistic characterization of the phenomenon would appear to be most advantageous.

Representation of surface flaw crack growth rates in terms of the shape and plasticity-normalized flaw size, or d(a/Q)/dN, was evaluated by Little (Reference 15). By combining data from Reference 16 on crack growth rates (da/dN) for several D6AC steel specimen configurations (Figure 3-10),

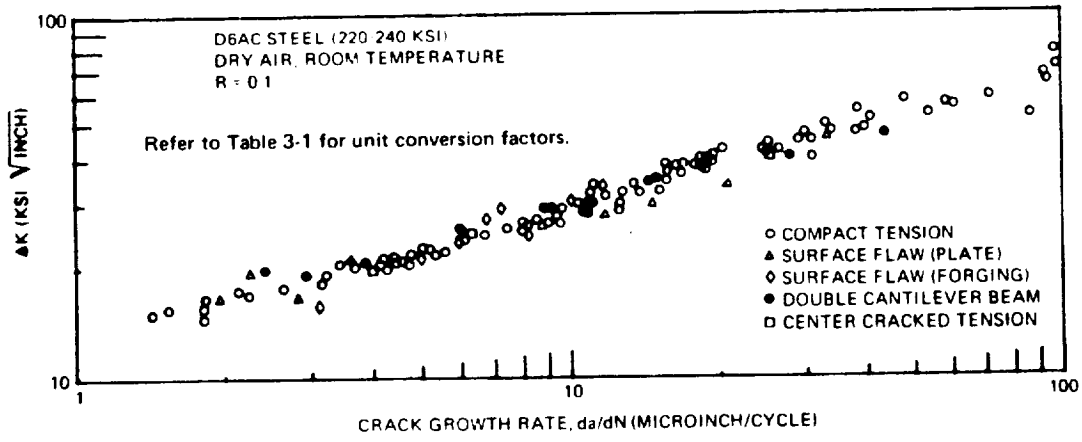

Figure 3-10. Specimen-to-Specimen Crack Growth Rate Correlation

it was concluded that the effects of the shape parameter, Q, on crack growth rates in surface-flawed specimens are adequately accommodated in the computation of stress intensity, K. To use Q a second time in the computation of crack growth rate appears to be an unnecessary complication which actually distorts correlation of crack growth rate data from the surface flaw with that obtained from other specimens.

End-point analysis of fatigue crack growth data has been employed by many investigators. This method of analysis is frequently utilized in the development of a proof test logic, as described in Reference 1. By representing cycles-to-fracture as a function of the initial-to-critical stress intensity ratio at the start of cycling, a characteristic relationship illustrated in Figure 3-11 is obtained. When end point analysis is restricted to conditions for which the critical flaw size is less than one-half the well thickness, it provides a convenient, one-dimensional representation of the cyclic life subsequent to the imposition of any initial stress intensity for surface flaw specimens. Where critical flaw sizes exceed one-half the specimen thickness, back surface stress intensity magnification becomes significant and is highly dependent upon flaw shape and depth-to-thickness ratio. In effect, the stress intensity gradients differ significantly between surface flaw specimens having identical stress levels and thicknesses but different flaw shapes. These conditions make the use of end-point analysis for representing cycles to penetration (leakage) a highly questionable procedure which would require complete correspondence among flaw shapes, thicknesses, and stress levels between specimen and component for reliable results. Such limitations on the use of end-point analysis make its use for generalization of crack growth data subject to possible errors and not a technique recommended as a versatile, general approach to analysis of proof test results.

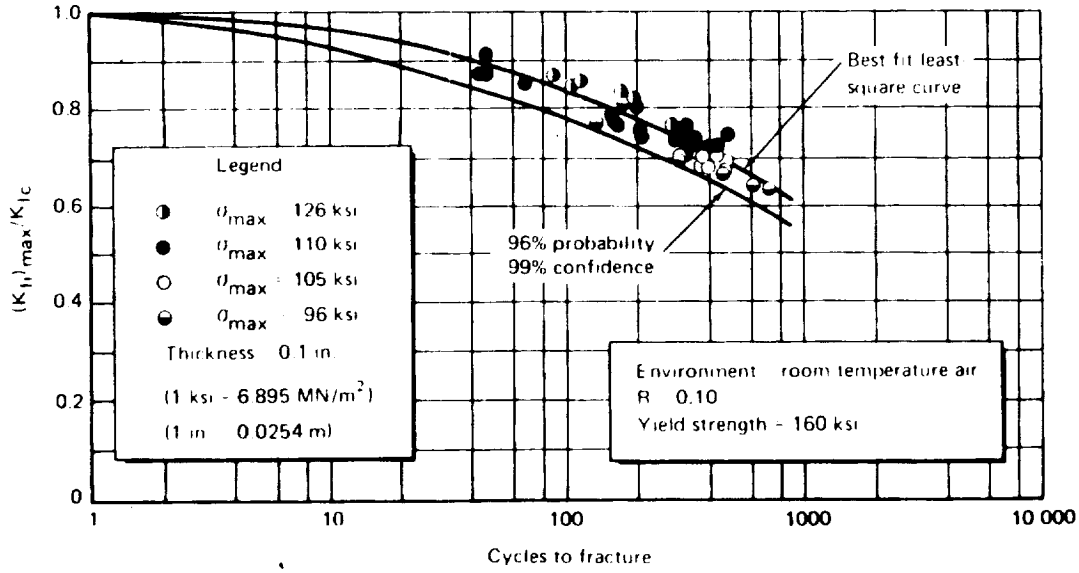

Figure 3-11. Cyclic Flaw-Growth Data for Heat-Treated 6Al-4V Titanium

Retardation and Closure Forces

The cyclic growth rate relationships described above provide reasonable agreement between predicted and actual crack growth for constant load amplitude conditions. However, significant variation between predicted and actual crack growth is frequently observed for cases of mixed load amplitude. In general, cyclic crack growth will be retarded when preceded by a higher maximum load application. The total effect of prior load history, however, is quite complex, and behavior more closely associated with the mechanisms of fatigue crack propagation must be considered.

Variable load amplitude conditions will occur in a variety of situations such as single-cycle overloads (e.g., produced by a proof test), constant amplitude block changes, and ordered flight load spectrum (see Figure 3-12).

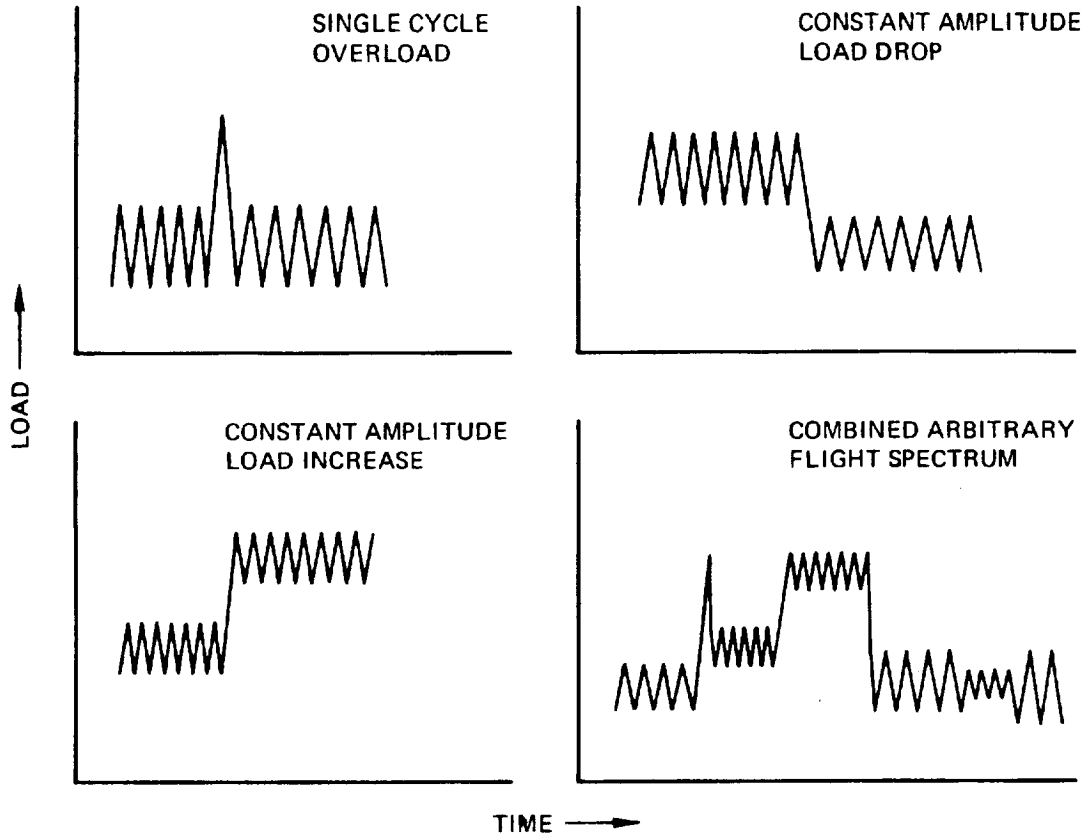

Figure 3-12. Typical Variable Load Amplitude Profiles

The crack growth rate following the single-cycle overload has been observed to be completely arrested following high overloads, to be severely retarded at moderate overloads, and to exhibit no measurable change at small overloads. In the most severe cases of overload, where test specimens were near failure, the subsequent cyclic life has been observed to decrease significantly because of crack extension during the overload application.

Similar behavior has been demonstrated following a constant amplitude load drop, where, depending on the magnitude of the change, complete arrest or moderate retardation, followed by a discrete recovery period to the normal growth rate, will occur. Sudden constant amplitude load increases, on the other hand, have been observed to increase and subsequently decay to the anticipated crack growth rate in what might be considered an inverse of the retardation mechanism.

Naturally, the desired product of any retardation model must be a demonstrated applicability to an identified complex load spectrum simulating anticipated service conditions.

Several papers have been published which touch on growth retardation in some way; however, the availability of computational techniques providing accurate accommodation of load change effects is very limited. Currently popular mechanistic approaches to the problem involve either yield zone interactions or crack closure forces.

Two retardation models using yield zone approaches have progressed to the point of operational use with general growth computation programs. These are the Wheeler model and the Willenborg model.

Analysis of crack propagation is usually performed by integration of one of the established functional relationships for crack growth rate as a function of the change in crack tip stress intensity. Since there are different forms of this relationship, only the functional dependence will be indicated, as follows:

$$da/dN = f(\Delta K)$$

Therefore, the generalized approach under constant amplitude load conditions is to sum the damage incurred during each load cycle to accumulate the total damage after N cycles, or

$$a_N = a_0 \sum_{i=1}^{N} f(\Delta K_i) \qquad (5)$$

where a_N is the flaw size following N load applications and a_0 is an initial flaw size.

To incorporate retardation effects into the cumulative damage approach from above, Wheeler (Reference 17) suggest modification of Equation 4 to the following:

$$a_N = a_0 + \sum_{i=1}^{N} C_{p_i} f(\Delta K_i)$$

where C_{p_i} is termed a retardation parameter which acts as a multiplier to reduce the growth rate described by $f(\Delta K_i)$. The retardation parameter is

required to increase from a minimum value immediately following a load drop to its maximum value of unity when the current crack size plus its yield zone moves past the residual yield zone from the previous maximum load (see Figure 3-13).

These boundaries conditions are quantified by the following relationships:

$$C_p = (R_y/a_p - a)^m$$

when

$$a + R_y < a_p$$

and

$$C_p = 1 \text{ when } a + R_y \geq a_p$$

where

R_y = Yield zone size at current stress
a = Current crack length
$(a_p - a)$ = Distance from crack tip to the residual elastic plastic interface (see Figure 3-13).
m = Shaping exponent

The exponent m is an empirical constant necessary to shape the retardation parameter to correlate with test data. Figure 3-13 shows the effect of various values of m on C_p for a hypothetical example.

The second retardation model involving yield zone interaction has been proposed by Willenborg (Reference 18). Growth rate retardation is accommodated by operating on the crack growth driving function, ΔK. An effective value of the stress intensity range is computed by quantifying a residual crack tip stress which is present following an overload or load reduction.

A reduction in applied stress due to crack progression through a residual plastic zone of size a_p is equivalent to:

$$\sigma_{red} = \sigma_{a_p} - \sigma_{max}$$

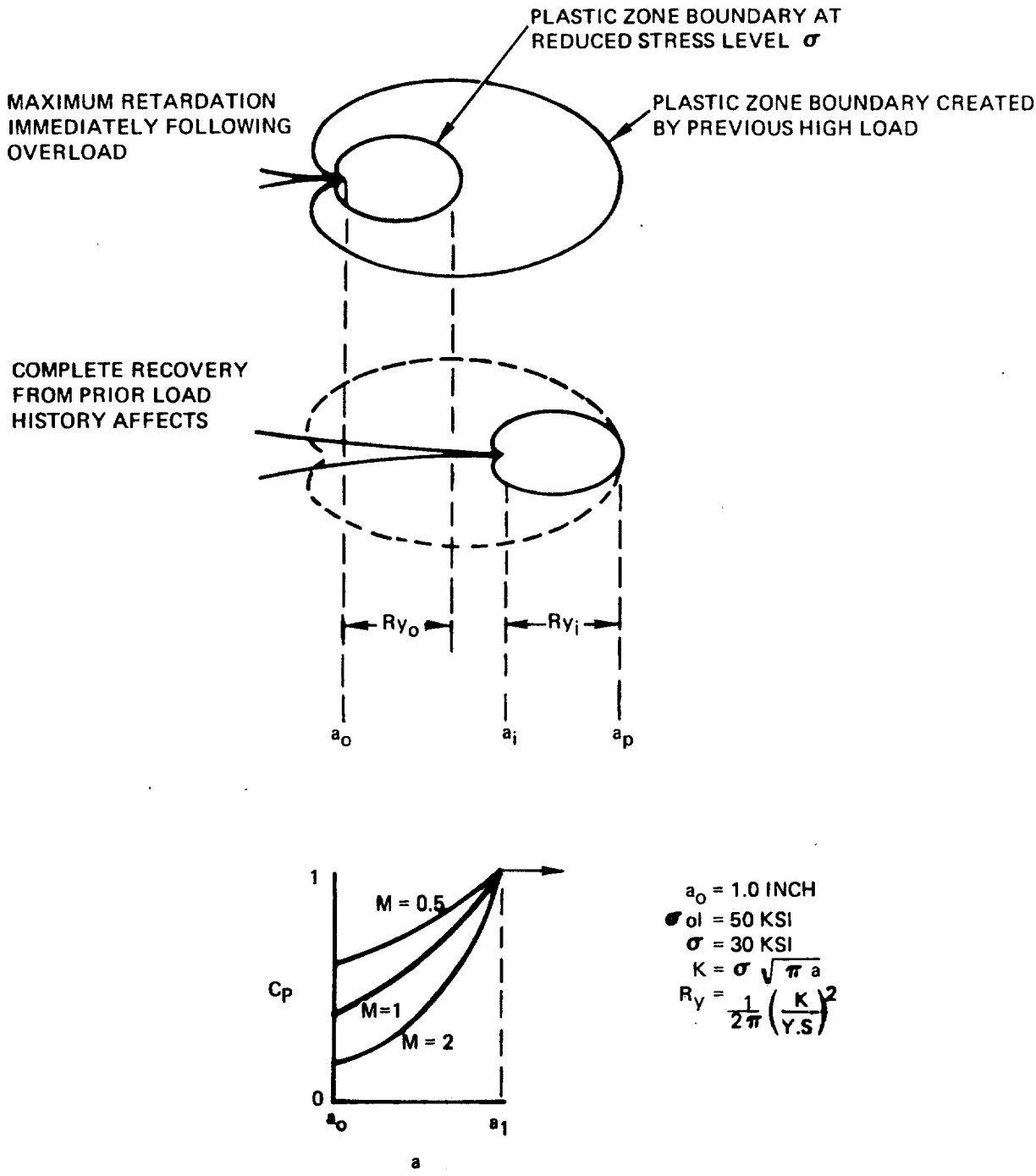

Figure 3-13. Wheeler Retardation Model

where σ_{max} is the maximum operating stress at the reduced load and σ_{ap} is the stress level required to produce a crack length plus plastic zone $(a + R_y)$ large enough to extend past the residual plastic zone dimension, a_p, created by a previous higher load.

For a generalized stress intensity relationship of $K = \beta \sigma \sqrt{\pi a}$, and a plastic zone size represented by

$$R_y = \frac{K^2}{2\pi\sigma_y^2} = \beta^2 a \sigma^2 / 2\sigma_{ys}^2$$

the reduction in applied stress can be calculated (with the consideration that $a_p = a + R_y$ when $\sigma = \sigma_{ap}$) as follows:

$$\sigma_{red} = \frac{\sigma_y}{\beta}\sqrt{\frac{2(a_p - a)}{a}} - \sigma_{max}$$

The effective values of the maximum and minimum applied stress are then calculated as:

$$(\sigma_{max})_{effective} = \sigma_{max} - \sigma_{red}$$

$$(\sigma_{min})_{effective} = \sigma_{min} - \sigma_{red}$$

When crack growth or load increase produces $a + R_y \geq a_p$, σ_{red} is set to zero. If either of the effective stresses is less than zero, it is set equal to zero

The effective values of R and ΔK are then used for evaluating an appropriate crack growth relationship. Following each load cycle, a test for the size of a_p must be performed and the corresponding effective stresses calculated.

Both of the above models depict maximum retardation at the point of overload or load reduction. Duration and rate of recovery calculation differ although all are related to nominal plastic zone calculations. The Wheeler model will never predict total crack arrest; the Willenborg model would predict growth arrest when $\sigma_{max} \leq 0.5\ \sigma_{ap}$. Neither of the models described is completely satisfactory in predicting spectrum load effects. Failure to accommodate delayed retardation following overload cycles and acceleration following a block loading increase are two specific deficiencies.

A somewhat different approach to retardation mechanisms has been proposed by Elber (Reference 19) and von Euw (Reference 2). The model rejects the implicit assumption of previous work that a crack is closed only under compressive or zero load. Instead, it is proposed that during crack propagation, a zone of residual tensile deformation is left in the wake of a moving crack tip. Upon unloading, these deformations can cause crack closure to occur above zero load which subsequently increases the effective minimum stress during cyclic load application. The net result of the increase in minimum stress is a decrease in the effective stress intensity range (ΔK) and a corresponding decrease in crack growth rate. The crack closure model requires that closure forces be continually in effect, regardless of loading spectrum, but that their magnitude is directly related to prior load history.

Evidence of crack closure forces can be found by analyzing load-displacement records. It would not be uncommon to observe a load-displacement record for a specimen following fatigue precracking to have the characteristics shown in Figure 3-14. The nonlinear behavior can result from either material nonlinearity (plasticity) or a change in geometric configuration. Since the relatively low loads should not involve plastic response or crack extension, the configuration change is then explained by crack closure. Referring to Figure 3-14, the crack is fully open between Points D and C during unloading, gradually closes between the Points C and B, and is closed between Points B and A.

For conditions of constant amplitude cyclic loading, crack propagation is then considered to occur only during that portion of the loading cycle in which the crack is fully open at the crack tip. Crack growth rates must

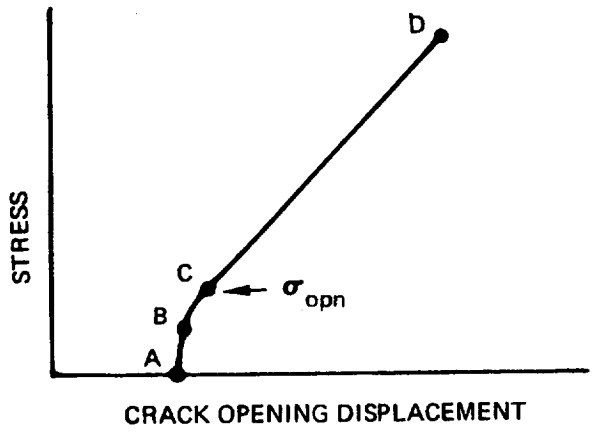

Figure 3-14. Typical Load-Displacement Record With Evidence of Crack Closure

then be evaluated using a minimum effective stress (σ_{opn}) and correspondingly adjusted load ratio ($R_{eff} = \sigma_{opn}/\sigma_{max}$), as indicated in Figure 3-14. Total crack arrest would be predicted if σ_{opn} is greater than σ_{max}.

When applied to crack growth retardation analysis, the closure model can account for several of the observed inconsistencies associated with the yield zone models, in addition to providing a rational basis for the more conventional retardation behavior.

Observations (Reference 2) that a fatigue crack may continue to grow at a decreasing rate for some time following a large overload and then completely arrest have been termed "delayed retardation." This behavior can be accounted for by examining the large plastic zone ahead of the crack tip which was created by the high load cycle. The elastic material surrounding the plastic zone acts like a clamp or closing force on this zone, causing the compressive residual stresses. While this plastic zone is ahead of the crack tip, it does not influence crack opening. The closure force action will build up as the crack propagates into the plastic zone, and then a larger applied stress will be required to open the crack. This causes crack growth to decelerate. At this point, the crack growth may or may not completely arrest. The growth rate should then recover as the crack progresses through the perturbed region.

Conversely, observations that crack growth rates may temporarily accelerate following a load amplitude increase (and then decay to the anticipated growth rate for this increased stress level) can also be accounted for by closure concepts. Immediately following a load increase, the effective ΔK is large. As the crack progresses at the higher load, the closure forces will build up to a new and characteristic value of ΔK and thereby gradually decreasing the growth rate to its anticipated value.

In a recent investigation by Jones (Reference 20), it was reported that strain hardening can result in an increase in constant amplitude cyclic crack growth rate for 6Al-4V titanium. This result negates the influence of strain hardening mechanisms as a viable retardation influence when yield zone models are employed. However, using the closure model, strain hardening may act to locally strengthen closure forces in the wake of the moving crack and thereby increase the retardation effects.

In summary, the effects of retardation forces on crack growth and corresponding structural lives could provide significant weight savings if accurately accommodated in a structural design. It does appear, however, that for Space Shuttle applications, the benefits of retardation cannot be realized without a dramatic and timely breakthrough in quantifying retardation effects.

Environmental Effects on Fatigue Crack Growth

Environmental influence on fatigue crack growth rate will often be a major consideration when attempting to generate useful estimates of service life. An environment is classified, with respect to fatigue crack propagation, as either passive (inert) or active (agressive).

A passive environment will define a baseline characteristic crack growth behavior free from chemical and thermal influence. For example, room temperature dry argon or nitrogen or a vacuum are all classified as passive environments. For practical engineering applications, it is necessary to extend this definition of passive environment to include room temperature dry air (unless a significant deviation from a truly passive environment has been identified). A chemical or thermal environment which will not measurably affect crack growth rate behavior, after due consideration of known affecting variables, is also defined as a passive environment.

Alternately, an active environment will change the baseline crack growth rates by some electrochemical mechanism such as stress corrosion, or any number of other observed phenomena. Since there exist approximately as many theories for environmentally influenced cracking mechanism as there are theorists, it would not be prudent to attempt to relate observed test results to cracking mechanisms. Rather, a display of observed environmental influences on fatigue crack growth rates will be presented to illustrate the need to avoid sweeping generalizations and to properly represent the complex nature of the subject.

Many factors will influence the effect of active environments on fatigue crack growth rates. Such factors include the chemical nature of the environment, the interactions between gases in the environment, the environment used for baseline data, the cyclic frequency of the test, the stress states and stress intensity levels, alloy chemistry, prior thermal and mechanical treatment of the alloy, the strength level of the material, and the sample geometry used in the test.

The most common active environment for aluminum is water vapor. Less dramatic effects are associated with oxygen, and somewhat controversial results have been obtained in hydrogen (Reference 21). Figure 3-15 illustrates the effect of humid versus dry argon atmosphere on the fatigue crack growth rate of 7075-T6 aluminum sheet (Reference 9). A water vapor pressure effect has been shown (Reference 22) whereby crack growth rate is virtually unaffected until a threshold pressure is reached and then increases rapidly with pressure until eventually no further increase is noted; however, the threshold pressure is also observed to be a sensitive

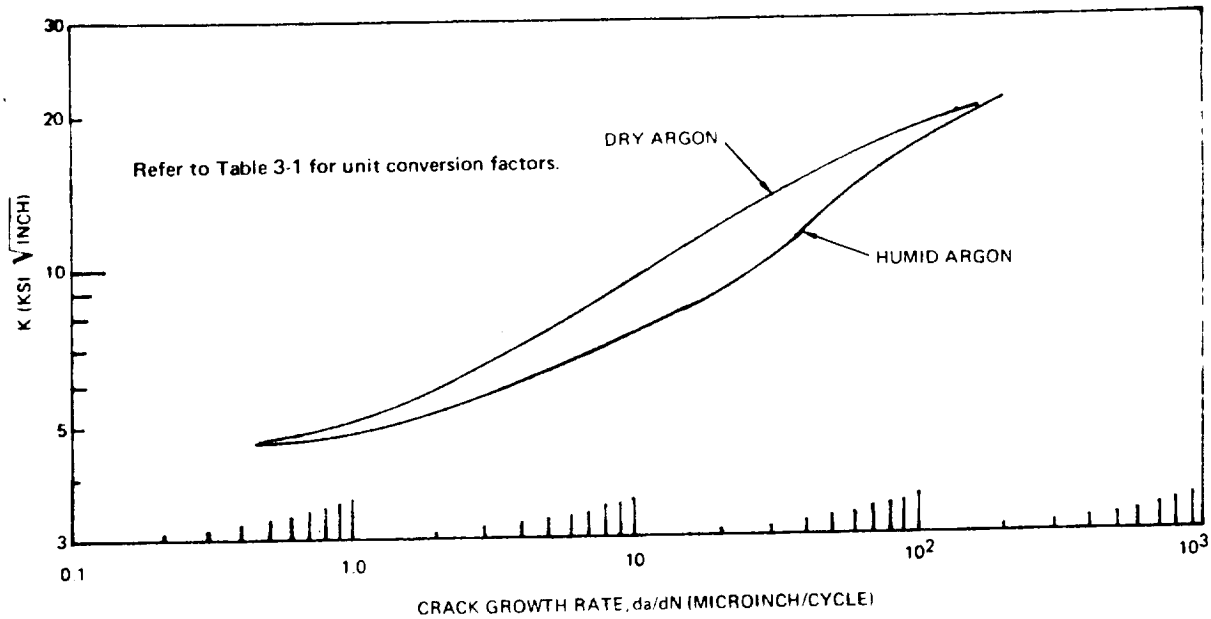

Figure 3-15. Influence of Humidity on Crack Growth for 7075-T6 Aluminum Sheet

function of test frequency. The limited magnitude of moisture effects on the fatigue behavior of aluminum, however, does not seriously restrict normal application of most aluminum alloys.

The effect of distilled water on the crack propagation rate of D6AC steel was reported by Feddersen (Reference 16) and is illustrated in Figure 3-16. Over the range of stress intensities evaluated, the crack growth rate is uniformly accelerated by approximately one-half an order of magnitude.

The effect of hydrogen gas as a fatigue crack growth accelerator is often quite large in ferritic steels, nickel base alloys, and titanium alloys but small or nonexistent for aluminum and copper-base alloys. Figure 3-17 illustrates effects of gaseous hydrogen at ambient temperature on 6Al-4V titanium and weldments (Reference 23). The reported increase in crack growth rate due to hydrogen was shown to diminish with decreasing temperature and essentially disappear at temperatures approaching -200°F.

Figure 3-18 illustrates an effect of salt water environment on fatigue crack growth rates for titanium (Ti-6Al-4V MA) sheet. For these particular data, it was observed that the merging of laboratory air and salt water growth rates corresponds with a flat to slant rotation of the crack plane. This behavior may be attributed to stress-accelerated corrosion

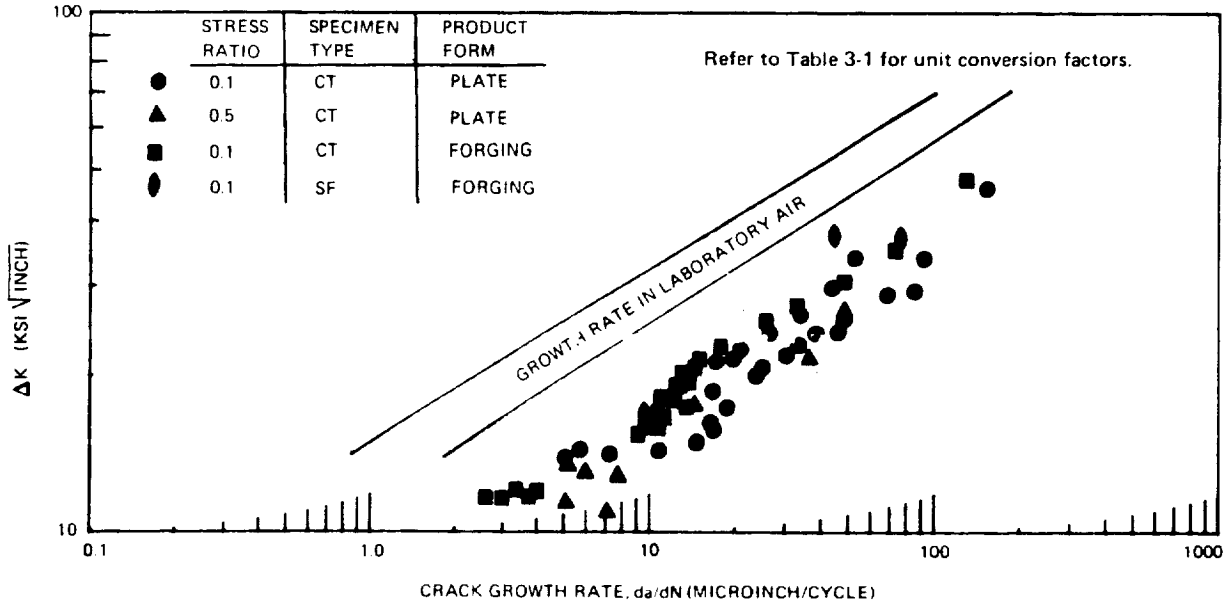

Figure 3-16. Effect of Distilled Water on Fatigue Crack Propagation Rate for D6AC Steel

mechanisms requiring particular stress state conditions at the crack tip. An equally significant observation from the test data, however, is that crack growth rates are accelerated at lower values of stress intensity. This result contradicts a common generalization that there is no influence of environments on fatigue crack growth rates at stress intensities below K_{Iscc}.

This observation was further illustrated by Crooker and Lange (Reference 24) for several high-strength structural steels. Figures 3-19 through 3-21 illustrate a lack of correlation between fatigue crack growth behavior in salt water environment and the stress corrosion cracking parameter, K_{Iscc}. In this instance, the lack of correspondence between the two modes of subcritical flaw growth was attributed to the time-dependent behavior of stress corrosion mechanisms in these alloys. Regardless of the cause for environmental acceleration of fatigue crack growth rates below measured K_{Iscc} values, the need for its consideration in service-life analysis approaches has been demonstrated.

The influence of cyclic rate during corrosion fatigue testing has been observed for many years. Due primarily to the time-dependent mechanisms associated with many corrosion cracking theories, it is reasonable to conclude that the relative amount of time that a crack is exposed to a stressed condition can be proportional to the rate of crack extension.

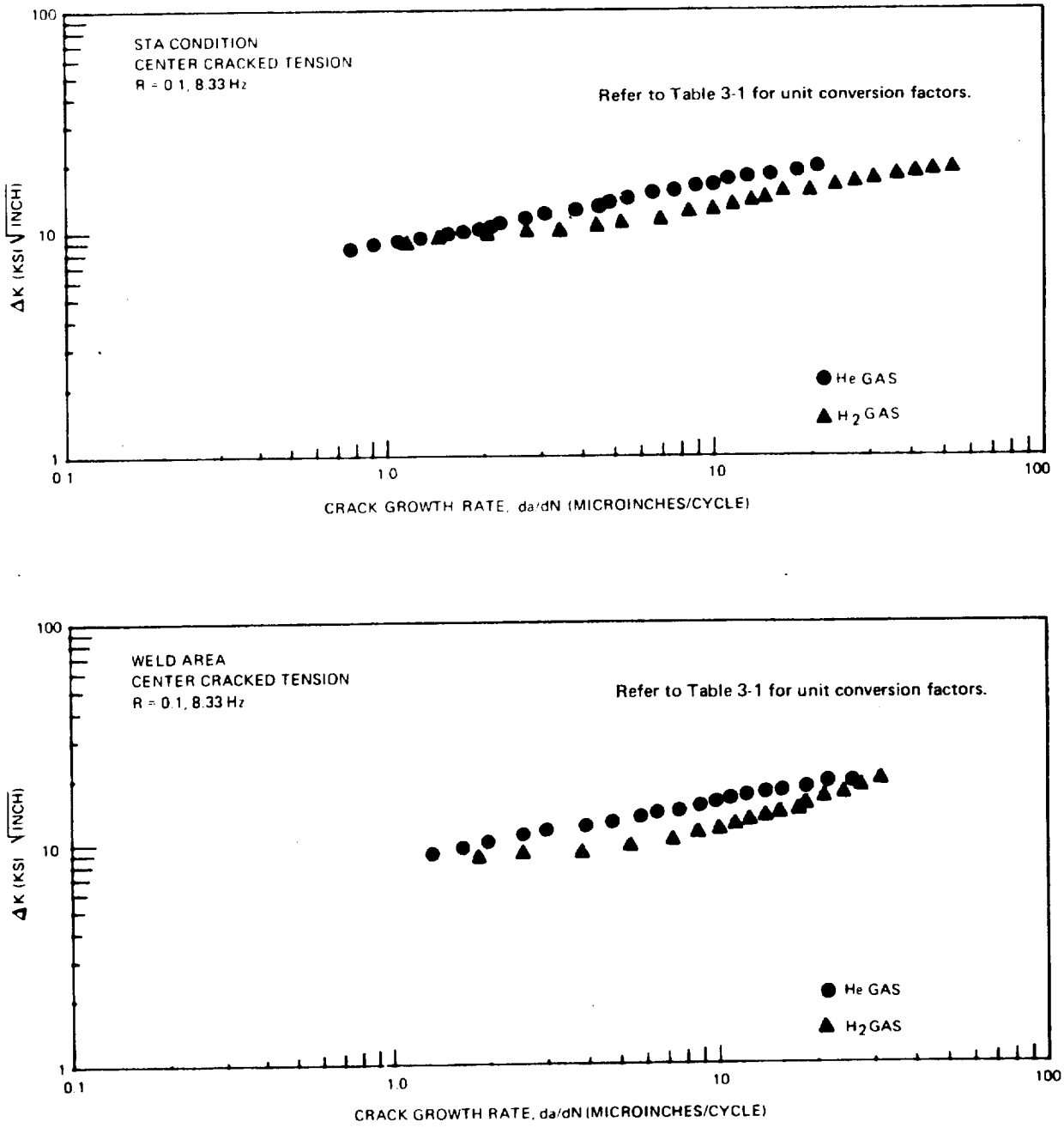

Figure 3-17. Effect of Hydrogen Gas on Fatigue Crack Propagation for Ti-6A-4V ELI Forged Material Tested at Ambient Temperature

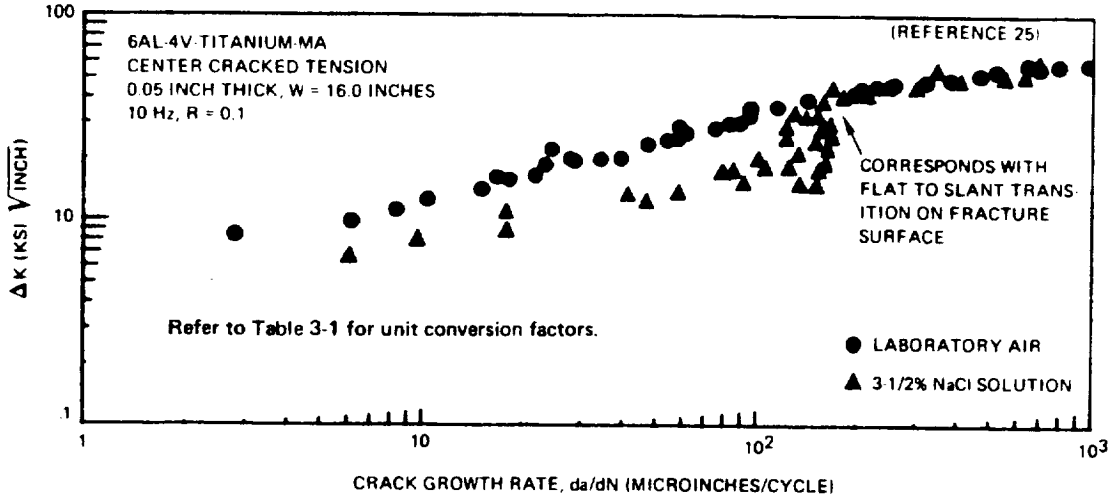

Figure 3-18. Effect of Salt Water Environment on the Cyclic Crack Growth Rate for 6AL-4V Titanium

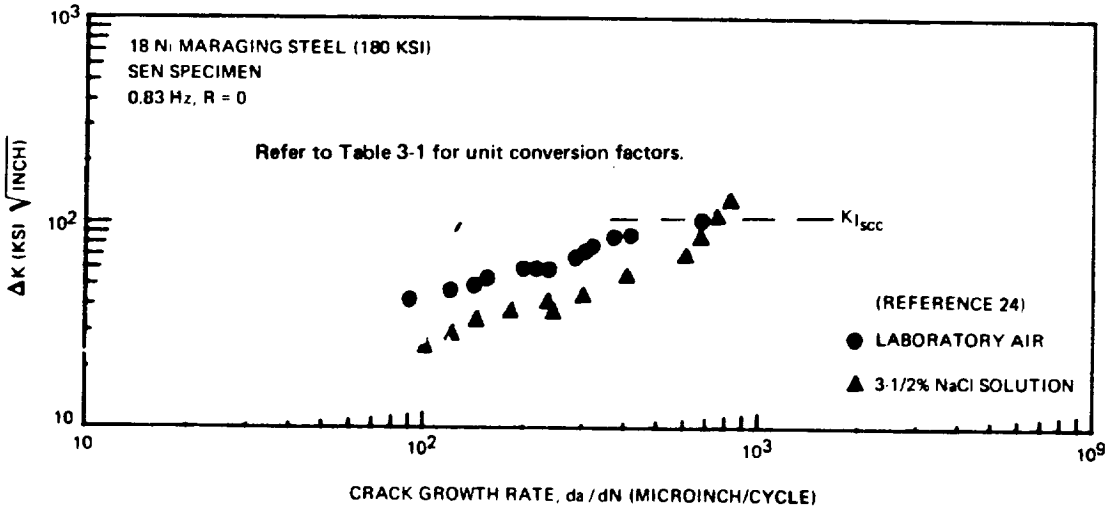

Figure 3-19. Effect of Salt Water Environment on the Cyclic Crack Growth Rate for 18Ni Maraging Steel

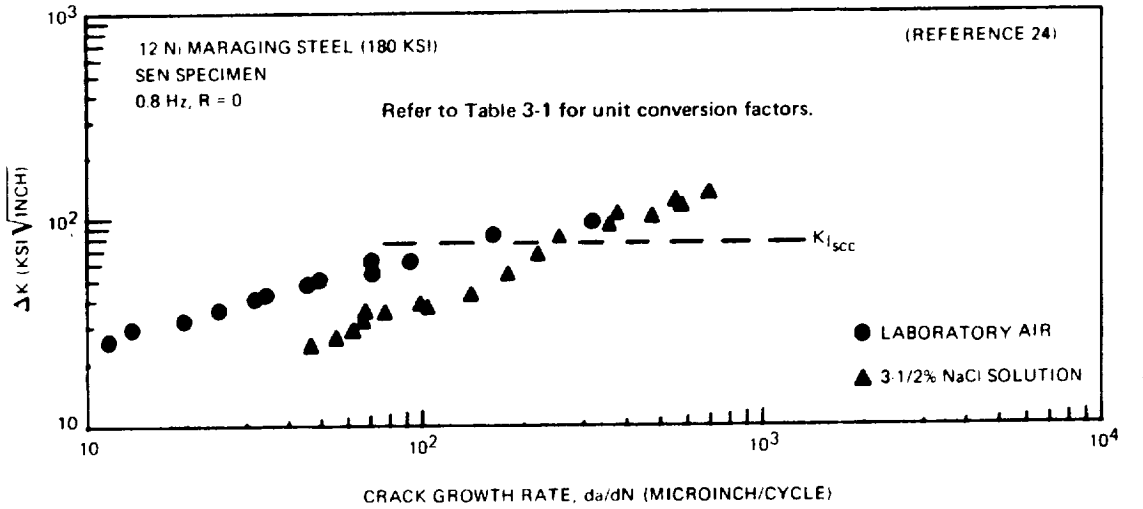

Figure 3-20. Effect of Salt Water Environment on the Cyclic Crack Growth Rate for 12Ni Maraging Steel

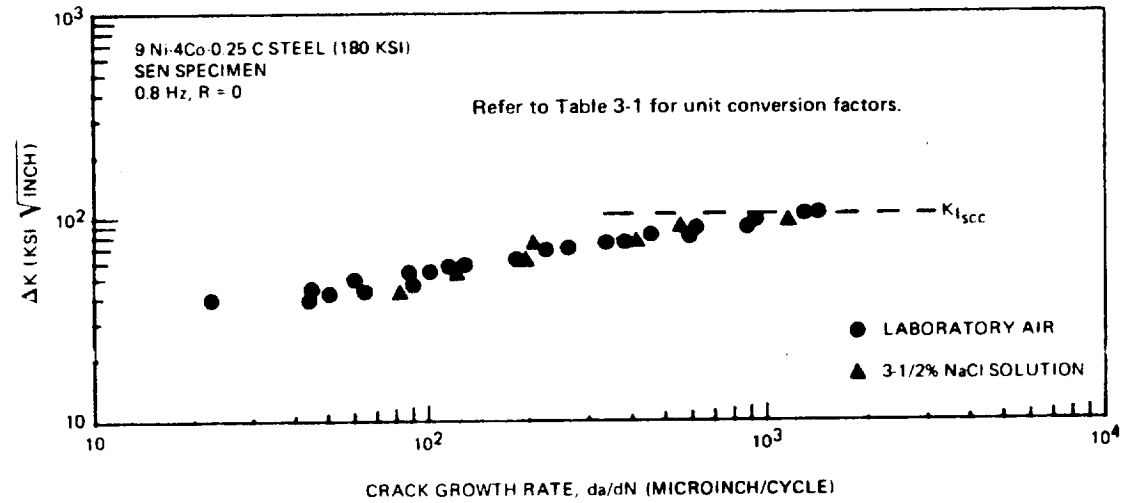

Figure 3-21. Effect of Salt Water Environment on the Cyclic Crack Growth Rate for 9Ni-4Co-0.25C Steel

Frequency effects are illustrated in Figure 3-22 for 12Ni maraging steel (Reference 26) in a salt water environment.

Extremely fast cyclic rates (~500 Hz) have, on the other hand, been shown to cause an increase in crack growth rates at low stress intensities in a relatively inert environment for 2024-T3 aluminum (Reference 27). Such an effect, as illustrated in Figure 3-23, has been attributed to local crack tip heating since no effect below 200 Hz was observed.

A quantitative method for estimating the effects of agressive environments on fatigue crack growth in high-strength steels was suggested by Wei and Landes (Reference 28). In this method, the rate of fatigue crack growth in an agressive environment is considered to be equal to the sum of the rate of fatigue crack growth in an inert reference environment and that of an environmental component computed from the applied load profile and sustained-load crack growth data obtained from an identical active environment. This approach, however, requires that no growth rate acceleration occur below the sustained load environmental threshold stress intensity which, as has been demonstrated; this is not the case for many alloy systems. Additionally, the simple additive nature of fatigue and environmental acceleration has not been demonstrated.

The recommended approach at this point in time, for providing a reliable accounting of the influence of active environments on fatigue crack behavior is simulated service life testing. Such a test would involve the actual anticipated service environment, cyclic frequency, flaw geometry, and loading modes. Such testing has been termed "suslic" (sustained load plus cyclic load) and is currently employed in several fracture prevention programs.

Test Methods

Constant amplitude cyclic crack growth rates are usually determined by measuring some incremental flaw extension, Δa, which has occurred over a discrete number of load cycles, ΔN. The growth rate, $\Delta a/\Delta N$, is subsequently related to some driving mechanism parameter such as stress intensity or range of stress intensity excursion.

A rudimentary approach to the required crack size monitoring is to optically measure crack length while a test is in progress. This approach, in addition to not being practical when testing in hazardous or extreme environments, provides no supplemental information with regard to plasticity or closure force influences.

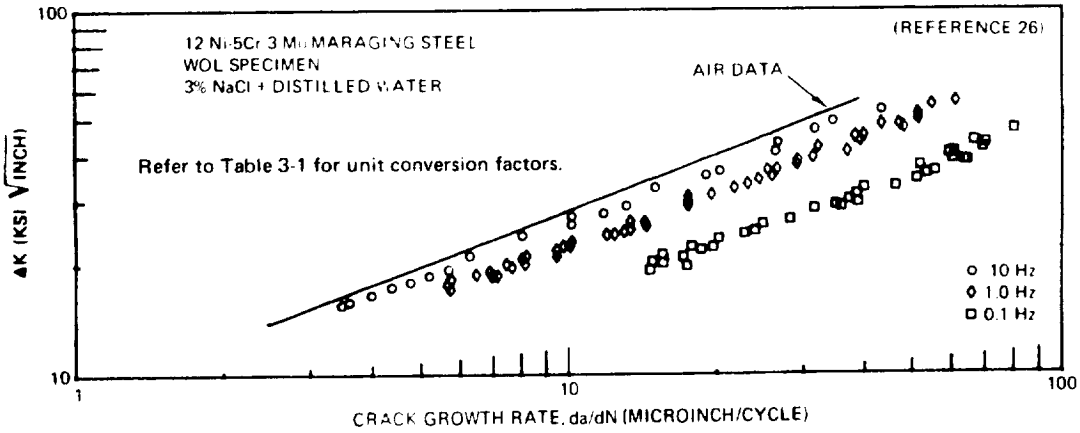

Figure 3-22. Effects of Load Frequency on Crack Growth Rate of 12Ni Maraging Steel in Salt Water Environment

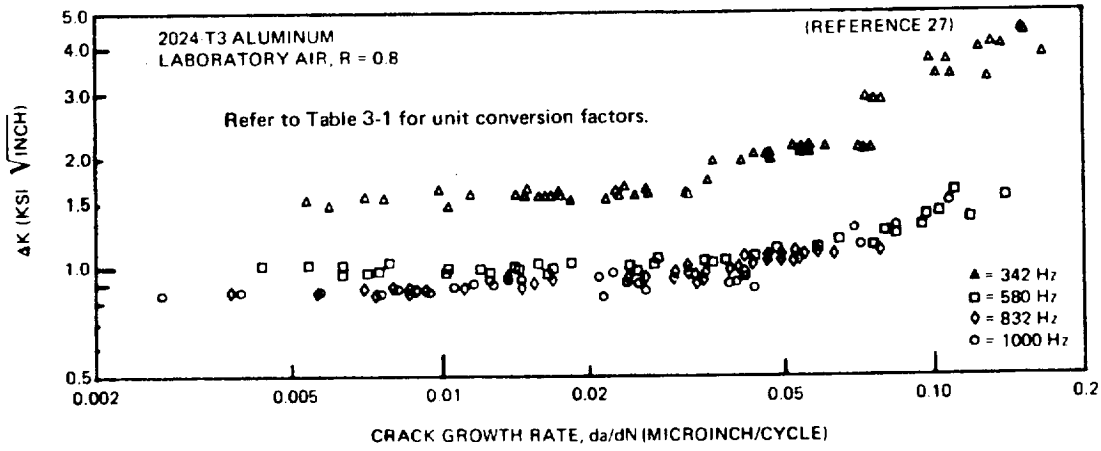

Figure 3-23. Effect of High Cyclic Rates on Crack Growth for 2024-T3 Aluminum

Many alternate methods have been developed. Ink staining, chemical etching, heat tinting, and fatigue marking leave discernible evidence on the crack surface. However, some secondary effects may be experienced. Other (more passive) methods include measuring changes of electrical resistivity, acoustic emission monitoring, and eddy current and ultrasonic crack detection. Some of these methods have been essentially abandoned; each has deficiencies which tend to offset their advantages.

A more viable method frequently employed for crack size approximation is elastic compliance monitoring, in which elastic compliance, C, may be considered the inverse of the spring constant. C is defined as γ/P, where γ is the elastic crack opening displacement (COD) produced by the load, P. The elastic compliance is geometry-dependent whereby slight flaw extension (for a given elastic modulus) will produce rational compliance changes or

$$C = f(a)$$

The linear or elastic portion of a record of crack opening displacement versus applied load will provide a measure of elastic compliance; and, with the aid of a compliance versus flaw size calibration for the particular specimen, the crack size can be determined.

By measuring incremental changes in elastic compliance, the increase in crack size corresponding to the number of applied cycles will provide a crack growth rate. In this manner, several data points can be realized from a single specimen in addition to providing a permanent record of plasticity and closure forces.

An extension of the incremental compliance approach to growth rate measurements is the continuous compliance derivative method (Reference 8) developed from the relationship:

$$da/dN = \lim_{\Delta N \to o} \frac{\Delta C/\Delta N}{dC/da}$$

where $\Delta C/\Delta N$ is the measured change in elastic compliance over a small number of cycles and $dc/da = f'(a)$ is the derivative of the relationship of elastic compliance to crack size.

The absolute flaw size for use in stress intensity calculations is measured by occasional load versus COD records. The term $\Delta C/\Delta N$ is measured from the net slope (upper slope minus lower slope) of a time-COD record as illustrated on Figure 3-24. If evidence of crack closure

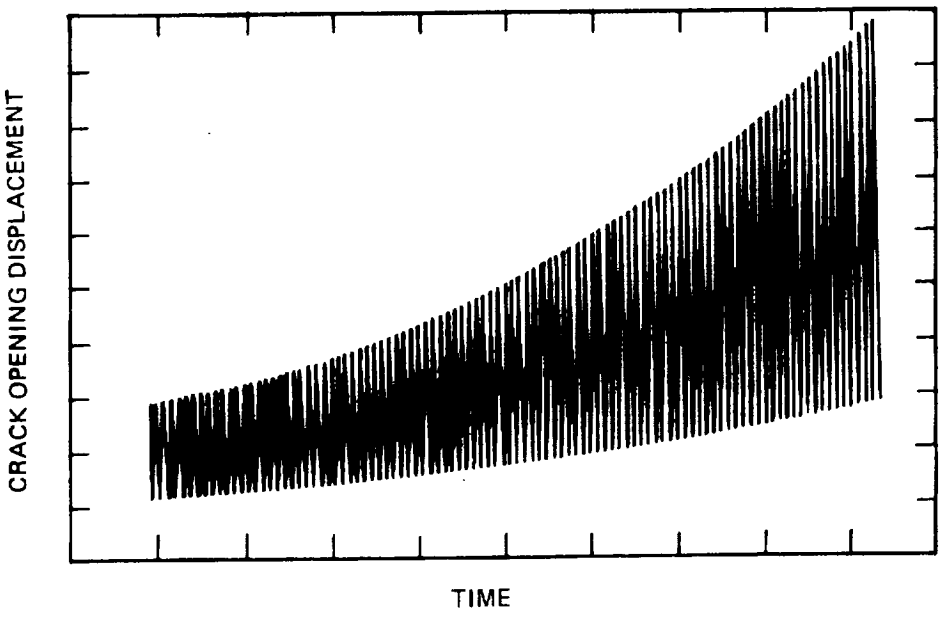

Figure 3-24. Typified Time-COD Cyclic Test Record

forces are present on the load-COD record, they must be considered when measuring the lower slope.

For example, the compliance to flaw size relationship for a center-cracked-tension specimen under conditions of sufficient width and crack length (and normalized by the elastic modulus, E) can be expressed as $CEA = (COD) \cdot E/\sigma \cong 4a$ (Reference 4) and the crack growth rate subsequently can be evaluated from

$$da/dN = \frac{\Delta C \cdot EA/\Delta N}{EA \cdot dc/da} = \frac{(\Delta COD/\Delta N) \cdot E}{4\sigma}$$

This approach to crack growth rate testing is most useful for test specimens that have characteristically high stress intensity gradients or that can accommodate only small amounts of crack growth like thin sheet surface flaw specimens. Additionally, for PTC testing, the time-COD record often provides considerable insight into the influence of approaching flaw breakthrough on crack growth rates (see Section 4).

Until such time that a standard method of test for cyclic growth testing has been adopted, review and analysis of cyclic growth rate test

data cannot be responsibly performed unless all pertinent test procedures and results are reported. These include as a minimum the following:

1. Test specimen type
2. Material designation with corresponding mechanical properties data
3. Flaw/load orientation
4. Actual test loads
5. Test frequency
6. Environment and temperature
7. Flaw size measurement techniques
8. Stress intensity solution used in data reduction
9. Net stress
10. Some record as to the presence of closure forces

Specimens for crack growth rate testing must be carefully selected. They should be sized before test to determine that sufficient crack growth can be accommodated at the desired load levels without net section yielding. Depending on the flaw growth mechanism under study, the stress intensity gradient for the specimen may also merit considerable attention. Also, if retardation mechanisms related to crack closure forces are being investigated, compliance behavior is particularly important since closure forces may diminish due solely to an increase in specimen compliance resulting from crack extension.

3.3 SUSTAINED LOAD FLAW GROWTH

Structural failures resulting from environmental cracking have been observed for many years. Stress corrosion cracking refers to cracking caused by the simultaneous presence of tensile stress and a specific corrosive medium. The stress corrosion phenomenon involves evaluation of smooth specimens and is usually assumed to include crack initiation as well as subsequent growth under sustained load. A supplementary, but certainly not an alternative, analytical approach is evaluation of sustained-load flaw-growth behavior of preexisting flaws in an aggressive environment. Use of stress intensity solutions to describe such a phenomenon is a logical extension of the limits of applicability of fracture mechanics.

Early investigative attempts met with encouraging success in correlating stress-intensity factors with precritical sustained-load flaw growth in agressive environments. Of primary significance was observation of an apparent threshold stress intensity level (K_{th}) below which time-dependent, precritical flaw growth will not take place. Where flaw growth is attributed to stress corrosion cracking, this apparent threshold value has been termed K_{Iscc}.

An explicit example of the stress intensity dependence was provided by Brown and Beachem (Reference 29). They explored the consistency of sustained stress crack growth test results with three different specimen types: the center-cracked tension, surface flaw, and precracked cantilever beam. For 4340 steel in dilute NaCl solution, the same K_{Iscc} value was obtained for all three specimens, as illustrated in Figure 3-25, where initial stress intensity, K_{Ii}, is plotted versus time to failure. The difference in time to failure at stress intensities above K_{Iscc} is attributed to the different functional dependencies of the stress intensity upon crack size for the three specimens. The shortest failure times were observed for the precracked cantilever beam, which has the highest K gradient. The longest failure times were observed for the center-cracked specimens, for which the K gradient is smallest.

For comparing relative effects of various environments on different materials, K_{th} data are often displayed as a ratio of the threshold stress intensity to the critical stress intensity, K_{th}/K_{Ic}. Unfortunately, since a majority of available threshold data was generated before publication of

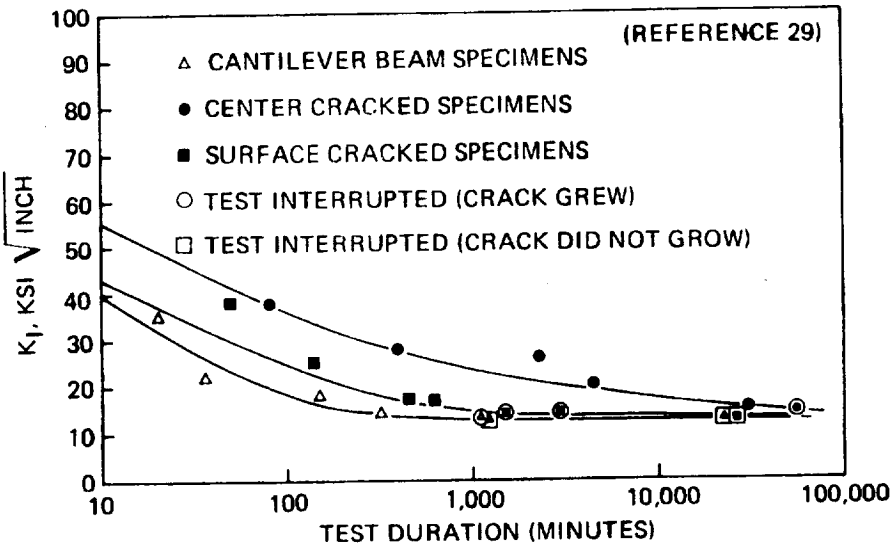

Figure 3-25. Correlation of Threshold Stress Intensity (K_{Iscc}) Results for Three Different Specimen Configurations, 4340 Steel in Dilute NaCl Solution

ASTM recommended procedures, the validity or applicability of the K_{Ic} data must be scrutinized. In many instances, the K_{Ic} used to calculate threshold ratios will be part-through-crack failure stress intensity values; i.e., K_{IE}. Again, no standard method of test is available for threshold stress intensity measurements, and scatter in reported results will reflect this deficiency as much as the irresolute nature of the phenomenon being measured.

As illustrated, the lower bound of a plot of K_{Ii} versus time to fracture or time for measurable growth is designated as K_{th}. Measurements are usually made by loading a preflawed specimen in an environment of interest and maintaining a constant load for a prescribed time. If the specimen has not fractured, it is removed from the environment, the flaw front is fatigue-marked, and the flaw growth recorded. Figure 3-26 presents typical room-temperature data for titanium alloy in environments of distilled water and methanol. For this example, as with many other material-environment combinations, two distinct types of behavior result. In methanol, environmental cracking mechanisms produce crack extensions, causing an increase in stress intensity, and the specimen eventually fractures. This behavior is consistent with stress corrosion cracking characteristics and would be anticipated in very aggressive environments. On the other hand, the distilled water environment results in crack extension without subsequent growth to failure. This behavior was also noted by Lorenz (Reference 30). Lorenz defined two threshold stress intensities for 5Al-2.5Sn (ELI) titanium and 2219-T87 aluminum in the environment of room air, liquid nitrogen, and liquid hydrogen. The one threshold stress intensity was defined as that value above which growth could be expected to occur without resulting in

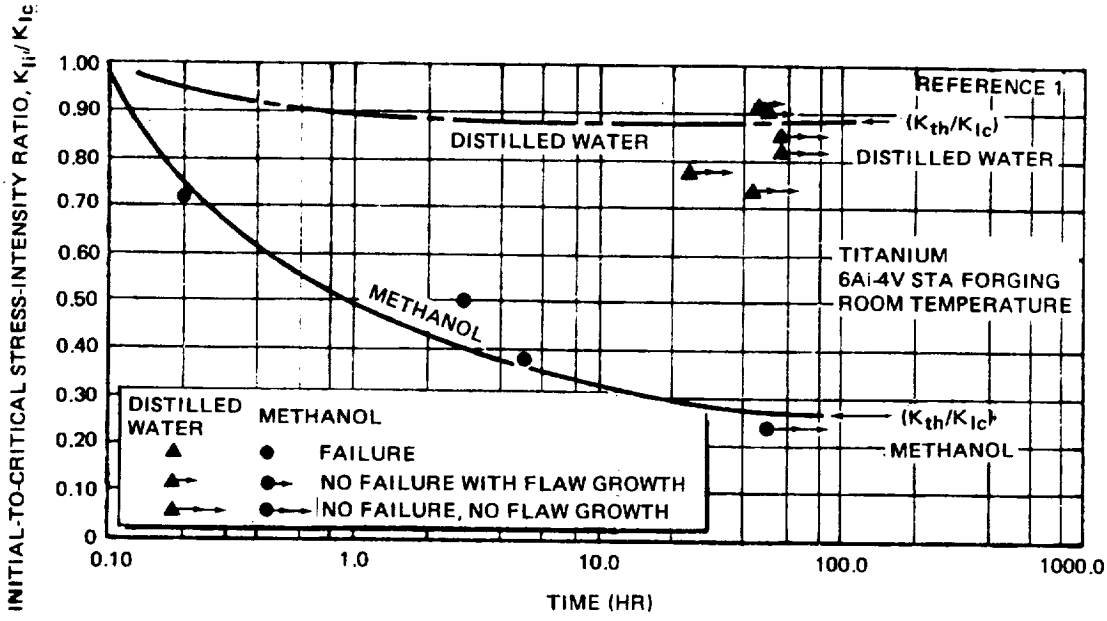

Figure 3-26. Typical Representation of Sustained Load Flaw Growth Data

failure. A higher threshold stress intensity was defined as that value above which growth to failure could be expected.

The observation that crack growth will arrest in an agressive environment under a positive stress intensity gradient is not consistent with the concepts of environmental cracking mechanisms. Therefore, accommodation of the observed behavior with other precritical flaw growth mechanisms must be attempted. One obvious source of crack extension during K_{Iscc} testing is flaw growth during initial load application for the constant load test. Failure to account for this phenomenon properly can result in reports of environmental crack extensions that, in reality, result entirely from flaw-growth on loading. Recent sustained load growth data generated at the Boeing Company (Reference 31) exemplify the type of measurements necessary for differentiation between environmental and growth-on-loading components of flaw growth. These data are shown in Figure 3-27, where flaw extension is plotted as a function of applied stress intensity. In these tests, control specimens of similar configuration were subjected to load-unload tests in a relatively inert environment. The flaw front was fatigue-marked, and the growth on loading was measured from the fracture surface. The point where load-unload growth intersects the sustained load growth data is then designated as K_{th} for that material-environment combination.

Another, more subtle, possible contributor to arresting flaw growth in some environments is environmental cracking accompanying increasing load application; i.e., environmentally enhanced crack growth upon loading. This behavior was illustrated recently by Barsom (Reference 32) in a simple but revealing experiment in which several loading profiles were used to

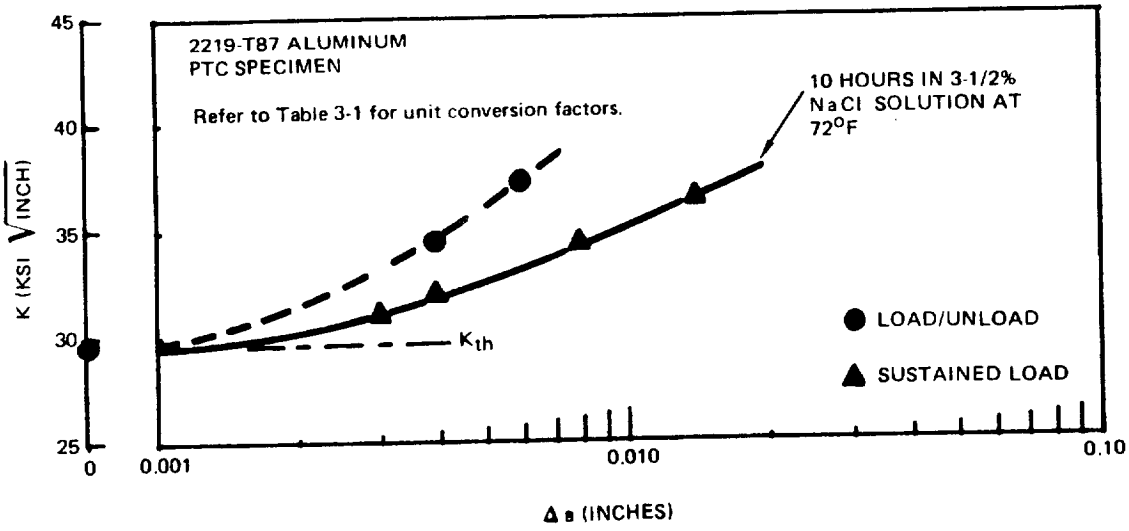

Figure 3-27. Flaw Depth Growth During Sustained Load and Load/Unload Tests of 2219-T87 Aluminum

propagate fatigue cracks in steel. One profile applied a rapidly increasing load followed by a more deliberate unload. The other load profile reversed the order. The increasing load was applied slowly and the unload was abrupt. Although the average cyclic rates were equivalent, the flaw growth in the slowly increasing load profile progressed at a much faster rate than opposite profile. In view of the aforementioned observations, it may be wise to include load-unload tests in the test environment to complement the type of data generated in Figure 3-27 and thereby assure that the factors contributing to flaw growth are recognized and properly evaluated.

Indeed, if environmentally induced flaw growth under sustained load conditions can be shown to be restricted to the initial load cycle for particular material-environment combinations, accommodation of environmental effects in safe-life analyses can be greatly simplified. Additionally, revaluation of the reported K_{th} data may increase reported threshold values for some material-environment combinations.

Another possible contributor to flaw arrest in environments can be related to changes in stress state as a flaw increases in size. Although little work has been performed in this area, it has been generally concluded that in many instances plane strain conditions will promote environmental cracking while plane stress conditions will inhibit it. Since constraint in the area of surface flaws in thin sheet material is not well understood, stress state changes with small increases in crack size may occur and subsequently influence precritical growth.

A convenient method of monitoring flaw behavior during threshold stress intensity testing is by crack opening displacement (COD) measurements. A continuous record of COD versus time will indicate whether crack growth is taking place. When evaluating a time-COD record for flaws subjected to near critical stress intensities, it will be necessary to consider creep relaxation immediately after the initial load application. In such instances, plastic flow characteristics may dominate the specimen behavior.

Another approach to stress intensity threshold testing is to maintain the specimen at a constant crack-opening displacement in the test environment. As environmental cracking progresses, the stress intensity will decrease and crack growth will arrest when the threshold stress intensity is reached. The equivalency of this test method with the increasing stress intensity tests was demonstrated by Smith, Piper, and Downey (Reference 33) for Ti-8Al-1Mo-1V alloy in 3-1/2 percent salt solution. They used center-cracked specimens to determine the threshold stress intensity for crack initiation with end loading, and crack arrest with wedge-force loading. The measured threshold for crack initiation was 20 to 25 ksi

$\sqrt{\text{inch}}$, and for crack arrest, 20 to 22 ksi $\sqrt{\text{inch}}$. The equivalence of test methods for very aggressive cracking environments has been demonstrated. However, when more subtle environmental influences on sustained load flaw growth are being experienced, the two test methods may lead to different results.

Because the environmental effects on sustained-load crack growth are quite complex, design for operation above K_{th} should naturally be avoided. Where applications above K_{th} are required by cost or by weight restrictions, the time-dependent flaw growth behavior must be incorporated into the analysis. Measurements of the sustained-load flaw growth rate, da/dt, as a function of applied stress intensity are often represented in a manner similar to cyclic flaw growth rates.

Figure 3-28 shows sustained load flaw growth rates for 4340 steel in 3.5 percent NaCl (Reference 34). The form of the curve is similar to that obtained for cyclic flaw growth rates in that a lower threshold corresponding to K_{Iscc} and an upper limit corresponding to K_{Ic} bound the stress intensity range. The transitions in the curve are much more abrupt, depicting a somewhat constant growth rate over a wide range of stress intensities. The observed behavior can be adequately accommodated by the sigmoidal cyclic growth rate equation formulated by Collipriest (see Section 3.2). The accuracy of a single expression for growth rate is naturally limited by the quality and repeatability of the test data.

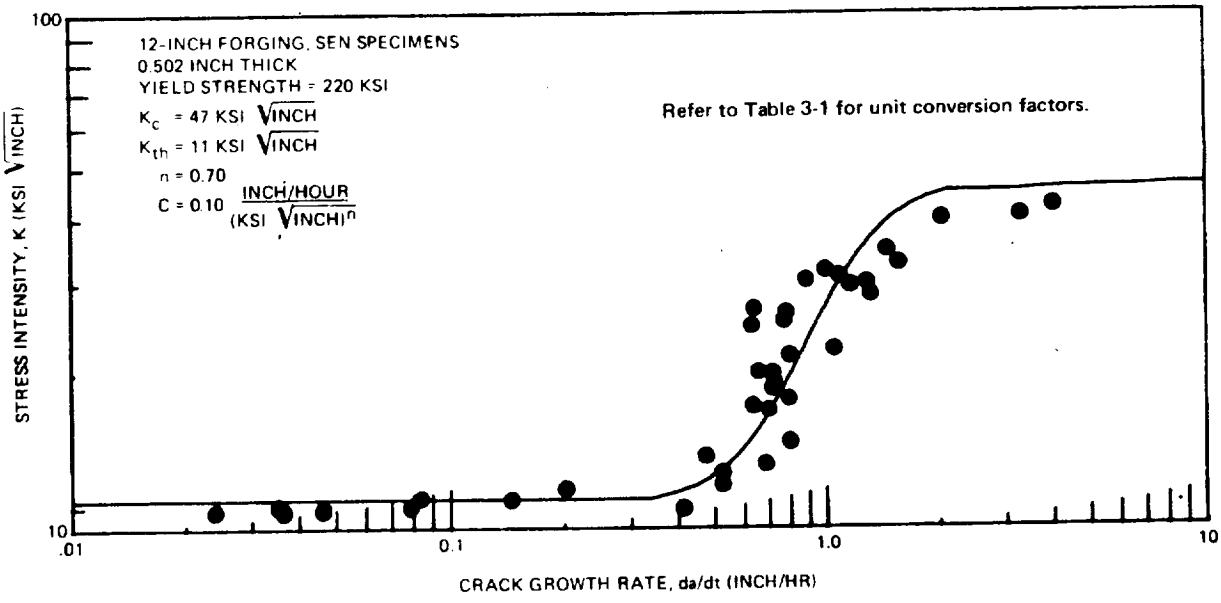

Figure 3-28. Sustained Load Crack Growth Rate Data for AISI 4340 Steel in 3.5-Percent NaCl Solution

Such data are incorporated into predictive analysis in a manner identical with cyclic growth rate analysis; that is, integration of the growth rate expression over a discrete time period (i.e., time at maximum operating pressure) provides the amount of anticipated flaw growth. It must be emphasized again, however, that the accuracy of such an analysis depends entirely on accurate accommodation of the flaw growth phenomenon by the growth rate data.

REFERENCES

1. Tiffany, C.F. Fracture Control of Metallic Pressure Vessels. NASA SP-8040 (May 1970).

2. von Euw, E.F.J., R.W. Hertzberg, and R. Robert. Delay Effects in Fatigue Crack Propagation. Presented at the Fifth National Symposium on Fracture Mechanics, University of Illinois (September 1971).

3. Tiffany, C.F., J.N. Masters, and W.D. Bixler. Investigation of Crack Growth Threshold of Inconel 718 Exposed to High Pressure Oxygen. NASA CR-108485 (August 1970).

4. Ehret, R.M. A Study of Deep Surface Flaws in Aluminum. Master's thesis, California State University at Long Beach (June 1972).

5. Bixler, W.D., and J.N. Masters. Study of Deep Flaws in Weldments of Aluminum and Titanium. Quarterly Progress Report No. 3, NASA Contract NAS3-14386 (April 1972).

6. Paris, P., and R.A. Erdogan. "A Critical Analysis of Crack Propagation Laws," Journal of Basic Engineering, Transactions of the ASME (December 1963).

7. Forman, R.G., V.E. Kearney, and R.M. Engle. "Numerical Analysis of Crack Propagation in Cyclic-Loaded Structures," Journal of Basic Engineering, Transactions of the ASME, Vol. 89 (September 1967), pp. 459-464.

8. Collipriest, J.E., Jr., and R.M. Ehret. Computer Modeling of Part-Through-Crack Growth. Space Division, Rockwell International Corporation, SD 72-CE-0015 (1972).

9. Unpublished data generated at the Space Division, Rockwell International Corporation.

10. Brock, D., and J. Schijve. The Influence of the Mean Stress on the Propagation of Fatigue Cracks in Aluminum Alloy Sheet. National Lucht-en Ruimtevaart/Aboratorium, NLR-TR M.2111 (January 1963).

11. McMillan, J.C., and R.M. N. Pelloux. "Fatigue Crack Propagation Under Program and Random Loads," Fatigue Crack Propagation. American Society for Testing and Materials, ASTM STP 415 (1967), p. 505.

12. Erdogan, F. Crack Propagation Theories. NASA CR901 (October 1967).

13. James, L.A. "The Effect of Frequency Upon Fatigue Crack Growth of Type 304 Stainless Steel at 1000°F." Fifth International Symposium on Fracture Mechanics, Urbana, Illinois (August 1971).

14. Jaske, C.E., C.E. Fedderson, K.B. Davies, and R.C. Rice. Analysis of Fatigue, Fatigue-Crack Propagation, and Fracture Data. Battelle Memorial Institute, Columbus Laboratories (January 1973).

15. Little, D.C., and P.M. Bunting. "The Surface Flaw in Aircraft Structures and Related Fracture Mechanics Analysis Problems," The Surface Crack: Physical Problems and Computational Solutions. ASME (1972), pp. 11-42.

16. Fedderson, C.E., D.P. Moon, and W.S. Hyler. Crack Behavior in D6AC Steel. Battelle Memorial Institute, Columbus Laboratories, MCIC-72-04 (January 1972).

17. Wheeler, O.E. Crack Growth Under Spectrum Loading. Fort Worth Division, General Dynamics, FZM-5602 (June 1970).

18. Willenborg, J., R.M. Engle, and H.A. Wood. A Crack Growth Retardation Model Using an Effective Stress Concept. AFFDL-WPAFB, TM-71-1 FBR (January 1971).

19. Elber, W. The Significance of Fatigue Crack Closure. NASA Langley Research Center. Presented at the 1970 Annual Meeting of American Society for Testing and Materials.

20. Jones, R.E. Fatigue Crack Growth Retardation After Single-Cycle Peak Overload in Ti-6Al-4V Titanium Alloy. Air Force Technical Report AFML-TR-72-163 (April 1972).

21. Marcus, H.L., J.C. Willimas, and N.E. Paton. The Influence of Gaseous Environments on Corrosion Fatigue. Science Center, Rockwell International Corporation, Technical Memorandum, Preprint No. 71-69 for Proceedings, International Meeting on Corrosion Fatigue (June 1971).

22. Bradshaw, F.J., and C. Wheeler. Applied Materials Research, Vol. 5 (1966), p. 112.

23. Pittinato, G.F. The Effects of a Hydrogen Environment on the Mechanical Properties of Forged Ti-6Al-4V ELI Weldments. NAS8-21470, McDonnell Douglas Astronautics Company (November 1969).

24. Crooker, T.W., and E.A. Lange. "The Influence of Salt Water on Fatigue-Crack Growth in High-Strength Structural Steels," Effects of Environment and Complex Load History on Fatigue Life. American Society for Testing and Materials, ASTM STP 462 (1970), pp. 258-271.

25. Walker, K., S. Pendleberry, and R. McElwee. "Tensile and Shear Mode Cracking of Titanium Sheet in Air and Salt Water," Effects of Environment and Complex Load History on Fatigue Life. American Society for Testing and Materials, ASTM STP 462 (1970), pp. 239-240.

26. Barsom, J.M. Mechanisms of Corrosion Fatigue Below K_{Iscc}. U.S. Steel Co.

27. Schmidt, R.A., and P.C. Paris. Threshold of Fatigue Crack Propagation and the Effects of Load Ratio and Frequency. Lehigh University.

28. Wei, R.P., and J.D. Landes. "Correlation Between Sustained Load and Fatigue Crack Growth in High-Strength Steels," Materials Research and Standards (July 1969), p. 25.

29. Beachem, C.D., and B.F. Brown. A Comparison of Three Specimens for Evaluating the Susceptibility of High-Strength Steel to Stress Corrosion Cracking. Internal report, U.S. Naval Research Laboratory.

30. Lorenz, P.M., et al. Extended Loadings of Cryogenic Tanks. NASA CR-72252 (July 1966).

31. Hall, L.R., and W.D. Bixler. Subcritical Crack Growth of Selected Aerospace Pressure Vessel Materials. NASA CR-120834 (December 1972).

32. Barson, J.M. Effect of Cyclic Corrosion Fatigue Crack Propagation Below K_{Iscc} in a High Yield Strength Steel. Preprint for presentation at the International Conference on Corrosion Fatigue, University of Connecticut, Storrs, Connecticut (June 14-18, 1971).

33. Smith, H.R., D.E. Piper, and F.K. Downey, "A Study of Stress Corrosion Cracking by Wedge Force Loading," Engineering Fracture Mechanics, Vol. 1, No. 1 (June 1968), pp. 123-128.

34. Fedderson, C.E., et al. Damage-Tolerant Design Handbook. Battelle Memorial Institute, Columbus Laboratories, MCIC-HB-01 (December 1972).

35. Collipriest, J.E., Jr. Part-Through Crack Fracture Mechanics Testing. An IR&D Summary Report. Space Division, Rockwell International Corporation, SD 71-319 (June 1971).

4.0 FAILURE MECHANISMS

4.0 FAILURE MECHANISMS

The science of fracture mechanics attempts to draw together the analytical techniques of applied mechanics and the physical realities of the fracture process. The aftermath of fracture has been studied in great depth on both a macroscopic and microscopic scale as a part of routine failure analysis. By combining knowledge available from the surface of a fracture with fundamental fracture mechanics principles, a much more complete picture of specific failure mechanisms is often available.

An alternate mode of failure, as opposed to total fracture, is surface flaw penetration to a through-crack (leakage). Such failures are of a particular interest for pressurized structures where either leakage is preferred to fracture or where flaw penetration is equivalent to catastrophic failure.

The following paragraphs will briefly review fracture mechanisms from both a microscopic and macroscopic viewpoint and summarize available techniques for analyzing surface flaw breakthrough.

4.1 MICROSCOPIC FRACTURE PROCESSES

The advent of electron microscopy as a tool for analyzing fracture surfaces has provided much needed information regarding the physical mechanisms of crack behavior. Electron microscopes permit high magnification and high-resolution examination of materials. Two types of electron microscopes are presently being used to study fracture surfaces: the transmission electron microscope and the scanning electron microscope. The transmission microscope has a higher resolving power than the scanning microscope; however, the fracture itself is not directly observed. Very thin replicas of the fracture surface must be prepared and transferred into the microscope. The scanning microscope permits, with limited resolution, direct study of the fracture surface itself with substantially improved depth of field and field of view.

When fracture surfaces are observed at increasingly higher magnifications, the extremely complex nature of the fracture process becomes apparent. However, in spite of the complex appearance of a fracture surface at high magnification, it has been possible to relate several mechanisms of fracture with certain characteristic fracture features.

From a metallurgical viewpoint, a brittle fracture is associated with cleavage of crystallographic planes with crack extension perpendicular to the

tensile axis, and it generally occurs with the presence of minimal plastic deformation. The cleavage facet is flat and frequently contains sets of gradually diverging lines, associated with cleavage fracture, occurring on parallel sets of planes (Figure 4-1). The origin of fracture for such facets is the focal point for the cleavage lines. On other cleavage facets, a network of cleavage steps in the shape of a "river pattern" may be observed where fine steps continually merge into larger ones. These markings again reflect the propagation of cracks on parallel planes. In this case, the origin of failure is in the direction of finer and more numerous steps in the pattern. A ductile fracture is considered the result of a process of extremely localized plastic deformation. In crystalline solids, plastic deformation tends to be confined to crystallographic planes of atoms which have a low resistance to shear. This shear fracture, in single crystals, occurs when the two halves of the crystals slip apart on glide planes that have the largest amount of shear stress resolved across them.

A ductile fracture mechanism common to most materials, regardless of fundamental differences in crystal structure and alloy composition, is that of void coalescence. It is believed that stress-induced fracture of brittle particles, particle-matrix interface failure, and, perhaps, complex dislocation interactions lead to the formation of microcracks or pores within the stressed component. At increasing stress levels, these mechanically induced micropores (not to be confused with preexistent microporosity sometimes present as a result of processing) grow larger and finally coalesce into a broad crack front. At some point, this growing flaw reaches critical dimensions, resulting in total failure of the component. Even after the point of instability, the unstable crack often grows by a repetitive process of void formation and subsequent coalescence with the main crack front.

Three distinct processes for void formation and coalescence can be envisioned, depending upon the state of stress. Under simple uniaxial loading conditions, the microvoids will tend to form in association with fractured particles and/or interfaces and grow out in a plane generally normal to the stress axis. The resulting microsized "equiaxed dimples" are generally spherical in shape (Figure 4-2).

When failure is influenced by shear stresses, the voids which nucleate in the same manner as cited above grow and subsequently coalesce along the planes of maximum shear stress, which are often inclined to the surface of the component. Consequently, these voids tend to be elongated and result in the formation of parabolically shaped depressions on the fracture surface. If one were to compare the orientation of the "elongated dimples" from matching fracture faces, one would find that the voids are elongated in the direction of the shear stresses and that they point in opposite directions on the two surfaces.

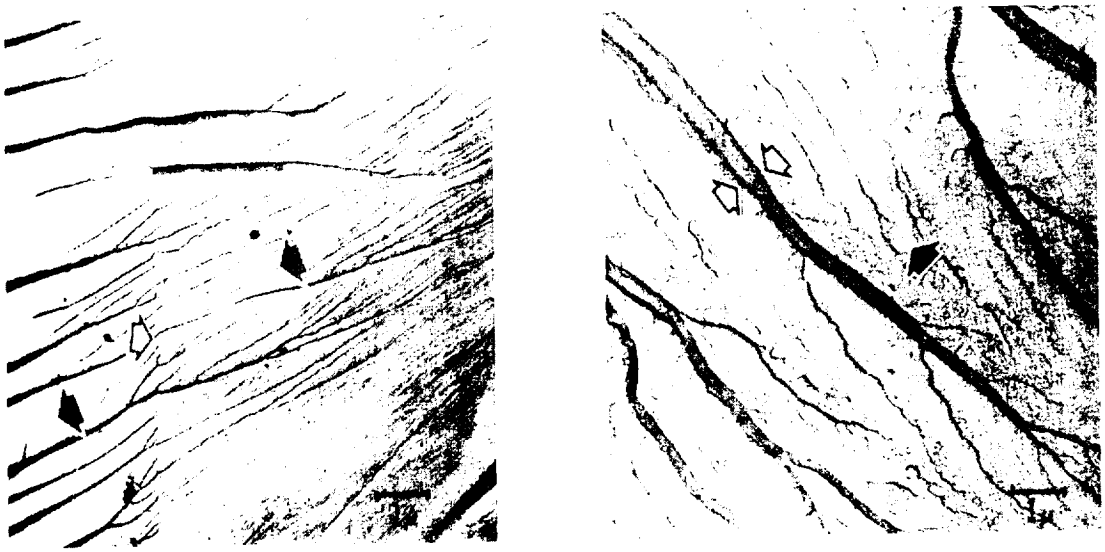

BLACK ARROWS INDICATE FRACTURE DIRECTION. WHITE ARROWS INDICATE CLEAVAGE STEPS.

Figure 4-1. Typical Fractrographs of Cleavage Fracture (Reference 1)

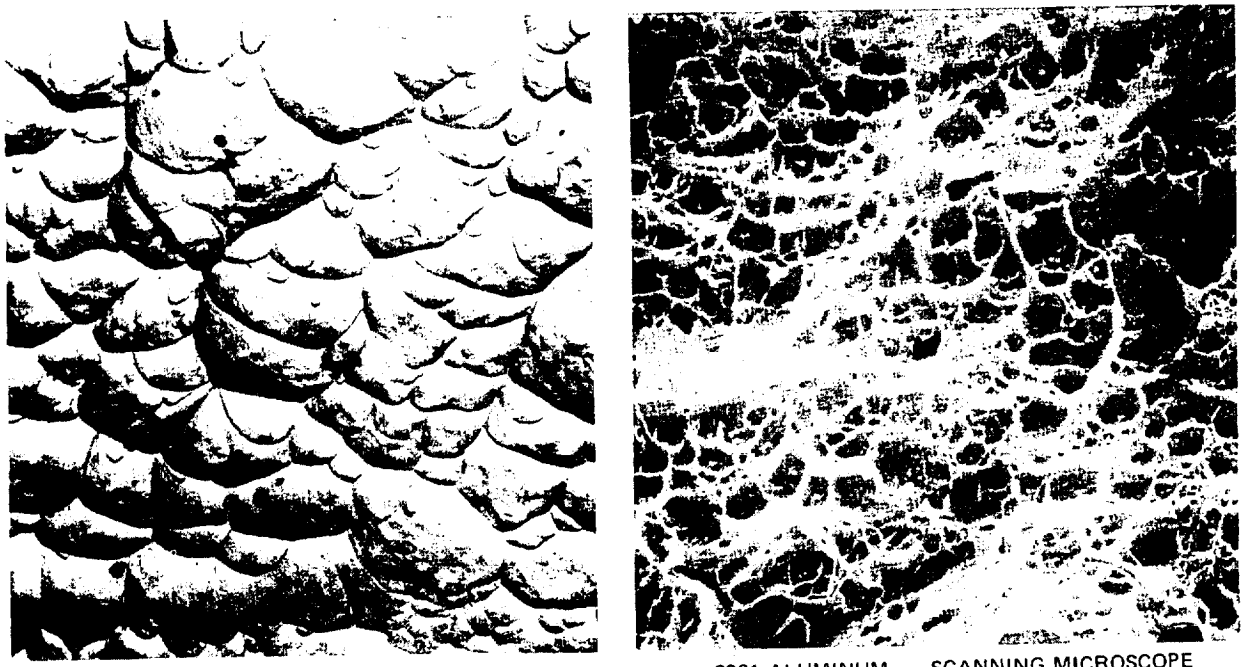

6AL-4V-STA - TRANSMISSION MICROSCOPE (REFERENCE 1)

6061 ALUMINUM - SCANNING MICROSCOPE

Figure 4-2. Fractrographs Showing Microvoid Coalescence Associated With Ductile Fracture

Finally, when the stress state is one of combined tension and bending, the resulting tearing process produces elongated dimples which can appear on gross planes normal to the direction of loading. The basic difference between these elongated dimples and the ones produced by shear is that the tear dimples point in the same direction on both halves of the fracture surface. It is important to note that these dimples point back toward the crack origin. A schematic diagram of the various types of microvoid coalescence is shown in Figure 4-3.

A fatigue fracture surface often reveals the presence of fatigue striations, which represent the successive position of the crack front after a given loading cycle (Figure 4-4). In addition to these striations are other regions on the fracture surface that contain mixtures of dimples, quasi-cleavage, and other fracture mechanisms. The relative ease in observation of striations seems to vary with stress state and alloy content. Striations are most clearly observed on flat surfaces associated with plane strain conditions. Elongated dimples and evidence of abrasion are the dominant fractographic features found on plane stress slant fracture surfaces. It is a much easier task to find striations on fatigue surfaces in aluminum alloys than in high-strength steels. In some cases, it is virtually impossible to identify clearly defined areas of striations in the latter material, thus making the fractographic interpretation very difficult.

The spacing between striations is a measure of crack growth during a given load cycle. Several investigators have shown that the striation spacing is equivalent to the macroscopic growth rate measures as a crack traverses a test panel. Since striation formation is a highly localized event, it is dependent upon both stress intensity and metallurgical factors. It has been repeatedly shown in laboratory experiments that, for constant stress intensity conditions, striation spacings in a local region may vary by a factor of two to four. To arrive at a meaningful estimate of crack growth rate at a particular crack length, many measurements of striation spacing should be made.

4.2 MACROSCOPIC FRACTURE PROCESSES

The macroscopic description of the fracture surface usually involves the orientation of the fracture plane and a visual interpretation of the texture of the fracture surface. In general, the orientation of the fracture surface can be placed in one of two categories: (1) square or flat fracture or (2) slant fracture, as illustrated in Figure 4-5. The term "flat fracture" is used when the plane of the fracture surface is perpendicular to the axis of the applied tensile stress. When the plane of the fracture surface is oblique to the axis of applied stress, the term "slant" is used. In many cases, the fracture surface is composed of both a slanted segment and a square or flat segment. The slant fracture is sometimes referred to as a shear fracture

REFERENCE 2

(For each mode the sketches show from left to right: material stressed almost to the point of local rupture; local rupture; and the directional sense of dimples on the rupture surfaces. The three coalescence modes are called (a) normal dimpled rupture, (b) shear rupture, and (c) tearing.)

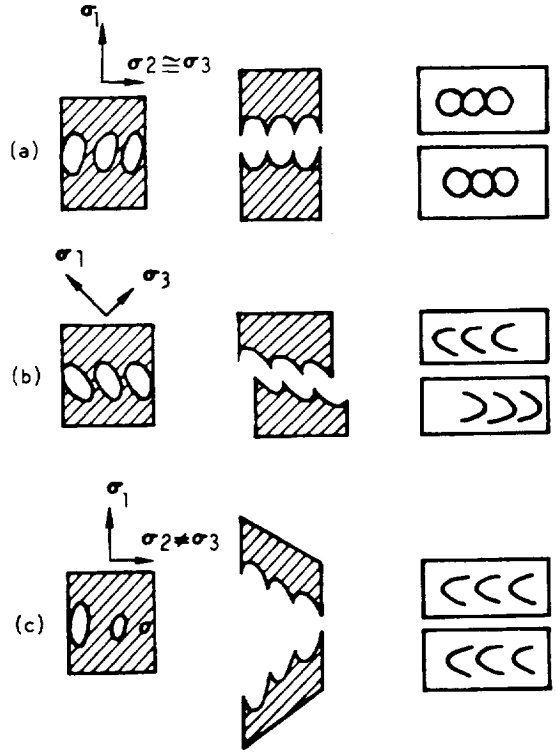

Figure 4-3. Three Observed Basic Modes for the Coalescence of Microvoids

6061 ALUMINUM - TRANSMISSION MICROSCOPE
MAGNIFICATION 6500X (REFERENCE 1)

2024-T861 ALUMINUM - SCANNING MICROSCOPE
MAGNIFICATION 8000X

Figure 4-4. Fractrographs of Fatigue Striation

(referring to the failure mechanisms, not the applied loads), and the slant portions at the edges of mixed orientation fracture surfaces are commonly referred to as shear lips. It should be pointed out, however, that cleavage or shear mechanisms present on the crystalline level may not necessarily be reflected by the orientation of the fracture plane; that is, flat surfaces do not automatically represent brittle fracture, nor do slant surfaces represent a ductile fracture. Many examples can be provided where predominantly flat fracture surfaces are produced by failure of very ductile material, and subsequent microscopic analysis reveals predominant evidence of microvoid coalescense.

The previously mentioned influence of plate thickness on the measured critical stress intensity, K_c, can also be used to illustrate an observed relationship between the stress state at the crack tip and the fracture surface orientation. In general, as the orientation of the fracture surface changes with increasing plate thickness from 100-percent slant fracture to nearly 100-percent square fracture, the measured critical stress intensity factor decreases to approach K_{Ic}. This effect, illustrated in Figure 4-6, has led to the generally accepted conclusion that the flat fracture is indicative of plane strain conditions (more constraint and less deformation), and that the slant fracture results from a plane stress influenced fracture (less local constraint and more plastic deformation).

From the preceding discussion, it becomes apparent that several terms are often used interchangeably to describe a particular fracture characteristic (i.e., tough, ductile, etc.). However, considerable confusion will often arise regarding implied relationships between these terms. In the interest of clarity, Table 4-1 catalogs a few of the more common descriptive terms associated with flaw-induced fracture. The terms are separated into generally desirable characteristics from an engineering/fracture mechanics viewpoint, and their undesirable counterparts.

Items listed within a particular subgroup appear to be mutually inclusive by either definition or observation, and no sound arguments are available that suggest their dissociation. It would not be surprising to find a single material/structure system that exhibits all the desirable or all the undesirable properties. On the other hand, generalitites regarding the exclusive commonality of the characteristics between the subgroups can be very misleading; that is, a flat fracture surface will not automatically preclude the possibility of a ductile fracture in a relatively thin structure, nor will testing thin sections preclude the possibility of brittle behavior. In failure analysis or interpretation of laboratory test results, it is important that interdepencency (or lack of dependency) among the different characteristics be well understood.

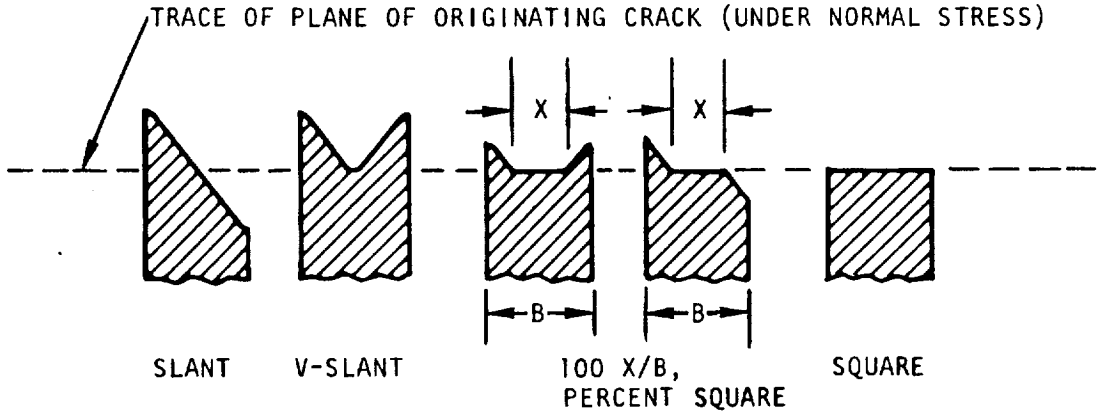

Figure 4-5. Descriptive Terms for Types of Fracture Surfaces

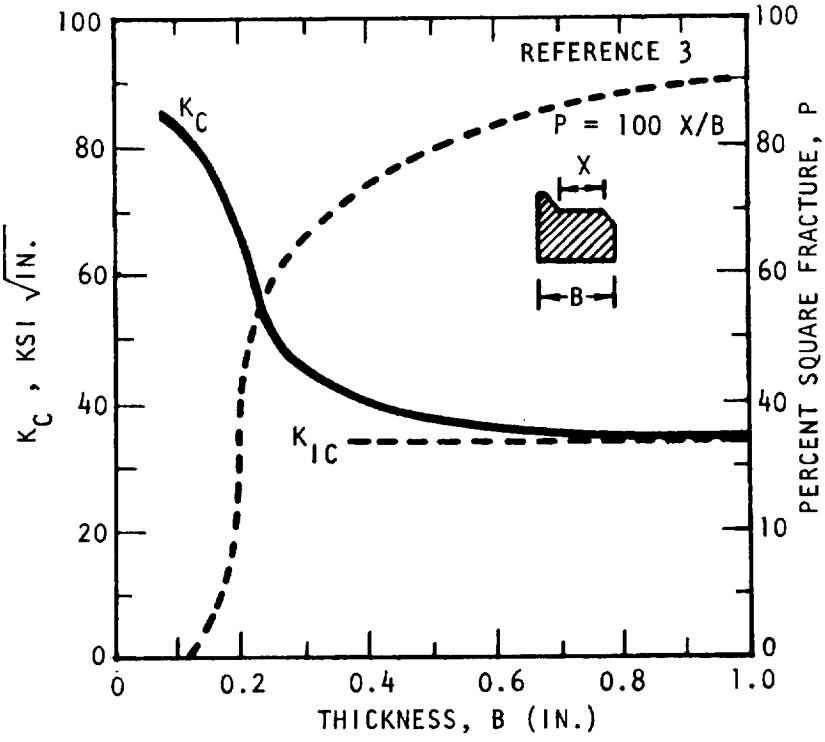

Figure 4-6. Dependence of K_c and Fracture Appearance

Table 4-1. Popular Descriptors of Flaw-Induced Fracture Characteristics

Generally Desirable	Generally Undesirable
Ductile High toughness Stable flaw extension Microvoid coalescence	Brittle Low toughness Abrupt instability Cleavage
Plane stress constraint Slant fracture surface	Plane strain constraint Flat fracture surface
Thin	Thick

Other observations available from a macroscopic viewpoint involve the textural appearance of the fracture face. For example, fatigue crack growth at low to moderate load levels is usually distinguishable on a fracture surface by exhibiting a relatively smooth, flat surface when compared to slow, growth-upon-loading or fast fracture. Figure 4-7 shows a part-through crack fracture surface that was monotonically loaded to near failure several times to produce slow, stable growth. Between monotonic loads, the specimen was fatigue cycled to extend the crack. The amount of crack growth by fatigue is readily visible as distinct bands of high reflectivity while the slow, stable growth is characterized by a much more coarse and subsequently less reflective surface. Changes in fatigue load amplitudes or single-cycle overloads are also often observable on the fracture surface. Fatigue crack growth at very high stress intensities will often cause fretting of plastically deformed material in the wake of the advancing crack. This fretting will often cause textural or color changes on the fracture surface. This effect is illustrated in Figure 4-8, which shows an aluminum specimen that was cycled at high stress intensity and subsequently cycled at a lower stress intensity. The black constituents (attributed to aluminum oxide) on the fracture surface are no longer apparent once the load level is reduced. A similar effect can be seen in the Inconel-718 example shown in Figure 4-9. This specimen was fatigue-cracked at relatively low stress intensity levels and subsequently cycled at extremely high stress intensities. Once again, distinct color differences are apparent on the fracture surface. Additionally, the large amount of crack tunneling is also indicative of very high stress intensity application. Examples of the many other interesting and revealing fracture surface characteristics would not be appropriate within the scope of this document, and the examples given were presented only to illustrate that much can be learned regarding the physical nature of flaw growth by a detailed macroscopic study of fracture surfaces.

Reference 4

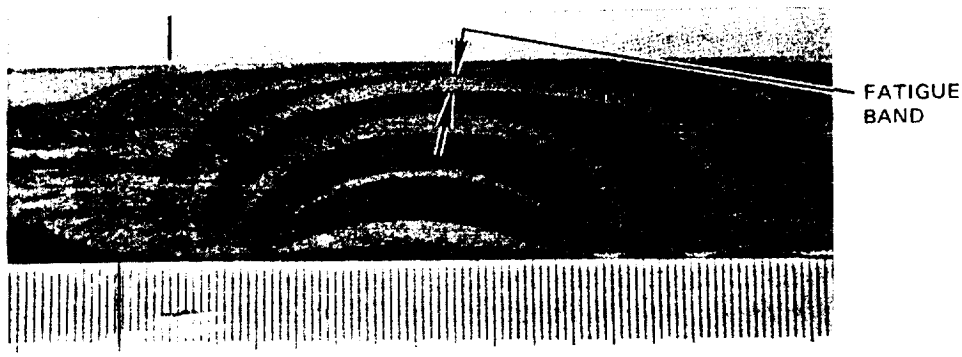

Figure 4-7. Photograph of 0.25-Inch-Thick Titanium Fracture Surface Showing Distinguishable Evidence of Fatigue Crack Growth and Flaw Growth During Monotonic Load Application

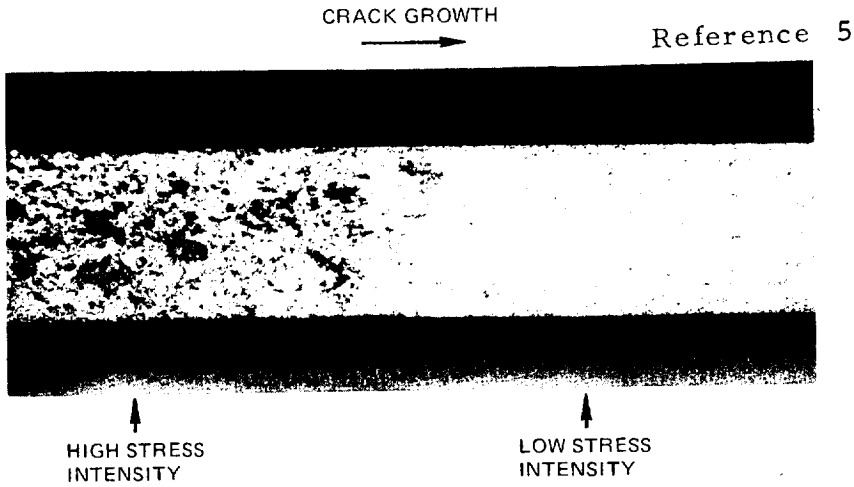

Figure 4-8. Photograph of 2024-T851 Aluminum Showing Distinct Difference in Fracture Surface Corresponding to a Decrease in Cyclic Load Levels

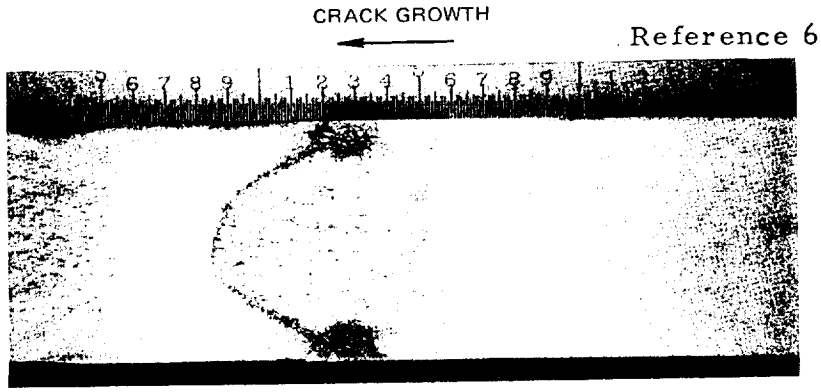

Figure 4-9. Photograph of Inconel 718 With Fracture Surface Evidence of High Cyclic Load Application

4.3 LEAK-BEFORE-BURST

Pressure vessel design often requires that preexisting flaws would grow to through-the-thickness cracks and subsequently leak rather than precipitate catastrophic failure, i.e., "leak before burst." In instances where hazardous or indispensable contents are involved, leakage cannot be tolerated but will often be a preferred or required failure mode when the alternative is rupture.

Efforts to categorize a structures' tendency to leak-before-burst have resulted in definitions of thick-walled and thin-walled structures, referring to critical flaw sizes that are respectively small and large with regard to the material thickness (Reference 7). Such a definition, however, must be restricted to describing flaws of small aspect ratios ranging from semi-circular to long, shallow flaws. For example, a very small hole completely through a thick material would naturally leak-before-burst but would not be consistent with the "thick" definition.

Leakage or flaw breakthrough can occur as a result of either cyclic load crack propagation, sustained load growth, or growth from an increasing monotonic load. As a flaw under load approaches the far surface, a depression on that surface will often be observed. This depression, or dimple, has been attributed to an extension of the plastic zone at the crack tip through the sheet thickness. In thin sheet material, this deformation can be enhanced by localized bending in the area of the flaw. This bending, resulting from load eccentricity due to the presence of a flaw, can cause the dimple area to experience compressive loads.

In leak situations, as either the load and/or flaw size increase, the flaw will abruptly penetrate through the material thickness. As with fracture, this point of one-dimensional instability has been attributed, by various investigators, either to net stress overload of the remaining ligament behind the crack front or to stress intensity instability confined to the thickness direction.

Evaluation or characterization of flaw breakthrough behavior is severely limited by the minimal amount of data available for different alloy systems. Discrepancies among flaw breakthrough measurement techniques complicate the problem further. Visual observations of flaw breakthrough are virtually useless, since dimple formation will usually obscure evidence of crack opening on the back surface. Additionally, since a surface flaw may penetrate to a stable backside length which is a small fraction of the front-face length (2c), it can easily go undetected.

Several techniques are currently employed to accurately indicate the point at which flaw breakthrough occurs. One such method involves

attaching a thin wire to the back surface. As breakthrough occurs, the wire is broken, opening a circuit which will either control the test equipment or signal the test operator. A similar technique involves affixing a strain gauge over this back surface and monitoring strain to give evidence of flaw breakthrough (Reference 8). This approach can provide some supplementary information regarding the events leading up to breakthrough.

For testing in liquid environments, leakage may be assessed by containing the liquid (at the anticipated operating pressure) on the cracked surface of the specimen. In this manner, leakage can be visually observed. Obviously, provisions for containment of the leaking fluid must be made to avoid hazards associated with aggressive environments.

For situations where testing is confined to laboratory air or moderate temperature gases, breakthrough can be identified by a vacuum cup technique (Reference 9). Using a vacuum pump, a rubber cup is attached to the back surface. Once evacuated, the cup is sealed from the pump by a valve and the vacuum monitored by a line gauge. When breakthrough occurs, a sudden loss of vacuum will result. A pressure transducer in the vacuum system can be used to control the test equipment when leakage occurs.

Evidence of flaw breakthrough is often present and can be detected when elastic compliance over the mouth of the flaw is monitored. For cyclic load applications, a continuous record of time versus crack-opening displacement (COD) will often inflect at the point of breakthrough. This transition is related to the different elastic compliance relationships associated with the geometry of the PTC and through-crack (Reference 10). Figure 4-10 shows a typical time-COD record for cyclic loading near flaw breakthrough. Evidence of ligament yielding and a corresponding decrease in minimum-load compliance is a precursor to breakthrough and is evidenced by a decrease in the lower slope of the test record. Additionally, since the bending component of the crack-opening-displacement is reduced by ligament yielding, the total COD will decrease at breakthrough, producing a dip in the upper slope of the test record. Following breakthrough, the elastic compliance behavior will correspond to the center-cracked tension compliance as the flaw growth accelerates to failure.

Measurements of compliance shifts associated with breakthrough under increasing monotonic load application have also been reported (Reference 10). This behavior, however, is much more subtle than that for cyclic load application, and its value as a flaw breakthrough indicator is minimal.

Several models have been formulated to predict or account for the breakthrough of surface flaws to through cracks. The primary application of such a model is in predictive analysis programs designed to calculate the

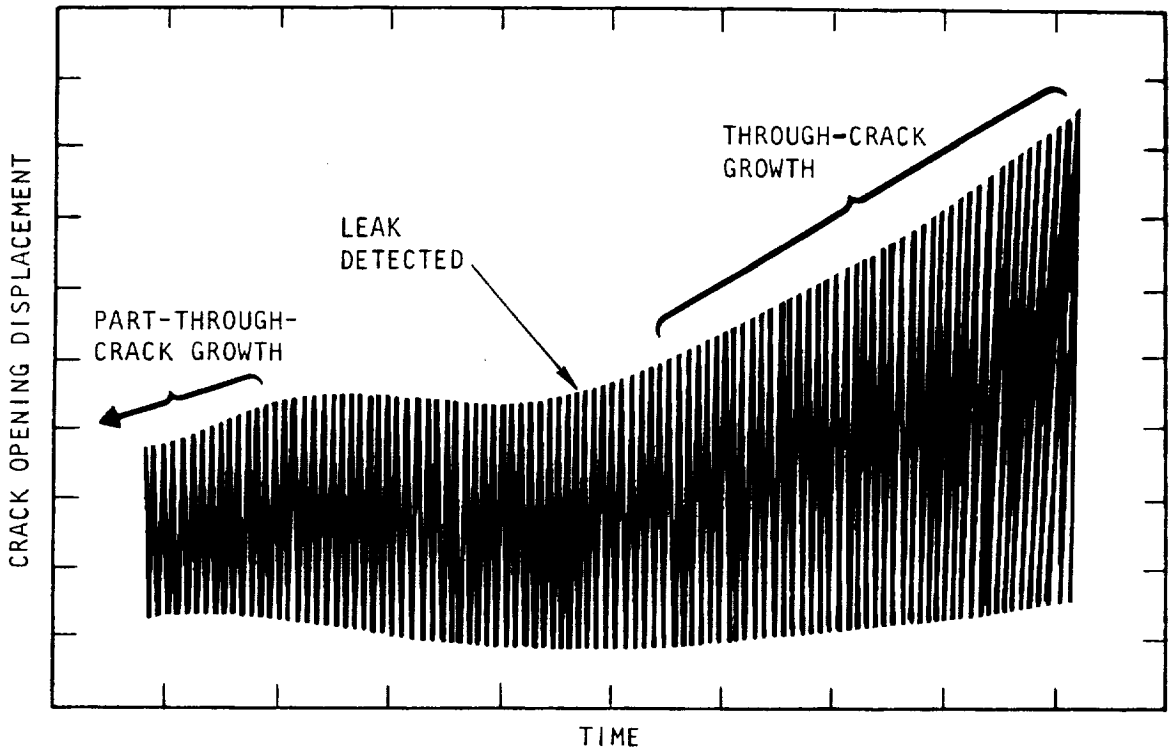

Figure 4-10. Typified Cyclic Compliance Record During Flaw Breakthrough

total life or life-to-leakage of a structural component. As stated earlier, these models are usually attributed to net stress overload of the ligament or stress intensity instability confined to the thickness direction.

From a stress intensity viewpoint, a transition from part-through-crack behavior to through-crack behavior has been approximated by assuming that the ligament area directly behind the flaw carries an increased load proportional to the decreased cross-sectional area (Reference 11). This transition then occurs when the effective stress through this reduced cross-section exceeds the material's yield strength. This type of relationship is expressed by the following equation:

$$(a/t)_{transition} = \frac{4}{\pi}(1 - \sigma/\sigma_{ys}) \qquad (1)$$

For an applied stress level of 50 percent of the yield strength, this equation requires that the transition occur when the flaw depth exceeds only 62 percent of the material thickness. Use of such a model naturally would not be applicable for predicting the occurrence of actual flaw breakthrough. Additionally, the conservative nature of any relationship, which assumes breakthrough occurs by some yielding criterion, is realized only when it can be demonstrated that actual additional flaw growth in the structure will not preclude leak-before-burst behavior when it is a mandatory requirement.

Many investigators prefer to estimate a ligament size at breakthrough by suggesting that when the plastic zone at the crack tip extends to the far surface, breakthrough will occur. Again, however, this implies that a yielded ligament constitutes breakthrough, which is not generally the case, and a serious underestimate of the maximum flaw size at breakthrough may result. Further confusion stems from the variety of equations available in the literature to predict plastic zone size.

For cyclic crack growth predictive analysis, reasonable agreement with experimental life-to-penetration has been demonstrated by simply assuming breakthrough occurs when the actual flaw depth becomes tangent with the far surface (Reference 12). Such an approach assumes essentially elastic behavior up to the point of flaw breakthrough.

In a study by Orange (Reference 13), it was demonstrated that predictions of whether a flaw will precipitate leak or fracture could be made by assuming that through-cracks are governed by plane-stress conditions and surface flaws by plane strain. Figure 4-11 is constructed by evaluating the following stress intensity solutions for surface flaws and through-cracks, respectively:

$$K_{Ic} = M \sigma_c \sqrt{\pi a / \phi^2} \tag{2}$$

$$K_c = \sigma_c \sqrt{\pi c} \tag{3}$$

where K_{Ic} and K_c are the critical stress intensity factors corresponding to plane strain and plane stress, respectively, σ_c is the applied gross stress at fracture, and M is the combined near and far surface correction factor as described in Section 2.

By plotting the flaw length, 2c (the common flaw dimension between the two configurations) as a function of applied stress, evidence of the controlling failure mode is indicated. In the example, K_{Ic} was taken as 40 ksi $\sqrt{\text{inch}}$, K_c as 70 ksi$\sqrt{\text{inch}}$, and the thickness was specified as 0.200 inch. The surface flaw equation is plotted twice: once for constant a/t and a second time for constant a/2c. By locating the surface flaw of interest (i.e., specifying a and 2c), the fracture stress can be located. If the equivalent through-crack size failure stress is greater than the surface flaw failure stress, then leak-before-burst conditions will prevail (Point A). If, on the other hand, the part-through-crack failure stress was greater than the equivalent through-crack failure stress, then fracture before leakage would be expected. For this particular example, flaws of aspect ratio greater than 0.2 and depth-to-thickness ratios in excess of 0.5 would be expected to leak before fracture.

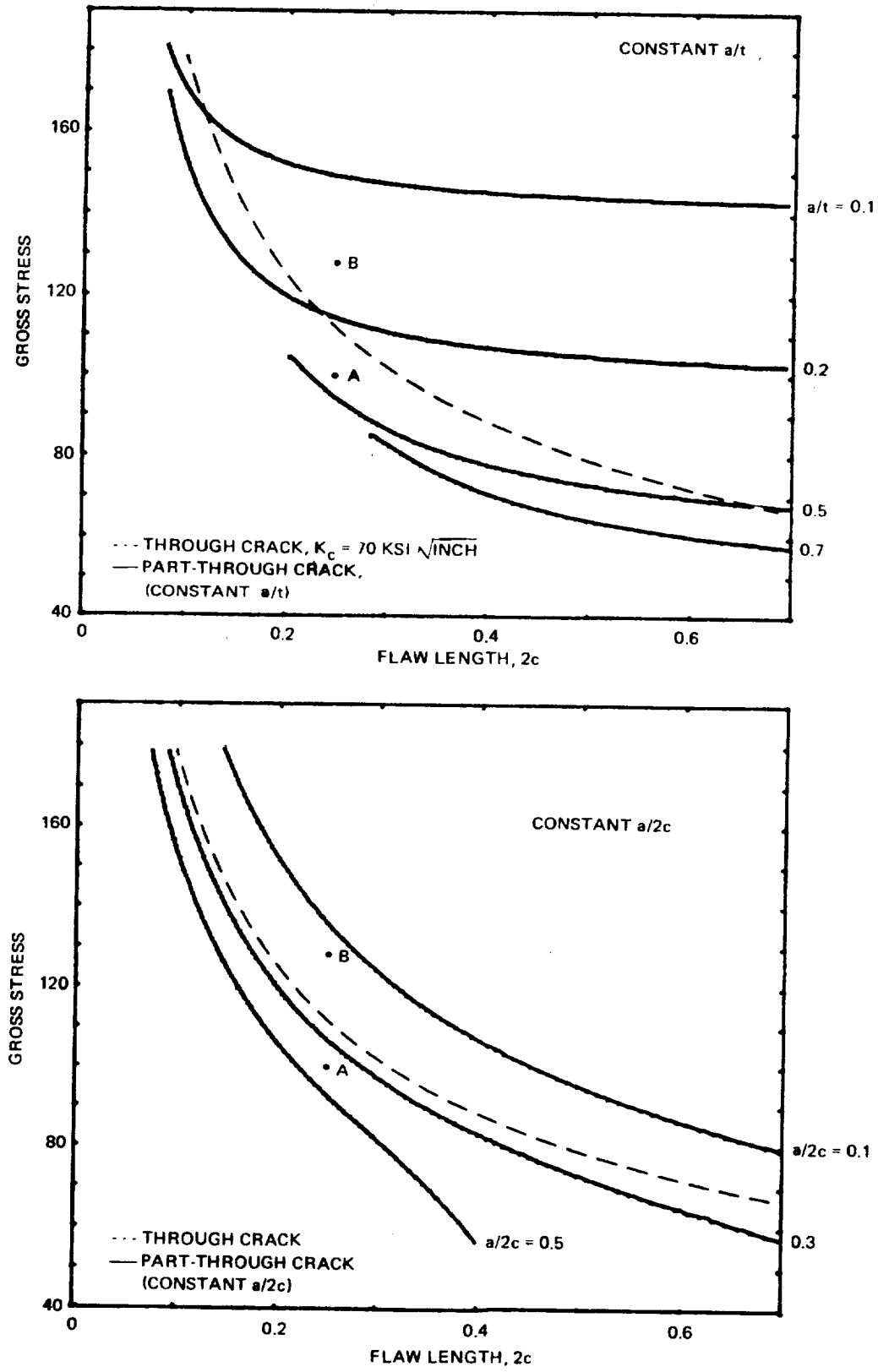

Figure 4-11. Effect of Crack Geometry on Predicted Fracture Stress for Through- and Part-Through Cracks

By equating the stress levels between Equations 2 and 3, specifying that the stress intensity of the part-through crack is equal to K_{Ic} and applying the criteria of leak-before-break that the stress intensity of the equivalent through-crack be less than the plane stress critical stress intensity K_c, the following relationship can be formulated:

$$K_{Ic} < K_c \frac{M}{\phi} \sqrt{\frac{a}{c}} \tag{4}$$

when

$a < t$

$K_{PT_c} = K_{Ic}$

$K_{through\text{-}crack} < K_c$

The leak-before-break criteria of Equation 4 are dependent on thickness only as M and K_c are dependent on the thickness. An immediately apparent consideration resulting from the above analysis is that accurate evaluation of K_{Ic} and K_c values is necessary to properly evaluate the potential for leakage.

Unfortunately, the preceding approach does not consider the elements of flaw growth upon loading and flaw shape changes due to precritical growth, and the deficiencies associated with these omissions have not been fully explored.

As a surface flaw penetrates the far surface, the backside flaw length is frequently seen to grow to stability at a considerably smaller length than the front side length, 2c. Figure 4-12 illustrates the crack front geometry under consideration. For cyclic loading, the backside flaw length increases much faster than the front until the through-crack has achieved a more uniform front. To account for this phenomenon, a correction factor can be applied to the through-crack stress intensity solution to increase the stress intensity as a function of the reduced effective cross-sectional area caused by the semi-elliptical shape of the through-crack front.

Effects on stress intensity due to this type of irregular through-crack front can be approximated as

$$K_{backside} = \sigma \sqrt{\pi c_B} \left\{ \sec \frac{\pi c_B}{w} \right\}^{1/2} \cdot \left(\frac{t}{t - a} \right)^{1/2} \tag{5}$$

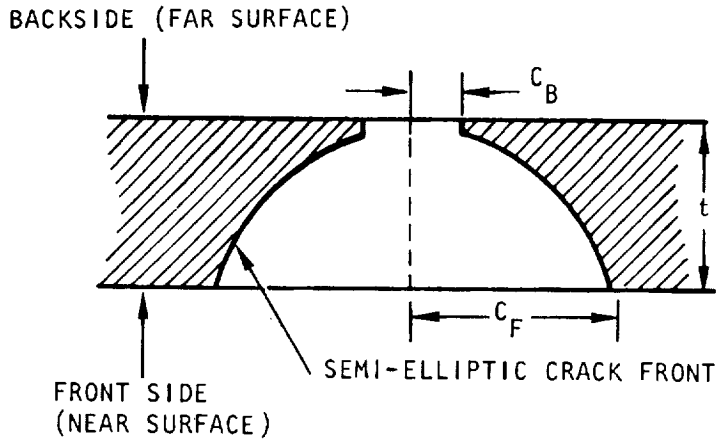

Figure 4-12. Transitional Crack Geometry

By considering the remaining part-through crack front as a regular semi-ellipse, the flaw depth, a, at any point along c can be evaluated from

$$a = t\sqrt{1 - c^2/c_F^2} \tag{6}$$

For c equal to c_B, the magnification factor is expanded to

$$(t/t - a)^{1/2} = \left\{ \frac{1}{1 - \sqrt{1 - c_B^2/c_F^2}} \right\}^{1/2} \text{ where } c_B < c_F . \tag{7}$$

and

$$K_{backside} = \sigma\sqrt{\pi c_B}\left\{ \sec\frac{\pi c_B}{w} \Big/ 1 - \sqrt{1 - c_B^2/c_F^2} \right\}^{1/2} \tag{8}$$

When the backside length equals the front side flaw length, the magnification factor is unity and is dropped from further consideration.

By iteration of Equation 8, an estimate of the stable backside flaw length can be calculated by assuming that the flaw will propagate until the stress intensity falls below K_c. Unfortunately, very little data is available

where backside flaw lengths are measured or reported, and adequate verification of such a model is not possible. Figure 4-13 illustrates the results of a predictive analysis program for cyclic load crack growth incorporating the crack transition model of Equation 8. In this instance, crack size was measured for both the front and backside, and therefore provides a good comparison with the computational output. For this particular example, failure to accommodate the transitional flaw growth behavior would impart a thirty-percent underestimate of the total cyclic life following breakthrough.

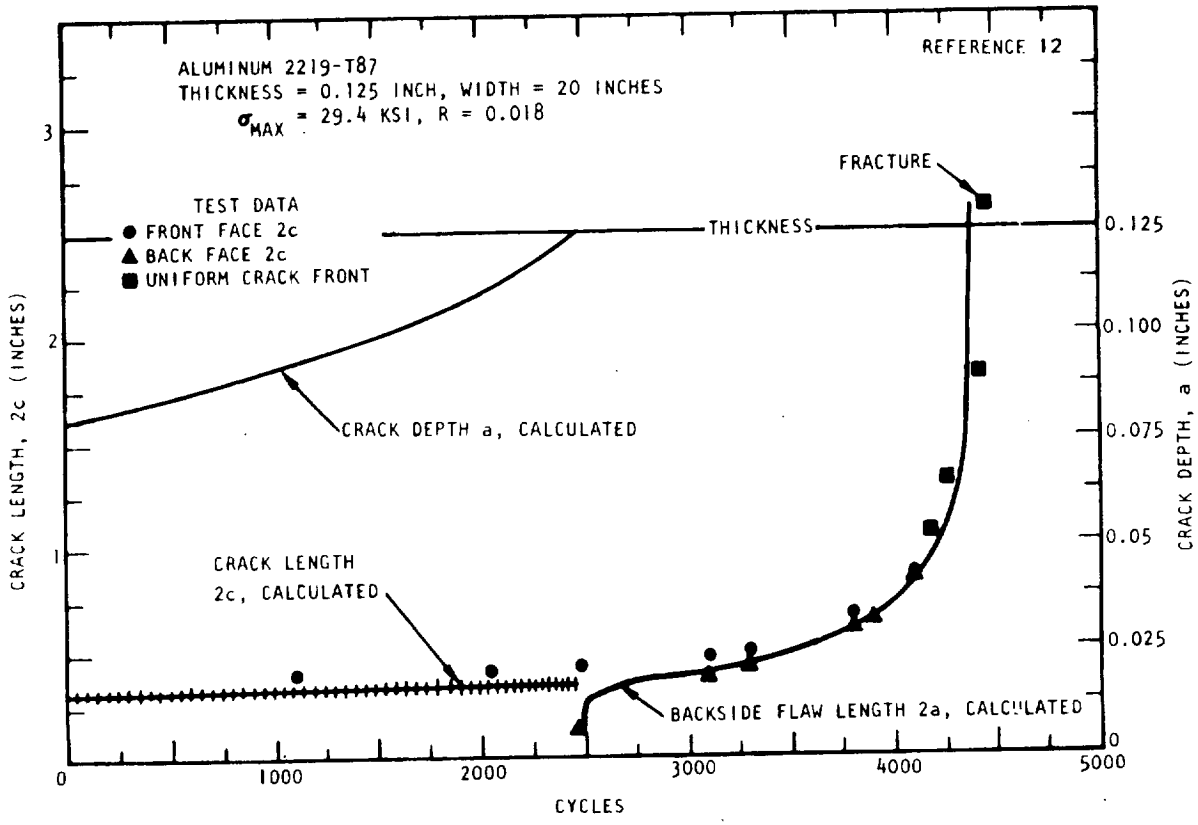

Figure 4-13. Comparison of Predicted With Actual Back Side Flaw Length Following Breakthrough

REFERENCES

1. Electron Fractography Handbook. Air Force Materials Laboratory, Wright-Patterson AFB, Ohio, ML-TDR-64-416, (January 1965).

2. Beachem, C.D., and D.A. Meyn. "Fracture by Microscopic Plastic Deformation Processes," Electron Fractography. American Society for Testing and Materials, ASTM STP 436 (1968), pp. 59-88.

3. Srawley, J.E., and W.F. Brown, Jr. "Fracture Toughness Testing Methods," Fracture Toughness Testing and Its Applications, American Society for Testing and Materials, ASTM STP 381 (1965).

4. Collipriest, J.E., Jr. "An Experimental PTC Study of Pre-Critical Crack Growth in Thick (0.25-Inch) Titanium 6Al-4V, Condition STA," Part-Through-Crack Fracture Mechanics Testing IR&D Summary Report, Space Division, Rockwell International Corporation, SD 71-319 (June 1971).

5. Thatcher, C.S. "Investigation of Cyclic Flaw Growth Behavior of 2024-T851 Aluminum." SD 73-SH-0070. Space Division, Rockwell International Corporation, August 1973.

6. Thatcher, C.S., and R.M. LaSalle. Ki (5) Fracture Mechanics Tests on Inconel 718 Plate. Space Division, Rockwell International Corporation, Laboratories Test Report LR9790-4053 (April 1973).

7. Tiffany, C.F. Fracture Control of Metallic Pressure Vessels. NASA SP-8040 (May 1970).

8. Masters, J.N. W.P. Harse, and R.W. Finger. Investigation of Deep Flaws in Thin-Walled Tanks. NASA CR-72606 (December 1969).

9. Demonet, R.J. Fracture Mechanics Test and Analysis Summary Report. Space Division, Rockwell International Corporation, SD 72-SA-0019 (February 1972).

10. Ehret, R.M. A Study of Deep Surface Flaws in Aluminum. Masters thesis, California State University at Long Beach (June 1972).

11. Vroman, G. Correlation of PTC Growth to CT Specimen Data. Los Angeles Division, Rockwell International Corporation, NA-71-879 (1971).

12. Collipriest, J.E., Jr., and R.M. Ehret. Computer Modeling of Part-Through-Crack Growth. Space Division, Rockwell International Corporation, SD 72-CE-0015 (1972).

13. Orange, T.W., T.L. Sullivan, and F.D. Calfo. "Fracture of Thin Sections Containing Through- and Part-Through Cracks," Fracture Toughness Testing at Cryogenic Temperatures. American Society for Testing and Materials, ASTM STP 496 (1971), pp. 61-81.

5.0 INSPECTION

5-1

5.0 INSPECTION

Over the past several years, fracture mechanics principles have been vigorously applied toward facilitating improved flaw-detection capabilities. This is a somewhat natural result of the characteristic dependence of fracture mechanics on flaw size, and the inherent necessity that the current or initial flaw size within a structure be known in order to perform a predictive analysis. Also, specification of minimum detectable flaw dimensions is of primary importance when attempting to construct realistic fracture control procedures.

While conventional nondestructive evaluation techniques will often provide sufficient information concerning the size of existing flaws in a structure, it is sometimes necessary to supplement these techniques. Proof test logic employs fracture mechanics principles to characterize the maximum flaw size that could survive a proof load. For relatively brittle materials, where the flaw size screened by a proof test is below that which can be confidently found by conventional nondestructive evaluation (NDE), the proof test can be of significant value.

Other fracture mechanics-related inspection aids are currently in various stages of development. Acoustic emission technology intends to relate sounds emitted in the vicinity of a crack to the crack tip stress intensity. Back surface dimple formation attendant with deep surface flaws under load has also been related to the applied stress-intensity factor.

The conventional nondestructive evaluation techniques and their apparent limits on flaw detectability are briefly summarized in the following paragraphs. A more detailed review of the proof test logic, as it applies to Space Shuttle materials, is presented. Additionally, the theory and applicability of acoustic emission technology and back surface dimple formation are reviewed.

5.1 NONDESTRUCTIVE EVALUATION

The NDE techniques that are within the present technology and that are applicable to the Space Shuttle structure are briefly reviewed in the following paragraphs. Five nondestructive testing techniques widely used for crack detection and measurement are: visual, penetrant, ultrasonic, eddy current, and radiography.

1. Visual/Optical Inspection

Visual inspection, the most elementary method for detecting surface cracks, relies on object illumination and optical surface examination. To improve visual inspection, optical aids such as mirrors, microscopes, and boroscopes (fiber and rod optics) can be used to provide magnification and direct-viewing conditions.

2. Penetrant Inspection

As an extension of visual inspection, the liquid penetrant method can be performed faster, and with greater confidence, than the visual inspection technique. Within the confines of smooth surface finish, and recognizing the spatial resolution limits of the human eye, the penetrant method detects smaller surface cracks, those beyond the scope of visual techniques. The penetrant method depends on the ability of an applied low viscosity, low surface tension liquid to penetrate the surface crack by capillary action. Excess penetrant is removed and an absorbent, emulsified power developer is applied to enhance the indications. Penetrants containing fluorescent dyes are generally viewed with black light to find surface cracks. Several grades of sensitivity are available for penetrant inspection depending on the type of penetrant used. The limiting factor in penetrant inspection is the background fluorescence, which is a direct function of the surface finish for a given material. Hence, flaw sensitivity results depend upon surface finish for penetrant inspection. Penetrant inspection is often used on welds after machining off the weld bead. In this case, etching of the weld bead is necessary to remove smeared metal and assure a quality inspection operation. Penetrant inspection is one of the most cost-effective inspection techniques, and deals directly with the most critical-type flaw, the surface crack.

3. Ultrasonic Inspections

Ultrasonic methods use low-energy, high-frequency mechanical vibrations (sound waves) which are produced by a transducer (piezoelectric element) and transmitted into the part through a couplant material at the transducer/part interface. A change in acoustic properties is detectable because of flaws (surface or internal) which reflect or scatter the sound energy. The reflected waves generate a received signal which is amplified and displayed on a cathode-ray tube. This interaction of sound wave energy with materials is used to determine physical properties of structural materials. Typically, pulsed ultrasonic compression or shear waves are reflected from acoustical impedance interface mismatches. Various types of ultrasonic flaw-detection techniques

exist, these include pulse echo, through-transmission, and resonance techniques. Various wave propagation modes may be employed; these include compression or longitudinal, shear, Lamb, and surface or Rayleigh waves.

The fundamental limitations of ultrasonic inspection other than the material inhomogeneities, common to all nondestructive evaluations, relate to the ultrasonic wavelength in the material being inspected. The usefulness is also limited by the electronic signal-to-noise ratio, speed of the electronics, and transducer response. Because of the advances made in the electronics industry, improvements have been made, and will continue to be made in the ultrasonic equipment field. In particular, the adoption of digital techniques and large-scale integration promises even more rapid advancements in the future.

4. Eddy Current Inspection

The eddy current method involves a coil carrying a high-frequency alternating current, which is brought into the vicinity of an electrical conductor (the structure) to induce eddy currents in the structure. The current field generated by the flow of the eddy currents is interrupted or changed by cracks. This change, which affects the induced currents and magnetic field produced, is detectable. Conditions of material inhomogeneity, especially in terms of the microelectrical conductivity which can reflect small variations in alloying constituents, grain refinement, heat treat condition, etc., represents the most limiting factor as far as crack sensitivity is concerned. Present-day research to refine and improve eddy current techniques includes pulsed eddy current equipment and multiparameter instrumentation where several frequencies can be used. Present work indicates that eddy current techniques are well suited for the detection and measurement of tight, small surface fatigue cracks.

5. Radiographic Inspection

The radiographic method is based on the ability of X-ray, gamma, or neutron radiation sources to penetrate a material, with the attenuation of transmitted radiation proportional to the effective density of the material. Internal cracks or voids are revealed because of the local change in effective density they cause and consequent image they produce on the radiographic film. The detectable size of defects is directly influenced by material thickness. Maximum sensitivity is obtained when the crack plane is oriented parallel to the direction of source radiation.

Penetrating radiation, in the form of X-ray, gamma ray, or neutrons, is used to obtain shadow graph projects of the internal constituents of materials. Radiography detects only the absence or presence of materials. It does not detect lack of bond or crack openings directly. Radiography is principally used for the inspection of welds, brazed assemblies, and castings.

X-ray inspection is a widely practiced technology and the results are well respected. Even so, X-ray inspection is a relatively gross inspection technique and does not represent a precise fracture mechanics inspection tool. Present areas of active research include image enhancement, application of neutron radiography, and development of portable neutron sources.

During operational service, the application of nondestructive evaluation methods will rely heavily upon the accessibility of the structural element. To expose the critical location and surface of some of the reference structural elements, some disassembly may be required. For this reason, it is necessary that qualified NDE personnel evaluate specific configurations for accessibility before minimum detectable flaw sizes are specified for fracture mechanics analysis.

NDE Capabilities

The flaw-detection capabilities of any given NDE technique are, at best, difficult to define precisely. The present trend is to apply statistical methods to demonstrate the validity of critical flaw-detection capabilities. Samples with known flaws (artificially grown fatigue cracks) of various sizes are inspected; then statistical analysis of the detection results is made to determine the crack size range for which 90-percent probability of detection at a 95-percent confidence level has been demonstrated. Actual capabilities and reliability may be influenced by many detailed factors such as material, surface finish, protective coatings, geometric complexity, etc. Currently available literature regarding NDE capabilities, and the results to date of Rockwell International B-1 Division qualification tests on NDE techniques to be applied to the B-1 program have been reviewed. Results of this review are reflected in the estimated curves of "design values" for reliable detection of crack-like flaws summarized in Figure 5-1. Individual curves are given for the NDE techniques of interest. The curves are applicable to cracks partially through the thickness of material, and the attempt to provide a reasonable estimate of interaction between crack length and crack depth as it affects detectability. There are threshold values of crack depth or length below which reliable detection cannot be assured regardless of the other dimension. This concept is reflected in the shape of the estimated detectable/nondetectable boundary curves.

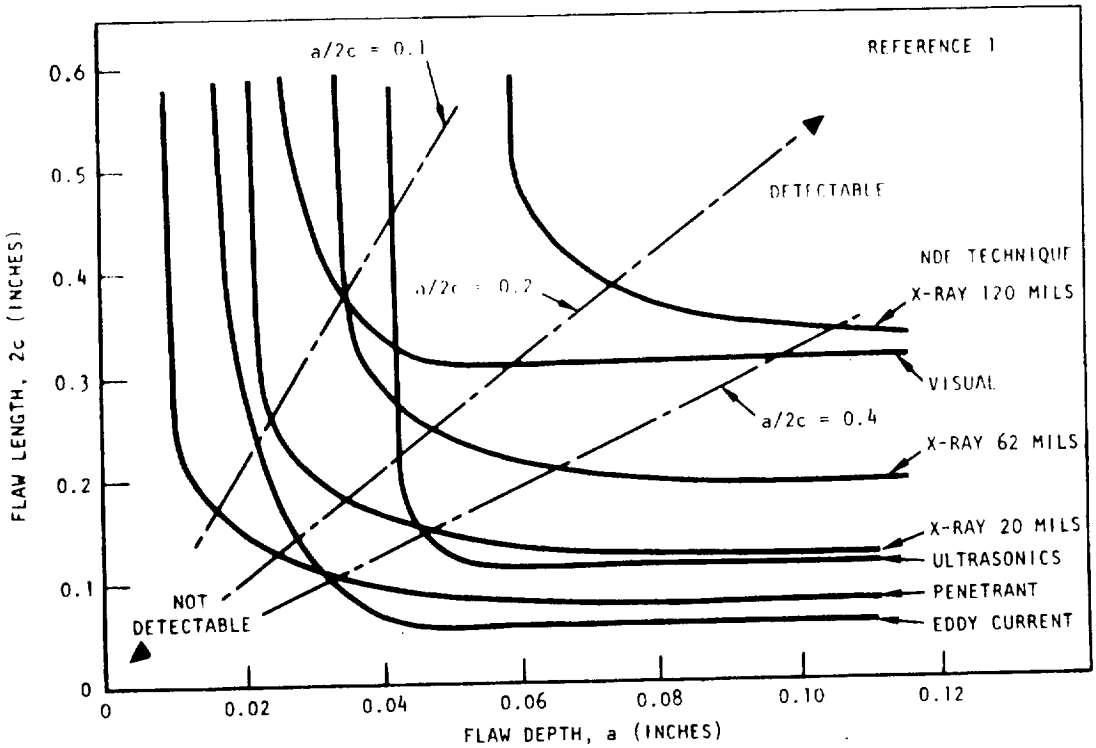

Figure 5-1. Estimated NDE Capabilities for Flaw Detection

The complementary nature of nondestructive evaluation techniques is of prime consequence relative to successful application of NDE. Often, several NDE techniques can be used on a single structure and thereby increase confidence that some specified minimum flaw dimension will be successfully screened. Thus, the availability of the specific detectability limits of conventional NDE techniques is necessary in order that requirements of supplemental inspection techniques can be properly defined.

5.2 PROOF TEST

Proof-test logic can probably be credited with being the single concept most influential in establishing the discipline of fracture mechanics as essential to the design and evaluation of high strength, lightweight, aerospace structural systems. As a technique for limiting the maximum flaw size that could exist in a structure, its value was quickly recognized and accepted. However, not always recognized or appreciated, are the factors which must be satisfied in order to obtain an accurate interpretation of the consequence of a successful proof test. Advancements of fracture mechanics analysis and testing techniques have resulted in comprehensive methods for quantifying the maximum initial flaw size. The following paragraphs review the simplified proof test logic and the important test variables. Identification of the salient features of a more comprehensive proof test logic is also discussed.

Simplified Proof-Test Logic

Given an ideally brittle material of sufficient thickness with an absolute and invarient measure of its fracture toughness, K_c, the following relationship among critical flaw size, stress, and toughness, is obtained from linear elastic stress-intensity analysis:

$$K_c = \beta \sigma \sqrt{a_c} \tag{1}$$

where β is a geometry-dependent constant and, for the present, is considered independent of stress level and flaw size.

This equation will construct the relationship illustrated in Figure 5-2. The maximum flaw size that could survive an applied proof stress (σ_p) is then identified as a_1. Additionally, the final flaw size that will precipitate failure at the reduced operating stress (σ_{op}) is identified as a_2. By evaluating flaw

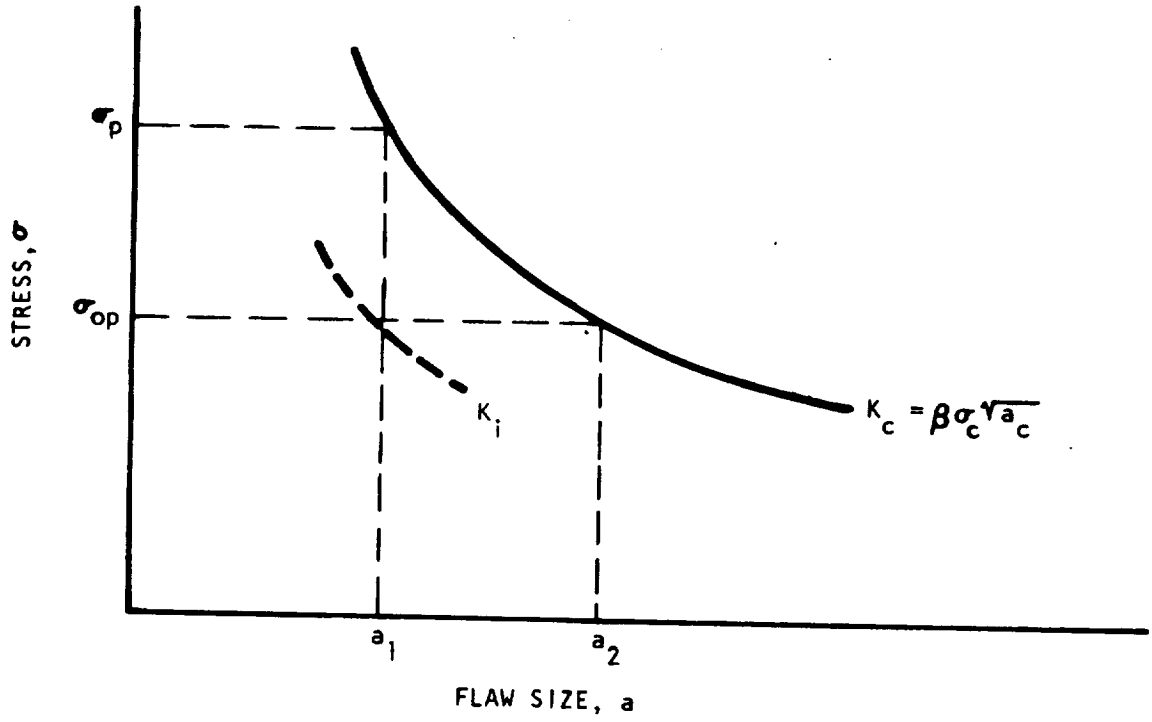

Figure 5-2. Simplified Proof-Test Logic

growth characteristics at the operating stress conditions, the life of the structure (i.e., time and/or load cycles required to grow a flaw from a_1 to a_2) following a successful proof test can be calculated or estimated.

Since service life and operating stresses are commonly specified before a proof test is constructed, the proof stress or proof factor, $\alpha = \sigma_p/\sigma_{op}$, then becomes the dependent variable. A reexamination of Figure 5-2 shows that immediately following the proof load, the structure's maximum initial stress-intensity factor (K_i) at the operating stress can be expressed as:

$$K_i = \beta \sigma_{op} \sqrt{a_1} \tag{2}$$

and since

$$K_c = \beta \sigma_p \sqrt{a_1} \tag{3}$$

the proof factor, α, can then be related to the initial-to-critical stress-intensity ratio, i.e., $K_i/K_c = 1/\alpha$.

By using end-point analysis (see Section 3) to evaluate precritical flaw growth, the K_i/K_c ratio has been related to the time or cycles required to precipitate failure. Based on required service life, a desired K_i/K_c ratio is selected and the necessary proof stress is then calculated.

Complicating Factors

The stress versus critical flaw size relationship of Figure 5-2 becomes more complex with the introduction of free surface and plasticity considerations. For two-dimensional flaw systems, such as the surface flaw, the shape of the fracture curve will change with variables such as yield strength, toughness, thickness, and flaw shape.

Fracture toughness for the surface flaw can be related to flaw size by the following equation (refer to Section 2.3):

$$K_c = M \sigma_c \sqrt{\pi a/Q} \tag{4}$$

where

σ_c is the applied stress at fracture

a is flaw depth at fracture

Q is a flaw shape and plasticity correction factor

M is a combined near and far free surface correction factor dependent upon flaw depth-to-thickness and flaw aspect ratios.

Since the applied stress is included in the plasticity correction and relative flaw size in the M factor, the additional extent of the stress, thickness, and flaw shape dependency on the critical stress intensity becomes evident.

For ideal fracture mechanics materials (very thick, high yield, and low toughness), a single value of the surface flaw size parameter a/Q will adequately describe the critical flaw dimension as illustrated in Figure 5-3. However, for "real engineering" materials, i.e., moderate or high toughness and yield strength in relatively thin gauges, the inadequacy of a/Q as a single critical flaw parameter is demonstrated in Figure 5-4.

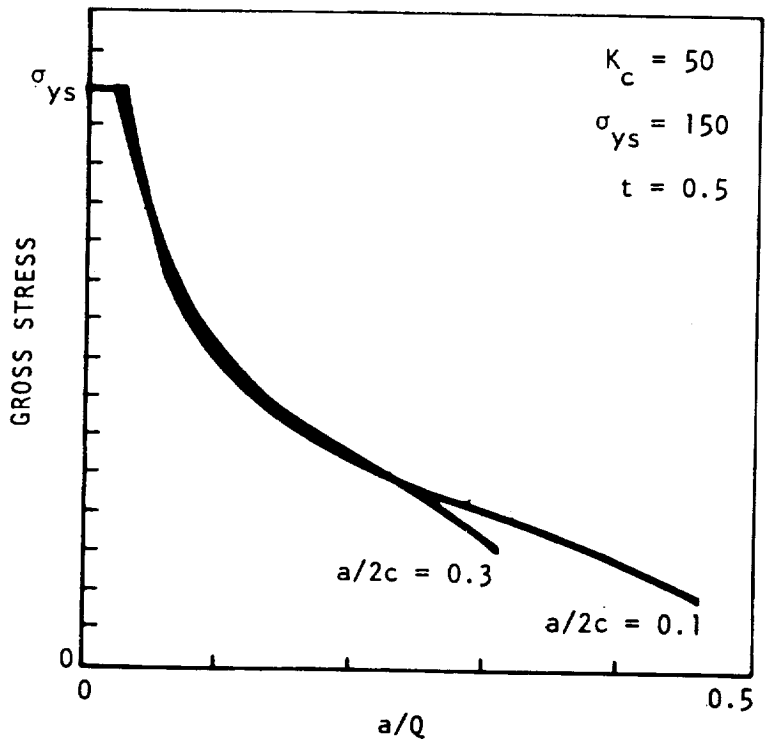

Figure 5-3. Surface Flaw Fracture Curve for an Ideal Fracture Mechanics Material

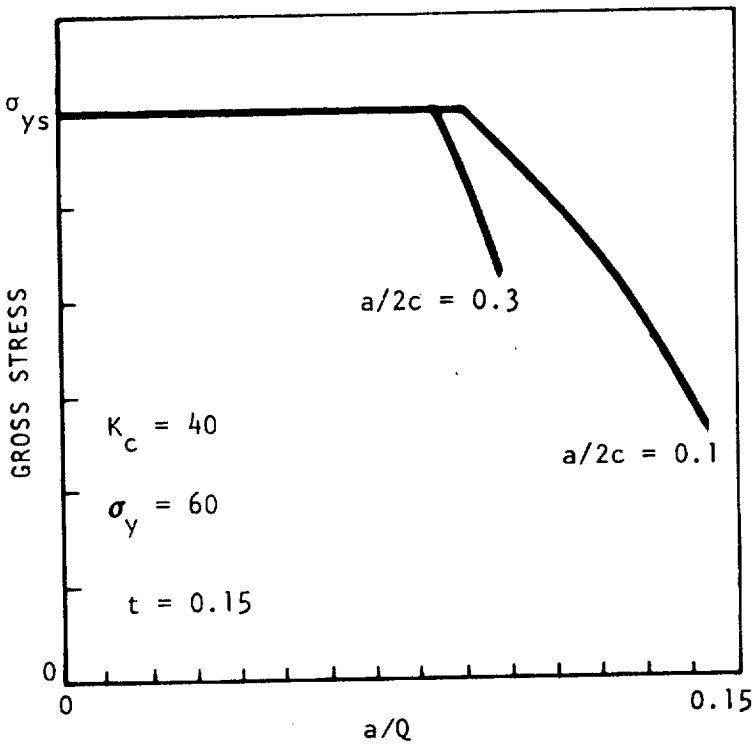

Figure 5-4. Surface Flaw Fracture Curve for a "Real" Engineering Material

Figure 5-5, a replot of Figure 5-4 with flaw depth-to-thickness ratio, a/t, as the abscissa, reveals those (flaw size and shape combinations) which would cause failure at any stress level. Specifying an applied proof stress will provide the matrix of maximum-size flaws which could survive, according to Equation 4. This is illustrated in Figure 5-6. For the more brittle fracture mechanics material, it is evident that a relatively moderate proof test would provide information regarding the entire range of flaw shapes from aspect ratios near zero to semicircular flaws. For the thin-gauge material, it is illustrated that some flaws of high aspect ratio will not result in fracture even as near-through cracks.

The fracture curves previously illustrated have been considered from a single value of fracture toughness. However, whether plane strain or plane stress conditions prevail in the structure being analyzed, considerable variability among critical stress-intensity measurements will be present. As discussed in Section 2.0, the temptation to assign a "conservative lower bound" to toughness values can lead to totally nonconservative results when applied to proof test logic. This can be illustrated by considering the normal relationship between flaw size and the number of applied load cycles as shown in Figure 5-7. The shape of this curve is attributed to the increased flaw growth rates caused by the increase in stress intensity range (ΔK) associated with flaw extension. Analysis using a lower bound measure of toughness will indicate a smaller initial crack size after proof in addition to

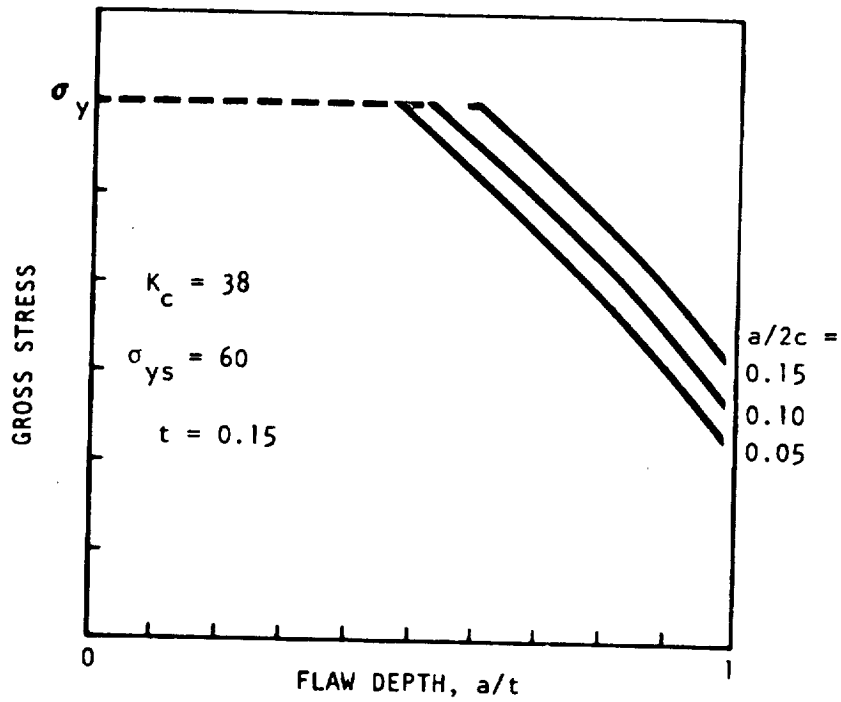

Figure 5-5. Surface Flaw Fracture Curve for Absolute Flaw Depths

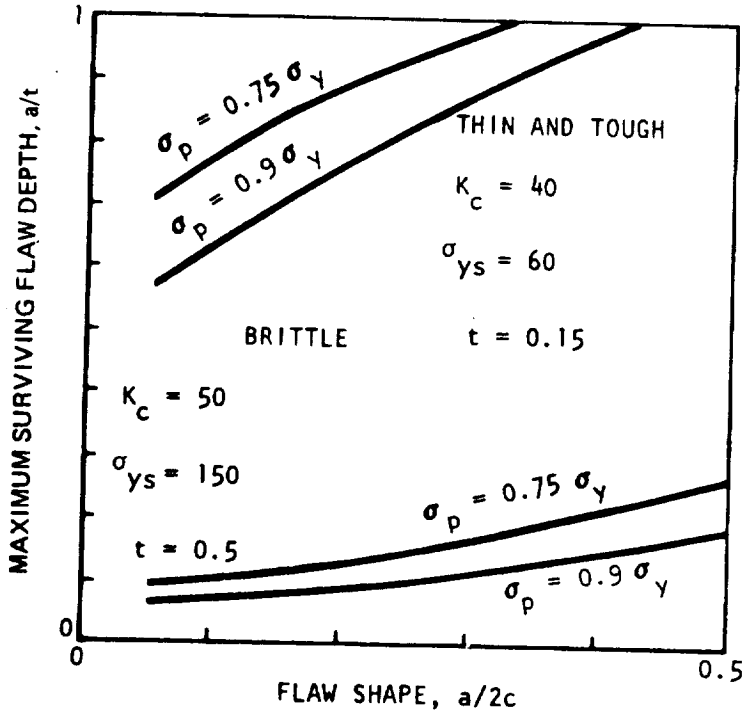

Figure 5-6. Matrix of Flaws to Survive a Given Proof Stress for Real and Ideal Fracture Mechanics Materials

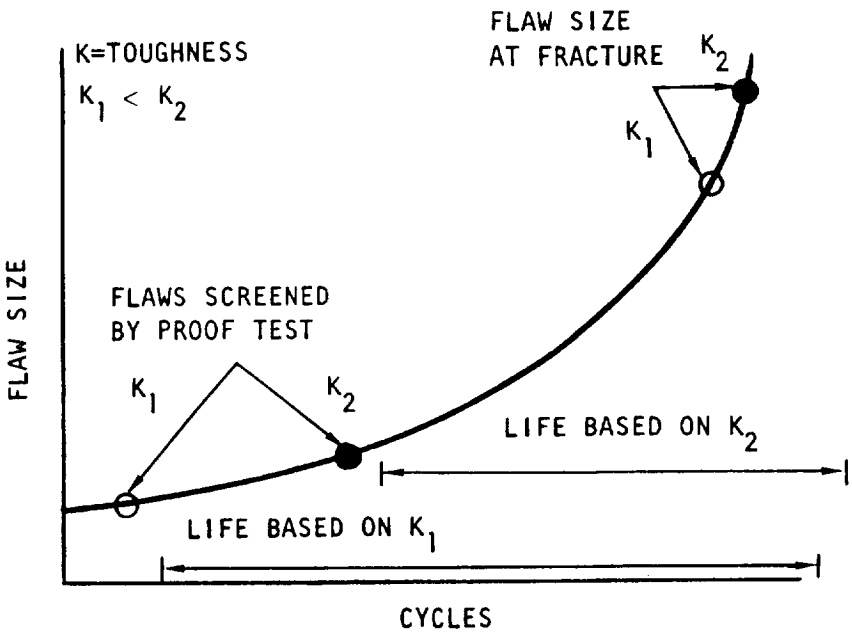

Figure 5-7. Service Life Analysis Curve Illustrating The Unconservative Nature of Lower Bound Toughness Values For Proof-Test Logic

a smaller critical crack size. However, Figure 5-7 illustrates that the total service life is much more severely affected by the initial crack size than by the critical size, and the lower value of toughness predicts the longer service life. Additionally, if the failure mode is penetration (leakage) then the end point of the analysis is not affected by the critical K value which further increases the unconservatism of the analysis.

Additionally, this error can be compounded by flaw shape changes when severe aspect ratio surface flaws (a second assumed conservatism) are being analyzed. That is, when the depth of the smaller initial flaw grows to match the depth of the larger initial flaw, its aspect ratio may be less severe which reduces the stress intensity gradient and extends the predicted life.

At stress levels above the yield strength, the elastic analysis used to formulate the stress-intensity solution fails to account for the large plastic strains, and stress-intensity equations no longer describe observed crack behavior. In general, the fracture curve will deviate above the yield strength to intercept the materials ultimate strength on the ordinate. The net effect of this behavior is a reduction of critical flaw size well below values predicted by Equation (1).

If a proof stress exceeds the yield strength without fracture, the maximum predicted initial flaw size could be significantly overestimated, thus producing a conservative proof prediction. However, high proof-stress levels would significantly increase the risk of structural mortality during the proof test.

As discussed repeatedly in previous sections, flaws subjected to increasing monotonic load are subject to discrete and potentially significant growth. Small flaws that are not too close to being critical may grow insignificant amounts. Near-critical flaws, conversely may grow significantly during proof. If not properly accounted for, this damage could be severe enough to result in the structure failing to meet its first operating stress following the proof stress (Reference 2). This is a worst-case example and although the probability of such an occurrence is minimal, the tendency to characterize the proof test as a guarantee of maximum initial flaw size determination requires that the phenomenon be accommodated.

Assuming that the principles of fracture mechanics analysis still apply, and requiring that instability corresponds to some critical stress-intensity factor, flaw growth on loading might be accommodated by increasing the measured toughness value. For the surface flaw, use of final crack size and failure stress will usually provide a significant increase in the critical stress-intensity factor when compared with K_{IE} values measured from initial flaw size and failure stress. This "survival" stress-intensity (K_S) can be used to identify the maximum flaw to survive the proof load and K_{IE} used to identify that flaw which might cause failure on the next load cycle.

An example of how the resistance curve (R-curve) concept can be used to identify the maximum flaw size that will survive a proof stress is illustrated in Figure 5-8. The more growth-upon-loading experienced by the material, the more gradual the contour of the R-curve (a characteristic of ductile materials). Instability is anticipated at the point of tangency between the R-curve and the stress-intensity curve corresponding to the constant proof stress. The flaw size at this point is labeled, a_s. If a flaw greater than a_o had been present at the start of the proof load application, the entire R-curve would be shifted to the right, causing flaw instability at a stress lower than σ_{proof}.

The stress intensity corresponding to a_s is then termed the survival stress-intensity factor, K_S. This factor, if found to be relatively constant for a particular material and, if necessary, configuration, could be used to establish the necessary matrix of maximum initial flaw sizes that could survive a given proof load. The stress intensity corresponding to the initial flaw size and failure stress (proof stress in the example) should then be equivalent to measured K_{IE} values. The larger the difference between K_{IE} and K_S, the more tolerant the material is to the presence of flaws and the more difficult the application of proof test logic. The current major drawback of such an analysis approach is the lack of credible R-curve data, especially for the surface flaw configuration. As more data become available, however, it is anticipated that application of R-curves to proof test logic will be provided a much needed analysis tool for accommodation of flaw growth on loading during the proof test.

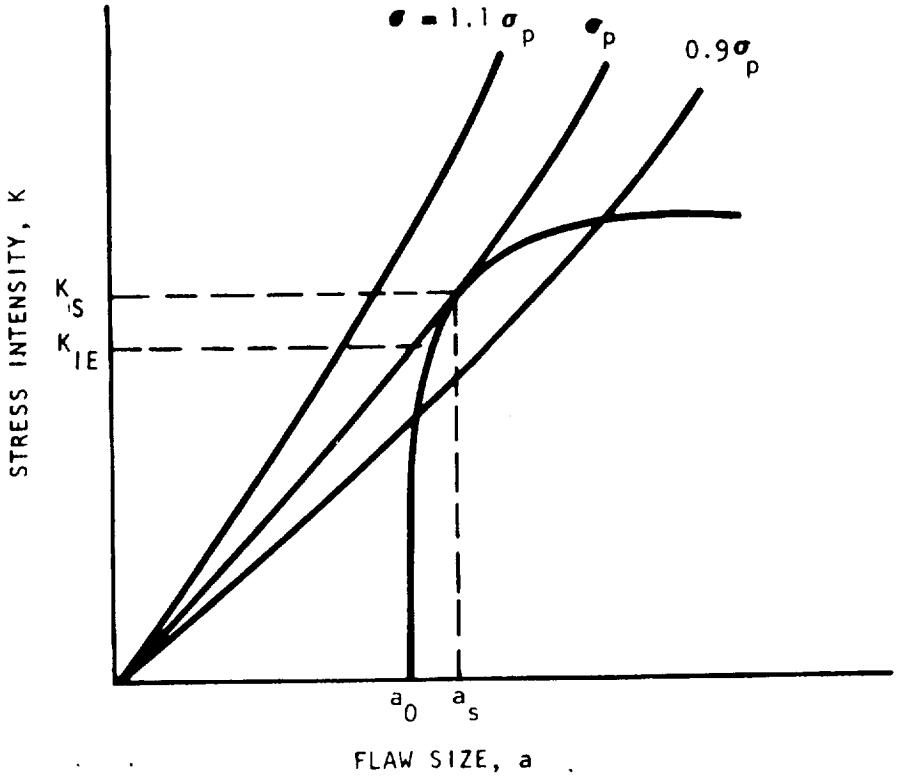

Figure 5-8. Application of Resistance Curves to Proof-Test Logic

When a required initial screened flaw size is smaller than that which minimum detectable flaw size by a lower-temperature proof test. In many engineering materials, as temperature is decreased it is generally observed that the yield strength (Y.S.) increases and the fracture toughness decreases. Each of these conditions will tend to improve the screening severity of the proof test, as shown in Figure 5-9.

In this example, a normal-temperature proof test at a stress level equal to 85 percent of the material's yield strength will screen a flaw of size 0.2 a/t. A proof at 85 percent of yield at the liquid nitrogen temperature would detect a similarly shaped flaw of 0.1 a/t. The difference for the full matrix of detectable flaws between room temperature and cryogenic proof at the yield strength is shown in Figure 5-10.

Before implementing cryoproof as a structural qualification requirement, several factors must be considered. The first would be in assessing the cost of cryoproof as opposed to incremental proof or alternative inspection procedures. Secondly, for consistent application of a cryoproof, an accurate knowledge of how the materials fracture properties vary with temperature is required. This consideration must be extended to include

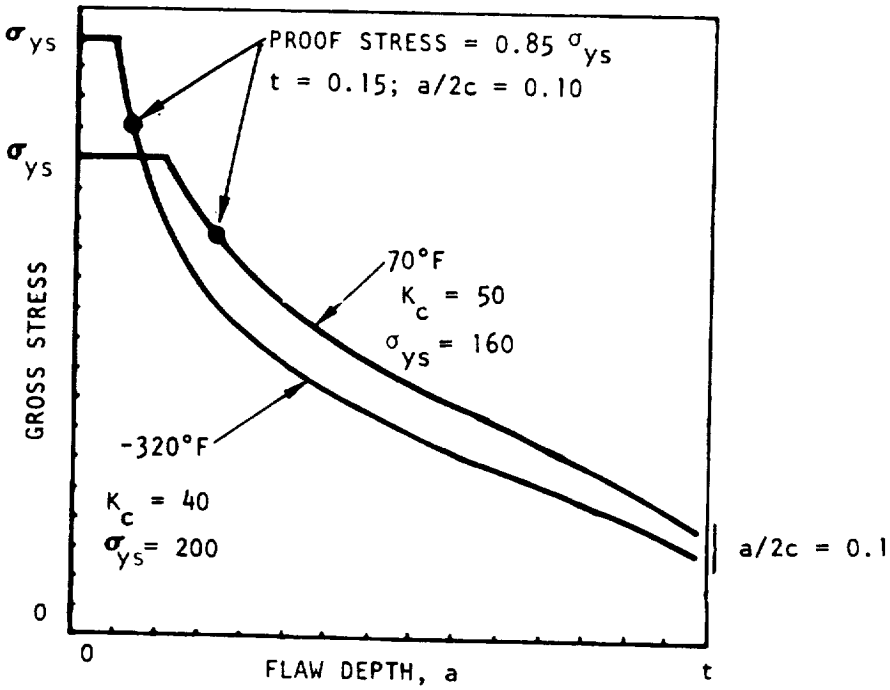

Figure 5-9. Surface Flaw Fracture Curve at Ambient and Cryogenic Temperatures

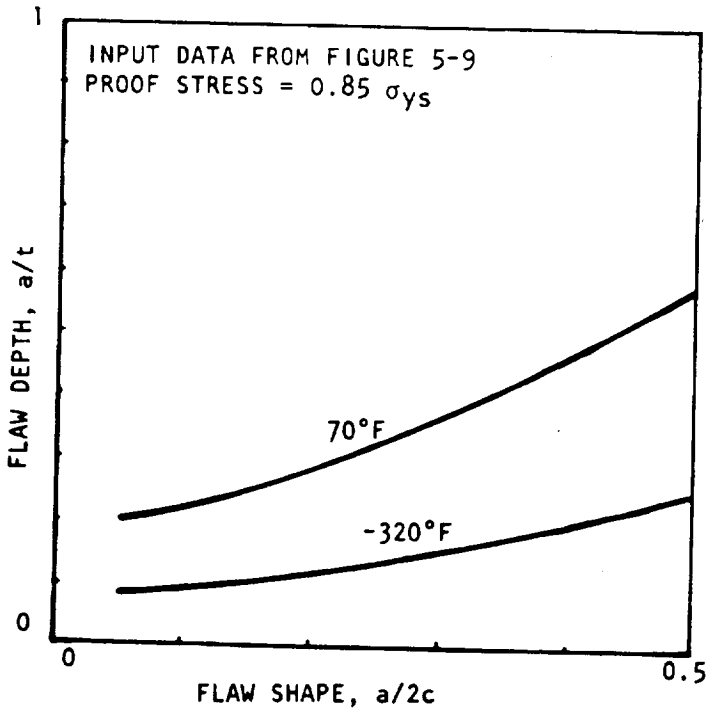

Figure 5-10. Matrix of Maximum-Sized Flaws Surviving Ambient and Cryogenic Temperature Proof Test

all materials within the structure. While one material may be of secondary concern for a normal-temperature proof test, it may become extremely critical if its toughness decreases significantly at cryogenic temperatures.

The effect of temperature on precritical flaw growth behavior during proof loading must also be evaluated. Based on available test results (References 3 and 4) where significant flaw growth during cryogenic proof simulations has been observed, it is not possible at this point in time to generalize concerning temperature and flaw growth-upon-loading.

Comprehensive Proof-Test Logic

Formulation of a comprehensive proof-test logic encompassing all anticipated application situations is naturally beyond the scope of this document. The salient features of such a logic are presented, however, as a guide for construction of viable proof-test logic that accommodates known affecting variables. In the majority of instances, a proof-test logic will be constructed to assure that following proof test the structure will survive an intended service life at operating stresses and environments. The proof test analysis should effectively indicate when an insufficient factor of safety has been applied, or when incremental inspections or periodic replacement of structural components, would be required. Attempts to justify reduction of the design safety factor primarily on a proof-test logic analysis should be avoided; and, if necessary, made only after carefully considering any assumptions made in constructing the proof-test logic. Thus, implementation of a proof test for evaluating structural integrity of hardware does not mean that normal engineering design practice, including safety factors, is no longer controlling structure design.

The following paragraphs outline the primary consideration features involved in constructing a comprehensive proof-test logic. Since the major area of intended implementation of the proof test for Space Shuttle applications will be for pressure vessels, many areas of the following outline will be so oriented.

1. Size the Structure and Choose Materials

The size and function of a structure are usually determined either by mission requirements or management dictate. Producibility, past experience, and cost will most likely govern the material selection. Fracture mechanics analysis will usually play little or no role in this phase of the design. However, subsequent proof test analysis will require a detailed summary of anticipated loads and service environments, in addition to information regarding the size and configuration of the structure.

2. Identify Criteria for Determination of Maximum Initial Flaw Size Following Proof

As previously discussed, the flaw size normally screened by the proof test is one that would cause failure (or leakage) at a designated proof stress. Using such a criterion, it is necessary to establish which of the two failure modes would be anticipated. Flaws which cause stable detectable penetration during a proof test are much more desirable since a proof-test "failure" would not be catastrophic for expensive hardware where repairs could be made. As discussed in Sections 3.0 and 4.0, the assessment of failure modes under increasing monotonic load can be approximated by evaluating the stability of a through-crack equivalent to the surface length of the part-through-crack. In such an analysis, a long shallow flaw, as would be expected, would have a lesser chance of stability following breakthrough than would a semicircular flaw of equivalent effective size. By identifying the critical surface flaw length at the proof stress and comparing it to the flaw size which can be reliably detected by conventional NDE methods, a first-order approximation of the failure mode can be made. In structures where leakage is the anticipated failure mode, it is necessary that leak detection capabilities be sufficient to allow only minimal further load increase or immediate unloading to prevent fracture of the structure.

Criteria other than fracture or leakage have been proposed to determine the maximum initial flaw size that will survive a given proof stress. For example, acoustic monitoring of flaws under increasing monotonic stress intensity has been credited with the ability to detect precritical flaw growth. By experimentally relating the emission counts to the applied stress intensity, the actual initial flaw size, or possibly a smaller size corresponding to a minimum detectable stress intensity, K_d, can be characterized. Acoustic monitoring techniques, however, are presently restricted by structural geometry considerations and insufficient data relating absolute flaw size or stress intensity to acoustic output.

Other approaches which attempt to quantify an initial flaw size during a proof stress will often involve increasing the effectiveness of standard detection methods. For example, by relating far surface dimple formation to stress level and flaw size, the presence and possibly the size of deep surface flaws can be detected by visual methods (Reference 5). Since dimple formation is

most pronounced at maximum load, some hazard may be encountered while monitoring the structure. Given time to properly quantify this dimple formation effect, problems involved in detecting noncritical deep surface flaws of high aspect ratio may be minimized.

3. Identify Fracture-Related Material Properties

A primary fracture property required for successful construction of a proof test logic is some measure of critical stress intensity. In limited situations where plane strain conditions prevail, the ASTM K_{Ic} might be appropriate. In most cases, however, the surface flaw K_{IE} or thin-sheet K_c values will apply.

Experimental characterization of flaw growth on the loading behavior must also be available for the material under consideration. Either R-curve, surviving stress intensity, or other experimental approaches can be employed. In the absence of such data, it becomes necessary either to use an upper bound critical stress intensity which could possibly be much too conservative, or to totally ignore the phenomenon of growth-upon-loading (a dangerous alternative).

4. Identify the Maximum Initial Flaw Screened by the Proof Test

The maximum initial flaw size that will survive a given proof stress can be calculated by combining both R-curves (or other measures which accommodate both growth-on-loading and fracture) and appropriate stress-intensity solutions. For two-dimensional flaw situations, such as the part-through-crack, a matrix of maximum initial flaw sizes must be determined.

The preliminary analysis should be performed anticipating an inert environment proof test at ambient temperature. An inert environment generally allows evaluation of the proof test without accommodating the time variable. That is, loading rates and hold times at the proof stress can be considered to offer an insignificant contribution to precritical flaw growth in an inert environment.

For the surface flaw, the matrix of initial flaws is often limited to aspect ratios at or below 0.5 (semicircular). The fracture behavior of flaws of higher aspect ratio is not adequately characterized and stress-intensity solutions cannot be used with confidence. This limitation necessitates that leakage be detectable during the proof test, or that the maximum initial through-crack size also

be evaluated. For example, a pressure vessel containing a surface flaw of very high aspect ratio (i.e., deep corrosion pit) may often not cause fracture during a proof test even though the defect may be almost completely through the wall thickness. Such a defect cannot be detected by the proof test but is naturally of considerable concern in structures where subsequent leakage is equivalent to catastrophic failure. For such a structure, the fracture/leakage criterion of the proof test can certify only that certain maximum flaws below a particular aspect ratio do not exist in the structure, and remaining flaws must be screened by other criteria or inspection techniques.

If leakage can be accepted as a "tolerated" failure mode and is detectable during service, then flaw growth predictive analysis of the matrix of starting flaws will often determine that aspect ratio below which fracture will take place without prior leakage, and the service life is so evaluated. For nonpressurized structures where flaw penetration might not be detected during proof or service, an initial flaw size analysis for both the surface flaw and the through-crack must be performed. The subsequent service life analysis is then performed for both situations, and the minimum predicted lifetime is then used to access the quality of the proof test or the frequency of inspections or replacement.

5. Perform Service Life Analysis

To adequately evaluate the post-proof test service life of a structure, a flaw growth predictive analysis must be performed on the entire matrix of initial flaw sizes. The predictive analysis techniques (described further in Section 6.0) require accurate precritical flaw growth behavior information for the operating or service environment. Failure must be accommodated by exceeding some critical stress-intensity factor. For relatively inert environments, a lower bound K_{Ic}, or more appropriately, a K_{IE}-type value determined from resistance-curve tests may be used. For application or service in an aggressive environment, it is recommended that failure be considered to occur when the applied stress intensity exceeds the environmental threshold stress intensity, K_{th} or K_{Iscc}, determined from sustained load flaw growth tests.

An example illustrating a typical surface flaw predictive analysis output is presented in Figure 5-11. The matrix of initial flaws is established by Equation (2) for a proof stress of 90 percent of the yield strength for 0.02-inch aluminum alloy. The flaw survival

stress intensity, K_S, was specified at 35 ksi$\sqrt{\text{inch}}$. In this example, the loading profile consists of simple constant amplitude cycles ranging from a 3.3 ksi minimum load to a maximum load of 33 ksi. Below an aspect ratio of 0.15, the analysis indicates that fracture will occur without prior flaw penetration or leakage. For starting flaws of aspect ratio above 0.15, the structure would be expected to leak before fracture. A "safe" difference between leakage and fracture will depend upon mission requirements and leak-detection capabilities.

For this example, the shape of the cycles-to-fracture curve shows a minimum value of 800 cycles at a/2c = 0.15, indicating a worst-case starting flaw aspect ratio. Examples with other starting conditions can be generated where the worst-case flaw shape will occur at aspect ratios of both 0.1 and 0.5 with the shape of cycles-to-fracture curve being much more significantly contoured. Therefore, generalizations regarding the most severe flaw aspect ratio must be avoided, and a complete analysis (as shown in Figure 5-11) should always be performed.

Depending upon the degree of confidence associated with the predictive analysis program, the minimum predicted lifetime of the

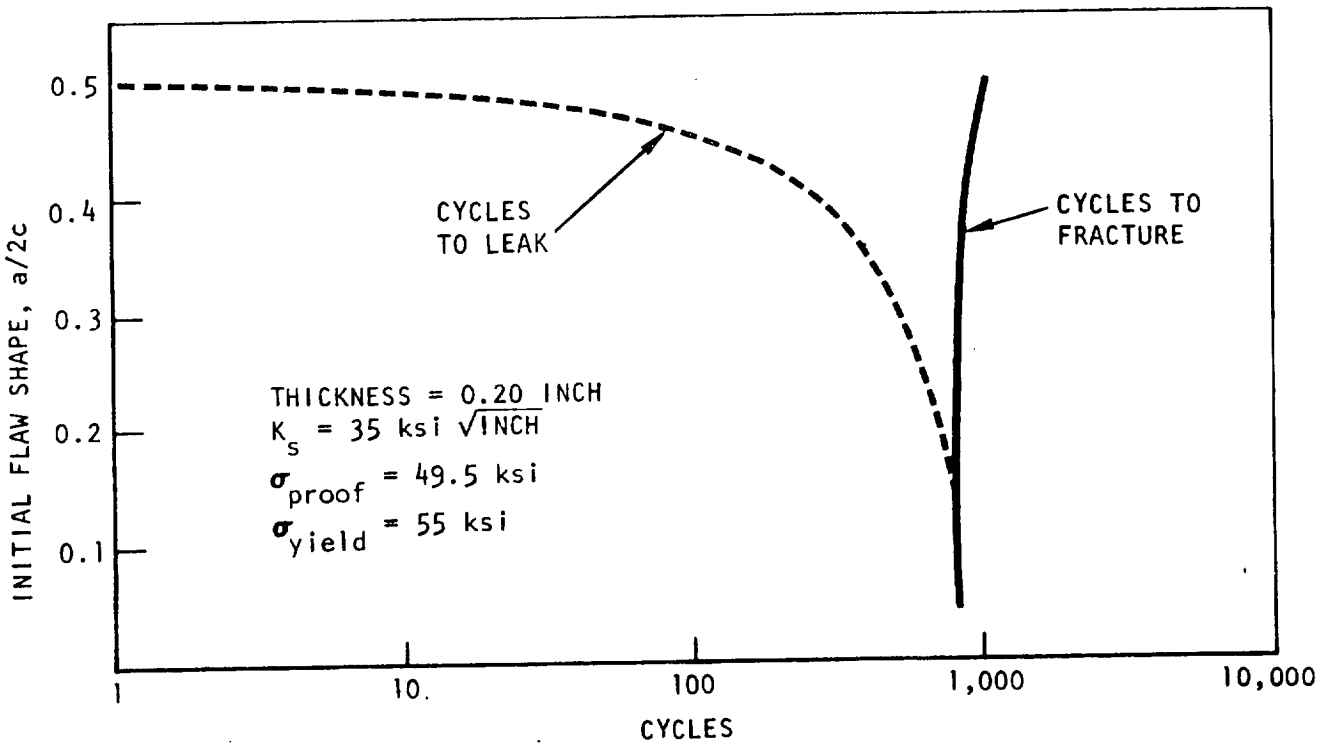

Figure 5-11. Post-Proof-Test Cyclic Flaw Growth Analysis

structure is then divided by some predetermined scatter factor (often ranging somewhere between 1 and 10) and the result compared to the required service life. Confidence in the analysis naturally degrades as the number of phenomena to be considered increases. If the operating conditions are comprised solely of inert environment constant amplitude cyclic loads, the scatter factor would be a minimum value. If, conversely, the analysis is required to accommodate a severe spectrum load (with crack retardation), hostile environments, periodic holds, and thermal cycling, the applied scatter factor should naturally increase. Additionally, if the total required service life is very short (i.e., less than 50 load cycles) a larger scatter factor should also be used since precritical flaw growth data usually averages large amounts of crack extension occurring over many load cycles.

6. Assess Position

If the predicted lifetime (adjusted by the appropriate scatter factor) exceeds the required service life, the proof test can then be used to support hardware qualification by providing some measure of confidence regarding the ability of the structure to meet its intended lifetime. If, conversely, the proof test analysis reflects insufficient service life, modification of either the proof test, the service life requirements, or the basic design of the structure must be considered. The alternatives are summarized in the following paragraphs.

A. Reconstruct the Proof Test to Screen Out Smaller Flaws

If insufficient service life is predicted by a proof-test logic analysis, several changes in the basic design of the proof test are possible. The minimum predicted service life can naturally be extended by decreasing the maximum initial detectable flaw size. Increasing the proof stress would be the first choice, provided that it has been demonstrated that proximity to the material's yield strength does not jeopardize the applicability of linear elastic theory, and that localized yielding (if it occurs) will not distort the structure beyond specified limits. If a proof test at stresses above 90 percent of the materials yield strength approaches this limit of applicability, other methods of improving the proof test should be sought.

A second, and quite common, approach to decreasing the maximum detected flaw size is use of the cryogenic temperature

proof test, the principles of which have previously been explored. Liquid nitrogen (-320 F) is the most used cryogenic proof media because of its inert characteristics. If the structure is not intended or designed for low-temperature service, a survey of all components must be made to assure that temperature-sensitive materials, such as many nonmetals, will not be damaged during a cryoproof.

The multiple-cycle proof test concept has been offered as a method of decreasing the maximum initial detectable flaw size by decreasing the probability of the presence of flaws large enough to experience significant growth-upon-loading. It has been proposed (Reference 6) that an optimum five-cycle proof test would allow near-critical flaws to grow to a critical size and cause failure during the multiple-cycle proof test, while smaller flaws could not grow significantly. The probability of the presence of a flaw of the exact size necessary to fracture on a sixth proof cycle is significantly less than the probability of a near-critical flaw just surviving a single proof load.

B. Reassess Precritical Flaw Growth Analysis

The service life predictive analysis will often omit some flaw growth phenomenon which, if incorporated, might significantly extend the predicted lifetime. One such phenomenon is crack-growth retardation (refer to Section 3.0). Since retardation mechanisms are far from exact in representing actual behavior, they are often "conservatively" omitted from the preliminary analysis. If the loading profile suggests possible benefits from incorporating retardation considerations, and the analysis without retardation shows insufficient service life, then characterization of the crack-growth retardation behavior would be appropriate.

It may also be possible to require that environmental controls be imposed which would allow application of less severe flaw-growth characteristics. For example, fluxuation of NO content in N_2O_4-titanium configurations has been demonstrated to significantly affect flaw-growth rates (Reference 7). Similar effects have been observed for elevated temperature in otherwise inert environments.

C. Reduce Required Service Life

One method often used to certify structural integrity by the proof test is through periodic replacement or requalification

by proof test at specified intervals in the structure's lifetime. Thus, the proof test must certify the structure for a smaller service life, thereby decreasing the severity to the test and increasing the probability of reaching its intended service. Although it may be argued that more damage is likely to occur during proof than in service, the incremental proof provides an alternative approach for handling negative proof analysis results. Naturally, one primary consideration to be evaluated in such a situation is the accessibility of the component for periodic replacement or reproof. Additionally, the cost of such procedures may, in many instances, be prohibitive.

D. Design Change

The predicted service life of a structure can be easily extended by design changes. Although system requirements usually dictate operating pressure or loads, it may be possible to decrease these load requirements if the situation demands it. Correspondingly, the operating stress can be decreased by increasing the material thickness. The corresponding weight penalty, however, will often restrict such a change. Additional assessments may be necessary to assure that leakage rather than fracture will be anticipated failure mode as a result of an increase in structural thickness.

A final possible alternative to increase service life would be a major material change. Such a decision requires reassessing the entire previous analysis and constructing a new proof-test logic for the alloy.

In summary, it must be reemphasized that the proof test often will not provide sufficient information regarding the full matrix of initial flaw sizes so that the full service life can be assured by successful proof test alone. A proper mix of dependence upon both the proof test and conventional NDE will allow these techniques to complement or supplement one another so that the most efficient and effective design will prevail.

5.3 BACK SURFACE DIMPLE FORMATION

One interesting and potentially important aspect of surface deformation phenomena studied in the laboratory is that of back surface dimpling. Preliminary consequences of this effect have been studied and reported by Francis and Davidson in Reference 5. When surface flaws are loaded in tension, a depression or dimple on the back surface is often observed. The

shape is that of an elongated surface depression, resembling an hour-glass configuration on the specimen surface, lying in the crack plane with a length approximating the front surface crack length, 2c. The dimple effect is strongly influenced by crack depth, a/t, and less so by crack aspect ratio, a/2c. For 2219-T87 aluminum alloy, the stress level at which back surface dimpling first develops was shown to be inversely related to the crack depth and directly related to the aspect ratio, as illustrated in Figure 5-12. It was also reported that the dimple depth, when first detected by eye, was typically on the order of 20 microinches.

The phenomenon of back surface dimpling has been suggested (Reference 8) as potentially forming the basis for detecting surface flaws which reside on the inside surfaces of tanks and thin-walled pressure vessels. If improved dimple detection techniques prove feasible, substantially more must be learned about the dependence of dimple size and depth upon flaw geometry, applied loads, and material properties.

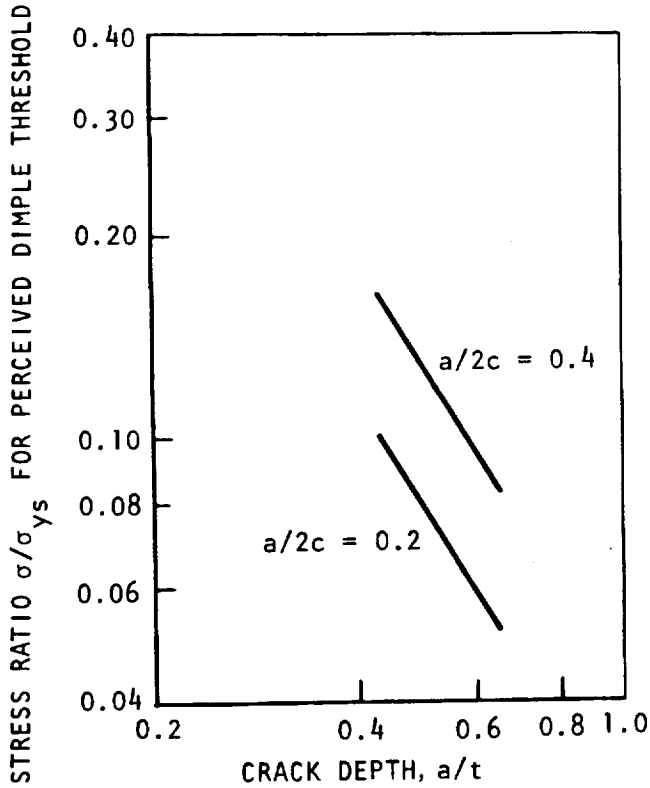

Figure 5-12. Perceived Dimple Thresholds for 2219-T87 Aluminum

5.4 ACOUSTIC EMISSION TECHNOLOGY

Acoustic emission technology addresses the subtle sonic emissions generated during metallic crack growth. Three fruitful areas for investigation have been: (1) scientific investigations of crack growth in the laboratory, (2) monitoring of pressure vessels during proof testing, and (3) monitoring of atomic reactor components to identify crack propagation before failure.

Basic theory tells us that all sound is generated by vibrating bodies. Large objects vibrate at low frequencies while small objects vibrate at high frequencies. Typically, the sonic emissions generated by crack growth extend from the audible range to over one megahertz. High-pass filters are usually used to reduce the low-frequency sound competition from extraneous sources. The majority of the research performed has addressed frequencies from 80 kHz to 700 kHz. The sounds are detected by a variety of transducers, piezoelectric crystals being the most common. Many factors influence the capabilities of present acoustic emission equipment to detect and monitor flaw initiation and growth. Generally, the gross factors can be categorized, as noted in Table 5-1. However, even the heat treatment of an alloy will affect the acoustic activity of a material, and sufficient data is not normally available even on one material to predetermine the degree of usefulness of acoustic emission tesing for a given structure without first performing preliminary testing for each specific application.

Acoustic emission has been handicapped with scaling problems. What works with small specimens and is simple, becomes increasingly difficult and complex with larger structures. With this in mind, it should be realized that the most encouraging results have been generally achieved with small tensile specimens.

Acoustic emissions are emitted from plastically deformed material occurring to the relation $N = AK^m$ (Reference 10), where N is the total number of acoustic emission signals resulting from dislocation movement in the plastic zone surrounding a growing crack, K is the local stress-intensity factor, and A and m are material-related constants. Experimentally, values of m have been observed from 4 to 8. A simplified theory predicts a value of 4 (Reference 11). The coefficient A is dependent on the instrumentation (gain) and transducer location in addition to material properties and, hence, is more difficult to relate to a specific material characteristic.

Acoustic emissions are essentially volumetric local phenomena. As with plastic deformation, the process is irreversible. That is, once a structure has been loaded, additional acoustic emission will not occur until the previous load level is exceeded (Kaiser effect, Reference 12). This is somewhat of a gross simplification since unload emission and reload emission

Table 5-1. Factors That Influence Acoustic Emission Detectability (After Reference 9)

Factors Resulting in High Amplitude Signals	Factors Resulting in Lower Amplitude Signals
High strength	Low strength
High strain rate	Low strain rate
Anisotropy	Isotropy
Nonhomogeneity	Homogeneity
Thick section	Thin section
Twining materials	Nontwining materials
Cleavage fracture	Shear deformation
Low temperatures	High temperatures
Flawed material	Unflawed material
Martinsitic phase transformations	Diffusion controlled transformations
Crack propagation	Plastic deformation
Cast structure	Wrought structure
Large grain size	Small grain size
Soft materials	Hard materials
Low dimensional stability	Low creep

have been reported, but these were at much lower signal levels than load emissions. It would appear that all solid materials, including glass, generate acoustic emission under sufficient loads. Acoustic emission activity is associated with numerous processes, including welding, stress corrosion, work-hardening, and metallurgical transformation. The transmission of sound (acoustic emissions) in metals is a complex situation highly dependent upon reflection losses and reflective geometry. The fundamental physical theory of sound transmission is fairly well established and computer analysis

of real-life geometries to determine theoretical sound transmission output at various points on a structure represents an area of research deserving closer attention.

Emission activity is basically an acoustic phenomenon and the basic laws of sound generation and transmission are applicable. Sound transmission and generation are associated with vibrating structures. Typically, vibrations are generated at frequencies determined by the general differential equation of motion:

$$\frac{\partial^2 u}{\partial x^2} + \frac{\partial^2 u}{\partial y^2} + \frac{\partial^2 u}{\partial z^2} = \frac{1}{\sqrt{T/\rho}} \frac{\partial^2 u}{\partial t^2}$$

where u is deflection, x, y, z are the three-dimensional cartesian coordinates, t is time, and $\sqrt{T/\rho}$ is the velocity of sound where T is the modulus in tension and ρ is mass density. By applying appropriate boundary conditions the vibrations of any object may be represented, the solution of which evolves as an eigenvalue problem defining the frequencies of vibration. In thick materials (>1/4 inch), the attenuation coefficient is proportional to the frequency to the fourth power, while in thin material (<1/4 inch), the attenuation coeffiecient is proportional to a lower power of the frequency because of the nature of the propagation. Direct attenuation of sound is not significant in metals at frequencies below 1/2 megahertz. However, reflection losses are quite significant and pose a difficult problem with respect to geometry considering the simple nature of the phenomena. In a practical sense, material thickness can have a large effect on apparent attenuation (signal amplitudes decrease). In general, however, the attenuation of sound is low in metals and monitoring of relatively large areas (10 to 100 square feet per sensor) is feasible.

Acoustic emission monitoring techniques have been applied to fracture mechanics laboratory studies for a variety of materials. Laboratory fatigue test techniques are well suited for acoustic emission studies, and it is possible to directly correlate acoustic emission activity with crack growth and number of fatigue cycles. Of course, numerous other nondestructive testing techniques have been used to locate, measure, and monitor fatigue crack growth. With acoustic emission testing, a new approach to nondestructive testing of flawed structures is possible. The passive nature of the flaw can be eliminated. The flaw must be an active source of crack growth under proof tests. Hence, the criticality of the flaw location, orientation, etc., is automatically controlled. Table 5-2 lists several types of acoustic emission testing.

Many problem areas exist, the foremost being the noise problem. This problem can be divided into two areas, instrumentation and extraneous noise sources. High gain is necessary because the signals are initially low and a

good signal-to-noise ratio is important. Other mechanical sources of noise, including the tensile testing machine, pinning, and associated laboratory equipment, must also be considered.

Preliminary testing on small specimens has revealed that it would be extremely difficult, if not impossible, to obtain useful information from a large structure by simple monitoring of the structure for acoustic signal count, or even the count rate. The many variables that could be involved made this an impractical approach. Additionally, a review of the research performed by others revealed that while adquate precursors were established from small specimens, confirmed on small specimen in-house tests, that the same precursors could not be established on large specimens or tanks except immediately preceding the actual failure. To take advantage of the monitoring success possible on small specimens and adapt the advantages inherent in small-area monitoring, systems have been designed to treat a large structure like a small structure by dividing it into small areas and then monitoring each individual area separately. The Space Division, under a NASA program, has developed a system to operate under this principle.

With this system, a single triangle of 390 square inches can be divided into 174 areas, approximately 2 square inches each. Each one of these small areas can then be monitored for acoustic activity. Unusual activity in any area, especially at a high rate, is cause to suspect the presence of a flaw. Common noises do not interfere with interpretation, using this concept, because they generate a rise in all the areas relatively evenly. Results to date have been encouraging and show that this concept principle is workable. System refinements are still needed to fully evaluate the concept.

Typical instrumentation used in acoustic emission monitoring is indicated in the block diagram of Figure 5-13. The most critical part is the transducer-preamplifier section. Lead-zerconate-titanate PZT polarized in the thickness expander mode is commonly used for the transducer because this piezoelectric crystal has the largest piezoelectric constant (response). Typically, a 1/2-inch-diameter by 0.05-to 0.2-inch disc is used. The geometry and backing determine the frequency response of the transducer which is a significant factor in the overall system sensitivity. The preamplifier must be of low noise (< 50 to 1 microvolts) and high gain (40 to 100 db), and should act as a line driver at low impedence for the line connected to the rest of the instrumentation. The preamplifier should be as close to the transducer as possible to minimize signal distortion. A fast cutoff active filter is invaluable in establishing a system bandpass optimized to receive acoustic emissions and to reject extraneous noise. The trigger of the electronic digital counter is critical and must have good stability and resolution.

Table 5-2. Acoustic Emission Testing Concepts and Approaches

1. Proof-Test Monitoring. Monitor structure during proof testing; high acoustic emission signal indicates damage during proofing and a weakened structure-low acoustic emission signal further assures a successful proof test. For an example of this approach refer to Reference 10.

2. Use Certification. Functionally proof structure before or during use, with acoustic emission monitoring. High counts indicate incipient failure diagnosis. Low counts certify part for a given life expectancy. In theory this is simple, in practice statistical complications abound. For an example of this approach refer to Reference 11.

3. Stress Level Certification. Proof structure at increasingly higher stress levels until acoustic emission activity occurs at various times in structure life. Activity during each proofing assures that the stress level has not been exceeded during use and flaw growth has not occurred. Low activity indicates that the structure was exposed to higher stress and/or flaw growth has occurred, and proofing should continue at higher levels to determine residual fatigue life. For an example of this approach refer to Reference 13.

4. Life Monitoring. Monitor structure during periods of stressing (testing and actual use). Accumulative counts are indication of life use. Several sources have suggested this approach, including References 10 and 12.

5. Flaw Detection. Use acoustic emission monitoring during proof testing to determine presence of flaws. Flaws are then located by triangulation of acoustic emission signal and other nondestructive inspection techniques. This approach is suggested in References 14 and 15.

6. Fatigue Growth Testing. Based on the irreversible nature of acoustic emission, it is possible to determine the extent of crack growth during a particular number of cycles of loading at a working stress σ_w by periodically stressing at a proof stress $\sigma_p = 1.5\,\sigma_w$. The stress-intensity factor, K, will increase if flaws have grown at σ_w and, hence, acoustic emission activity observed. Conversely, if no acoustic emission activity occurs this would indicate the absence of crack growth. This approach is detailed in Reference 10.

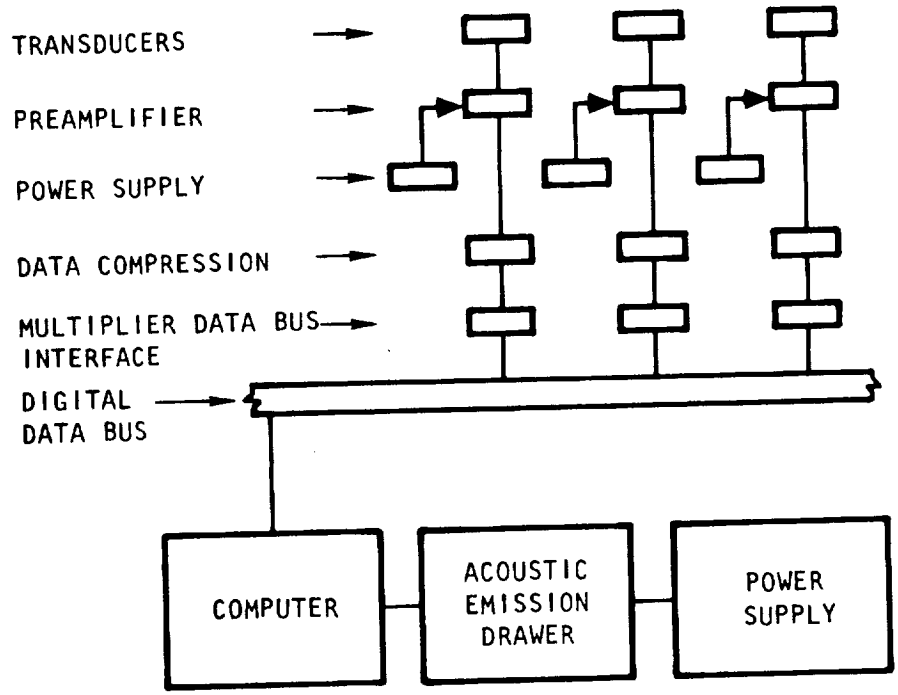

Figure 5-13. Acoustic Emission Test System Block Diagram

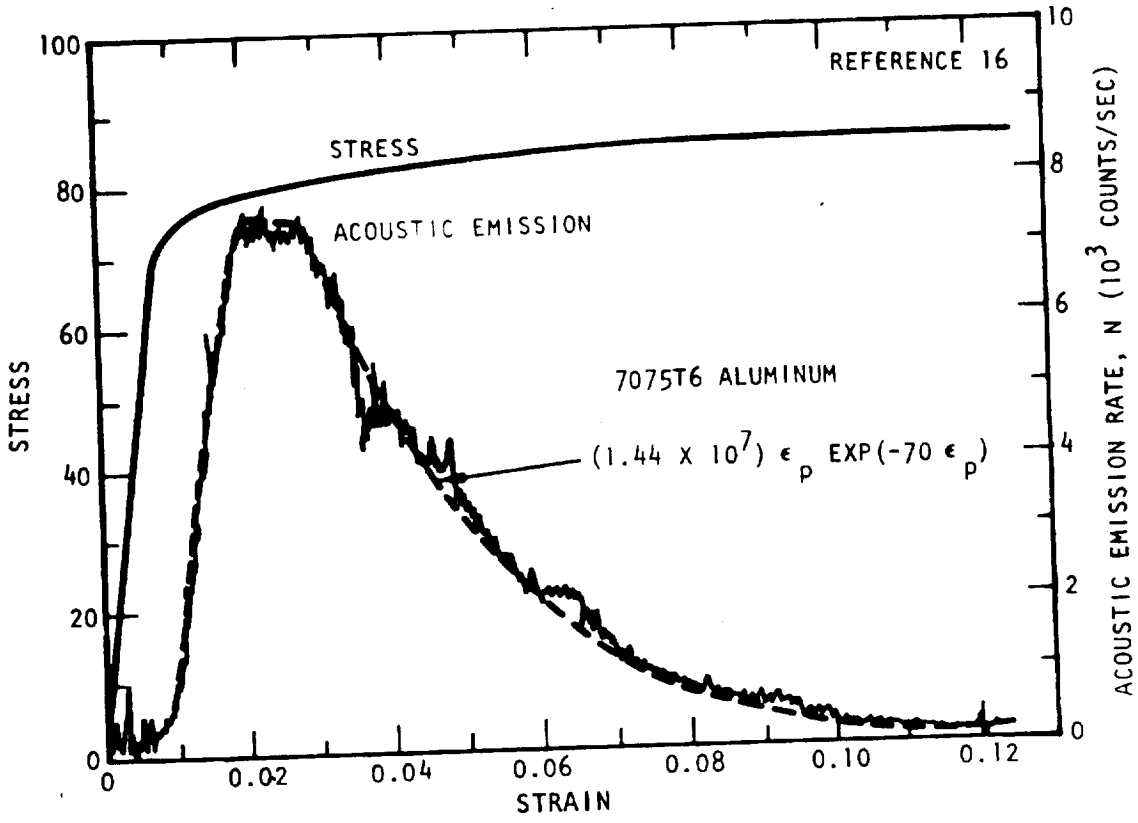

Figure 5-14. Correlation of Acoustic Emission Rate With Strain as Related to Stress

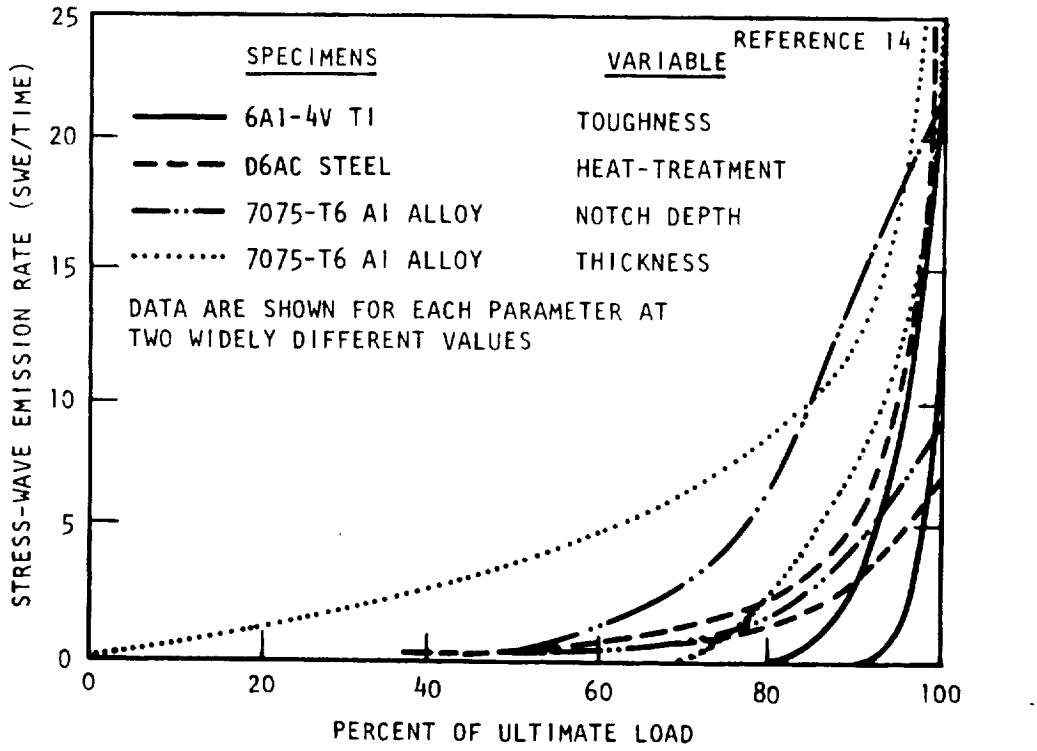

Figure 5-15. Acoustic Emission Rate as a Function of Percent Ultimate Load

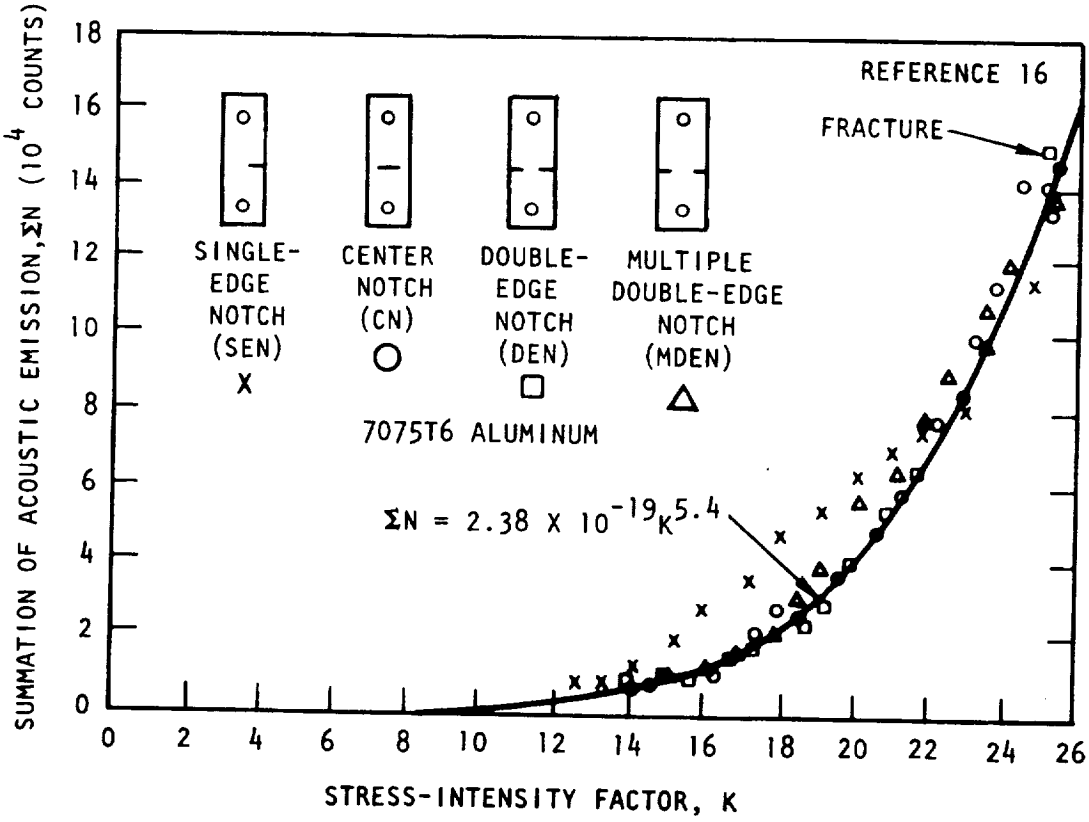

Figure 5-16. Acoustic Emission Summation Versus Stress-Intensity Factor

The nature of the acoustic emissions relative to the stress-strain diagram is shown in Figure 5-14. Initial results were commonly plotted against percent of yield, such as shown in Figure 5-15. This with the view that early emitters of acoustic events would be more receptive to acoustic emission monitoring. Such materials could now be identified on a theoretical basis calculated from the stress-instensity factor correlation (Figure 5-16). Because of the basic complex nature of sound transmission in large specimens, most investigators have devised triangulation techniques to locate the flaw and determine how large an area can be monitored.

The technical literature on acoustic emission technology has grown voluminous considering the relatively recent discovery of acoustic emissions. Reference 17 lists more then 200 technical papers in its bibliography, and this is by no means complete. However, the majority of the works contains little new technical data or original contributions. The technology is diverse and complex. Many papers mention further areas for work and discuss unanswered questions, many of which reflect lack of effort rather than technical limitations.

The future of acoustic emission monitoring is a relatively moot point in that present research and applications assure continued development and use. Acoustic emission testing represents one of the most fertile fields for applications development, and with adaptation of smaller, faster, and cheaper large-scale integrated devices, growth should accelerate and further practical application should evolve.

REFERENCES

1. Westrup, R.W. Final Report - Establishment of Design Criteria for Acceptable Failure Modes and Fail-Safe Considerations for the Space Shuttle Structural System. Space Division, Rockwell International Corporation, SD 72-SH-0046 (June 1972).

2. Collipriest, J.E., Jr. "The Influence of Pre-Critical Crack Growth in PTC Testing of D6-AC Steel," Part-Through-Crack Fracture Mechanics Testing IR&D Summary Report. Space Division Rockwell International Corporation, SD 71-319 (June 1971).

3. Hoeppner, D.W., D.E. Pettit, C.E. Fedderson, and W.S. Hyler. Determination of Flaw Growth Characteristics of Titanium 6Al-4V Sheet in the Solution-Treated and Aged Condition. Battelle Memorial Institute, Columbus Laboratories, NASA CR-65811 (January 1968).

4. Collipriest, J.R., Jr., and D.E. Kizer. Final Report - Saturn S-II Fracture Mechanics Research Program. Space Division, Rockwell International Corporation, SD 68-659 (December 1968).

5. Francis, P.H., and D.L. Davidson, "Experimental Characterization of Yield Induced by Surface Flaws," The Surface Crack: Physical Problems and Computational Solutions. American Society of Mechanical Engineers (1972).

6. Creager, M., and G.A. Vroman. Multiple-Cycle Proof Test Logic. Rocketdyne Division, Rockwell International Corporation, SSME 73-410 (February 1973).

7. Bixler, W.D. Flaw Growth of 6Al-4V STA Titanium in Nitrogen Tetroxide With Low Nitric Oxide Content. The Boeing Company, D180-14853-1 (May 1972).

8. Francis, P.H. "Elasto-Plastic Analysis of a Mode I Edge Crack With Application to a Surface Notch," International Journal of Fracture Mechanics, Vol. 7, No. 4 (December 1971).

9. Parry, D.L., and E.V. Waite. "Field Evaluation of Heavy-Walled Pressure Vessels Using Acoustic Emission Analyses," Materials Evaluation (June 1971).

10. Dunegan, H.L., and A.S. Tetelman. "Acoustic Emission," Research Development (May 1971).

11. Dunegan, H.L., and D.O. Harris. Prediction of Fatigue Lifetime by Combined Fracture Mechanics and Acoustic Emission Techniques. Air Force Conference on Fatigue and Fracture of Aircraft Structures and Materials, Miami Beach, Florida, December 15-18, 1969.

12. Frederick, J.R. "Acoustic Emission as a Technique for Nondestructive Testing," Material Evaluation (February 1970).

13. Green, A.T., H.L. Dunegan, and A.S. Tetelman. Nondestructive Inspection of Aircraft Structures in Materials via Acoustic Emission. ATAA Symposium (September 1971).

14. Green, A.T. "Detection of Incipient Failure in Pressure Vessels by Stress-Wave Emissions," Nuclear Safety, Vol. 10 No. 1 (January-February 1969).

15. Nakamura, Y. "Acoustic Emission Monitoring System for Detection of Cracks in a Complex Structure," Materials Evaluation (January 1971).

16. Liptai, R.G. Acoustic Emissions From Composite Materials. University of California, Lawrence Radiation Laboratories (1971).

17. Hartbower, C.E., W.G. Reuter, C.F. Morais, and P.P. Crimmins. Correlation of Stress-Wave-Emission Characteristics With Fracture in Aluminum Alloys. NASA CR-2072 (July 1972).

6.0 CRACK GROWTH PREDICTIVE ANALYSIS TECHNIQUES

6.0 CRACK GROWTH PREDICTIVE ANALYSIS TECHNIQUES

Analysis methods and techniques specifically related to Space Shuttle applications will be discussed in detail within other tasks associated with this contract. However, a general discussion of the more intrinsic features of flaw growth analysis methods is presented herein to provide the information necessary to properly evaluate or construct predictive analysis programs.

To obtain a valid crack growth prediction, proper consideration must be given to all major aspects of the problem. The initial flaw size must be described and the anticipated load history must be defined. Additionally, crack growth must be considered as a step-by-step process of accumulated damage in which crack extension progresses as a stochastic process to some point of instability.

From discussions in earlier sections it is evident that the calculation of flaw growth to failure of a structural component, if done rigorously, would require a very large number of known quantities and behavioral relationships, and a great deal of computation. Even with the current computational equipment, simplifying assumptions will have to be made and the objective then must be to choose these assumptions carefully to maximize the usefulness of the results.

Throughout the aerospace industry, there exist a number of crack growth predictive analysis programs. Of these, the Air Force Program CRACKS (Reference 1), the NASA-JSC Program CRACK (Reference 2), and the Rockwell International (Los Angeles Division) Program EFFGRO II (Reference 3) have received the most attention by the Space Division.

These three programs are all oriented strictly toward accumulative damage fatigue crack propagation. Each of the programs contains certain attractive features which will be incorporated into a Space Shuttle-oriented predictive analysis program. The EFFGRO II is the largest program and is capable of accommodating several geometric configurations. That program also incorporates the "range-pairing" technique for counting a complex load spectra and the Vroman crack growth retardation model (Reference 4).

The CRACK program, while using the Forman crack growth rate equation (Reference 5), is capable of evaluating two-dimensional crack growth behavior for surface flaws. This capability represents a very significant advancement in flaw growth prediction eliminating the necessity for

simplifying assumptions regarding flaw shape changes. A part-through-crack predictive analysis program prepared at Rockwell International Space Division also incorporates the two-dimensional crack growth analysis approach (Reference 6). Both programs using the two-dimensional approach show improved agreement with experimental results for constant load amplitude surface flaw growth treating a wide variety of starting flaw shapes (Reference 7).

COMPUTATIONAL TECHNIQUES

Most crack growth predictive analysis programs have been structured around fatigue crack propagation laws. As discussed in Section 3, a crack tip subjected to a constant load amplitude applied differential stress intensity, ΔK, has been observed to propagate at a material dependent rate, or:

$$da/dN = f\left(\Delta K,\ g\left(c,\ n,\ K_c,\ K_o\right)\right) \qquad (1)$$

where

ΔK = $h\left(a,\ \sigma,\ \sigma_y,\ \alpha\right)$

$c,\ n,\ K_c,\ K_o$ = material constants (see Section 3)

a = flaw size

$\sigma,\ \sigma_{ys}$ = applied and yield stress, respectively

α = geometry related coefficients or stress intensity factors often dependent upon crack size and/or shape

To estimate the crack extension over a discrete number of constant amplitude load cycles requires integration of Equation 1 along a, or:

$$N - N_0 = \int_{a_0}^{a_n} \frac{da}{f\left(\Delta K,\ \ldots\right)} \qquad (2)$$

Numerical integration of Equation 2 is required in most cases due to the complexity of the crack growth rate expression and/or the stress intensity solution. Two approaches can be taken to this integration, incrementing either crack size or cycles at a chosen fixed rate.

The number of cycles required to grow a crack a discrete distance, Δa, can be calculated by simply evaluating ΔK at the average crack length

$(a + \Delta a/2)$ and calculating the average growth rate, da/dN, from Equation 1 and solving:

$$\Delta N = \Delta a / (da/dN) = \Delta a / \left| f(\Delta K, \ldots) \right| \quad (3)$$

For a flaw configuration which experiences large stress intensity gradients (dK/da) the Δa increment must be small to preserve accuracy. For most applications, 2 percent of the "current" flaw size is a sufficiently small increment which still affords a reasonable computational time. By summing the number of cycles calculated from Equation 3, an output of a versus N can be generated and arbitrarily terminated at a specific stress intensity, crack size, or cyclic life. Output accuracy can be improved by various alternative methods of approximating the average growth rate; however, the improved accuracy (dependent upon the severity or possible inflections in the stress intensity gradient) normally will be obliterated by the scatter factors usually applied to the end result due to the inherent variability in the accuracy of Equation 1.

Conversely, an increase in crack size resulting from a discrete number of load cycles can be evaluated by:

$$\Delta a = \Delta N (da/dN) = \Delta N \left| f(\Delta K, \ldots) \right| \quad (4)$$

The average growth rate for this calculation is slightly more difficult to estimate; however, several integration techniques are available to provide an accurate evaluation of Equation 4. The Runga Kutta integration technique requires only the current flaw size as follows:

$$\Delta a = a_2 - a_1 = 1/6 (k_1 + 2k_2 + 2k_3 + k_4)$$

where

$$k_1 = \Delta N \cdot da/dN \Big|_{a_1}$$

$$k_2 = \Delta N \cdot da/dN \Big|_{a_1 + k_1/2}$$

$$k_3 = \Delta N \cdot da/dN \Big|_{a_1 + k_2/2}$$

$$k_4 = \Delta N \cdot da/dN \Big|_{a_1 + k_3}$$

Proper selection of the integration increment, ΔN, requires some prior knowledge of the expected service life to avoid excessive computer time. Routines which vary the integration increment are available. They start with a very large increment and decrease it until the total life is calculated in some prespecified number of cycle-increments. The increment

is systematically decreased as the remaining life approaches one load cycle and an output of flaw size versus cycles can be obtained. The speed and efficiency of this integration technique is often restricted by the number of times the increment must be changed and the accuracy can be most influenced by subroutines which interpolate the final result.

Multiple direction flaw growth analysis is necessary to properly evaluate many flaw configurations. For example, the stress intensity along the front of a surface flaw is expressed by the following equation (see Section 1):

$$K = 1.12\,\sigma\sqrt{a/Q}\left\{\sin^2\beta + (a/c)^2\cos^2\beta\right\}^{1/4}$$

where β specifies location along the crack front at which the stress intensity is being calculated as illustrated in Figure 6-1. Accordingly, the applied differential stress intensity, ΔK, for a given cyclic load and the corresponding flaw growth rate will vary along the entire front of the flaw.

Flaw extension, in such an instance, must be computed by evaluating the crack growth at different locations along the crack front. Conservation of the semi-elliptical flaw shape for the part-through-crack requires that a maximum of two locations be separately evaluated. The most convenient crack front locations, because of the availability of free surface correction factors, are at $\beta = 90$ degrees and 0 degrees. The corresponding stress intensity solutions are then

$$K_a = 1.12\,\sigma\sqrt{\pi a/Q} \text{ for } \beta = 90^o$$

$$K_{2c} = 1.12\,\sigma\sqrt{\pi a/Q\,(a/c)} \text{ for } \beta = 0^o$$

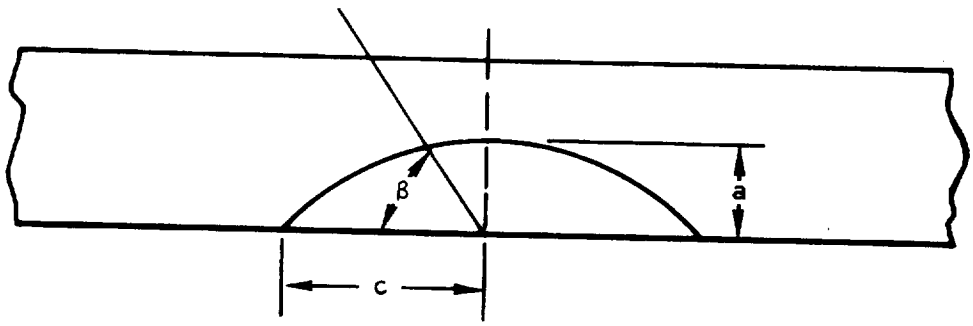

Figure 6-1. Surface Flaw Geometry

Appropriate free surface correction factors are then applied to both relationships and the flaw extension calculated from

$$\Delta a/\Delta N \simeq da/dN = f(\Delta K_a, \ldots)$$

$$\Delta c/\Delta N \simeq dc/dN = f(\Delta K_{2c}, \ldots)$$

A similar approach is applicable for corner cracks, or any other flaw configuration which experiences differing stress intensities along the crack front.

When material anisotropy causes a discernible change in the flaw growth rate as a function of crack orientation, provisions must be available within the analysis program to input and evaluate discrete growth rate equation coefficients for the appropriate crack orientations.

Transitional flaw growth behavior associated, for example, with surface flaw breakthrough to a through crack also requires consideration when evaluating service life. "Conservative" assumptions, i.e. at breakthrough the flaw length is assumed to jump to a through crack of length equal to the front face crack length, can significantly reduce a useful and sometimes very necessary portion of the service life as illustrated in Reference 8. The primary deficiency in transitional crack growth analysis is the lack of credible stress intensity solutions. In their absence, approximations or empirical solutions must be found and implemented.

Since very few structural applications will involve only constant amplitude load cycles throughout an intended service life, it is mandatory that the predictive analysis program accommodate a complex load spectrum representative of anticipated service conditions. One essential requirement for accurate prediction of fatigue life or crack growth rate is a correct interpretation of the load spectrum. A specific load spectrum constructed from estimated flight requirements may not be directly applicable to an analysis. This results from the observation that flaw extension is influenced not only by a load step currently being applied, but also by the total range between previous and current load levels. In analyzing the complex fatigue load spectra, many different methods are available which count the effective or damage causing load cycles. It has been reported by Dowling (Reference 9) that all of the current counting methods have serious flaws with the exception of the "range-pair" and "rain flow" methods. In the rain flow method, all closed stress-strain hysteresis loops are counted as cycles. The range-pair method, equivalent to rain-flow for most practical applications, is more convenient in computer programming.

The essence of the range-pair technique of counting spectrum load cycles can be explored by considering the following example taken from

Reference 10. Given a load trace as illustrated in Figure 6-2a the following criteria for counting a cycles is applied.

> If $P_2 > P_1$, then a cycle of amplitude $|P_2-P_3|/2$ and mean of $1/2\ (P_2+P_3)$ is counted if $P_2 \leq P_4$ and $P_3 \geq P_1$.
>
> Conversely (Figure 6-2b), if $P_2 < P_1$, the same cycle is counted if $P_2 \geq P_4$ and $P_3 \leq P_1$.

Given a complex load spectra, four consecutive peaks and valleys are considered. If the second and third peak or valley meet the above conditions, one cycle is defined and those two points are deleted from the load trace. The fourth peak or valley now becomes the second, and the next consecutive peak and valley of the load trace are added to again give four points. This counting continues until the four points being considered will not define a cycle. When this occurs (Figure 6-3), the first point is omitted from consideration and put into a residue trace and the next following peak is added to the load trace. This process continues, adding points to the residue trace as necessary, until there are only two or three points left. These points are added to the residue trace, which is then analyzed in the same manner as the original trace. The results of this counting process will

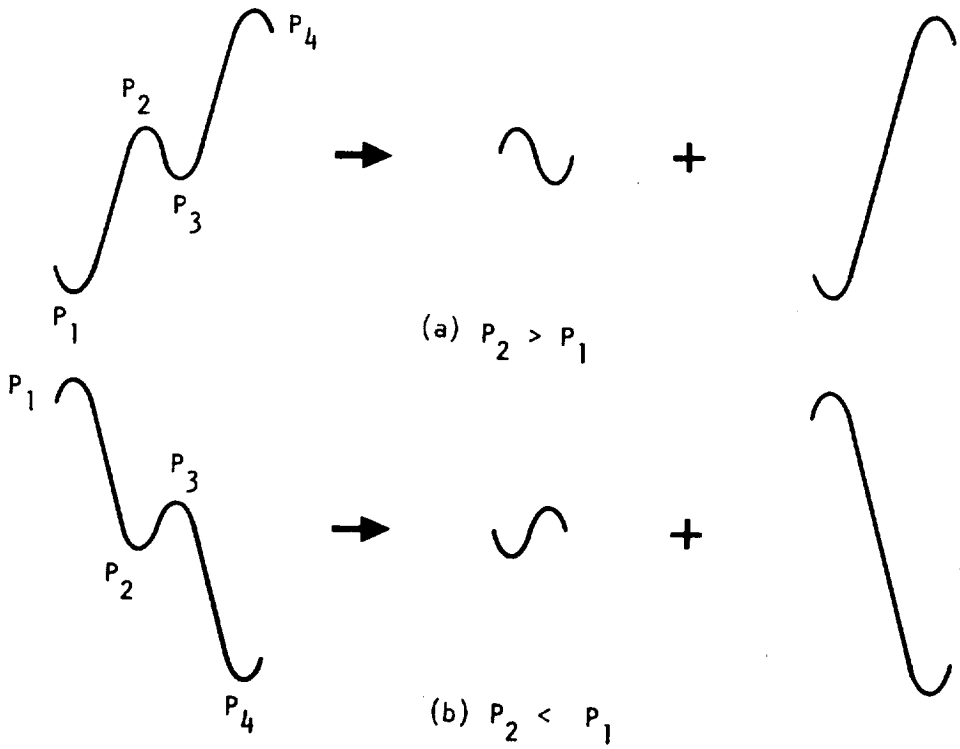

Figure 6-2. Range-Pair Technique of Counting Spectrum Load Cycles

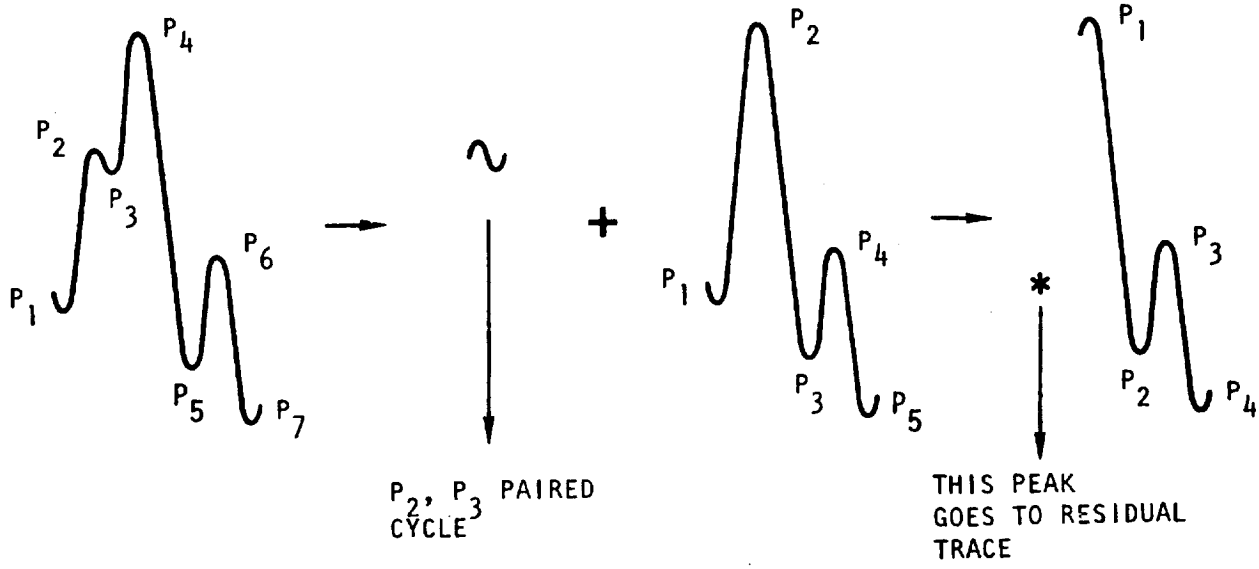

(A) REMOVAL OF "NONDEFINED" CYCLES

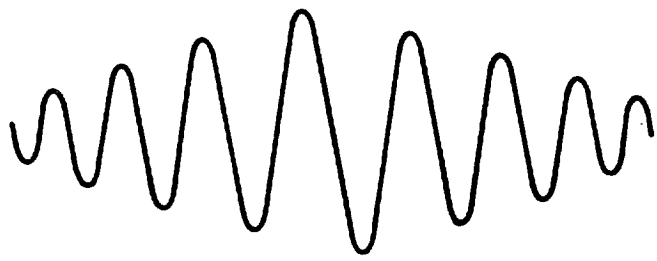

(B) FINAL RESIDUAL TRACE

Figure 6-3. Range-Pair Counting of Nondefined Load Cycles

eventually leave a residue trace which diverges to a maximum range and then converges as shown in Figure 6-3b. This trace will yield no cycles by the range pair counting method.

To count these remaining cycles, the highest peak is paired with the lowest valley to form a cycle. Moving away from this cycle in both directions, each successive peak and valley are paired together. If there is an extra peak or valley left on either side, it is omitted. A peak on one side of the maximum excursion cycle should never be paired with a valley on the other side. The load cycles resulting from this counting procedure now form the spectrum to be used in both fatigue and fracture mechanics analyses.

When employing a more ordered spectrum, i.e., steps consisting of several constant amplitude load cycles, the range pairing technique then attempts to account for the damage caused by changing load amplitudes. This feature is illustrated in Figure 6-4. A two-step block consisting of five cycles at one load range and four cycles at a higher load range is paired to produce a spectrum of three distinct steps.

When sequence becomes important, as in crack growth retardation, the peaks must be ordered, as well as possible, in the same sequence as the original load trace. The effectiveness of the reordering, however, is difficult to evaluate because of the inherent variability in retardation mechanisms and the strong dependency on exact load sequence.

As discussed in Section 3, the treatment of crack growth retardation usually requires, depending on the model chosen, that some effective stress or stress intensity be calculated. This requires that the load spectrum be

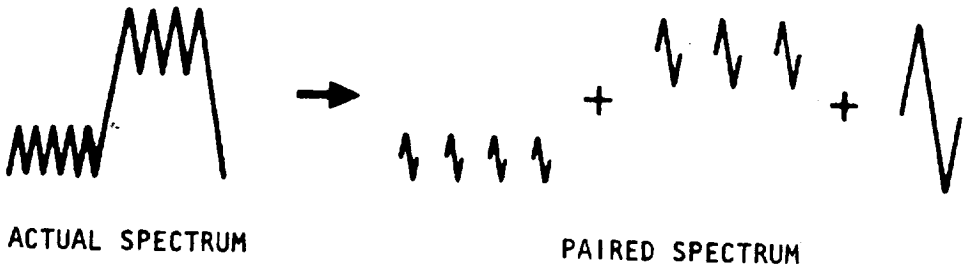

Figure 6-4. Range-Pair Counting of Ordered Spectrum

continuously monitored for prior load history effects and/or the current plastic zone boundary relative to the largest prior zone boundary. Since the different retardation models operate on different variables, it is difficult to provide for interchangeability of the models within a single program. Since the current "working" models are all based on very little mechanistic foundation, incorporation of any particular model cannot be recommended.

Of major concern when evaluating complex load spectra containing several single-cycle load applications is the applicability of cyclic crack growth representations. These representations usually are developed by averaging relatively large numbers of load cycles and their ability to accurately describe single-cycle events is questionable.

A complex load spectra containing many load steps of relatively few cycles and a large load block lifetime will require much computer time for cycle-by-cycle crack growth assessments. In a method proposed by Brussat (References 11 and 12) the computational time can be significantly decreased by separately evaluating the stress and flaw size components of the stress intensity solution. That is, by considering

$$K = \sigma \cdot \alpha$$

where σ is the applied stress and α is the part geometry and flaw size contribution to the stress intensity (independent of stress and therefore exclusive of plasticity considerations). By normal rigorous calculation of flaw growth only at selected blocks within a "lifetime," the separate contribution to flaw growth by the loads and the geometry (α) can be assessed. Since the loads contribution to flaw growth will not change, any shift in flaw growth rate results from geometry changes and this can be calculated without evaluation of the load spectra at every block.

The accuracy of such an analysis appears to depend upon minimal change of α (flaw growth) within a single block when compared to the flaw growth over the entire lifetime. Although sensitivity studies regarding the limits of applicability of this type of analysis to space shuttle systems have not been performed, the approach will be thoroughly reviewed prior to formalization of a shuttle analysis program.

Obviously, fatigue crack propagation is not the only mechanism by which cracks can grow to cause failure. Sustained load flaw growth, environmentally enhanced fatigue crack growth, and flaw growth during monotonic loading are all real and significant problems. While characterization of these phenomenon is not yet complete or very accurate, provisions for future incorporation into analysis programs should be considered.

Sustained load flaw growth probably will be best defined as a function of applied stress intensity in a manner similar to fatigue crack growth. If similar relationships are used to describe both flaw growth mechanisms, predictive techniques can be greatly simplified. For example, the Collipriest growth rate equation (see Section 3) requires four input variables (K_c, K_o, C, n) to describe the fatigue crack growth rate of a given material. Since the same form relationship appears to describe the sustained load flaw growth behavior for some material-environment combinations, then input of four alternate variables (K_c, K_{th} or K_{Iscc}, C, n) can be used in the same program to output crack growth as a function of time. Additionally, if a program is written to consider a new set of growth rate equation coefficients for each step within a spectrum load block, then a service spectrum which mixes both cyclic load applications and periodic holds at specified loads can be evaluated. Also, if effects on cyclic growth rate due to environments or temperature can be accommodated by adjusting the normal environment growth rate coefficients, a more complex and realistic service load spectrum can be evaluated.

Since the fracture-influenced crack growth rate equations can also provide an R-curve representation of flaw growth on monotonic load application it is possible also to consider this facet of observed behavior in predictive analysis. A single cycle load increase could then be treated by a separate set of growth rate equation coefficients and a complete service life load spectrum could be evaluated.

Cycle counting techniques, if used, are applicable only to that portion of a service spectrum which experiences load changes without changes in growth rate equations. Additionally, if monotonic load induced crack growth can be adequately characterized in the near future, then the need or applicability of cycle counting techniques must be re-evaluated.

RECOMMENDED PRACTICE

As knowledge of fracture-related material behavior is expanded, modifications or updates will be made to existing predictive analysis programs. Such modifications may be made at a very high rate during periods of significant technology advancements. For this reason it is mandatory that any analysis output always be accompanied by identification of the exact computational program used to generate it.

To facilitate convenient update of the analysis, it is advisable to construct the program logic so that subroutines are used to calculate the material related parameters such as stress intensity, complex free surface factors, and flaw growth rate expressions. In this manner, evaluations of the effects of changes to such parameters can be made easily.

With the current availability of large capacity desk-top programmable calculators, user access to the analysis program can be significantly improved. The use of such equipment can greatly reduce turn-around time and often will increase the incentive to perform parametric studies to evaluate the effects of selected variables. However, when a large volume of predictive analysis work must be performed, the speed of the large computers makes them cost effective.

Program flexibility regarding user options will add significantly to the effectiveness of the program. In addition to being able to output total lifetime as a function of initial flaw size and operating loads, other outputs should be available to the user. A continuous output (either print-out, X-Y plot, or CRT plot) of crack size versus applied load blocks or cycles should be available as an option. Additionally, it is useful to be able to obtain periodic outputs of factors such as "current" stress intensity or flaw growth rate. Also, it is often desirable to determine the amount of flaw extension and the residual strength of the structure after a specified limit on cycles or missions. These optional outputs require only minor adjustments to a program and their ability to eliminate waste and increase confidence in the analysis are well worth the additional program size.

For Space Shuttle fracture control applications, a new crack growth predictive analysis program is in preparation. The program is being formulated with due consideration of the previously mentioned variables while attempting to incorporate and consolidate the appropriate features of other predictive analysis programs currently in use.

REFERENCES

1. Engle, R.M., Jr. Cracks, A Fortran IV Digital Computer Program for Crack Propagation Analysis. Air Force Flight Dynamics Laboratory, Wright-Patterson AFB, Ohio, AFFDL-TR-70-107 (October 1970).

2. Forman, R.G., H.C. Kavanaugh, and B. Stuckey. Computer Analysis of Two-Dimensional Fatigue Flaw-Growth Problems. NASA TMX-58086 (February 1972).

3. Streitmatter, S. EFFGRO II, Crack-Propagation Analysis With Range-Pair Counting. Los Angeles Division, Rockwell International Corporation, TFD-72-729 (June 1972).

4. Vroman, G. Crack Propagation Analysis With Retardation. Presented to ASTM-E24 Committee. Northrop Corporation, Hawthorne, California (September 1971).

5. Forman, R.G., V.E. Kearney, and R.M. Engle. "Numerical Analysis of Crack Propagation in Cyclic-Loaded Structures," Journal of Basic Engineering, Transactions of the ASME, Vol. 89 (September 1967), pp. 459-464.

6. Collipriest, J.E., Jr., and R.M. Ehret. Computer Modeling of Part-Through-Crack Growth. Space Division, Rockwell International Corporation, SD 72-CE-0015A (September 1972).

7. Johnson, K. Fracture Mechanics Technology Requirements for Space Shuttle. Space Division, Rockwell International Corporation, IL No. SSD-FF&CM-73-004 (May 1973).

8. Christensen, R.H. Safe Operating Stresses for Reusable Space Shuttle Propellant Tanks To Ensure Leak Before Burst. Presented at the Fracture Control Technology Meeting, NASA/Lewis Research Center, January 1972. (McDonnell Douglas Astronautics Company.)

9. Dowling, N.E. Fatigue Failure Predictions for Complicated Stress-Strain Histories. University of Illinois, Urbana, Illinois, Report No. 337 (January 1971).

10. Streitmatter, S. A Method of Counting Spectrum Load Cycles. Los Angeles Division, Rockwell International Corporation, TFD-72-358 (March 1972).

11. Brussat, T. R. Rapid Calculation of Fatigue Crack Growth by Integration. Preprint prepared for presentation at the Seventh National Symposium on Fracture Mechanics, College Park, Maryland, August 1973 (Lockheed-California Company).

12. Brussat, T. R. An Approach to Predicting the Growth to Failure of Fatigue Cracks Subjected to Arbitrary Uniaxial Cyclic Loading. Presented at the 73rd Annual Meeting of the American Society for Testing and Materials, Toronto, Canada, June 1970. (Lockheed-California Company.)